Optimization of Patient Matching in Total Knee Arthroplasty through Improved Implant Sizing and Detailed Fit Assessment

Optimierung der Patienten-Anpassung in der totalen Knieendoprotethik durch verbesserte Implantat-Größen-Verteilung und detaillierte Fit Bewertung

Von der Fakultät für Maschinenwesen der Rheinisch-Westfälischen Technischen Hochschule Aachen zur Erlangung des akademischen Grades einer Doktorin der Ingenieurwissenschaften genehmigte Dissertation

vorgelegt von

Sonja Anke Gabriele Agathe Ehreiser (geb. Grothues)

Berichter: Univ.-Prof. Dr.-Ing. Klaus Radermacher
Prof. Eric Stindel, MD, PhD

Tag der mündlichen Prüfung: 29.05.2024

Diese Dissertation ist auf den Internetseiten der Universitätsbibliothek online verfügbar.

Danksagung

Die vorliegende Arbeit entstand im Rahmen meiner Tätigkeit als wissenschaftliche Mitarbeiterin am Lehrstuhl für Medizintechnik im Helmholtz-Institut für Biomedizinische Technik an der Rheinisch-Westfälischen Technischen Hochschule Aachen.

Ganz besonders danken möchte ich Univ.-Prof. Dr.-Ing. Klaus Radermacher. Danke für die hervorragende Betreuung der Arbeit, mit zahlreichen Ideen, wichtigen Diskussionen, sehr hilfreicher Kritik, und viel Begeisterung. Danke für das große Vertrauen und für die große Unterstützung, die ich sehr zu schätzen weiß.

Weiterhin möchte ich Prof. Eric Stindel, MD, PhD danken, für die Übernahme des Korreferats und für die weite Anreise nach Aachen anlässlich der Prüfung.

Teile der Arbeit wurden von der Firma Conformis, Inc., Billerica, Massachusetts, USA im Rahmen einer Industriekooperation gefördert, wofür ich mich ebenfalls bedanken möchte. Insbesondere danke ich Sumesh Zingde für die gute Zusammenarbeit.

Ich danke allen Kolleginnen und Kollegen am mediTEC. Durch euch war die Zeit am Institut etwas ganz Besonderes. Die Arbeit im Biomechanik-Team in seinen verschiedenen Konstellationen hat sehr viel Spaß gemacht. Danke an alle ehemaligen und neuen Teammitglieder und die dazugehörigen Studierenden. Danke insbesondere an Luisa Berger, Benjamin Hohlmann und Malte Asseln, für den tollen Austausch, die gegenseitige Begeisterung und Unterstützung. Außerdem möchte ich mich bei Anne Benninghaus, Manuel Vossel und Nina Reinhardt für die gegenseitige Motivation und einfach die gemeinsame Zeit, insbesondere in der Abschlussphase der Dissertation bedanken.

Mein abschließender und wichtigster Dank gilt meiner Familie. Meinen Eltern, die mich immer unterstützt haben, immer ein offenes Ohr für mich hatten und mir immer alles zugetraut haben. Meinem Bruder und meiner Oma, ebenfalls für das Zutrauen und den Zuspruch. Und ganz besonders meinem Mann Fritz, für die Unterstützung in allen Phasen dieser Dissertation, mit Ermutigung, Empfehlungen, Korrekturen, Probevorträgen und viel Geduld. Danke!

Summary

Total knee arthroplasty is one of the most performed surgeries worldwide. Indicators of treatment success, such as revision rates or patient satisfaction, are subject to multiple influences, with implant design and associated patient-specific implant fit being a relevant and variable factor. A considerable discrepancy between implant and bone shape in terms of size as well as individual morphologic parameters has been reported for various populations. Such mismatch can motivate the advising of a customized implant. However, there is currently no standardized method to support this decision, or for detailed assessment of knee implant fit in general. Hence, the aim of this thesis was to evaluate the potential for standard implant size optimization and to develop methods for patient-specific implant fit evaluation, with the goal of optimizing patient matching in total knee arthroplasty.

The possibility of improved size matching through numerically optimized sizing was demonstrated for a large database of over 85.000 knees. With the numerically optimized sizes an increase in population coverage of 19% to 26% compared to representative existing implant systems was reached. The need for further fit analysis beyond size was demonstrated by an exemplary documentation of size-independent shape variations using the femoral J-curve as an example, and by relevant morphological deviations even in the case of an ideal size fit. Many objective criteria for assessing implant fit have been defined in the literature, which were assigned to the categories interface, morphological, alignment and other. As morphological criteria are defined for the physiological, non-deformed knee morphology, a parameter-based deformity correction was developed and verified. Based on the analysis of existing imaging procedures, concepts for the evaluation of the identified criteria were defined. The chosen concept includes an initial fit assessment based on standardized radiographs and, if required, an additional detailed fit evaluation using computed tomography data. The potential for clinical integration was demonstrated in an exemplary implementation with a high level of automation. The fit evaluation was carried out for an exemplary implant and a large knee database, demonstrating the workflows robustness. With the implant size optimization and individual fit evaluation, more patients can be provided with an adequate standard implant and those requiring a customized implant identified objectively, thereby maximizing patient matching.

Zusammenfassung

Der totale Kniegelenkersatz ist eine der meist-durchgeführten Operationen weltweit. Indikatoren des Operationserfolgs wie Revisionsraten oder die Patientenzufriedenheit sind multifaktoriell beeinflusst, wobei das Implantat Design und die zugehörige Passgenauigkeit einen relevanten und veränderlichen Faktor darstellt. Für diverse Patienten Populationen wurde eine erhebliche Diskrepanz zwischen Implantat- und Knochen-Form berichtet, hinsichtlich Größen sowie einzelner Morphologie Parameter. Solch geringe Passgenauigkeit kann die Empfehlung eines Individual-Implantats motivieren. Bislang gibt es jedoch weder standardisierte Methoden welche diese Entscheidung unterstützen, noch generell für eine detaillierte Passform-Bewertung. Das Ziel dieser Arbeit ist demzufolge die Potenzial-Bewertung einer Implantat-Größen Optimierung sowie die Entwicklung von Methoden zur individuellen Passformbewertung, für eine insgesamt optimierte Patienten-Anpassung.

Die Möglichkeit einer verbesserten Patienten-Anpassung durch numerisch optimierte Implantatgrößen wurde für eine Datenbank von über 85.000 Knien demonstriert. Mit den optimierten Größen wurde eine um 19% bis 26% verbesserte Patientenabdeckung erreicht, im Vergleich zu bestehenden Systemen. Durch die exemplarische Dokumentation größen-unabhängiger Formvariation der femoralen J-Curve sowie relevanter Formabweichungen trotz idealem Größen-Fit, wurde der Bedarf an weiterer Passformanalyse gezeigt. In einer Literaturrecherche wurden Kriterien für die Passformbewertung identifiziert und als Interface, Morphologie, Alignment und Andere klassifiziert. Da die identifizierten, morphologischen Kriterien für das physiologische, nicht-deformierte Knie definiert sind, wurde eine parameter-basierte Deformitätskorrektur entwickelt und verifiziert. Basierend auf der Analyse bestehender Bildgebungsverfahren wurden Konzepte zur Fit-Bewertung definiert. Das gewählte Konzept beinhaltet eine initiale Risikoabschätzung mit standardisierten Röntgenbildern und, wenn erforderlich, zusätzlicher Detailanalyse mittels Computer-Tomographie. In einer beispielhaften Implementierung mit hoher Automatisierung wurde das Potenzial für die klinische Integration demonstriert. Die Passformbewertung wurde für ein beispielhaftes Implantat und eine große Kniedatenbank durchgeführt. Mit optimierten Implantatgrößen und individueller Passformbewertung kann der Anteil adäquat versorgter Patienten erhöht und diejenigen, welche ein Individual-Implantat benötigen, objektiv identifiziert werden, was insgesamt die Patienten-Anpassung maximiert.

Table of Contents

1. Introduction

The knee joint is central for locomotion during which it supports high loads while providing both flexibility as well as stability in extension and throughout knee flexion. This intricate function is enabled by a complex interplay between muscles, ligaments, menisci, and bones. However, this complexity renders the knee susceptible to various pathologies.

Among these pathologies, osteoarthritis (OA) is the most common joint disease, with the knee joint frequently affected (Buckwalter et al. 2004). OA can be characterized as a group of pathologies with various causes, affecting different articular and periarticular structures, including cartilage, ligaments, menisci, and the subchondral bone (Wirtz 2011). OA-related symptoms are pain and functional impairment (Buckwalter et al. 2004). The gold standard for the treatment of OA, after the exploitation of conservative treatment options or more bone preserving interventions such as osteotomies or unicondylar knee replacement, is total knee arthroplasty (TKA). TKA is one of the most performed surgeries in Germany. High costs are involved with TKA (Rabenberg 2013), but similarly high socio-economic savings are achieved, through the recovery of previously lost working power (Lombardi et al. 2014; Ruiz et al. 2013). Although TKA commonly provides pain relief and restores knee function, a notable proportion of patients remain dissatisfied post-surgery.

Current studies report that 10% to 19% of TKA patients are dissatisfied with their knee replacement (Jacobs and Christensen 2014; Bryan et al. 2018; Bourne et al. 2010). Respective patient-reported outcome measures (PROMs) primarily assess pain levels during different activities of daily living (ADLs) as well as the knee function, determined by the range of motion and the ability to perform various ADLs (Noble et al. 2012; Scuderi et al. 2012; Roos et al. 1998). Other factors to be considered for evaluating the treatment's success include surgery revision rates, the length of the hospital stay, as well as the amount of bone and blood loss during surgery (Culler et al. 2017). In TKA, the implant design is a relevant predictor of postoperative kinematics (Banks and Hodge 2004; Dennis et al. 2003; Shi et al. 2015), postoperative pain levels (Powers 2000;

Mahoney and Kinsey 2010), implant longevity (Nishikawa et al. 2014), as well as bone and blood loss (Gao et al. 2014).

Several decisions must be made about the implant system prior to surgery, including the selection of the implant components (Tanzer and Makhdom 2016). In clinical practice, standardized implant systems are commonly used. These systems vary in the number of components they encompass, the level of constraint they provide, and their size graduation. For the individual patient, the degree of constraint is determined mainly based on the patient's ligamentous status (Lützner and Kirschner 2017). The planned implant component sizes are identified by comparison with the bones' anteroposterior (AP) and mediolateral (ML) size on the respective radiographs, while the anterior-posterior dimensions are prioritized (Tanzer and Makhdom 2016). Different manufacturers follow different design philosophies (Delfosse et al. 2022) and also offer different sizing (Hitt et al. 2003; Budhiparama et al. 2021). Despite the variety available, most clinics use only one implant system. Potential advantages of this approach include the surgeons' experience with the implant system, while the clinical relevance of the learning curve with new knee implant systems is still debated (Whittaker et al. 2018). The disadvantage is that patients may receive an implant with a poorer morphological and functional fit.

Geometrical mismatch between the implant geometry and the patient's bone morphology adversely affects clinical outcomes (Bonnin et al. 2022). For an inadequate AP fit, the resulting impact depends on the referencing technique (Charette et al. 2018). With anterior referencing, an adequate anterior resection without notching or overstuffing is prioritized over the restoration of the flexion gap and posterior condylar offset (Charette et al. 2018), with potentially detrimental effects e.g., on the flexion range of motion (Bellemans et al. 2002). In contrast, with posterior referencing the restoration of the posterior condylar offset is targeted, and hence in case of size mismatch a compromise regarding the anterior resection is required (Charette et al. 2018). Inadequate femoral ML fit entails implant over-/ underhang relative to the bone (Dai et al. 2014b), with overhang being associated with increased risk for pain and reduced function (Bonnin et al. 2013; Chung et al. 2015; Mahoney and Kinsey 2010). The described mismatch between the implant and resected bone size has been reported in

the literature across implant designs and populations (Hitt et al. 2003; Mahoney and Kinsey 2010; Guy et al. 2012; Yue et al. 2014; Chung et al. 2015; Kim et al. 2010; Sharma et al. 2017), which underscores the need for optimizing implant size fit.

Apart from size matching, other morpho-functional parameters with relevance for post-operative knee function are to be considered. A well-known anatomical feature is the femoral J-curve, whose relevance for knee kinematics is reflected in different design philosophies of implant manufacturers, including Single-, Dual- and Multi-Radius designs. Corresponding morphological parameters and their alterations have been reported to be main influence factors for knee kinematics *in silico* (Fitzpatrick et al. 2012b; Asseln et al. 2021), *in vitro* (Asseln et al. 2021), and *in vivo* (Kessler et al. 2007). Other functionally relevant parameters are the posterior condylar offset, which is linked to the postoperative flexion range of motion (Bellemans et al. 2002) and parameters of the femoral trochlea, which affect patellofemoral kinematics and pain (Powers 2000). Some anatomical features and related morphological parameters including the distal femoral condyles (J-Curve) are often affected by OA (Neogi et al. 2013), necessitating reconstruction. This fact further complicates the determination of an adequate implant design.

In clinical practice, a comparison of different implant designs regarding such detailed morphological fit is not considered. Few clinics use customized implants apart from the one implant system, which is used regularly. Surgeons may recommend such a customized implant based on subjective evaluation of the mismatch between the standard implant's geometry and the patient's knee morphology. To date, no standardized and objective method exists, that supports surgeons in this decision. The resulting inaccurate and potentially insufficient allocation of customized implants to patients with non-conforming knee morphology, in combination with inadequate size offerings of available standard implant systems and resulting mismatch, represents one factor that may explain the aforementioned high percentage of dissatisfied TKA patients.

Hence, the aim of this thesis was

- to evaluate the potential for **standard implant size optimization** to address current size mismatch in TKA and
- to develop a parameter-based **deformity correction workflow**

- **to develop methods and a workflow for comprehensive implant fit evaluation** based on 3D-morpho-functional analyses

with the goal of supporting surgeons in the decision-making between standard implant systems and an adequate allocation of customized implants.

The background and motivation for the thesis are presented in **Chapter 2**, including the anatomy and biomechanics of the knee, as well as focus areas of TKA. With the first step in patient matching being an adequate size fit, **Chapter 3.1** presents the optimization of implant sizing for a large database with more than 85.000 cases. The method based on particle swarm optimization is explained and results of sensitivity analyses regarding the number of implant sizes and the error bounds are presented. The need for a comprehensive fit assessment beyond classical sizing is demonstrated by the variability of native knee morphology in the example of the femoral 2D and 3D J-Curves (**Chapter 3.2**) and by the study of remaining deviations in case of an ideal size fit (**Chapter 3.3**). Subsequently, concepts for a respective fit assessment are developed in **Chapter 4**. In the first subchapter, different workflows for the fit evaluation are defined based on existing imaging techniques. In **Chapter 4.2**, objective fit criteria are identified based on a literature research and classified into categories (interface, morphology, alignment, other). As the need for a deformity correction has been identified in the context of morphological fit criteria, **Chapter 4.3** describes a method for this task and gives an evaluation for exemplary parameters. **Chapter 5** presents the exemplary implementation of the patient-specific implant fit evaluation, both for the preliminary 2D fit analysis and for the subsequent detailed 3D fit assessment. A discussion and conclusions on standard and patient-specific implant designs as well as an outlook on further studies on fit evaluation and patient matching in general is given in **Chapter 6**.

2. Background and motivation

2.1 Medical background on the knee

The knee joint is central for locomotion, providing mobility as well as stability in flexion and extension. In reflection of its complex functionality, the knee is one of the most complex and largest joints of the human body. The knee joint consists of the tibiofemoral and patellofemoral joint, which are located in a common joint capsule. Regarding the functional anatomy of the knee joint, active and passive structures can be distinguished, with the active structures including muscles with tendons and the passive structures including bones, ligaments and menisci. **Figure 2-1** gives an overview of the respective functional anatomy.

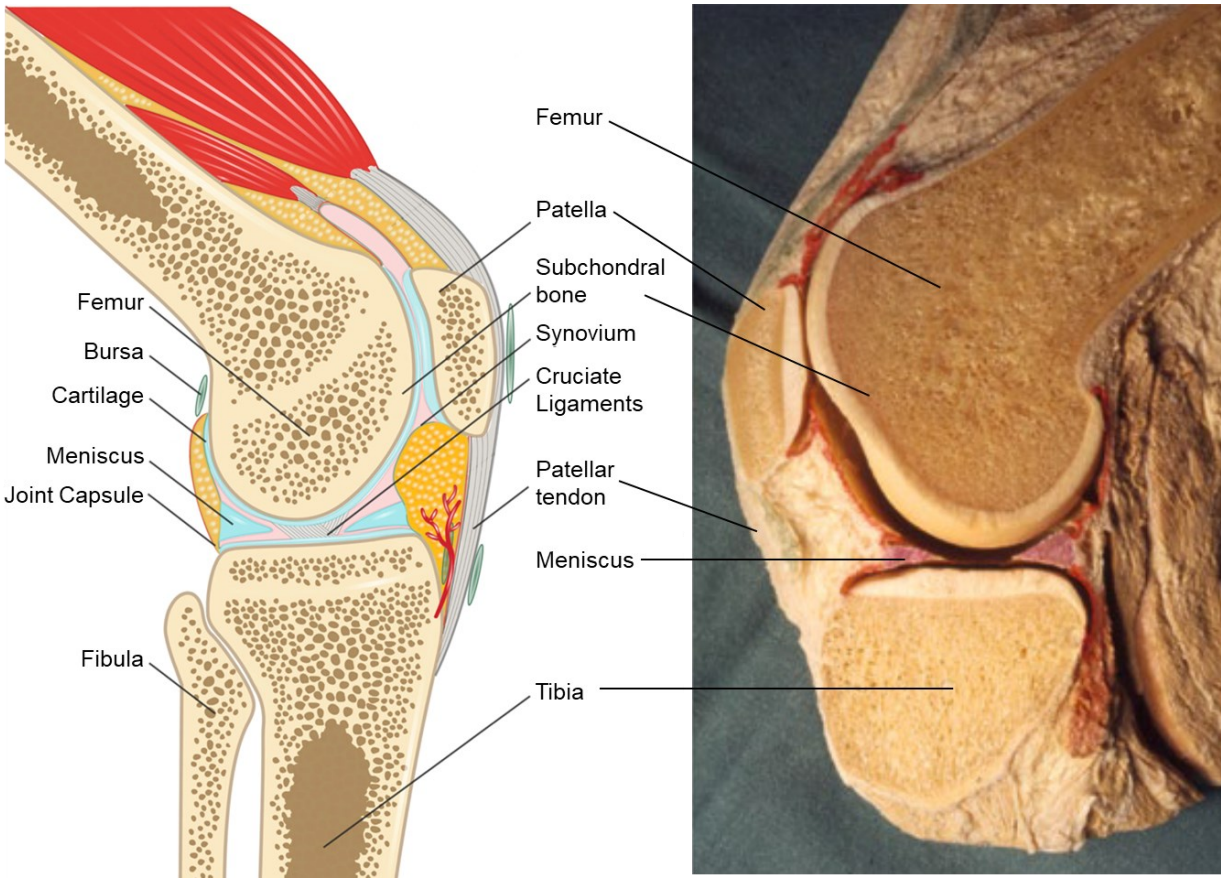

Figure 2-1: Functional anatomy of the knee. **(A)** Schematic representation of a sagittal cut through the lateral knee compartment (adapted from (Zhou et al. 2022), with permission from Wiley under CC BY 4.0). **(B)** Sagittal cut through the medial knee compartment of a cadaver knee (from (Jagodzinski et al. 2016), with permission from Springer Nature).

Articulating bony surfaces of the knee are those of the distal femur, the proximal tibia, and the backside of the patella, which are covered by articular cartilage. In general, the articular congruence of the knee's articulating surfaces is low, especially in the tibiofemoral joint (Jagodzinski et al. 2016). The low congruence emphasizes the relevance of the muscles and ligaments for stabilization of the knee joint.

The central ligaments of the knee are the anterior and posterior cruciate ligaments and the medial and lateral collateral ligaments. Furthermore, the medial patellofemoral ligament represents a main passive structure for patellar stabilization (Desio et al. 1998). The menisci are located on the tibial plateaus and are partly attached to the joint capsule. In the medial compartment, the meniscus further is indirectly attached to the medial collateral ligament, which results in a lower mobility of the medial compared to that of the lateral meniscus (Dürselen and Freutel 2015). The function of the menisci involves cushioning, increase of contact surface, proprioception, and guidance of synovial fluid (Dürselen and Freutel 2015).

The most important muscles of the knee joint are the corresponding main flexor and extensor muscles. The extensor muscles include the M. rectus femoris, the M. vastus medialis, the M. vastus lateralis and the M. vastus intermedius, together constituting the M. quadriceps femoris. The flexor muscles include the M. semimembranosus, the M. semitendinosus, and the M. biceps femoris (together constituting the so-called "hamstrings").

2.1.1 Knee morphology

The native articulating knee morphology highly influences active knee kinematics (Hodel et al. 2022; Klein and Sommerfeld 2012). In contrast, passive knee kinematics and stability are mainly determined by the ligamentous apparatus (Delport et al. 2013). During activities of daily living, muscle-driven active knee kinematics are mainly governed by knee (and implant) morphology. Nevertheless, the compatibility of active and passive knee kinematics has to be considered, as proprioception and nociception during knee motion are also based on ligament strain (Johansson 1991). This fact motivates the restoration of individual knee morphology in TKA, as it reduces the need for intraoperative adjustments in terms of ligament balancing through releases (Saffarini

et al. 2023). Consequently, the quantification of the native knee morphology is strongly relevant for developing adequate orthopedic treatments and implants.

Several approaches exist to quantify individual knee morphology. A classic method is the measurement of specific shape parameters such as anterior-posterior (AP) and medio-lateral (ML) sizes or distances respectively as well as angular parameters (Asseln et al. 2018). Those measurements enable a comparison with corresponding parameters of the implant shape, such as the sulcus angle (Dejour et al. 2014). A different approach considering the entire knee's surface are statistical shape models (SSM). By using an SSM, an individual knee shape can be defined by the mean shape and a combination of modes. Both approaches have been used to describe shape variations in populations differentiated by e.g., ethnicity (Mahfouz et al. 2012) or the presence of disease (Bredbenner et al. 2010).

With respect to such sub-populations, the presence of **morphotypes** is of interest in the context of total knee arthroplasty design. A clear differentiation of different morphotypes in the patient population would motivate an offer of specific implant shape variants. Bellemans et al. (Bellemans et al. 2010) analyzed the knee shape in the context of the constitutional morphotypes endomorph, ectomorph and mesomorph, however solely focusing on overall size measures. The size variation described can be addressed by optimized implant sizing, which is studied in this thesis (**Chapter 3.1**). Hirschmann et al. (Hirschmann et al. 2019b) and MacDessi et al. (MacDessi et al. 2021) presented classification systems for TKA patient knee morphology solely considering coronal alignment. Thereby they addressed the identification of an ideal alignment strategy, but did not consider other parameters of the detailed morphology of relevance for implant design. Mahfouz et al. (Mahfouz et al. 2012) comprehensively analyzed the morphology of the proximal tibia and distal femur and found several morphotypes related to ethnicity. However, most of the variation described applied to the general shape and respective ratios, which can also be addressed by optimized sizing studied in this thesis (**Chapter 3.1**). Regarding the concept of gender specific implants, Asseln et al. (Asseln et al. 2018) showed that gender differences are less relevant after normalization than inter-individual variations. In a recent study by Hohlmann et al. (Hohlmann et al. 2022), no clusters were found for a parameter database describing the knee morphology, after anisotropic

normalization of the measures. Those results suggest that generalized approaches for specific patient groups are not required due to the high interindividual deviations and missing clusters. Instead, an individualized approach and fit assessment should be used to assess the preoperative to postoperative changes in shape with TKA and the associated alterations in knee biomechanics that can be expected.

2.1.2 Knee biomechanics

Three-dimensional movement of the **tibiofemoral joint** involves six degrees of freedom each, three rotations and three translations along the axes of the bone-specific coordinate systems. Respective kinematics are displayed in **Figure 2-2-A**. For the tibiofemoral joint, the main movement with the largest range of motion is the flexion-extension movement. Relevant characteristics of physiological tibiofemoral kinematics furthermore describe internal-external rotation and anterior-posterior translation. Those characteristics include femoral rollback **Figure 2-2 C**, medial pivot, and the screw home mechanism. The screw home mechanism describes the internal rotation of the tibia in the last 5-10 degrees of extension (Freeman and Pinskerova 2005), leading to wrapping and tensioning of the cruciate ligaments, thus stabilizing the knee in extension. With the femoral rollback, the posterior translation of the femur over flexion is described, which is relevant for a sufficient range of motion (Fantozzi et al. 2006) and for limiting contact pressure in the patellofemoral joint. The presence of femoral rollback in combination with higher constraints and hence lower mobility in the medial tibiofemoral compartment results in the phenomenon of medial pivot, a continuous external rotation of the femur throughout flexion. Regarding TKA, also adduction-abduction rotation is of relevance in the context of the lift-off phenomenon (Dennis et al. 2001), which is reported to adversely affect wear rates (Jennings et al. 2007).

Likewise, the **patellofemoral joint** enables six degrees of freedom (**Figure 2-2-B**), but is constrained through the patellar tendon. Clinically relevant degrees of freedom include the patellar medial-lateral translation and rotation, as well as the patellar tilt rotation (Katchburian et al. 2003). Many factors determine patellofemoral kinematics and associated stability of the patella, including bony guidance, capsule and ligaments, and muscle forces (Klein and Sommerfeld 2012).

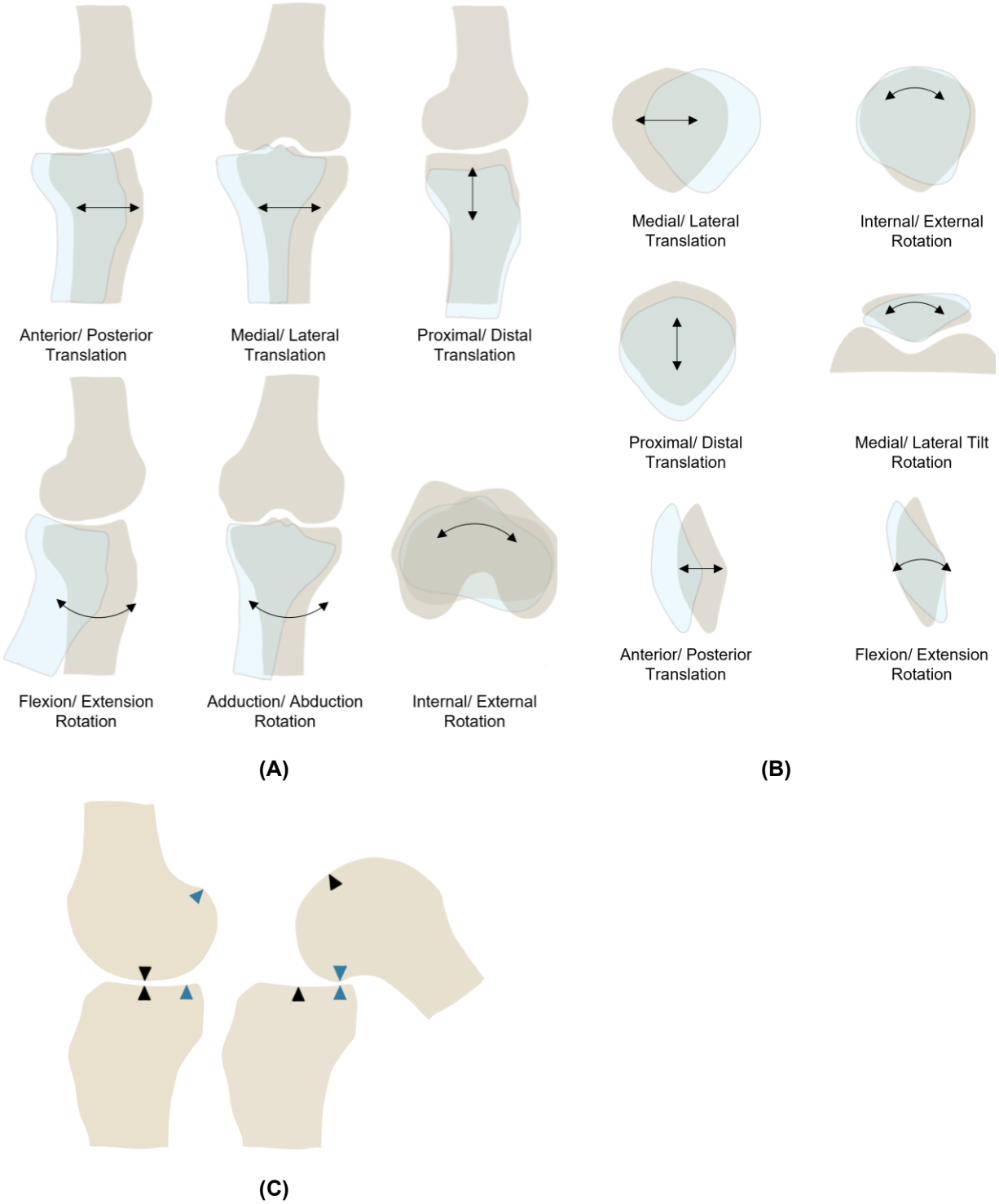

Figure 2-2: Degrees of freedom **(A)** of the tibiofemoral joint and **(B)** of the patellofemoral joint. **(C)** Sagittal view of the tibiofemoral rolling-gliding movement with "Femoral Rollback" during knee flexion movement.

The tibiofemoral and patellofemoral joint are subject to high loads, especially during active movement. Muscle activation mainly contributes to the high loads, while being crucial for stabilization and preservance of poses. Hence, depending on the activity

performed and muscle activation required, high differences in loads are observed. Instrumented prostheses were used to collect standard knee loads after TKA for several activities, which ranged from 160-280% of the body weight for level walking and 350% for stair descent (Bergmann et al. 2014). Similarly high maximum loads are estimated for the patellofemoral joint for stair descent (Mason et al. 2008). The lateral facet of the patella is generally exposed to higher forces, due to the lateral force vector of the M. quadriceps femoris. Loads in the tibiofemoral joint are strongly dependent on the leg axis. In the case of varus (valgus) leg axis deformities, the load transfer is shifted further to the medial (lateral) compartment and may ultimately result in osteoarthritis.

2.1.3 Osteoarthritis

Osteoarthritis (OA) of the knee joint (gonarthritis) is one of the most frequent pathologies worldwide, with an estimated **global prevalence** of 22.9% (95% CI, 19.8%-26.1%) in individuals aged ≥ 40 (Cui et al. 2020). OA is described as a group of pathophysiological processes, affecting not only cartilage but also the subchondral bone, ligaments, tendons, muscles, menisci, and synovium (Wieland et al. 2005; Bijlsma et al. 2011).

Two main types of OA are differentiated, being idiopathic (primary) and secondary OA (Altman et al. 1986). The disease is classified as idiopathic or primary, when the development is not attributed to a (single) known cause (Wirtz 2011; Altman et al. 1986). Instead, secondary OA originates from a specific cause or event, for example trough trauma or disease (Merle et al. 2012; Altman et al. 1986). In addition to these two main developmental mechanisms of osteoarthritis, various personal and environmental risk factors for the development and progression of OA have been identified, including increasing age and female sex (Creamer and Hochberg 1997). Of note, several of the OA risk factors relate to joint (over)loading, including leg axis deformations, missing ligaments or menisci, specific sports or occupation, and obesity (Doherty 2001), which emphasizes the role of joint forces in OA pathogenesis (Felson 2013).

OA can be classified as uni-/ bi- or tricompartimental, depending on the compartments affected. In addition, the severity of OA is differentiated and classified. The most frequently used radiological classification is the Kellgren-Lawrence scale, considering osteophyte formation, joint space narrowing, subchondral sclerosis, cyst formation, and

joint deformation as classification factors (Kellgren and Lawrence 1957). For the patient, OA is often accompanied by pain and functional impairment, including restricted mobility. When conservative therapy has been exhausted, TKA is indicated in the case of severe radiological OA (Kellgren-Lawrence grade 3-4) in combination with pain and functional impairment, leading to a reduced quality of life and physiological strain (Kayaalp and Becker 2022).

2.2 Total knee arthroplasty

Total knee arthroplasty (TKA) describes the replacement of the native joint surfaces by artificial implant components and represents the gold standard for the treatment of advanced OA. Knee OA in combination with severe pain constitutes the main indication for TKA (Carr et al. 2012), with 90% of TKAs being attributed to primary knee OA (Wirtz 2011). The number of TKA surgeries has been increasing steadily until the Covid pandemic. Over one million primary TKA surgeries are performed every year worldwide (Kurtz et al. 2011). In 2019, ~194.000 primary and additional ~26.000 revision TKA surgeries were performed in Germany (Statistisches Bundesamt 2020). In the context of the Covid pandemic, the numbers decreased to ~173.000 primary and ~23.000 revision surgeries in the years 2020-2021. Despite this decrease, a current study estimates an average increase of 43% in the total number of primary TKA and of 88% in the total number of TKA revision surgeries in Germany by 2050 (Klug et al. 2021). Because of the increasing confidence in TKA outcomes and higher rates of OA in the younger population, their proportion of the patient population has steadily increased (Kurtz et al. 2009; Klug et al. 2021; Le Stum et al. 2023), placing greater functional demands on TKA. In combination with the increasing life expectancy, revision rates are expected to increase rapidly (Klug et al. 2021; Harrysson et al. 2004).

2.2.1 Clinical workflow

The clinical workflow of TKA can be divided into the following steps: examination, indication, preoperative planning, patient information, surgical intervention, postoperative control, and rehabilitation (Lützner and Kirschner 2017). **Figure 2-3** depicts patient data within the workflow of TKA, with relevance for implant fit evaluation.

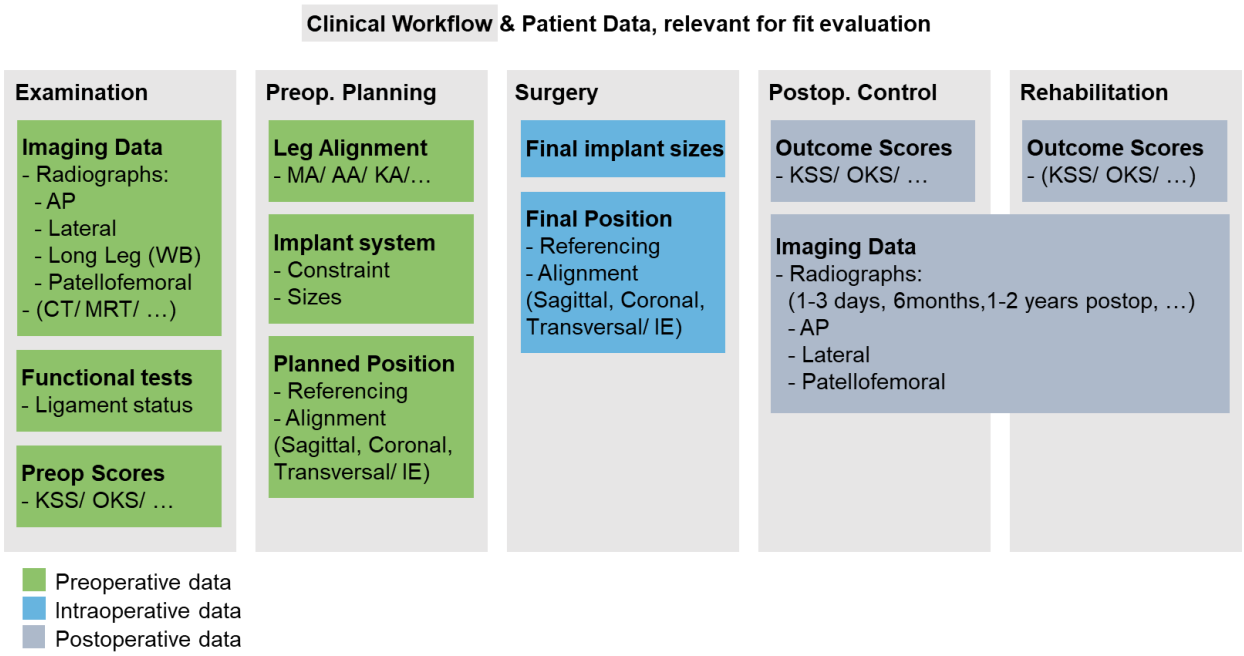

Figure 2-3: Clinical workflow of total knee arthroplasty with focus on patient data, relevant for patient-specific fit evaluation. WB = Weight-Bearing. KSS = Knee Society Score. OKS = Oxford Knee Score. MA = Mechanical Alignment. AA = Anatomical Alignment. KA = Kinematic Alignment. (Wirtz 2011; Lützner and Kirschner 2017; Meyer et al. 2022; Reichel 2005).

The **examination** includes the patient's anamnesis, functional tests, and imaging. X-Ray imaging is the gold standard for the radiological diagnosis of knee OA and for preoperative planning. Regularly the following X-ray images are taken for TKA planning: an anterior-posterior view, lateral view, patellofemoral view, and weight-bearing long leg radiograph (Lützner and Kirschner 2017; Meyer et al. 2022; Reichel 2005; Halder and Köhler 2011). When patient-specific instrumentation or implants are used, detailed 3D imaging of the knee is required, either by MRI or CT (Schotanus and Kort 2022). Hess and Hirschmann (Hess and Hirschmann 2022) have proposed a general switch to 3D imaging to overcome the limitations of 2D-based planning, such as the inability to comprehensively assess extra-articular deformities and the precise patient positioning, as well as the potential measurement inaccuracies that may result (Radtke et al. 2010). However, preoperative planning for TKA is still routinely performed in 2D (Hess and Hirschmann 2022). In addition to the data acquired through functional tests and imaging, preoperative scores may be obtained at this stage to allow for direct comparison with the postoperative scores (Lützner et al. 2022). Consequently, the results of the examination include the treatment **indication** and, if TKA is indicated, the patient data required for surgery and planning.

Standard **preoperative planning** for TKA involves planning of the leg axis correction and required bone resections (Halder and Köhler 2011), selecting the implant system and planning the components' alignment (Meyer et al. 2022; Halder and Köhler 2011), as well as estimating the implant sizes (Tanzer and Makhdom 2016; Meyer et al. 2022; Halder and Köhler 2011). Leg alignment strategies currently considered include patient-specific, hybrid, and systemic techniques (Rivière et al. 2018b), which are displayed in **Figure 2-4**. The degree of constraint of the implant system used is determined based on the results of the examination including the functional tests assessing knee stability (Lützner and Kirschner 2017), with the least constrained implant system always favored (Rodriguez-Merchan 2011). The factors influencing correct sizing include the bone anatomy, implant design, and surgical technique (Bonnin et al. 2022). The sizes of standard implant components are routinely selected based on the AP bone dimensions derived from the selected imaging method (Tanzer and Makhdom 2016). Templating is performed either analogue or digitally, involving a comparison of size measurements of the respective implant component with those of the bone to decide on a specific size. Generic boundaries for the implant component positioning may be considered in this step (Kim et al. 2014; Slevin et al. 2022). The subsequent step to preoperative planning is the **patient information**.

Of note, the mean time spend on preoperative planning in TKA and THA is reported to be below 5 min per case (Krueger et al. 2020), despite its relevance for minimizing intraoperative complications and optimizing postoperative outcomes (Hess and Hirschmann 2022). In addition, current reimbursement systems do not adequately account for preoperative work (Krueger et al. 2020; Wasterlain et al. 2019; Grosso et al. 2020), thereby even motivating a reduction of the limited time spend on preoperative planning.

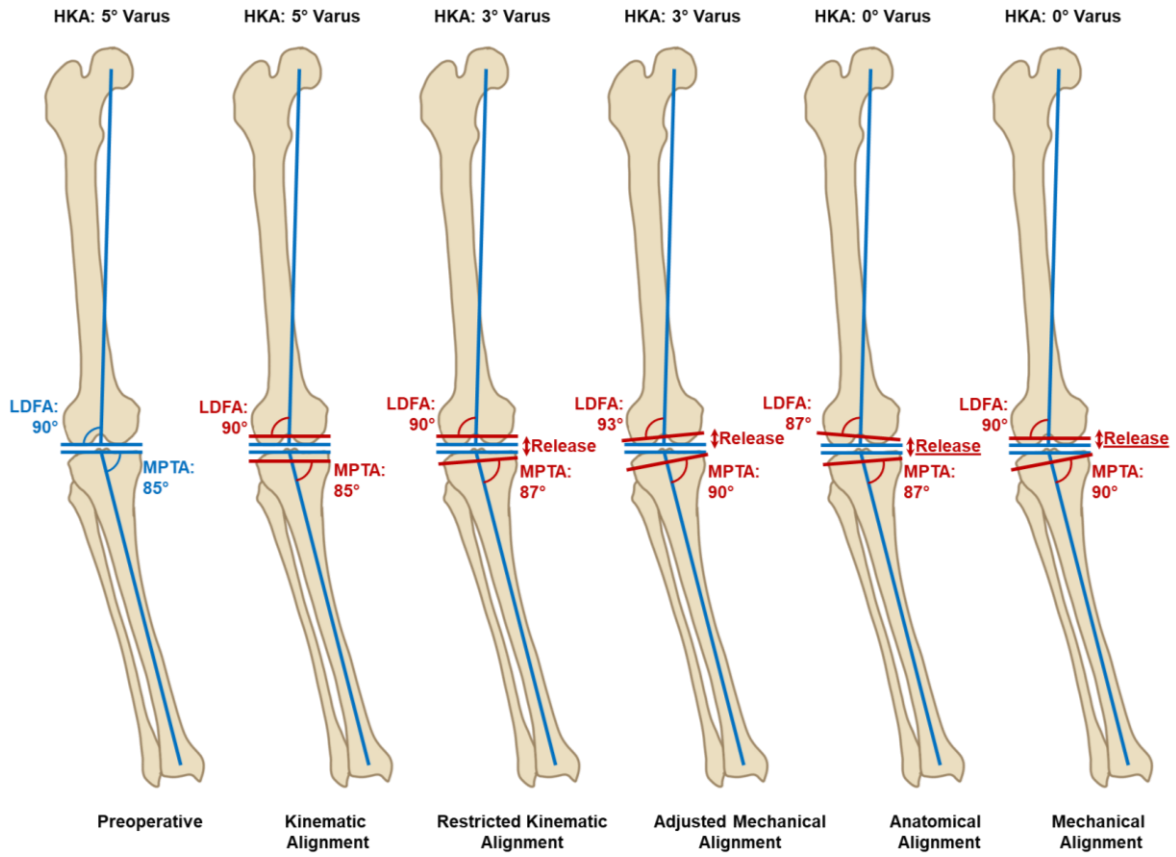

Figure 2-4: Leg alignment strategies in TKA with exemplary HKA, LDFA, and MPTA values: kinematic alignment, restricted kinematic alignment, adjusted mechanical alignment, anatomic alignment, mechanical alignment. Adopted from Rivière et al. (Rivière et al. 2018b) and Tuecking et al. (Tuecking et al. 2020).

The **surgical intervention** in standard primary TKA regularly begins with the classical approach of a midline skin incision and a subsequent medial parapatellar arthrotomy (Mattiassich and Hochreiter 2022). The next steps include the resection of the hypertrophic synovium, of the menisci, of the (anterior) cruciate ligament(s) (depending on the implant type), and of osteophytes (Röhrig 2011). After the required resections and resection of the fat pad, the patella is tilted or everted to the lateral side (Röhrig 2011; Weir et al. 2022). The following steps for bone resection and their sequence depend on the selected technique, being either femur-first or tibia-first (Merle et al. 2012; Röhrig 2011). Corresponding surgical instrumentation, provided with implant system, includes rods for intra- or extramedullary alignment and cutting blocks (Weir et al. 2022; Merle et al. 2012). After the bone resection, the final bone dimensions are determined and trial components are selected accordingly (Weir et al. 2022). The knee is then moved to evaluate laxity in extension and flexion under varus and valgus stress, by use

of spacer blocks, the trial components, and/or a tensioning device (Mihalko et al. 2009; Weir et al. 2022). Techniques for balancing of the knee include soft-tissue releases and further bone resections (Mihalko et al. 2009; Röhrig 2011), with the goal of creating a symmetrical and balanced flexion and extension gap (Röhrig 2011; Merle et al. 2012). Subsequently, the patella is treated and optionally prepared for resurfacing (Röhrig 2011). Afterwards a jet lavage is performed and the selected implant components are implanted using cement (Weir et al. 2022; Wirtz 2011; Merle et al. 2012). Final steps include functional tests and (multilayer) wound closure (Weir et al. 2022).

The **postoperative procedures** include documentation, mobilization, laboratory, imaging, and post-treatment medication (Seuser 2011). Aspects of documentation include results of functional assessment and of postoperative physiotherapy as well as clinical scores (Seuser 2011). The hospital stay is regularly followed by outpatient or inpatient **rehabilitation**. During rehabilitation and follow-up appointments further functional tests, laboratory, and imaging are performed, and optionally clinical scores are obtained (Seuser 2011).

2.2.2 Implant design

Implants for artificial knee replacement can generally be distinguished regarding the number of compartments replaced, their constraint level, and their type of fixation (ISO ISO 7207-1). **Figure 2-5** exemplarily displays a bi-compartmental, unconstrained knee replacement system. Respective implant components include a femoral component, a tibial tray, and tibial insert(s). Regularly the femoral component and tibial tray are made from cobalt-chrome while the tibial insert(s) and the optional patellar button are made from ultra-high-molecular-weight polyethylene (Delfosse et al. 2022). Overall, the cruciate retaining (CR) is the most used implant type according to national arthroplasty registers (Robertsson et al. 2001; Grimberg et al. 2023). Cementation is the most-used fixation technique in Germany (Grimberg et al. 2023), for which alternatives are press-fit systems and hybrid fixation.

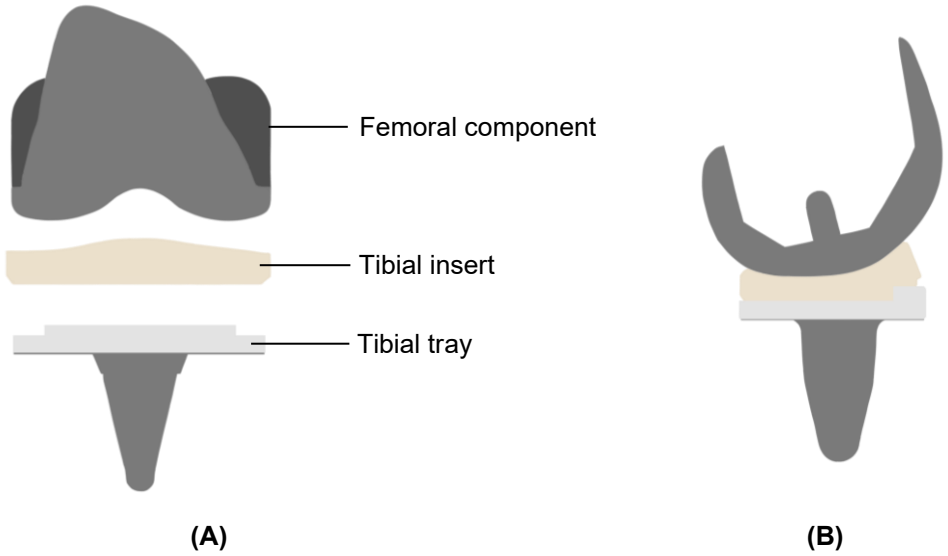

Figure 2-5: Components of a tri-compartmental, cruciate-retaining total knee replacement system in **(A)** frontal view and **(B)** lateral view.

In addition to the classification of implant type, implant systems can be distinguished by their **geometric shape**. However, only few established parameters are present to describe this shape. The standard ISO 7207-1 (ISO ISO 7207-1) gives a classification, definitions, and designation of dimensions for total and partial knee joint prostheses. For CR systems, the standard lists nine parameters describing the geometry of the femoral component and seven describing the geometry of the tibial tray and inserts. The description of the patellar component is limited to its width and length. In contrast, many more parameters for the differentiation of knee implant shape are discussed in the literature (Saffarini et al. 2014; Kessler et al. 2007; Clary et al. 2013). In terms of shape, the first distinction is between standard or “off-the-shelf” (OTS) implants and customized or patient-specific implants. Both concepts are discussed in more detail in the following.

Standard implant design

With standard total knee replacement design, one specific shape is offered in different sizes. Currently, manufacturers offer in the range of 7-21 femoral and 7-10 tibial implant sizes (e.g., e.motion, Aesculap AG, Tuttlingen, Germany | Attune, Depuy Synthes, Raynham, MA, US | Persona, Zimmer Biomet Holdings, Inc, Warsaw, IN, US). The size distribution of available implant systems suggests regression fitting, while the manufacturers in general did not specify the method used for sizing. The femoral and tibial size distribution of an exemplary set of current implant systems is given in **Figure**

2-6. In the diagrams, the implant sizes are compared against size information from a database of cadaver knees, including measurements from 416 femora and 416 tibiae. The corresponding CT data was acquired for surgical training purposes and provided by Conformis (Conformis Inc., Billerica, MA, USA). No prior selection was performed and also no donor identifying information was accessed for the conduct of the analysis. The bone measurements were performed according to the workflow described by Asseln et al. (Asseln et al. 2018).

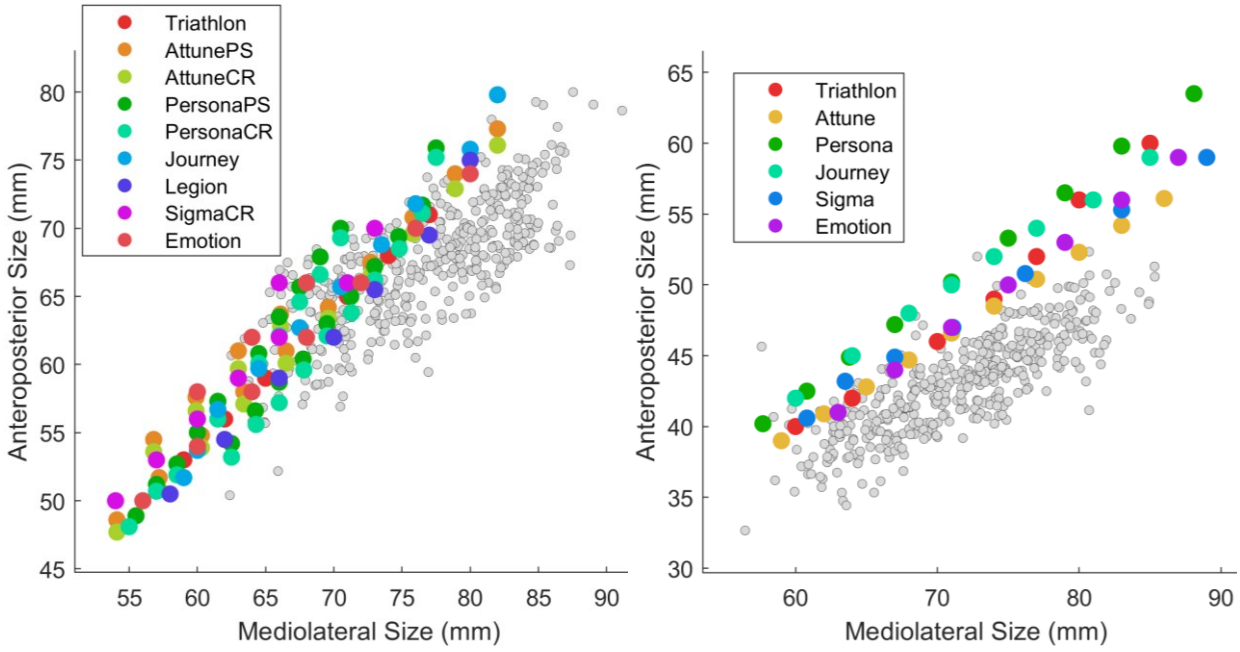

Figure 2-6: (A) Femoral and **(B)** tibial size distribution of an exemplary set of current implant systems together with cadaver knee size data, including measurements from 416 femora and 416 tibiae. Manufacturer information: Triathlon, Stryker Corporation, Kalamazoo, MI, US | Attune, Depuy Synthes, Raynham, MA, US | Persona, Zimmer Biomet Holdings, Inc, Warsaw, IN, US | Journey, Smith & Nephew plc, Watford, UK | Legion, Smith & Nephew plc, Watford, UK | Sigma, Depuy Synthes, Raynham, MA, US | e.motion, Aesculap AG, Tuttlingen, Germany)

Different manufacturers of TKA implants follow different **design philosophies** and features, of which examples are displayed in **Figure 2-7**. A design aspect extensively analyzed and discussed is the sagittal shape of the femoral condyles (J-curve), which has motivated different types of femoral implant design. Those include single-, dual-, multi-, and gradually reducing radius designs, of which examples are depicted in **Figure 2-7 A**. High-flexion designs address the proximo-posterior end of the J-Curve, with the theoretical advantage of higher range of knee flexion (Argenson et al. 2004). Tibiofemoral conformity (**Figure 2-7 B**) influences tibiofemoral kinematics, contact

pressure, etc., and has been reported to affect both polyethylene wear rates (Schwarzkopf et al. 2015) (*in vitro*) and postoperative range of motion (Walker and Garg 1991) (*in silico*). Willing et al. (Willing and Kim 2011) addressed this design aspect using rigorous numerical optimization, with the goal of defining a generically optimized tibiofemoral implant conformity for increased range of motion while preserving native AP and internal-external knee constraints. The study however, included several limitations. First, they did not consider patient-specific factors influencing range of motion, such as individual knee kinematics (e.g., femoral rollback) and individual knee anatomy with relevance for impingement. Second, they neglected many other targets such as the required compatibility e.g., regarding PCL strain, patellofemoral ligament strain, the TT-TG distance, etc. Therefore, a patient-specific optimized tibiofemoral conformity still needs to be researched. A comprehensive change in knee implant design addressing several shape aspects represents the gender-specific knee implant design, which was first introduced by Zimmer Inc. (Zimmer Inc., Warsaw, Indiana, US). The design change was motivated by the issue of ML oversizing frequently reported in female patients (Mahoney and Kinsey 2010). The design included a reduced aspect ratio, a thinner anterior flange, and a larger trochlear orientation angle (**Figure 2-7 C**). Those deviations have been reported for the female patient population for example by Conley et al. (Conley et al. 2007). Other authors have highlighted the extent of inter-individual deviations rather than gender-specific differences in knee morphology (Asseln et al. 2018; Hohlmann et al. 2022), which motivate the use of customized implants for TKA.

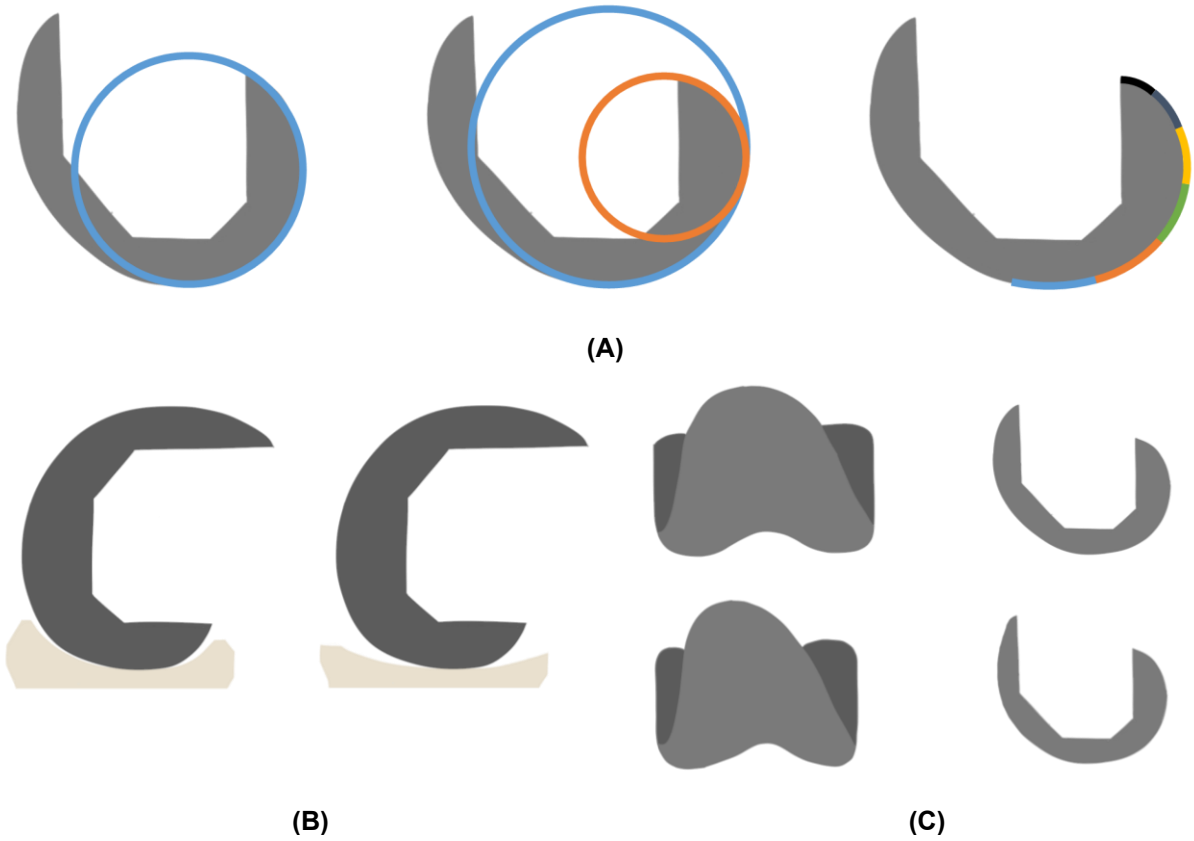

Figure 2-7: Design variations of standard implant systems: **(A)** Different J-Curve designs: single-, dual-, multi-radius design. **(B)** High-conforming vs. low-conforming CR implant design. **(C)** Standard (upper images) and Gender-specific/ "Female" design (lower images): „Female knee" design with a smaller aspect ratio, thinner anterior shield, and a higher trochlea orientation angle.

Patient-specific implant design

Instead of using standardized implants, the implant design can also be customized to the individual patient's knee morphology. The decision for such an implant is currently made by the surgeon, without standardized systematic analyses. The basis for the respective implant design is 3D surface information of the patient's native bone. For this purpose, regularly CT image data is acquired (Koch et al. 2013). Promoted advantages of customized implants include improved rotational alignment, optimal bony coverage without implant overhang (Schroeder and Martin 2019), and an ideal J-Curve matching. Customized implants are also reported to have a lower bone resection volume, which is attributed to the adaptation of the implant design and related resection cuts to the specific patient (Kurtz et al. 2016). Furthermore, a customized implant shape is expected to restore physiological ligament tension throughout knee flexion and thereby to reduce the need for intraoperative adaptations such as ligament releases (Saffarini et al. 2023).

Current disadvantages include the required 3D bone geometry data based on CT imaging with associated radiation exposure and waiting time, both for the CT and for implant manufacturing, as well as the additional costs involved.

2.2.3 Causes of revision

Revision surgeries make up ~12% of the yearly TKA surgeries in Germany (Statistisches Bundesamt 2019, 2020, 2021, 2022). During revision, the affected implant components are replaced, either directly or in case of infection in a two-step procedure including antibiotic spacers. Causes for implant failure have been analyzed extensively in the literature. The most frequent causes for revision of TKA for treatment of OA include **aseptic loosening**, **infection**, and **instability** (Sharkey et al. 2014; Schroer et al. 2013; Delanois et al. 2017). Pain is another common complication after TKA which is detrimental to patient satisfaction and in severe cases can require revision (Postler et al. 2018). **Anterior knee pain** specifically describes the phenomenon of pain in the patellofemoral region, which requires a complex analysis, as the origin often is multifactorial (Petersen et al. 2014). A summary of studies reporting on the causes of TKA revisions is given in **Figure 2-8**. The chart displays the proportion of each cause of revision in the total number of revision surgeries considered in the respective study.

The design of TKA implants has been shown to influence various factors relevant to TKA revision, including postoperative knee kinematics (Kessler et al. 2007; Dennis et al. 2003), knee stability (Clary et al. 2013; Jo et al. 2014), wear performance (Essner et al. 2011) which is associated with aseptic loosening and infection (Hodges et al. 2021). Most of the listed causes of revision represent failures related to implant and/or bone mechanics and resulting postoperative knee function, with the only clear exception being arthrofibrosis and malalignment. Hence, when excluding unknown causes of revision (“other”) in mean >99% of revisions may be directly or indirectly attributed to the implant design (percentage based on 402.081 revisions, **Figure 2-8**). Exemplary relationships between individual causes of revision and the implant design are discussed in more detail in the following section.

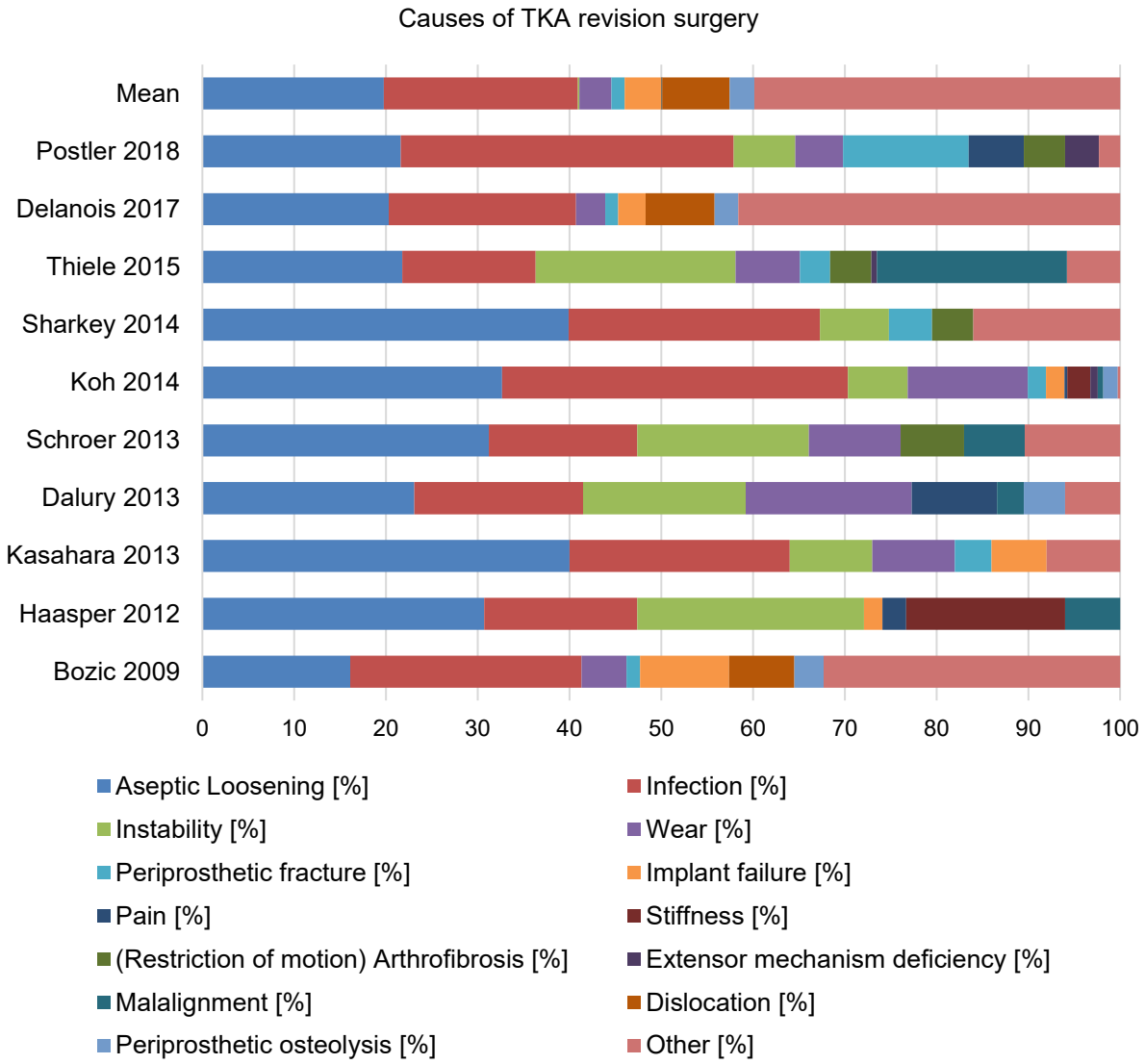

Figure 2-8: Overview of studies reporting on the causes of TKA revision surgery. The graph shows the proportion of each revision cause in the total number of revisions considered in each study. Of note: The average percentages reported are similar to the percentages reported by Delanois et al. (Delanois et al. 2017), as the study analyzed by far the highest number of revisions (n=337.597). (Postler et al. 2018; Delanois et al. 2017; Thiele et al. 2015; Sharkey et al. 2014; Koh et al. 2014; Schroer et al. 2013; Dalury et al. 2013; Kasahara et al. 2013; Haasper et al. 2012; Bozic et al. 2010).

Relation of revision to the implant design

The number of OTS implant sizes as well as their theoretical and even more their actual compatibility (Young et al. 2015) are limited. Therefore, the size selection in TKA is often a compromise. Current studies on implant size mismatch in TKA for different populations are listed in **Figure 2-9** (femoral overhang) and in **Figure 2-10** (femoral underhang). From the relevant errors it can be concluded that the implant systems considered in these studies did not adequately match the respective patient populations.

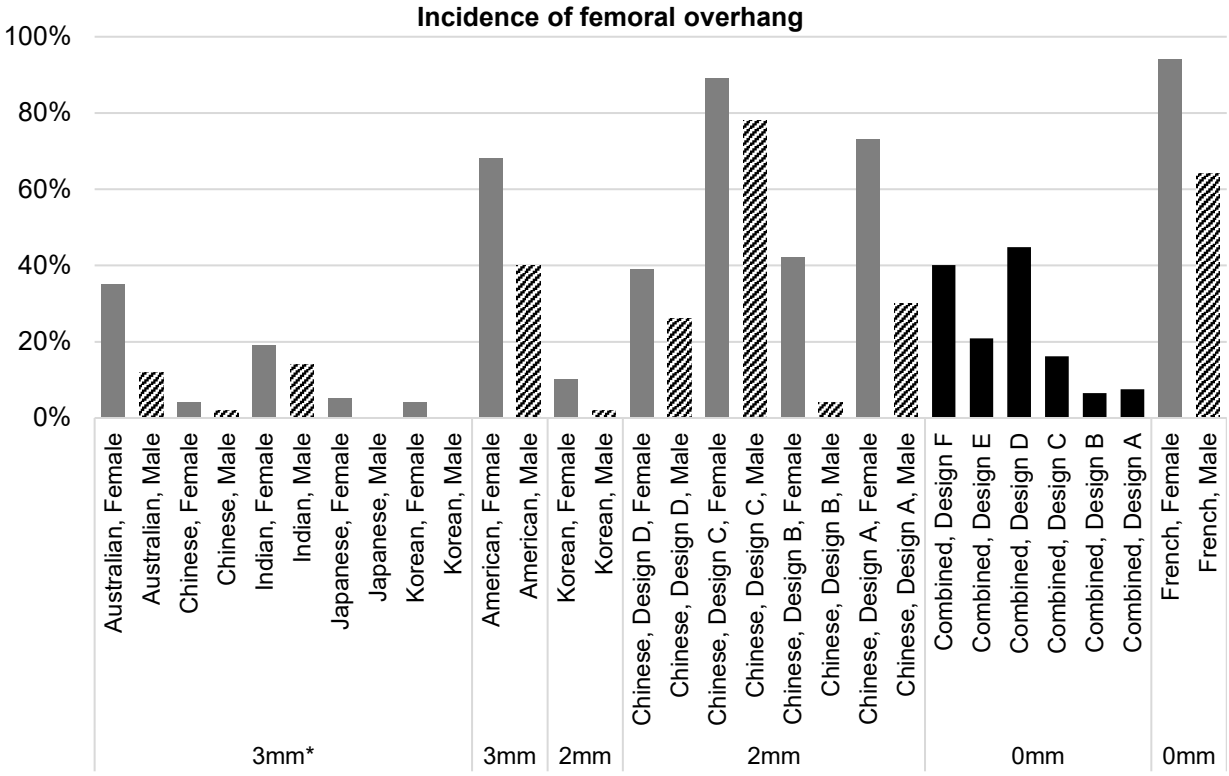

Figure 2-9: Incidence of femoral overhang with different overhang limits (3mm*: (Sharma et al. 2017) 3mm: (Mahoney and Kinsey 2010) 2mm: (Chung et al. 2015; Yue et al. 2014) 0mm: (Dai et al. 2014b; Bonnin et al. 2013)

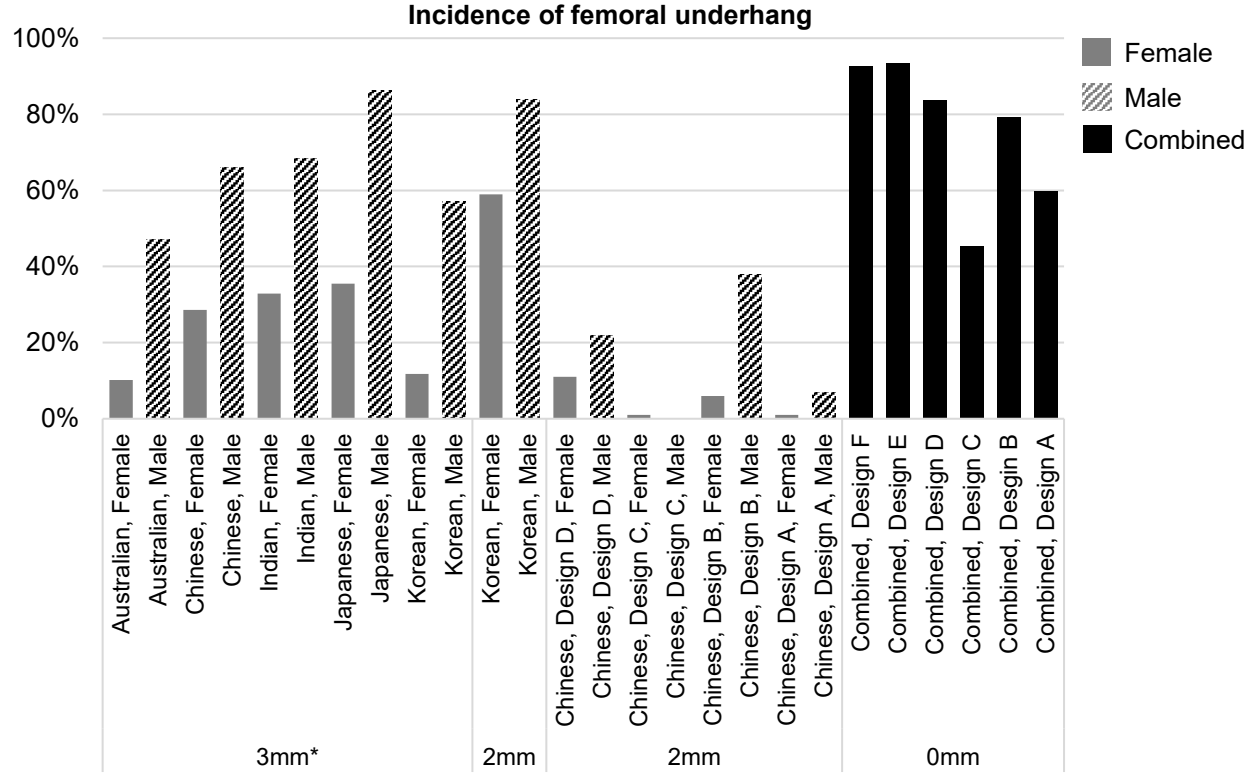

Figure 2-10: Incidence of femoral underhang with different underhang limits (3mm*: (Sharma et al. 2017) 2mm: (Chung et al. 2015; Yue et al. 2014) 0mm: (Dai et al. 2014b)).

The consequences of respective **mismatch** are discussed below exemplarily for the femoral component, depending on the referencing technique used. In the case of anterior referencing, an inadequate femoral AP size fit results in either an insufficient or an excess resection of the posterior condyles. Such a change in the posterior condylar morphology impacts flexion laxity (Mueller et al. 2014) and thereby may lead to instability and/or impact forces in flexion. Furthermore, the posterior condylar offset is changed, for which a negative impact on flexion range of motion has been reported by Bellemans et al. (Bellemans et al. 2002). In the case of posterior referencing, an inadequate AP size fit leads to an insufficient or an excess resection of the anterior femoral flange, which can affect patellar tracking and/or involve femoral notching. Kawahara et al. (Kawahara et al. 2012) have reported higher patellofemoral forces for anterior oversized femoral components, which may be linked to overstuffing and resulting **anterior knee pain** (Petersen et al. 2014). ML over-/ underhang of the implant relative to the bone is the result of an inadequate ML fit. The impact of respective size mismatch has been studied by several groups. Mahoney et al. (Mahoney and Kinsey 2010) found a twofold increased risk for clinically relevant knee pain at two years postoperative, with overhang ≥ 3 mm. Chung et al. (Chung et al. 2015) reported decreased flexion range of motion with condylar ML overhang > 4 mm. In the study by Bonnin et al. (Bonnin et al. 2013) any level of overhang (> 0 mm) was associated with statistically significant negative impact on pain and function scores as well as on flexion range of motion.

Even in the case of an ideal AP and ML size fit, **inter-individual variations** in knee morphology can lead to high local deviations between implant and bone cut contours. The extent of such deviations is scarcely analyzed but may lead (e.g., in case of implant overhang) to soft tissue irritations (Bonnin et al. 2017). Independently of respective inter-individual variations, **distinct shape differences** between the physiological, native knee shape and the implant geometry have been reported (Akbari Shandiz et al. 2018), especially for the femoral trochlea (Du et al. 2017; Dejour et al. 2014; Kuo et al. 2020; Rosa et al. 2023). Those include differences in the sulcus angle, lateral trochlear height, trochlear coronal alignment, and anterior flange thickness (Kuo et al. 2020; Rosa et al. 2023; Dejour et al. 2014). One could argue whether respective changes may better accommodate a matching patellar implant design (which in general differs significantly from native patella shapes). However, patellar resurfacing is performed in Germany only

in ~10% of all TKAs reported in a national registry (Grimberg et al. 2022, 2023; Grimberg et al. 2021). Consequently, the shape differences are expected to lead to undesirable changes in (patellofemoral) kinematics and stability.

The **clinical impact** of changes in morphology with TKA is scarcely analyzed, as specific design parameters cannot easily be evaluated independently of others. Kessler et al. (Kessler et al. 2007) and Pfitzner et al. (Pfitzner et al. 2018) reported differences in kinematics with different J-Curve designs *in vivo*. Clary et al. (Clary et al. 2013) also found relevant variation in kinematics with different J-Curve designs in a combined *in vitro* and *in silico* analysis. Comprehensive sensitivity analyses assessing several morphological parameters of the knee implant shape reported significant impact on kinematics and/or contact mechanics *in vitro* (Leichtle et al. 2017; Dai et al. 2018; Asseln et al. 2021) and *in silico* (Ardestani et al. 2015; Fitzpatrick et al. 2012b; Fitzpatrick et al. 2012a; Asseln et al. 2021). The link to clinical outcome measures needs to be established.

2.2.4 Outcome scores

Outcome scores are means to evaluate the success of a treatment, which include various different measures as sub-scores. In general, a distinction can be made between patient-reported outcome measures (PROMs) and clinician-reported outcome measures (CROMs). CROMs mostly include objective measures such as the postoperative leg alignment, flexion range of motion, and knee stability. In contrast, PROMs mostly include subjective measures, such as the patient-reported levels of pain during different ADLs.

A relevant application of outcome scores is the assessment of the suitability of different treatment options available. For example, when deciding on the treatment of knee OA with varus deformity, the outcome scores of the respective patient population for high tibial osteotomy and those for unicompartmental knee arthroplasty may be compared (Spahn et al. 2013; Serbin et al. 2023). Another application example of outcome scores is the decision for an implant system, which could be based on the comparison of outcomes with the available implant designs (Pfitzner et al. 2018).

Outcome scores commonly used in TKA surgery include general health or quality of life scores, such as the EQ-5D, SF-12/-36 and Forgotten Joint Score, as well as scores

specific to the joint and/or disease, such as the KSS, KOOS, OKS, and WOMAC (Lan et al. 2020; Giesinger et al. 2014). The dissatisfaction rates in TKA across different scores have been comparably high, with up to 19% of the TKA patients report to be unsatisfied after surgery (Bourne et al. 2010; Noble et al. 2006; Scott et al. 2010). To address this issue, several authors have proposed the use of outcome measures, and especially of PROMs, for optimizing postoperative satisfaction in TKA (Tew et al. 2020; Ayers 2017).

However, the suitability of existing TKA PROMs as sole optimization criteria has also been questioned e.g., due to the missing consideration of other success criteria such as implant survivorship as well as the PROMs limited sensitivity (Leonard et al. 2023). Possible explanations for the limited sensitivity include the effects of modifiers on PROMs (Wilson and Cleary 1995), for which numerous have been reported in the context of TKA and THA (Brembo et al. 2017; Singh and Lewallen 2013; Singh et al. 2023; Theiss et al. 2011). In addition, floor and ceiling effects have been reported for PROM scores commonly used in TKA (Busija et al. 2008; Giesinger et al. 2014), especially in the growing group of younger TKA patients (<60 years) (Klit et al. 2014). Thus, respective limitations of available scores prompt a particular emphasis both on increased individualization in outcome measures and on more sensitive criteria (Leonard et al. 2023), for which examples have been presented in the literature (Maffiuletti et al. 2010; Leonard et al. 2023). Sensitivity and accuracy of TKA outcome measures are also of relevance with regard to cost-effectiveness analyses, for which the respective scores are used as input (Losina et al. 2009).

2.2.5 Cost effectiveness

The optimal allocation of limited health care resources is a difficult task. On a patient-specific level, this allocation involves deciding between different treatment options, taking into account the associated costs and potential benefits (Gray et al. 2011). Here, cost-effectiveness analyses (CEA) are typically performed. An exemplary statistic of CEA is the incremental cost-effectiveness ratio (ICER), which weighs incremental costs against the associated effects. In the example of TKA, the (incremental) cost of the procedure compared to that of living with end-stage knee OA

is weighed against the (incremental) effect measured, for example, by the gain in quality-adjusted life years (QALY) (Losina et al. 2009).

Müller and Schürmann (Müller and Schürmann 2001) reported mean costs of 18 649,40 DM (= 9.535,29 Euro) for a TKA in Germany. The implant costs account for ~25% of the cost of TKA (Pogonke 2012; Müller and Schürmann 2001). In general, the implant cost strongly varies depending on the implant system and design, and has been reported to range between 1.000-5.000 Euro in 2012 (Merle et al. 2012)

When the direct cost of TKA with a customized are compared with those of TKA with an OTS implant, clearly the procedure with **customized implant** is more expensive, as CT imaging is required and the implants are more expensive. However, there are also cost-relevant disadvantages of OTS implants compared with customized implants. One example is the need for multiple implant sizes for possible adjustments during surgery, which must be available in a sterilized state. This effort and the associated costs would be avoided with a customized implant. Culler et al. (Culler et al. 2017) and Namin et al. (Namin et al. 2019) have reported the use of a customized implants in TKA to be of similar or even lower cost compared to standard implants. In their studies, the lower risk of complications and revisions and the reduced need for rehabilitation led to cost reductions for the TKA with customized implant. In addition, a recent study on patients with bilateral TKA (1. Knee: standard implant; 2. Knee: customized implant) found significant differences in KOOS and FJS, with patients favoring the customized implant (Schroeder et al. 2022). In contrast, a recent meta-analysis reported higher revision rates in the customized compared to the OTS TKA group and no difference in early outcome measures (Müller et al. 2023). The differences between studies in the literature regarding the performance of customized versus standard implants in the literature may be related to the different need for customization in the patient population.

In conclusion, also in terms of cost-effectiveness, the identification of patients who will benefit most from a customized implant, would be favorable. As a result, fewer unnecessary customized implants would be used for which the additional cost is not outweighed by an additional gain in, for example, QUALYs. In addition, fewer patients would receive an inadequately fitting OTS, which can lead to dissatisfaction or the need for revision surgery.

2.3 Conclusion

In the previous chapters, the relevance of TKA for restoring function and relieving pain in patients with advanced OA has been presented. The increasing number of TKA procedures, especially in younger, more active patients motivates, further optimization of the treatment. Various known causes for revision and poor patient dissatisfaction have been discussed, of which the majority is expected to be directly or indirectly associated with the implant design.

In a review of studies on available OTS designs, a **discrepancy between provided implant sizing and population size distribution** has been identified. Previous methods for implant sizing have not been described in the literature, however the results often resemble a regression fit. As ML and AP size are normally distributed, it becomes apparent that a regression fit is an inadequate sizing method. In contrast, numerical optimization methods appear to be more applicable, and consequently their potential is evaluated (**RQ1**).

Furthermore, advantages and disadvantages of customized implants, among others regarding cost and cost-effectiveness, have been discussed. Because of the disadvantages of the required CT, longer waiting periods, and higher implant-related cost, an adequate selection of cases requiring customized implants should be implemented. To date, there is **no method to support the decision-making which OTS implant design would fit best, and whether this fit is sufficient or if a patient-specific implant should be advised**. In light of the limited time available for preoperative planning, and its partially inadequate compensation, this deficiency is even more critical.

Consequently, the need for further fit evaluation beyond size is assessed, by evaluating the variability in knee morphology (**RQ2**) and by analyzing the correlation of morpho-functional with size parameters (**RQ3**). Subsequently, potential objective criteria are assessed (**RQ4**). Regarding morphologic fit, deformities have to be considered, whose corrections may significantly alter morphological parameters of the knee. Hence a method for parameter-based deformity correction is developed (**RQ5**). Finally, the

feasibility of the method is examined (**RQ6**). The research questions identified and addressed in the following chapters are listed below.

RQ1. Can patient population coverage be significantly improved by numerical optimization of implant sizing?

RQ2. Does native knee morphology involve shape variation independent of overall size?

RQ3. Is there a correlation between the individual morphological parameters and the overall knee size? What residuals remain in the case of an ideal size fit?

RQ4. Are objective criteria available for patient-specific morphological and functional implant fit evaluation?

RQ5. In the case of deformities, can those be clearly identified and adequately corrected by a parameter-based, data-driven approach?

RQ6. Can the proposed implant fit evaluation be integrated in the clinical workflow?

3. Preliminary studies

3.1 Optimization of standard implant sizing

Work in this chapter has been presented in parts in:

S. Grothues, B. Hohlmann, S.M. Zingde & K. Radermacher: Potential for femoral size optimization for off-the-shelf implants: A CT derived implant database analysis. Journal of Orthopaedic Research, 2023, 41(6), pp. 1198-1205 [DOI: 10.1002/jor.25464]

3.1.1 Introduction

Relevant mismatch regarding AP and ML fit between the sizing of available implant systems and different patient populations has been reported in the literature, as described in **Chapter 2.2.2**. Hence, potential for optimization of implant sizing was demonstrated. As a basis for an optimization study, knee size information of TKA patients is required. With the advent of patient specific total knee implants and instruments, as well as robotic TKAs, large databases of patient CT scan information are now available. In prior studies (Meier et al. 2019; Meric et al. 2015) such databases have been used to document the variation in the distal femoral geometry. However, there is no paper to the author's knowledge that has used such a database to determine an optimized implant sizing matrix that can be used in future implant design. Hence, the aim of this chapter was to find implant size distributions, which maximize the percentage of the patient population adequately provided for, to evaluate the sensitivity regarding error bounds and the number of implant sizes, and to compare the results against standard regression sizing, for a large case database of 85.143 TKA patients.

The research question addressed in this chapter is the following:

> *RQ1: Can patient population coverage be significantly improved by numerical optimization of implant sizing?*

3.1.2 Materials and methods

Basis of the analysis was a comprehensive database of 85,143 implant design datasets provided by Conformis Inc. (Conformis Inc., Billerica, MA US). The database includes CT derived anatomic and implant design parameters used in the design of customized total knee implants (iTotal CR and iTotal PS). All implants are either cruciate-retaining (CR) or posterior-stabilized (PS) types of the iTotal knee replacement (Conformis Inc., Billerica, MA US). Different size boundaries apply to the PS and CR implants according to the clearance of the Food and Drug Administration (FDA). The AP lower (upper) bound for the CR implants is 55 mm (80 mm) and for PS implants it is 56 mm (81 mm). The ML lower (upper) bound for the CR implants is 57.5 mm (90 mm) and for PS implants it is 55 mm (90 mm). All patients undergoing TKA were provided with a customized implant reconstructing the native femoral J-curves and interface bone contour (Slamin and Parsley 2012; Schroeder and Martin 2019). No selection of implant data took place before the analysis. Left (48.4%) and right (51.6%) consecutive femoral components of female as well as male patients were included. The gender distribution is unknown and was neglected based on the findings of Asseln et al. (Asseln et al. 2018). The cohort includes design data for patients residing in North America and Europe. However, the analysis did not stratify patients based on ethnicity-related factors. Overall AP and ML sizes were measured using the implant's design data. Ethics approval for this study was obtained from the Ethics Committee at the Faculty of Medicine of the RWTH Aachen University (EK 240/22).

Since the data set contains information on implant design data, the first step was to quantify and validate the difference between the native bone and corresponding customized implant designed for that bone. This is important, since implant design, in some cases, requires modifications from the native geometry to accommodate for e.g., congenital or acquired deformities or OA-related bone wear. Moreover, engineering design limits and technical constraints regarding manufacturing could result in minor differences between the bone model and the resultant implant. To quantify the difference between native bone and implant measurements, a subset of 1049 patients was used, for which the three-dimensional bone surface models were available. The AP and ML size were determined automatically using the approach described by Asseln et al. (Asseln et al. 2018). AP and ML measures were identified in a bone-specific coordinate

system. The AP length was measured as the distance between the most anterior point on the trochlea and the most posterior point on the condyles, along the AP axis. The condylar ML width was calculated between the most lateral and medial bone surface points along the ML axis at 10 mm above the most distal condylar point. A multivariate two-sided t-test with unequal variances was applied, to compare both measurements (Welch 1947). **Figure 3-1-A** shows both distributions. In addition, to ensure that the ML and AP measures were representative for all TKA patients, and not only for patients with customized implants, implant measures were also compared with measures of 386 cadaveric femora.

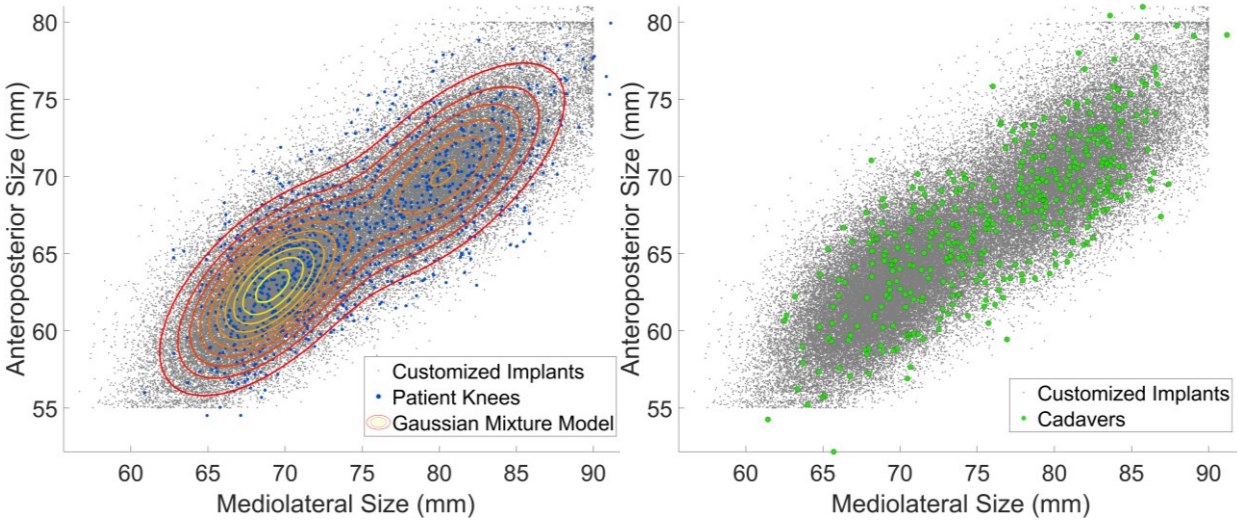

Figure 3-1: Analysis of the size distribution in the databases analyzed: (**A)** The distribution of AP and ML sizes for implants (gray dot) and bone (blue circle). A gaussian mixture model with two components is fitted to the implant data. **(B)** The distribution of AP and ML sizes for implants (gray dot) and cadavers (green circle).

Upper bounds for AP and ML mismatch were defined according to the following design rules: As stated earlier, the AP size relates to the biomechanical function. No differentiation between over- and undersizing was made, and the maximal bone to implant deviation was varied from 1 to 5 mm. This covers the wide range of implant size gaps seen in current commercial manufacturer's models. For example, size gaps from 2 mm (Persona, Zimmer Biomet Holdings Inc, Warsaw, IN, US) to 5 mm (Legion, Smith & Nephew plc, Watford, UK) regarding the AP size can be found. For ML mismatch, only underhang was allowed, with bounds from 1 to 5 mm. As this limit was applied on either side, the overall ML size may deviate twice as much.

Given the design bounds, a set of standard implant sizes was defined that optimizes the percentage of the patient population adequately provided for (“Coverage”). The optimization was performed in MATLAB (MathWorks, Inc., Natick, MA, US), using the particle swarm algorithm (Kennedy and Eberhart 1995). As the algorithm is non-deterministic, each run was repeated 50 times, and the best set of sizes was kept.

The particle swarm algorithm is an iterative method inspired by the behavior of swarms in nature that optimizes an objective function. In the application at hand, the objective is the population coverage. A brief pseudo-code implementation is given in **Figure 3-2**: A set of possible solutions, where each solution constitutes one particle is initialized randomly. In every iteration, the objective function is evaluated on all particles. Updates on the particles are determined by their velocity, which in turn is increased in the direction of the best-known solutions for the individual particle (i) known so far and (ii) in a random neighborhood, respectively. Thus, the velocity drives the particles to the current optimum. The optimization ends when the change in the objective functions becomes too small, indicating convergence on a (potentially local) optimum. **Figure 3-3** shows an example of a single iteration: in **Figure 3-3 A** two solutions are shown, each of which constitute a single particle. As the particle shown in green exhibits the highest objective function, the velocity of the orange particle is redirected to this solution. In the next iteration (**Figure 3-3 B**), the orange particle achieves a higher objective function. In contrast to linear regression, this optimization algorithm does not impose any bounds on the individual implant sizes.

Particle Swarm Algorithm

Initialize particles $P \in \mathbb{P}$ randomly

while ($\Delta f(P) < \varepsilon$):
   evaluate $f(P)$
   for every $p \in P$:
      Add current p to T_p
      Select random subset $S \in P$
      Update velocity v using $arg\,min\, f(S)$ and $arg\,min\, f(T_p)$
      Update particle $p = p + v$

Figure 3-2: Brief Pseudo-code implementation of the particle swarm algorithm.

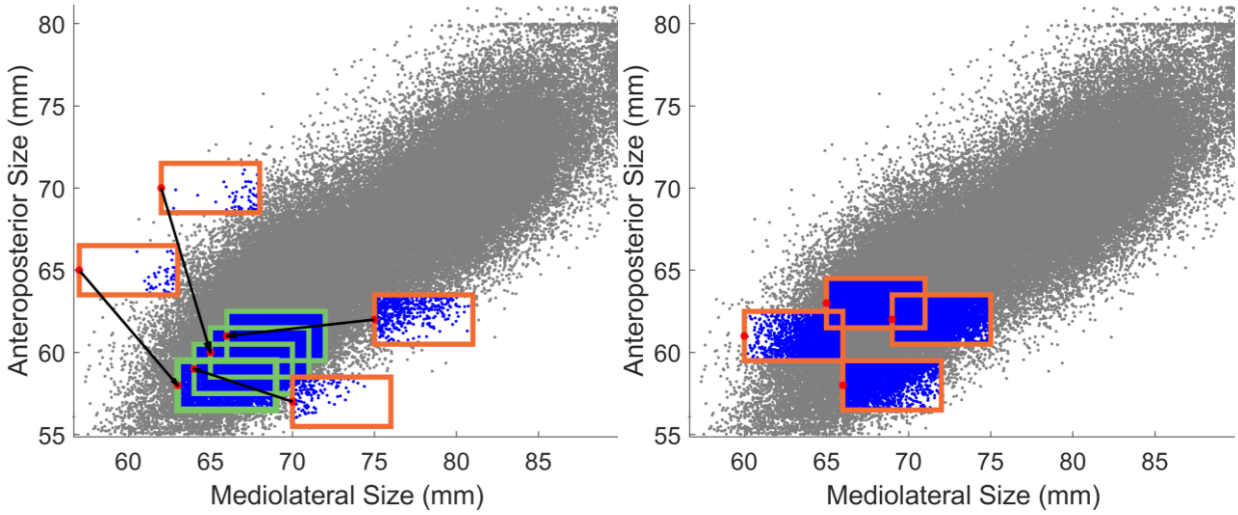

Figure 3-3: Visualization of the particle swarm optimization: **(A)** Visualization of two particles, colored in green and orange. Initially, the green particle achieves the highest coverage. **(B)** In the next iteration, only the orange particle is shown. It is driven to the best-known solution, achieving an even higher coverage

Two parameters were varied to investigate their respective effect on the coverage: The number of sizes, and the bounds on AP and ML mismatch. The bounds were linked with a factor of two, so that the ML mismatch may be twice as much as the AP mismatch (s. above). For every parameter set (number of implant sizes and mismatch bounds), the respective set of implant sizes was derived as described above and the population coverage was calculated. Finally, the coverage of the optimized implant sizes was compared against the coverage of existing implant systems, which are presented in **Table 3-1** and in **Figure 3-4**.

Table 3-1: Sizing information about existing implant systems considered for patient coverage analysis.

Implant Name	**Number of Sizes**	**AP Range** (mm)	**ML Range** (mm)	**Manufacturer (HQ)**
Triathlon	8	53.0 - 75.0	59.0 - 80.0	Stryker Corporation (Kalamazoo, MI, US)
Journey II CR	10	51.7 - 79.8	59.0 - 82.0	Smith & Nephew plc (Watford, UK)
Attune CR	14	47.7 - 76.1	54.1 - 82.0	Depuy Synthes (Raynham, MA, US)
Persona CR	21	48.1 - 75.2	55.5 - 77.5	Zimmer Biomet Holdings, Inc (Warsaw, IN, US)

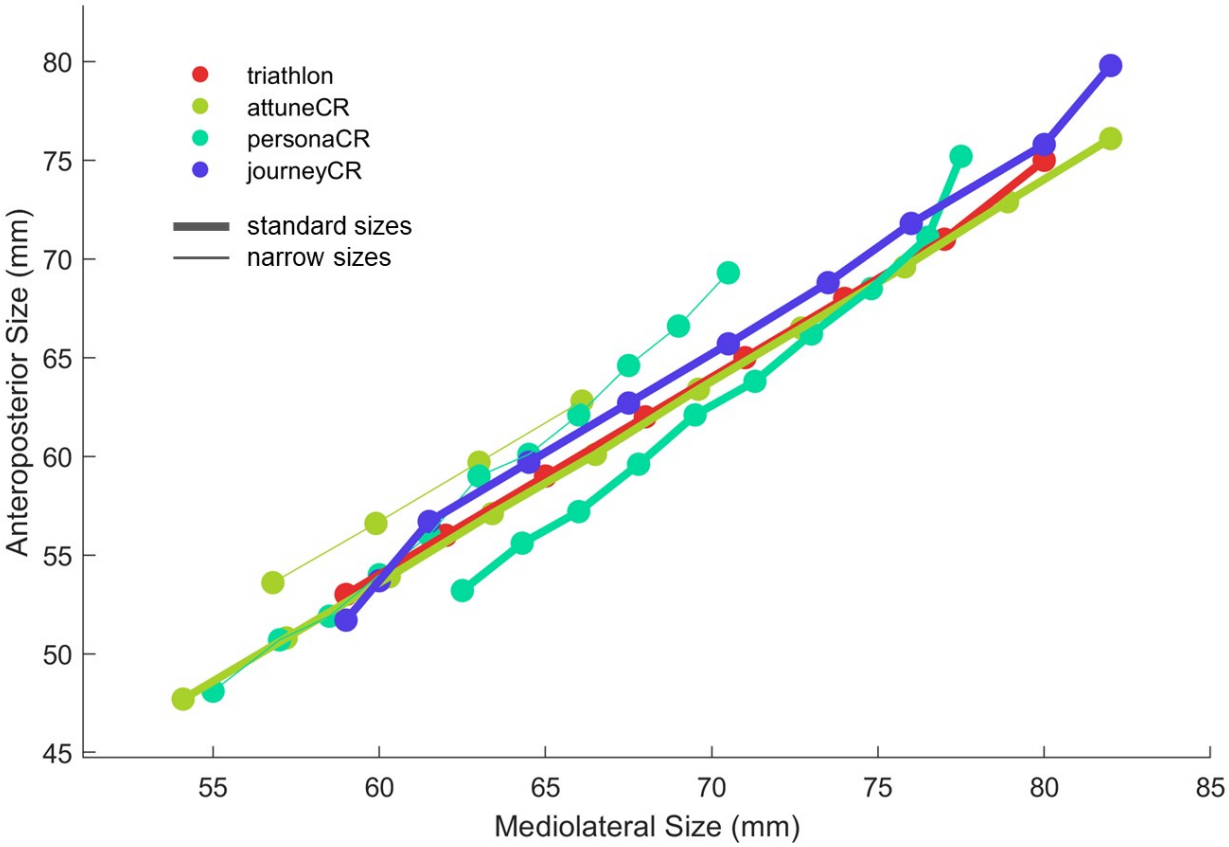

Figure 3-4: Size information of the knee implant systems analyzed in the context of population coverage.

3.1.3 Results

The multivariate t-test with unequal variances showed a significant difference ($p = 0.0005$) between the bone and implant measurements. The 95% confidence intervals of the mean value deviation for univariate tests ranged from 0.35 to 1.1 mm for ML and 0.03 to 0.6 mm for AP. However, these small differences between native bone and implant AP/ML sizes are not expected to be of clinical significance. **Figure 3-1 B** displays the comparison of the implant and cadaveric bone measures, demonstrating good agreement between the two datasets. Hence, it can be concluded that the implant geometry data are a valid basis for this sizing analysis.

In the following, the results of the sensitivity analysis regarding the number of implant sizes and the tolerated mismatch are presented. **Figure 3-5 A** shows the covered population over the number of sizes, given fixed size mismatch bounds of e.g., ±1.5 mm for the AP size and up to 3 mm ML underhang on either side. Starting from six sizes, 60% of the population could be provided with an adequately sized implant. Only 15 sizes

were required to fit 90% of the population. Yet, even 30 sizes were not sufficient to achieve a 100% coverage of the population. In **Figure 3-5 B**, the number of sizes is fixed. Instead, the bounds on AP and ML mismatch were varied: From ±0.5 to ±2.5 mm AP mismatch and 1 to 5 mm ML underhang on either side. This strongly influenced the coverage, with only 20% covered for a strict bound and a full coverage of the population when loose bounds were applied.

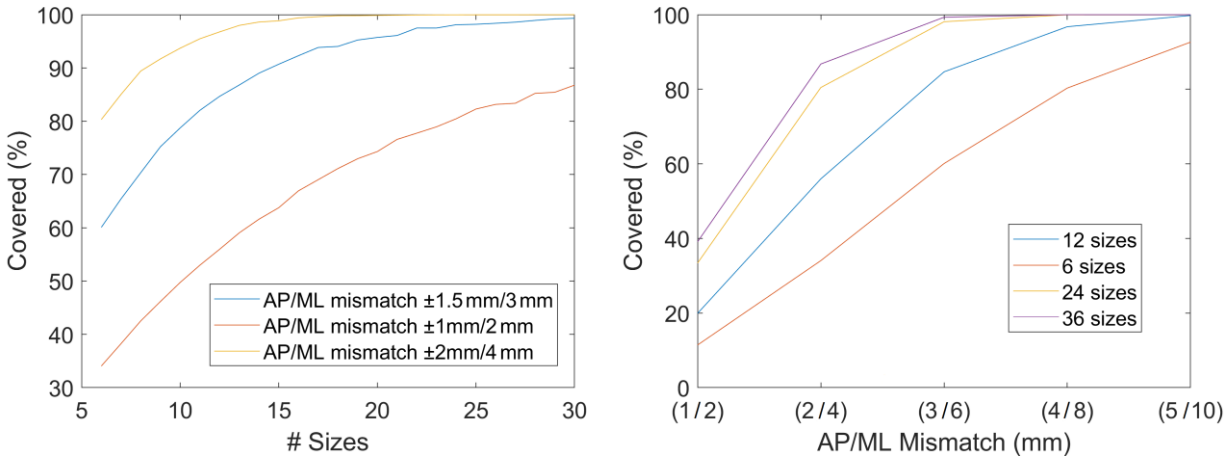

(A) **(B)**

Figure 3-5: Quantitative results of the sizing optimization analysis: **(A)** The percentage of population covered over the number of different implant sizes. An AP mismatch of ±1.5 mm and an underhang of up to 3 mm on either side is shown in blue, along with a less strict version with ±2 mm in AP and 4 mm in ML (yellow), as well as a strict requirement of ±1 mm in AP and 2 mm in ML (red). **(B)** The percentage of population covered over the allowed sizing mismatch. ML underhang may be twice as high as AP mismatch. This function was evaluated for 6 (red), 12 (blue), 24 (yellow), and 30 (purple) implant sizes.

Table 3-2 the percentage of population covered for all tested combinations of sizes and mismatch bounds. Within the bounds for mismatch and the numbers of implant sizes considered in the present analyses, the impact of changes in tolerated AP and ML mismatch had a greater influence on population coverage (for 12 sizes: range of coverage = 19.91%–99.78% based on allowed AP and ML mismatch) compared to changes in the number of sizes (for max ±1.5 mm AP error and 3 mm underhang on both sides: range of coverage = 60.08%–99.32%).

Table 3-2: Population coverage for the number of sizes varying from 6 to 30 and different AP & ML mismatches, ranging from ±0.5mm to ±2.5mm in AP direction and 1mm to 5mm underhang in ML direction. The exemplary setup presented in **Figure 3-5** is highlighted in blue. The number of implant sizes of existing implant systems in the setup analyzed are highlighted in grey.

# Sizes	AP / ML Mismatch				
	1/2 mm	2/4 mm	3/6 mm	4/8 mm	5/10 mm
6	11.43	34.05	60.08	80.32	92.64
7	12.94	38.25	65.43	85.04	95.14
8 (Triathlon)	14.34	42.52	70.35	89.42	97.68
9	15.97	46.17	75.22	91.70	98.62
10 (Journey II)	17.40	49.74	78.75	93.71	99.27
11	19.00	52.98	82.05	95.48	99.63
12 (example)	19.91	55.97	84.67	96.77	99.78
13	21.36	59.06	86.81	97.99	99.97
14 (Attune)	22.58	61.62	89.02	98.62	99.97
15	23.83	63.77	90.70	98.85	99.98
16	25.08	66.94	92.30	99.40	99.99
17	26.21	69.03	93.84	99.63	99.99
18	27.15	71.12	94.04	99.81	100.00
19	28.87	72.96	95.24	99.82	100.00
20	29.73	74.31	95.73	99.86	100.00
21 (Persona)	30.86	76.59	96.09	99.90	100.00
22	31.77	77.76	97.49	99.94	100.00
23	32.74	78.95	97.49	99.96	100.00
24	33.41	80.47	98.11	99.97	100.00
25	34.18	82.29	98.19	99.98	100.00
26	35.87	83.16	98.38	99.98	100.00
27	37.05	83.37	98.60	99.98	100.00
28	38.56	85.23	98.92	99.99	100.00
29	37.70	85.44	99.21	99.99	100.00
30	39.12	86.77	99.32	100.00	100.00

Figure 3-6 exemplarily displays the optimized sizes for 12 implants with size mismatch bounds of ±1.5 mm for AP and up to 3 mm ML underhang on either side. The 85,143 femoral component AP and ML sizes in the database are represented by gray dots. It has to be noted, that the density of cases represented by dots is much higher in the center of the distribution due to overlap. This is visualized by the Gaussian mixture model in **Figure 3-1 A**. Along with the patient-specific implant sizes, 12 standard implant sizes (red dots) optimized by the model are shown. Their respective bounds on AP and ML mismatch are visualized as rectangles. The rectangles are aligned to be on the right of the OTS implant size, as overhang is ruled out. Implants covered by the suggested OTS

sizes are highlighted as blue dots. The distribution is cut off at certain bounds: 55 and 81 mm for AP and 57 and 90 mm for ML. These bounds correspond to the boundaries of the FDA clearance of the iTotal implant (Conformis Inc., Billerica, MA, US), which are described in the Methods section.

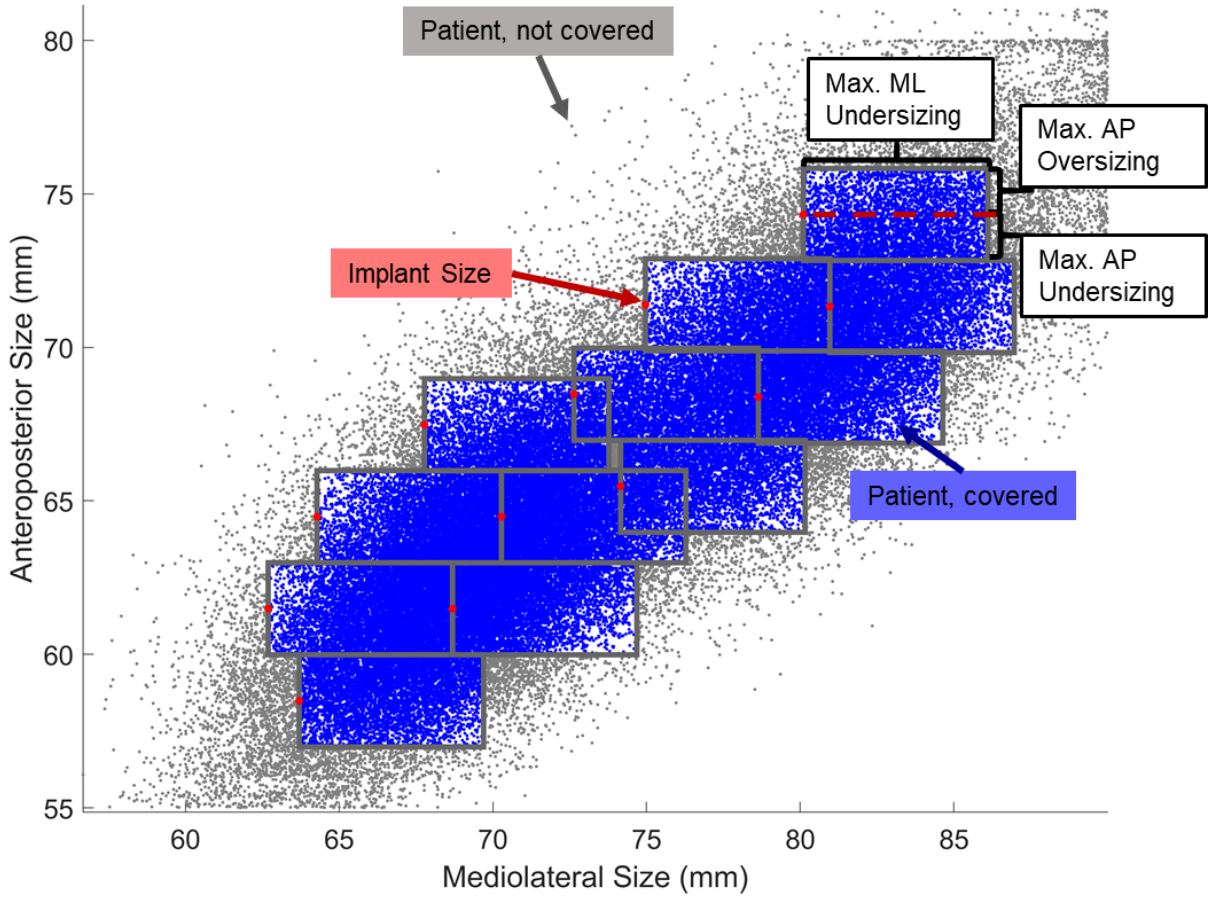

Figure 3-6: Distribution of femoral component AP and ML measures of the implant sizes in the data set. Every implant manufactured is shown as a dot. One exemplary set of 12 OTS implant sizes optimized by the model is shown as red dots, along with rectangles showing the covered range of sizes. Patients covered by such an OTS size are shown in blue. Gray dots are outliers.

Apart from the optimization, the coverage of existing implant sizing was evaluated and compared against the optimized implant sizing of this study. The results are given in **Table 3-3** and **Figure 3-7**. As an example, the Persona knee implant system (Zimmer Biomet Holdings, Inc., Warsaw, IN, US) offers 21 femoral implant sizes, with which a coverage of 73.32% of the cases analyzed was reached. With 21 optimized implant sizes from the approach presented, an increase in coverage by 22.77% (→96.09%) was achieved. Similar improvements were seen for the femoral component sizing of other implant systems.

Table 3-3: Population coverage of existing implant systems and potential improvements in population coverage through optimization.

Error: Max 6/0mm ML and Max 1.5/1.5mm AP	**Triathlon** (Stryker)	**Journey II** (Smith & Nephew)	**Attune** (DePuy Synthes)	**Persona** (Zimmer Biomet)
Number of Sizes	8	10	14	21
Coverage	51.51%	54.10%	63.50%	73.32%
Achievable coverage with optimized sizes	70.35%	78.75%	89.02%	96.09%
Coverage increase through optimization	18.84%	24.65%	25.52%	22.77%

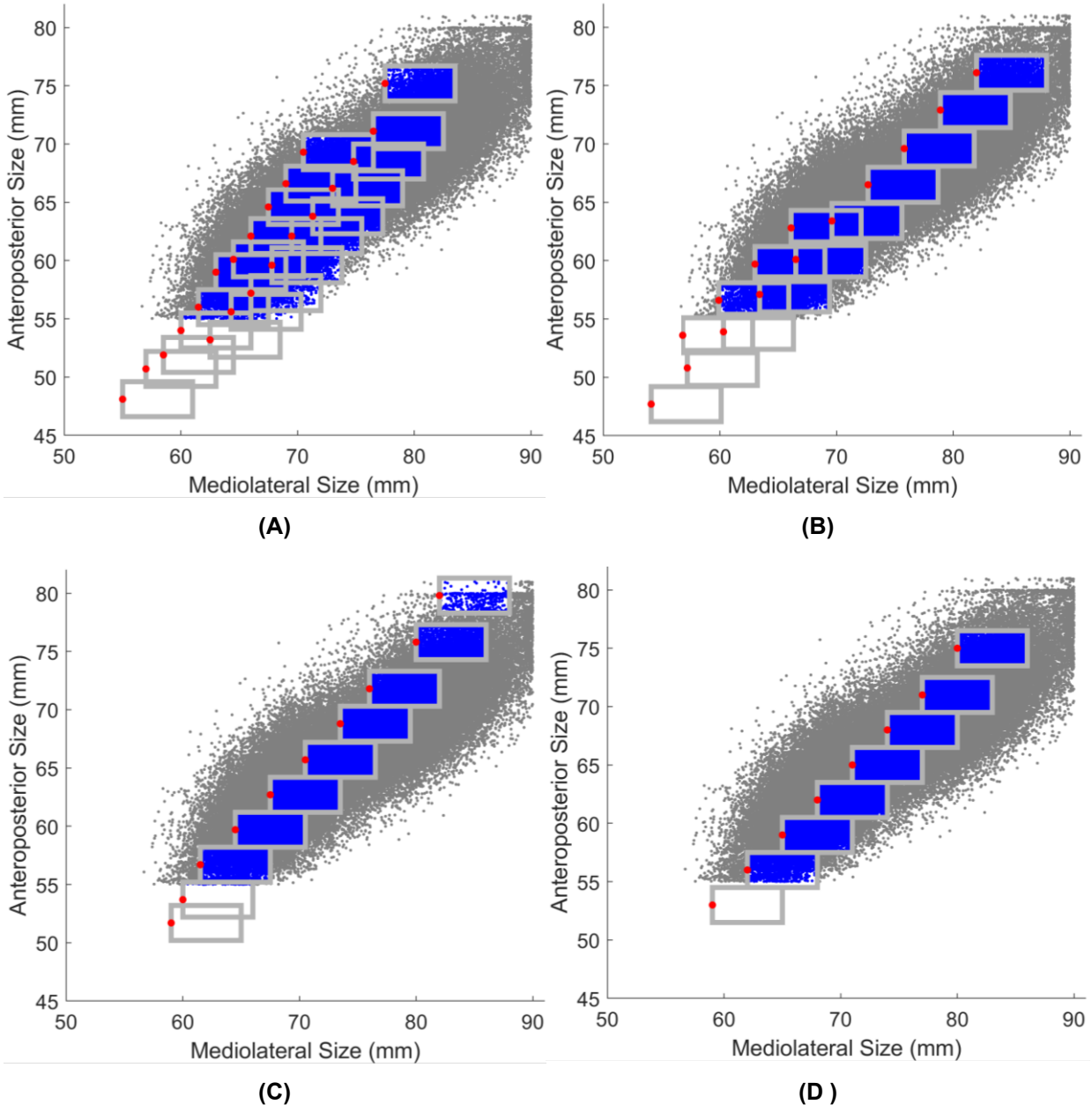

Figure 3-7: Population coverage of existing implant systems. **(A)** Persona (Zimmer Biomet Holdings, Inc., Warsaw, US-IN) **(B)** Attune (Johnson & Johnson, New Brunswick, US-NJ) **(C)** Journey II (Smith & Nephew plc., London, UK). **(D)** Triathlon (Stryker Corp., Kalamazoo, US-MI).

3.1.4 Discussion

In the present study, the bounds for AP and ML mismatch as well as the number of implant sizes highly affected the population coverage. Dai et al. (Dai et al. 2014b) reported improved fit for implant systems with increased size offerings, confirming the rather apparent positive relationship between the number of implant sizes and the percentage of adequately matched cases reported in the present study. In addition, the gradient of coverage per implant size decreased with increasing size offerings. This effect is highly plausible, considering the normal distribution of ML and AP measures. With an increasing number of implant sizes, more of the tails of the respective normal distributions will be covered, hence leading to a decreasing gradient in coverage. The same effect was seen for increasing AP and ML mismatch bounds. Again, this effect can be explained by an increasing coverage of the normal distributions' tails, with increasing error bounds. Within the bounds for mismatch and the numbers of implant sizes considered in the present analyses, the impact of changes in tolerated AP and ML mismatch had a greater influence on population coverage.

When applying the findings to the development of an implant system, clearly a trade-off between the tolerated AP and ML mismatch, the number of implant sizes and population coverage has to be found. With respect to AP and ML mismatch, conservative error bounds of ±1.5 mm for AP and up to 3 mm ML underhang on either side were selected, with the aim of minimizing the risk for pain and instability. When applying those bounds, a population coverage of 84.67% was achieved with 12 implant sizes. With the double number of implant sizes (24), an increase of only 13.44% of population coverage was achieved. Moreover, with the given bounds for AP and ML mismatch, even 30 implants could not cover the entire population. Hence, the use of patient-specific implants is advisable for the remaining cases.

When comparing the results against sizing of existing implant systems, a significant improvement in coverage through optimization was seen. The increase in population coverage ranged from 18.84% to 25.52%. However, industry related factors regarding sizing have to be considered, when evaluating the results of this analysis. Those results provide a theoretical upper limit of the patient population that can be covered by a certain set of femoral implants under different clinical mismatch criteria. Realistic possibilities

for population coverage will be lower, once engineering considerations such as cross compatibility of femoral and tibial sizes, surgeon preferences with regards to intra-operative flexibility and market dynamics such as the need for implant manufacturers to provide multiple variations (CR/PS, cemented/pressfit, etc.) in their implant systems and their implications on inventory management are taken into consideration. Conversely, this study highlights a new technique that can be utilized by implant manufacturers to design the next generation of implant systems, which leverages the use of large databases of patient data to drive engineering design decisions, which were not available to the industry when the current generation of implants were designed.

The present study was based on data from 85.143 patient-specific femoral implants, which is a much more extensive database compared to those of previous studies on the comparison of implant and bone morphology (Dai et al. 2014b; Hitt et al. 2003; Mahoney and Kinsey 2010). Despite this strength, there were several limitations associated with this study. First, the study was limited to a North American population. Hence, the optimization may not be adequate for e.g. the Asian population (Kim et al. 2017). Depending on the patient population, the optimization may have to be repeated with a different, representative database. Second, AP and ML measures of the patient-specific implants were used and not of the bones. However, the implants were designed individually, based on the patient's bone, hence leading to an adequate approximation of the bony measures. While a t-test proofed a significant difference between the two measures, its absolute difference is below 1.1 mm. The FDA bounds for the iTotal custom implant system measures may limit the morphologic spectrum considered. Yet, very few implant measures are close to the FDA bounds, which suggests this fact not to be a relevant limitation. Third, only AP and ML measures were considered, while many more parameters such as the femoral J-curve or the posterior condylar offset are linked to the clinical outcome (Bellemans et al. 2002; Kessler et al. 2007). The variation of the patient-specific J-Curve is therefore analyzed in more detail in **Chapter 3.2**. In addition, interface mismatch was only considered with regard to the overall AP and ML size, while (in contrast to patient specific implants) mismatch of OTS implants, can occur along the entire implant-bone interface contour. This aspect is addressed in the course of this thesis (**Chapter 5.3.2**). Lastly, only the femoral component was considered. Further analyses should include the tibial as well as the patellar component for a more

comprehensive assessment of population coverage in TKA. With tibial sizing, a similar optimization should be performed. Depending on the compatibility between femoral and tibial components, the overall population coverage can be calculated.

In conclusion, the study presented showed that in TKA, a high population coverage of 84.67% can be achieved with 12 optimized implant sizes, ensuring excellent AP fit while avoiding clinically relevant ML overhang as well as excessive ML underhang. As even with 30 implants a coverage of the entire population cannot be achieved, remaining patient population (about 15% for 12 sizes) should be provided with a patient-specific implant to avoid a clinically relevant mismatch between knee morphology and implant geometry. Since AP and ML sizing are the only established sizing parameters of commercial OTS implants, this study already provides insights into a potential optimization. However, only size fit was analyzed in this study. Deviations in other functionally related parameters were not addressed and are therefore the subject of the following chapters.

Summarizing, the research question addressed in this chapter can be answered as follows:

> *The size coverage of a representative dataset of >85,000 TKA patients was significantly improved with the numerically optimized sizing compared to available implant sizing. When comparing the results with the sizing of available implant systems, an increase in population coverage from 18.84% to 25.52% was achieved.*

3.2 Variation of native knee morphology

Work in this chapter has been presented in parts in:

S.A.G.A. Grothues & K. Radermacher: Variation of the Three-Dimensional Femoral J-Curve in the Native Knee. Journal of Personalized Medicine, 2021, 11(7), pp. 592 [DOI: 10.3390/jpm11070592]

S.A.G.A. Grothues, M. Asseln & K. Radermacher: Variation of the femoral J-Curve in the native knee. In: F. Rodriguez Y Baena & F. Tatti (ed.): CAOS 2020. The 20th Annual

Meeting of the International Society for Computer Assisted Orthopaedic Surgery, 4, 2020, pp. 86-91 [DOI: 10.29007/5k32]

3.2.1 Introduction

As presented in the previous chapter, the majority of a representative TKA patient population (~85%) could be provided with an adequate ML and AP sized femoral implant component of only 12 sizes, when optimization methods are used to define implant sizing. However, many more parameters are of relevance for patient satisfaction and for the overall clinical outcome. One relevant example is the sagittal shape of the femoral condyles, which is often referred to as J-Curve. The J-Curve represents a significant determinant of native knee biomechanics (Klein and Sommerfeld 2012). Similarly, in TKA, the J-Curve of the femoral component is reported to have a high impact on knee kinematics (Kessler et al. 2007) and its relevance is reflected in various implant design philosophies, including single-, dual-, and multi-radius designs. The medial and lateral J-Curve approximate the contours being in contact with the tibial plateaus and thereby they are highly relevant for tibiofemoral articulation. Therefore, the J-Curve is related to relevant motion phenomena of the native knee, such as femoral rollback and medial pivot (Freeman and Pinskerova 2005; Klein and Sommerfeld 2012; Pfitzner et al. 2018). Those phenomena are linked to flexion range of motion (Pfitzner et al. 2018) and patient satisfaction in general (Fantozzi et al. 2006). In addition, the J-Curve or rather its alteration is highly relevant for ligament strain and tension as well as for the resulting tibiofemoral contact forces. With a ligament stiffness of 60-80 N/mm of medial and lateral collateral ligaments (MCL/LCL) (Völlner et al. 2019; Wilson et al. 2012), a local condylar offset compared to the native J-Curve of only 1 mm will result either in 60-80 N additional lateral and medial tibiofemoral contact force and increased ligament. strain; or in ligament relaxation and potential (mid-flexion) instability. In addition, first structural damage is occurring in ligaments from about 5% strain (Provenzano et al. 2002). With an assumed average length of the MCL(LCL) of 100(60) mm, a medial (lateral) offset limit would be 5(3) mm (corresponding to 5% maximum strain) which would result in additional medial (lateral) forces of ~300-400 (180-240) N for an average knee. Taking into account, that TKA should not extend ligament strain up to the limits of structural damage, and that loads of 10 N (corresponding to less than 1 mm offset) already activate

afferent nerves from receptors in the ligaments triggering the knee joint stabilizing muscles (Sojka et al. 1991), it can be assumed, that local J-Curve offset limits would have to be reduced to the range of 1–2 mm maximum. These limits are in agreement with literature regarding recommendations for varus-valgus laxity between 0.5-1 mm for extension and 0.7-1.2 mm for flexion from Delport et al. (Delport et al. 2013).

Consequently, the analysis of the native femoral J-Curve is essential for a better understanding of native knee biomechanics and for optimizing the femoral implant component design in TKA. Previous analyses of the femoral J-Curve have focused on its 2D shape in one specific cutting plane or through projection. Most studies used geometrical primitives such as ellipses and circles and fitted them to the respective 2D J-Curve contours for investigation (Biscević et al. 2005; Howell et al. 2010; Li et al. 2012; Li et al. 2010; Martelli and Pinskerova 2002; Nuño and Ahmed 2001). However, variations in the contour itself have not been investigated in detail yet. In addition, because of the 3D nature of knee motion, the restriction to a 2D evaluation represents a relevant limitation. Hiss and Schwerbrock (Hiss and Schwerbrock 1980) analyzed the condylar extremum points of a cadaveric knee in 3D, by a comprehensive manual analysis. A limitation of their labor-intensive method is that it is not applicable to large sample sizes. A limitation of their analysis was that they neglected the J-Curve's orientation with regard to the mechanical axis, whereby a relevant amount of variation was neglected. Other authors analyzed the tibiofemoral process of contacts e.g., by finite element simulations (Gu and Pandy 2020), but did not evaluate the points identified regarding shape variation.

Consequently, the aim of this chapter was to investigate and compare the 2D and 3D J-Curves of the native knee by principal component and geometric parameter analysis.

The research question addressed in this chapter is the following:

RQ2: Does native knee morphology involve shape variation independent of overall size?

3.2.2 Materials and methods

Patient Datasets

Bone surface models of 90 cadaveric femora, which have been segmented semi-automatically (control by experts) from CT data (voxel size: 0.49/0.53 mm), were provided by Conformis (Conformis Inc., Billerica, MA, USA). Of the 90 cadavers, 56 were male, 32 were female, and for two no gender information was available. The bone models showed no osteophytes or other signs of osteoarthritis. All further processing was performed in semi-automatic MATLAB scripts.

Contour Derivation

First, the bone models were transferred to a bone-specific coordinate system (Asseln 2019) and left femora were mirrored. The 2D J-Curves of the medial and lateral condyles were extracted, using a semi-automatic workflow implemented by Asseln et al. (Asseln et al. 2019). To derive the 3D J-Curve shapes, the concept of rotating cutting planes was used, which has been previously applied in the context of surface parametrization (Asseln et al. 2015; Asseln 2019). The concept is depicted in **Figure 3-8**. The transepicondylar axis was used as origin of the cutting planes. In total 300 cutting planes between extremum points of the articulating areas on the condyles and the trochlea were used (note **Figure 3-8 A** shows only 18 cutting planes for better visibility of the individual cutting planes). From each cutting plane a cutting contour was derived. Subsequently, for each contour an extremum search was performed, as it can be seen in **Figure 3-8 B**. For this purpose, the contours were transformed to the x-y plane, and extrema (maxima) regarding the y-axis were identified.

For both the 2D and 3D contours (defined by the extrema), a curvature analysis was performed, in order to determine the boundaries of the articulating area, according to Li et al. (Li et al. 2010). The contours were then cut accordingly and interpolated by 300 equidistant points.

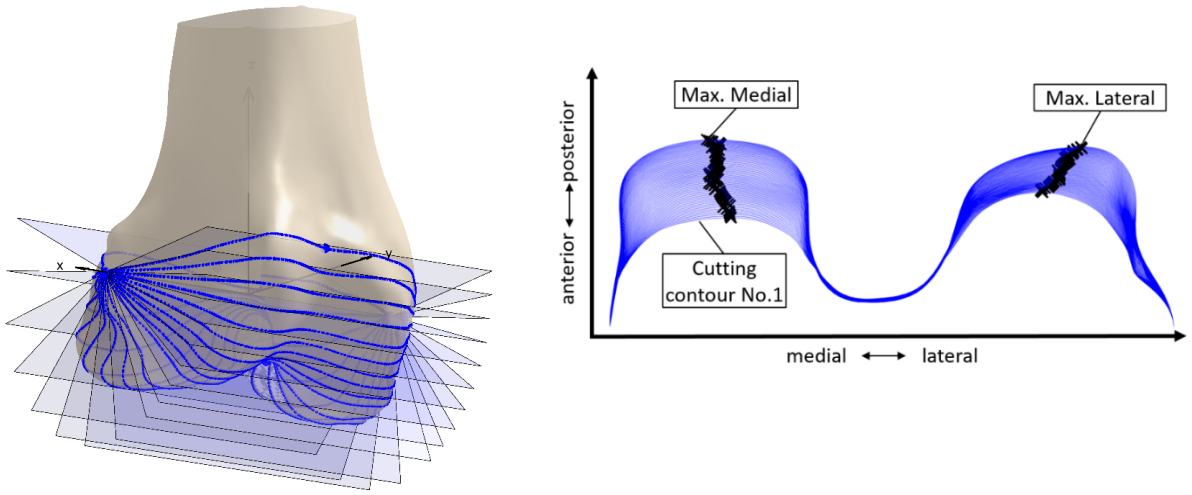

(A) **(B)**

Figure 3-8: Elements of the process of 3D J-Curve contour derivation. **(A)** Example femur with rotating cutting planes for the derivation of cutting contour (note: only 18 cutting planes displayed here, to enable better visualization of the individual planes). **(B)** Cutting contours (blue) and extrema (black) for cutting planes 1 to 63.

To evaluate the analyzed variance with regard to the one in implant design, the 2D J-Curves from two different standard implant systems of various sizes, including narrow versions, were extracted from the planning software mediCAD (mediCAD Hectec, Altdorf, Germany). For this purpose, images were taken from the software and contours were extracted by thresholding. All contours were scaled to the corresponding first size, for qualitative evaluation of their variance.

Principal Component Analysis

Principal component analysis (PCA) is a mathematical method, which is used for reducing dimensionality of multivariate datasets. In PCA, the principal components are calculated, which represent the directions along which the data varies the most. The principal components can be determined by calculating the eigenvectors of the covariance matrix, and they are ordered according to the amount of variance they account for (Ringnér 2008). In the present study, PCA was used to identify dominant patterns of contour variation. PCA requires corresponding data points (landmarks) between the subjects. The analysis is enabled by the use of a consistent bone-specific coordinate system for the contour derivation, and the standardized definition of boundary points. The PCA was performed combined on both the medial and lateral femoral 3D

J-Curves. The analysis was performed according to Shlens (Shlens 2005). The principal modes were defined according to Stegmann and Gomez (Stegmann and Gomez 2002). The female and male cadavers were analyzed separately as well as combined, in order to evaluate differences in gender.

Geometric Parameter Analysis

For the 2D J-Curves, the derived mean shapes were analyzed with regard to height, AP length, and the radii describing the posterior and distal proportion of the condyles (Asseln et al. 2019) as well as their center position. The parameters are listed and described in detail in **Table 3-4**. In addition, effect sizes for the first three PCs were calculated with regard to the respective mean shape. The combined PCAs results were evaluated qualitatively.

A more extensive geometric parameter analysis was applied to the mean shape as well as to the first five modes of the 3D bone contours. General size parameters, arc lengths, radii describing the curvature, and the mean and maximum local condylar offsets were considered (**Table 3-4**). In addition, exemplary parameters of the 3D J-Curves are displayed in **Figure 3-9**. Changes in parameter measures originating from the modes were quantified in absolute deviations and in percent.

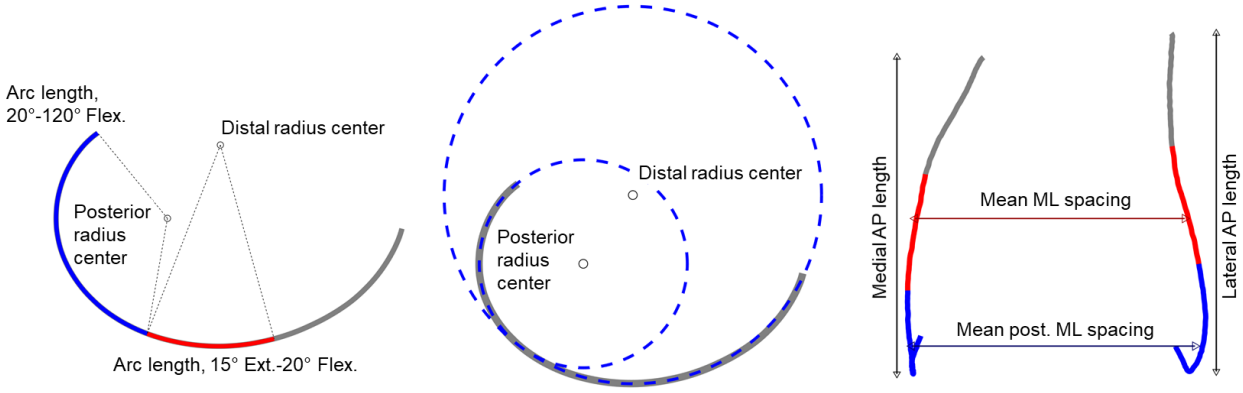

Figure 3-9: Visualization of the geometric parameter analysis of the 3D femoral J-Curves.

Table 3-4: Description of the parameters considered in the 2D and 3D J-Curve geometric parameter analyses. Parameters are either defined for the combined overall shape of both J-Curves or individually for the medial and lateral side (column: overall/medial and lateral).

Parameter Name	Overall/ Medial and Lateral	Description
Mean distal ML spacing	Overall	Mean mediolateral distance of the distal points of the lateral/medial 3D J-Curve (15° of extension to 20° of flexion, reference: radius of the circle fitted to the distal portion of the condyles). Inspired by Walker (Walker 2005)
Mean posterior ML width	Overall	Mean mediolateral distance of the posterior points of the lateral/medial 3D J-Curve (20°-120° of flexion, reference: radius of the circle fitted to the posterior portion of the condyles). Inspired by Mahfouz (Mahfouz et al. 2012)
Height	Overall	Proximodistal height of the medial/lateral J-Curve.
AP length	Medial and lateral	Anteroposterior length of the medial/lateral J-Curve.
Distal radius	Medial and lateral	Radius of the circle fitted to the distal portion of the medial/lateral J-Curve. The calculation was performed according to Nuno and Ahmed (Nuño and Ahmed 2001) and is described in more detail for the 3D J-Curve in Asseln et al. (Asseln et al. 2019)
Posterior radius	Medial and lateral	Radius of the circle fitted to the posterior portion of the medial/lateral J-Curve. The calculation was performed according to Nuno and Ahmed (Nuño and Ahmed 2001) and is described in more detail for the 3D J-Curve in Asseln et al. (Asseln et al. 2019)
Functional arc length	Medial and lateral	Arc length of the medial/lateral 3D J-Curve between 15° of extension until 120° of flexion (reference: center of the circle fitted to the distal/posterior portion of the condyles).
Arc length 15° Ext.–20° Flex.	Medial and lateral	Arc length of the medial/lateral 3D J-Curve between 15° of extension until 20° of flexion (reference: center of the circle fitted to the distal portion of the condyles).
Arc length 20°–120° Flex.	Medial and lateral	Arc length of the medial/lateral 3D J-Curve between 20° until 120° of flexion (reference: center of the circle fitted to the distal/ posterior portion of the condyles).
Mean abs. deviation	Medial and lateral	Mean absolute deviation (mean condylar offset) regarding anteroposterior and proximodistal direction.
Max abs. deviation	Medial and lateral	Maximum absolute deviation (maximum condylar offset) regarding anteroposterior and proximodistal direction.

3.2.3 Results

2D J-Curve

In total, 85 of the 90 cadaver cases could be processed without errors (54 male, 29 females, 2 without gender information). Results of the PCA and GPA are displayed in **Figure 3-10** and **Table 3-5**.

The mean shapes of the male, female and combined population differed regarding the morphological measures considered. However, after normalization of the measures according to their direction of measurement, as suggested by Asseln et al. (Asseln et al. 2018), those normalized measures were comparable for the male, female, and combined population. Consequently, only the results of the analysis of all knees are presented in the following.

The mean width and mean distal radius were greater in the lateral condyle than in the medial while the mean height and mean posterior radius were similar. The results of the isolated PCA of the medial and lateral side showed similar J-Curve variations (**Figure 3-10 A1:A2**). The analysis revealed a dominant first principal component (PC), accounting for 62.2% (73.1%) of variance in the medial (lateral) condyle. It comprised changes in the orientation and arc length of the J-Curves. In addition, the overall size of the lateral side and the width of the medial side was changed by the first PC. The second PC of the medial and lateral J-Curve accounted for 33.1% and 22.5% of variance, respectively. They both mainly contained changes of the contour's overall size and height. The third PC accounted for 3.5% and 3.0% of variance of the medial and lateral J-Curve, respectively. It mainly involved changes in the contours' circularity. The combined PCA of medial and lateral side involved the beforehand described individual side variations in combination with changes in relative position (**Figure 3-10 A3**). The PCs were less distinguishable and the accounted variance was more distributed (PC1 48.4%, PC2 24.4%, PC3 15.8%). The extracted standard implant J-Curves showed no changes in shape but only changes in size.

Table 3-5: Results of the 2D J-Curve geometric parameter analysis: Measures of the mean shape as well as effect sizes for the first three modes are listed (+3SD). Deviations with regard to the mean shape are quantified in millimeter and in percent. Changes exceeding predefined limits are highlighted (color code below). L=Lateral. M=Medial.

		Side	Height	AP length	Radius distal	Radius posterior	Radius center distal	Radius center posterior
Mean Shape		L	37.1 mm	45.9 mm	32.0 mm	18.9 mm	11.9 mm	10.9 mm
		M	35.5 mm	63.8 mm	36.8 mm	19.8 mm	2.0 mm	10.5 mm
Mode	**1**	M	-0.2 mm (-0.6 %)	+12.0 mm (+26.2 %)	+2.5 mm (+7.8 %)	+1.5 mm (+7.9 %)	-5.3 mm	+2.0 mm
		L	+6.6 mm (+18.7 %)	+13.8 mm (+21.6 %)	+6.7 mm (+18.2 %)	+2.9 mm (+14.7 %)	-5.0 mm	-0.6 mm
	2	M	+10.9 mm (+29.5 %)	+9.9 mm (+21.6 %)	+5.4 mm (+16.9 %)	+4.3 mm (+22.7 %)	+2.0 mm	+0.6 mm
		L	+9.0 mm (+25.3 %)	+8.7 mm (+13.7 %)	+8.4 mm (+22.9 %)	+4.1 mm (+20.7 %)	+2.0 mm	+1.4 mm
	3	M	+1.0 mm (+2.8 %)	+1.8 mm (+3.9 %)	+6.3 mm (+19.7 %)	+2.2 mm (+11.4 %)	+4.9 mm	+3.1 mm
		L	-1.1 mm (-3.1 %)	+3.9 mm (+6.1 %)	-0.1 mm (-0.2 %)	+2.6 mm (+13.3 %)	+1.2 mm	+3.4 mm

Color code: Deviations: ≥ ±10%: ■ | ≥ ±20%: ■ | Mean abs. deviation: ≥2 mm: ■ | ≥5 mm: ■.

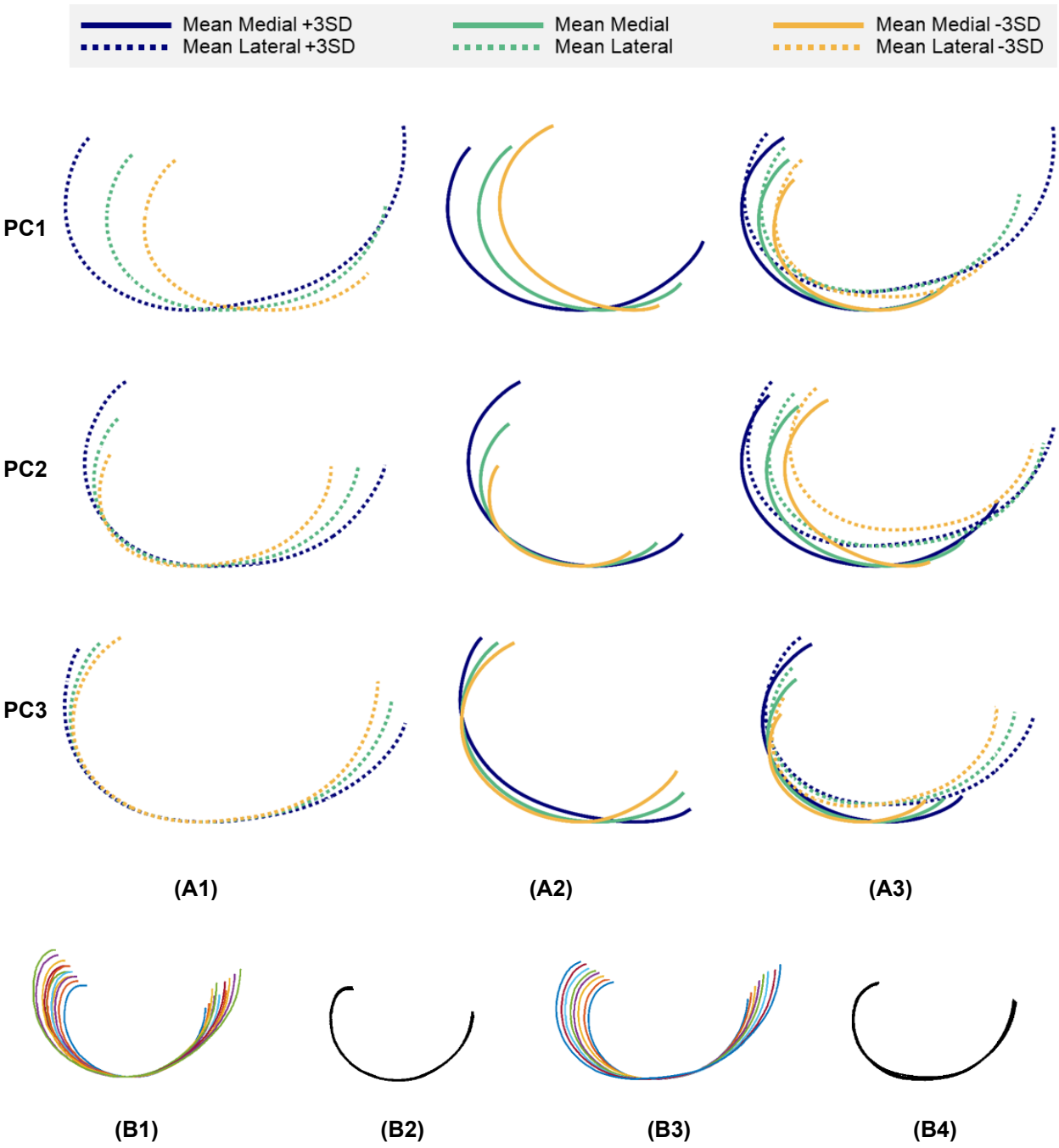

Figure 3-10: The first three PCs of **(A1)** the lateral, **(A2)** the medial and **(A3)** the combined femoral cadaveric 2D J-Curves. For the combined PCA the point coordinates of both lateral and medial side were included. (Solid line: medial, dashed line: lateral. 3SD = 3 standard deviations). In comparison, Implant J-Curves **(B1)** of sizes 1-8 from the Attune knee system (DePuy Orthopaedics, Warsaw, IN, US) and **(B3)** of sizes 1-6 from the Triathlon total knee system (Stryker, Kalamazoo, MI, US), which were scaled to their corresponding size 1 (**(B2)**: Attune, **(B4)**: Triathlon). All contours were oriented to their most distal point in proximodistal direction, for better comparison of the respective variance.

3D J-Curve

Analogue to the 2D analysis, 85 of the 90 cadaver cases could be analyzed with regard to the femoral 3D J-Curve without errors (54 male, 29 females, 2 without gender

information). **Figure 3-11** shows an example of the 3D bone contours of one femur, together with the respective bone model. An overview of all 3D J-Curves is given in **Figure 3-12**.

(**A**) (**B**) (**C**)

Figure 3-11: Example of the 3D J-Curve contours. **(A)** Anterior/lateral-posterior/medial view. **(B)** Lateral-medial view. **(C)** Medial-lateral view.

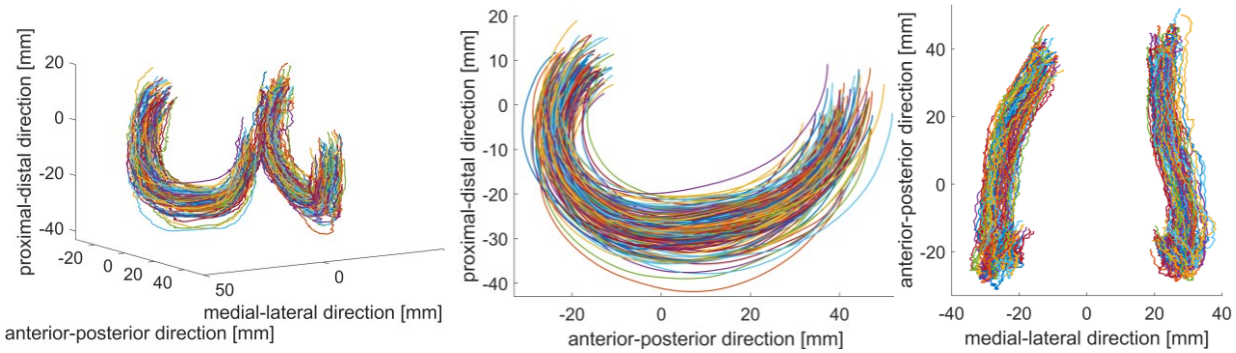

(**A**) (**B**) (**C**)

Figure 3-12: 3D J-Curve contours of both genders. **(A)** Anterior/lateral-posterior/medial view. **(B)** Lateral-medial view. **(C)** Superior-inferior view.

Similar as for the 2D analysis, the normalized J-Curve measures were comparable for the male, female, and combined population. The results of the separate PCA of female and male 3D J-Curves showed similarities regarding the aspects of shape variations (e.g., arc lengths, orientation, aspect ratio). For the combined analysis (**Figure 3-13**), the first mode consisted almost solely of changes in size, highlighting size differences between female and male femora. Apart from this first mode, the aspects of shape variation were similar for all analyses. Because of the similarities in normalized

measures of the mean shapes and in the aspects of shape variation, in the following only the detailed results of the combined analysis of both genders are presented.

Figure 3-13 shows the PCA results regarding the first five modes. The percentage of variation explained by modes 1-5 was 31.5, 23.4, 20.1, 7.4, and 5.5%, respectively (sum: 87.8%). In **Table 3-6**, the results of the respective geometric parameter analysis are presented. The first mode involved changes in size, which lead to an increase of all parameters in the geometric parameter analysis, when adding 3 standard deviations to the mean shape (**Table 3-6**). Furthermore, for the medial side, also slight changes in 3D J-Curve orientation were associated. With the second mode, the most prominent changes were seen regarding the anterior region of the lateral J-Curve. For the medial side, only slight changes in curvature and size were observed. The third mode consisted of changes in medial J-Curve orientation, in lateral J-Curve size and in ML width. The fourth mode primarily represented changes in aspect ratio. The fifth mode mostly consisted of changes in relative location of the medial vs. the lateral 3D J-Curve.

Table 3-6: Results of the 3D J-Curve geometric parameter analysis: Measures of the mean shape as well as effect sizes for the first five modes are listed (+3SD). Deviations with regard to the mean shape are quantified in millimeter and in percent. Changes exceeding predefined limits are highlighted (color code below). L=Lateral. M=Medial.

Mean Shape	Mean ML spacing	Mean post. ML width		AP length	Distal radius	Posterior radius	Funct. arc length	Arc length 15° Ext.-20° Flex.	Arc length 20°-120° Flex.	Mean abs. dev.
	51.2 mm	53.7 mm	L	64.2 mm	48.8 mm	20.3 mm	67.4 mm	32.5 mm	34.9 mm	64.2 mm
			M	60.1 mm	35.1 mm	19.3 mm	67.5 mm	22.8 mm	44.7 mm	60.1 mm

Mode											
	1	11.79 mm (23.0%)	10.96 mm (20.4%)	L	12.15 mm (18.9%)	7.31 mm (15%)	4.85 mm (23.9%)	12.3 mm (18.3%)	5.42 mm (16.7%)	6.88 mm (19.7%)	5.34 mm
				M	16.84 mm (28%)	8.31 mm (23.7%)	5.26 mm (27.2%)	13.35 mm (19.8%)	6.01 mm (26.4%)	7.35 mm (16.4%)	8.81 mm
	2	3.71 mm (7.2%)	−0.3 mm (−0.6%)	L	−7.11 mm (−11.1%)	2.33 mm (4.8%)	0.54 mm (2.7%)	10.85 mm (16.1%)	1.56 mm (4.8%)	9.29 mm (26.6%)	9.36 mm
				M	3.4 mm (5.7%)	1.99 mm (5.7%)	0.87 mm (4.5%)	6.84 mm (10.1%)	1.72 mm (7.6%)	5.12 mm (11.4%)	4.56 mm
	3	4.72 mm (9.2%)	7.7 mm (14.3%)	L	6.59 mm (10.3%)	9 mm (18.4%)	3.44 mm (16.9%)	16.2 mm (24%)	7.76 mm (23.9%)	8.44 mm (24.2%)	4.37 mm
				M	3.32 mm (5.5%)	4.08 mm (11.6%)	2.53 mm (13.1%)	11.75 mm (17.4%)	2.82 mm (12.4%)	8.93 mm (20%)	7.08 mm
	4	−4.72 mm (−9.2%)	−6.31 mm (−11.7%)	L	6.49 mm (10.1%)	7.97 mm (16.3%)	1.75 mm (8.6%)	12.93 mm (19.2%)	6.17 mm (19%)	6.76 mm (19.4%)	3.86 mm
				M	2.63 mm (4.4%)	-0.24 mm (−0.7%)	0.29 mm (1.5%)	3.45 mm (5.1%)	−0.07 mm (−0.3%)	3.52 mm (7.9%)	2.09 mm
	5	−0.56 mm (−1.1%)	−0.72 mm (−1.3%)	L	−0.49 mm (−0.8%)	−3.33 mm (−6.8%)	−0.17 mm (−0.8%)	−4.02 mm (−6%)	−1.61 mm (−4.9%)	−2.4 mm (−6.9%)	2.97 mm
				M	4.48 mm (7.4%)	3.28 mm (9.3%)	0.76 mm (3.9%)	6.22 mm (9.2%)	2.39 mm (10.5%)	3.83 mm (8.6%)	3.66 mm

Color code: Deviations: ≥ ±10%: □ | ≥ ±20%: ■ | Mean abs. deviation: ≥2 mm: □ | ≥5 mm: ■.

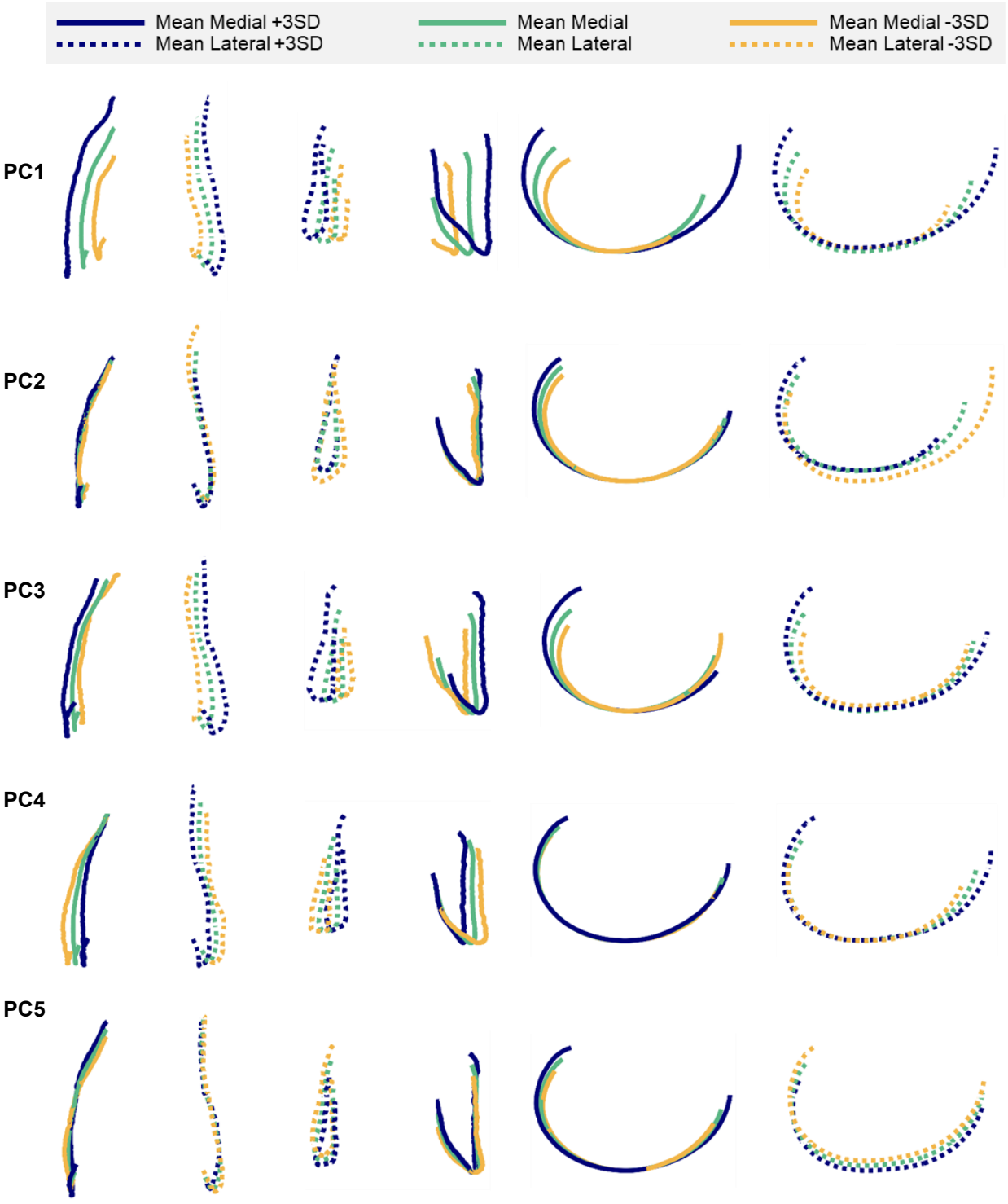

Figure 3-13: Modes 1–5 of the cadavers' 3D J-Curves in different views. Solid line: medial, dashed line: lateral. 3SD = 3 standard deviations. All contours were oriented to their most distal point in proximodistal direction, for better comparison of the respective variance. Variation explained by the modes 1–5: 31.5, 23.4, 20.1, 7.4, and 5.5%, respectively.

3.2.4 Discussion

2D J-Curve

The mean shapes of the lateral and medial cadavers' J-Curves showed relevant absolute differences, which are in agreement with other morphological studies of the native knee (Li et al. 2010; Asseln et al. 2019). The isolated PCA of medial and lateral J-Curves resulted in PCs involving changes in contour orientation, arc length, scaling and circularity. The combined PCA of both sides resulted in PCs comprising combinations of the individual variations together with changes in relative position. Thereby, further variation due to combination of the two contours were evidenced. The J-Curve variation e.g., due to changes in circularity amounted to several millimeters, being highly relevant for ligament tension and elongation. Scaling was a relevant aspect of the first 3 PCs of the combined analysis, accounting for 91.3% of the contours' variance. Fitzpatrick et al. (Fitzpatrick et al. 2008) analyzed the contours of the femoral resection cuts of 36 patients scheduled for TKA by PCA. They found that 59.7% of variation was due to changes in overall size. A direct comparison of the percentages however is not feasible, as the PCs of the present study involved relevant changes in shape. In contrast, the standard implants' 2D J-Curve variance consisted almost exclusively of changes in size.

3D J-Curve

For the combined analyses of the 3D J-Curve's mean shape, the identified radii are comparable to the respective 2D J-Curve analysis as well as to those of previous studies on the 2D J-Curve (Howell et al. 2010; Li et al. 2012; Nuño and Ahmed 2001; Asseln et al. 2018). However, a relevant difference regarding the AP length of the medial J-Curve can be seen. The medial 3D J-Curve shows a higher AP length compared to the medial 2D J-Curve, which may be explained by the distribution of the medial condyle's extremum points in the transversal plane (**Figure 3-12 C**). The extrema of both condyles do not lie in a single sagittal plane. Especially the medial extrema rather form a curve. A single sagittal cutting plane was used for the 2D J-Curve derivation, hence, parts of the medial J-Curve may have been neglected. This effect may also be present to a lower extent for the lateral side, as the lateral 2D J-Curve is also slightly smaller in AP direction compared to the lateral 3D J-Curve.

Similar aspects of shape variation of the femoral 2D and 3D J-Curves were found in men and in women. The amount of variation explained by changes in size was higher for the combined than for the gender-specific analyses. This observation is plausible, as men in general have larger knees compared to women (Asseln et al. 2018; Hitt et al. 2003; Mahfouz et al. 2012). Hence, the combination of both genders probably is the reason for the increased variability in size. The analysis of the 3D J-Curves demonstrated similar aspects of shape variation as for the 2D J-Curve analysis, however, with a clearer differentiation of the individual aspects in the different modes. For example, the first mode consisted almost exclusively of changes in size, accounting for 31.5% of shape variation. In addition, the third mode involved relevant changes in size, accounting for 20.5% of shape variation. Hence, when focusing on the first five modes, the share of shape variation explained by size sums up to ~52.0%, which is in agreement with the results of Fitzpatrick et al. (Fitzpatrick et al. 2008), reporting size to account for 59.6% of femoral shape variation. The effect of shape variation on morphological parameters was analyzed for the first five modes.

In the PCA results, changes in the distal arc length differed between the medial and lateral side and were even counteracting for modes 4 and 5. Mean absolute condylar offsets in the range of 2.09-9.36 mm and local maximum offsets in the range of 2.61-16.0 mm were found. Those exceed the derived off-set limits of 1-2 mm. It has to be noted that with ±3 standard deviations, a wide range of variation was considered. However, every patient needs to be provided with an adequate implant. In addition, all mean offsets were larger than 2 mm, suggesting that a relevant share of the patient population may receive an implant with local condylar offsets exceeding those limits. Some of the variation regarding size and aspect ratio is accounted for by different implant sizes and narrow/ standard implant versions. Remaining variation, however, is not accounted for with standard implants.

Limitations

The study presented involved limitations. First, the start and end points of the 2D and 3D J-Curves were determined automatically by curvature analysis and not by a visual inspection of the clinical images. However, this automation was necessary to enable the processing of a large number of cases. Second, the use of an extremum search for the

3D J-Curve determination still is an approximation of an actual course of tibiofemoral contact points on the femur. Actual contact points will depend among others on the tibial articulating shapes, on local cartilage thickness, on the ligamentous status, on muscle activity, and on the activity performed. However, the extremum search used in this study identified relevant points on the contours, which correspond to contact points of femoral and tibial implant components in TKA. Third, the database was limited to 90 cases of unknown ethnicity. Further analyses are necessary to investigate more cases and evaluate differences between ethnicities. In addition, this study is restricted to the analysis of the femur. Future analyses should also investigate the tibial sagittal contours and the patellofemoral contact (native vs. alloplastic).

Conclusions

The results of this study suggest that variation in the native femoral 2D and 3D J-Curves does not only involve scaling and aspect ratio changes, but other aspects such as changes in curvature or circularity, arc lengths, and relative location. Current OTS implant manufacturers offer various implant sizes (i.e., scaling only) as well as narrow and wide implants, accounting for differences in size and in aspect ratio. Differences in other aspects such as in curvature are not accounted for so far.

Summarizing, the research question addressed in this chapter can be answered as follows:

> *The analysis of the native 2D femoral J-Curve showed shape variation involving changes in contour orientation, arc length, scaling, circularity and relative positions. The analysis of the 3D J-Curves demonstrated similar aspects of shape variation as for the 2D J-Curve analysis, however, with a clearer differentiation of the individual aspects in the different modes. The effect on local J-Curve offsets exceeds the derived offset limits of 1-2 mm for preservation of ligaments and compatibility with the extensor mechanism function. The share of scaling attributed to ~52.0% of 3D J-Curve shape variation. Other 3D J-Curve shape variation described in this study (~36.3%), is not accounted for in the current OTS implant systems, which only incorporate a simple scaling.*

3.3 Correlation of size and morphology

In the previous chapter, shape variations independent of size have been demonstrated exemplarily for the femoral J-Curve. Consequently, the question arises to what extent the size of the knee correlates with individual measurements and what residuals remain in the case of an ideal size fit.

Hence, the research question addressed in this chapter is the following:

> *RQ3: Is there a correlation between the individual morphological parameters and the overall knee size? What residuals remain in the case of an ideal size fit?*

3.3.1 Materials and methods

A database consisting of morphologic parameters of 248 female and 146 male knees from TKA patients was available for the analysis (Asseln et al. 2018). In addition, a database of 421 cadaveric femora (273 male/ 146 female/ 2 without information) and a previously described subset of 90 cadaveric femora without osteophytes or other signs of OA were considered (56 male/ 32 female/ 2 without information) (**Chapter 3.2.2**). The parameters with the highest impact on kinematics were selected from a previous morpho-functional analysis (Asseln et al. 2021). Angular measurements were excluded, as those are not expected to correlate with size (Asseln et al. 2018). Hence, the lateral trochlear elevation and the distal and posterior sagittal radii were considered for the correlation and residuals analysis. The condylar ML size and the AP distance from the most anterior to the most posterior point of the femur in its bone-specific coordinate system were used as size parameters. Pearson correlation coefficients were calculated with the morphological parameters from plausible cases only (Asseln et al. 2018).

In addition, for each parameter and each case a regression model was built, following the leave-one-out procedure. Hence, all remaining cases were used to identify the coefficient estimates for the patient- and parameter-specific regression model. The femoral AP and ML size of the individual case were then used to predict the respective parameter. The residuals were analyzed regarding their range and the mean was calculated.

3.3.2 Results

The correlations of functionally relevant parameters with the overall size parameters ranged from 0.28 to 0.86 and are given in **Figure 3-14**. The correlations were highest in the healthy cadaver subset and lowest in the patient database. Regarding different parameters, the highest correlations were found for the lateral trochlear elevation with the AP size. The results of the regression analysis are presented in **Figure 3-15** and in **Table 3-7**. The mean absolute errors were lowest for the healthy cadaver subset and highest for the patient database.

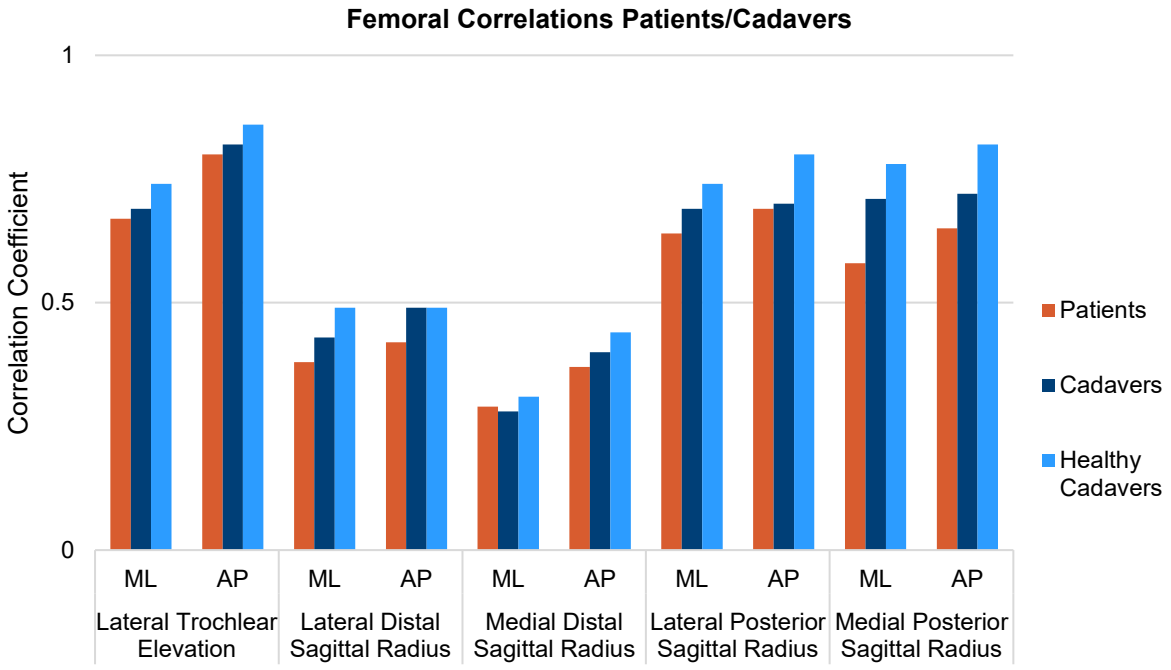

Figure 3-14: Correlations between overall size parameters and functionally relevant parameters of the distal femur for different populations.

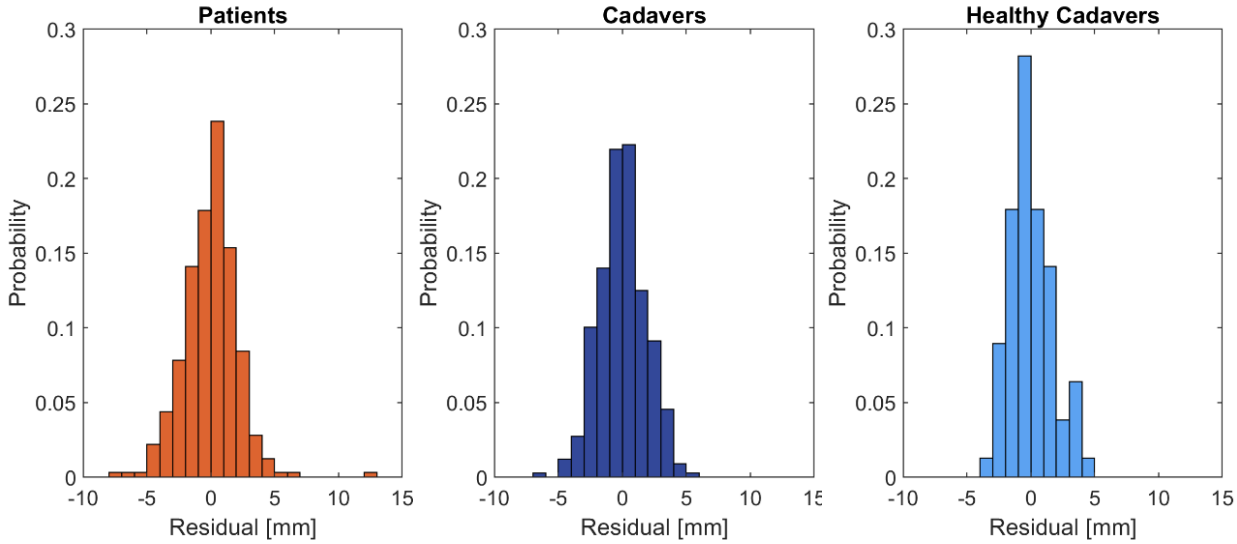

Figure 3-15: Residuals of the multiple linear regression analysis for the example of the lateral trochlear elevation.

Table 3-7: Results of the multiple linear regression analysis: The range and the mean of the residuals.

Parameter	**Residuals (**mean absolute error & range)		
Database	**Patients**	**Cadavers**	**Healthy Cadavers**
Lateral Trochlear Elevation (mm)	1.6 (-7.8/12.3)	1.5 (-6.1/5.5)	1.3 (-3.4/5.6)
Lateral Distal Sagittal Radius (mm)	4.6 (-11.3/33.6)	4.3 (-13.3/31.9)	4.2 (-10.6/31.2)
Medial Distal Sagittal Radius (mm)	4.4 (-13.0/33.7)	4.0 (-10.9/33.4)	3.9 (-11.0/14.7)
Lateral Posterior Sagittal Radius (mm)	1.2 (-6.4/4.4)	1.0 (-8.3/3.7)	0.9 (-3.1/3.8)
Medial Posterior Sagittal Radius (mm)	1.2 (-6.9/4.3)	0.9 (-3.6/3.5)	0.9 (-2.6/3.1)

3.3.3 Discussion

In this study, the correlations of functionally relevant parameters with the overall size parameters, showed a wide range. Higher correlations were seen for (healthy) cadavers than for patients, which suggests that morphologic relationships are affected by OA. However, the differences were limited (correlation coefficients: $\Delta \leq 0.2$, mean residuals: $\Delta \leq 0.5$ mm).

The overall highest correlation was seen for the lateral trochlear elevation and the femoral AP size. The strong relationship may be explained by the fact that the parameters' direction of measurement coincides, as already stated by Asseln et al. (Asseln et al. 2018). In contrast, the distal radii showed low correlations. An explanation could be, that their direction of measurement is not limited to one axis but spans the sagittal plane, while the proximodistal direction is not quantified by either AP or ML size.

The regression models based on femoral AP and ML size yielded variable prediction accuracy. In the healthy cadaver subset, a mean absolute error of below 2 mm and a small range of residuals was seen for the lateral trochlear elevation and the posterior sagittal radii. In contrast, a wide range of residuals was found for the distal radii. When interpreting the residuals, it has to be noted, that with the patient-specific regression model an implant with a perfect AP and ML size fit is imitated, which design is solely based on morphologic bone data. In contrast for actual OTS implants, often a compromise regarding the ML and AP fit is involved and technical restrictions do not allow for complete design freedom in patient specific implants either. Hence, actual deviations between functionally relevant parameter measures of the knee compared to those of the implant are expected to be even higher.

3.3.4 Conclusion

Summarizing, the research question addressed in this chapter can be answered as follows:

> *The correlation coefficients for the relationship of the knee size with the morphological parameters analyzed ranged from 0.28 to 0.86, depending on the parameter and population analyzed. Residuals in the case of an ideal fit frequently exceeded three standard deviations of the respective parameter value. Because of the often-required compromise in size fit and other technical design restrictions, acutal deviations are expected to be even higher.*

4. Concepts for detailed implant fit evaluation

Work in this chapter has been presented in parts in:

S. Grothues & K. Radermacher: X-ray based morphological analysis of the knee - a review. In: F. Rodriguez Y Baena, J.W. Giles & E. Stindel (ed.): Proceedings of The 20th Annual Meeting of the International Society for Computer Assisted Orthopaedic Surgery, 5, 2022, pp. 89-98 [DOI: 10.29007/sqcb]

4.1 Imaging for preoperative planning and fit assessment

Previous chapters have documented shape variations other than size variations of the femoral J-curve. Furthermore, limited correlations of morphologic parameters and overall size, as well as significant residuals in the case of an ideal size fit were determined. Thereby, the necessity for detailed, patient-specific implant fit evaluation was demonstrated.

To evaluate the implant fit with regard to a patient's individual knee morphology, image data are required. Depending on the imaging modality and image processing used, different concepts can be pursued. Standard imaging techniques and modern methodologies such as Upright CT or MRI respectively, 3D freehand US, as well as 2D-3D reconstruction from standard biplanar X-ray images are considered. In the context of TKA planning and implant fit assessment, the imaging techniques and respective processing methodologies can be evaluated regarding the following aspects:

- Accuracy
- Dimensionality *(2D/3D)*
- Representative position *(interbone parameter measurement)*
- Radiation dose
- Availability
- Contraindications
- Costs

For the imaging modality used to assess individual implant fit, the aim would be a minimal radiation dose, especially in younger patients. In addition, the availability of the imaging systems, respective contraindications, and costs are of relevance, in order to provide the service to the majority of TKA patients. Chairside imaging and bone-model reconstruction e.g., based on ultrasound or conventional x-rays potentially would enable the orthopedic consultant to instantaneously discuss and recommend optimal therapeutic options with the patient, potentially facilitating clinical workflows and increasing accessibility of optimal solutions for each individual patient. Further, an evaluation in 3D and a representative position (weight-bearing, active) would be advantageous, to enable a comprehensive and functional implant fit evaluation. For an adequate assessment, the reconstruction accuracy of the articulating surfaces (Hausdorff distance) would have to be 1 mm (Grothues and Radermacher 2021) to 3 mm (Mahoney and Kinsey 2010). However, differences in error definitions or missing specification of the metrics often complicate the assessment and comparison of reported accuracies. The characteristics of the different error metrics (MAE/ RMSE/ Hausdorff) and calculation methods used (point-to-point vs. point-to-surface, uni/bidirectional) must be considered when comparing reported accuracies. Respective characteristics and calculation methods are discussed in **Appendix A)**. The reported error limits for the articulating areas of 1-3 mm apply to the maximum absolute errors (or Hausdorff distance) and should be evaluated bidirectionally. The suitability and applicability of available imaging modalities and processing regarding the defined aspects are discussed in the following chapters.

4.1.1 Conventional radiographs

Conventional X-ray imaging is the gold standard for the diagnosis and for preoperative planning in TKA, hence the availability of respective imaging is high. In general, costs for X-ray imaging are comparably low, with an estimated total cost of 41.92$ for diagnostic radiography compared to 112.32$ for CT and 266.96$ for MRI in the study of Saini et al. (Saini et al. 2000). In addition, there are few contraindications to standard radiography. Reported radiation doses for a standard long-leg radiograph required for TKA planning from the literature are in the range of 0.1 mSv (Kloth et al. 2015; Aunan et al. 2023). Radiographs can be taken in various positions, hence, an assessment of

interbone parameters is possible in the active, weight-bearing position. With standardized positioning and the use of scaling objects, an assessment of morphologic parameters from single X-ray images is possible. However, the overall accuracy of measurements from radiographs still is lower compared to that of 3D imaging (Holme et al. 2011; Jud et al. 2020). In addition, when a parameter definition is based on landmarks that are inaccurately defined or are difficult to identify, large errors or deviations in measurement can occur. Therefore, an evaluation of inter- and intrarater reliability is necessary. **Table 4-2** lists parameters of the distal femur and **Table 4-1** those of the proximal tibia, to be evaluated on single X-rays, for which accuracies are reported. To achieve adequate measurements, requirements are defined, such as true lateral images or a scaling object. However, these requirements are similar to requirements for digital implant planning software. Seven studies evaluated intra class coefficients (ICC) for the respective parameter definitions, which ranged from 0.64 to 0.99 for interobserver- and from 0.77 to 0.98 for intraobserver reliability. Those ICCs can be interpreted as good to excellent (Cicchetti 1994) or moderate to excellent (Koo and Li 2016).

Table 4-1: Tibial morphological parameter definitions for the evaluation on single X-ray images. KF = Knee Flexion. AP = Anteroposterior. PA = Posteroanterior. * = more specific description to be found in the respective article. Studies for which both Inter- and Intra-Observer ICCs are above 0.75 (≙ excellent agreement (Cicchetti 1994) or good to excellent (Koo and Li 2016)) are highlighted in green.

Parameter name	**Xray info & requirements**	***in vivo/ in vitro*** (number of subjects/ knees)	**Reliability measure**	**Inter-observer reliability**	**Intra-observer reliability**	**source**
Anteroposterior depth [mm]	Lateral	*in vivo* (157/157)	ICC	~0.82	~0.89	(Zhang et al. 2018)
Posterior slope [°]	Lateral	*in vivo* (157/157)	ICC	~0.77	~0.9	(Zhang et al. 2018)
Mediolateral width [mm]	AP	*in vivo* (157/157)	ICC	~0.85	~0.85	(Zhang et al. 2018)
Coronal tibial slope (reference = anatomical axis) [°]	AP	*in vivo* (157/157)	ICC	~0.79	~0.89	(Zhang et al. 2018)
Plateau angle (reference = anatomical axis) [°]	AP, Weight-bearing	*in vivo* (390/n.a.)	ICC	0.93	0.89	(Higano et al. 2016)
Medial proximal tibial angle (reference = mechanical axis) [°]	AP, Standard, weight-bearing	*in vivo* (n.a./20)	ICC	0.979 (95% CI 0.948 – 0.992)	0.980 (95% CI 0.950 – 0.992)	(Springer et al. 2020)

Table 4-2: Femoral morphological parameter definitions for the evaluation on single X-ray images. KF = Knee Flexion. AP = Anteroposterior. PA = Posteroanterior. * = more specific description to be found in the respective article. Studies for which both Inter- and Intra-Observer ICCs are above 0.75 (≙ excellent agreement (Cicchetti 1994) or good to excellent (Koo and Li 2016)) are highlighted in green.

Parameter name	**Xray info & requirements**	***in vivo/ in vitro*** (number of subjects/ knees)	**Reliability measure**	**Inter-observer reliability**	**Intra-observer reliability**	**source**
Sagittal depth of the condyles [mm]	Lateral, Standard	*in vivo* (100/100)	Correlation coefficients	0.98	0.89	(Fridén et al. 1993)
Height of the condyles [mm]	Lateral, Standard	*in vivo* (100/100)	Correlation coefficients	0.96	0.95	(Fridén et al. 1993)
Posterior Condylar Offset [mm]	True lateral, overlapping condyles*	*in vivo* (n.a./105)	ICC	0.84 (95% CI 0.1 -0.95)	0.94 (95% CI 0.74-0.98	(Clement et al. 2014)
Posterior Condylar Offset Ratio (divided by cortical depth)	True lateral, overlapping condyles*	*in vivo* (n.a./105)	ICC	0.93 (95% CI 0.86-0.97)	0.9 (95% CI 0.63-0.96)	(Clement et al. 2014)
Posterior Condylar Offset Ratio (divided by condylar depth)	True lateral, overlapping condyles*	*in vivo* (100/100)	ICC	0.882	0.899	(Johal et al. 2012)
Lateral femoral condyle ratio	Lateral, Condylar overlap < 6mm	*in vivo* (200/n.a.)	ICC	0.80	0.77	(Pfeiffer et al. 2018)
Medial condyle height ratio	PA, Rosenberg, 45° KF	*in vivo* (66/n.a.)	ICC	0.64	n.a.	(Minami et al. 2018)
Lateral condyle height ratio	PA, Rosenberg, 45° KF	*in vivo* (66/n.a.)	ICC	0.72	n.a.	(Minami et al. 2018)
Joint line angle (method 1) [°]	AP, Standard	*in vitro* (n.a./5)	ICR (Eliasziw et al. 1994)	0.796 (95% CI 0.675–1.0)	0.973 / 0.85	(Weber et al. 2013)
Joint line angle (method 2)	AP, Standard	*in vitro* (n.a./5)	ICR (Eliasziw et al. 1994)	0.836 (95% CI 0.742–1.0)	0.958 / 0.832	(Weber et al. 2013)
Anatomical lateral distal femur angle [°]	AP, Standard, weight-bearing	*in vivo* (n.a./20)	ICC	0.992 (95% CI 0.979 - 0.997)	0.984 (95% CI 0.959 - 0.994)	(Springer et al. 2020)
mechanical lateral distal femur angle [°]	AP, Standard, weight-bearing	*in vivo* (n.a./20)	ICC	0.989 (95% CI 0.971-0.996)	0.978 (95% CI 0.944-0.991)	(Springer et al. 2020)

In conclusion, there are many advantages of a fit evaluation using standard X-Ray imaging, including low cost and high availability. In addition, several parameters with excellent inter- and intra-rater reliability have been presented in the literature. However, the number of parameters to be evaluated is limited due to the restriction to the frontal and sagittal plane. For example, radiographs can only provide an assessment of the projected bone-implant interface in the specific view (2D), which is a significant drawback compared to an adequate assessment of the full interface contour by CT (Simsek et al. 2020). Nevertheless, an X-ray based evaluation can serve as an **initial fit assessment**, to determine whether a more extensive OTS implant fit analysis by means of CT or even a customized implant should be advised.

4.1.2 Computed tomography and magnet resonance imaging

For the design of patient-specific instruments and implants, 3D imaging with high accuracy is required and hence regularly a CT (or MRI) is performed for these applications. In general, CT is the gold standard for bone segmentation. Magnetic resonance imaging (MRI) has been found to have similar accuracy compared to CT (Rathnayaka et al. 2012; Al Hares), with an exemplary RMSE of 0.85 mm for CT and of 0.98 mm for MRI for femoral bone models (Stephen et al. 2021). However, MRI is not routinely used for bone segmentation and has potential drawbacks due to motion artifacts. The disadvantages of both MRI and CT include comparably high cost (CT: 112.32$, MRI: 266.96$ (Saini et al. 2000)), limited availability and resulting waiting time. Furthermore, contraindications exist for the MRI such as pacemakers, metal implants, and severe claustrophobia, and higher costs compared to CT are involved. A disadvantage of CT is the comparably high radiation dose involved. The mean effective dose of a radiograph of the pelvis is 0.27 mSv whereas for a corresponding CT it is 4.2 mSv (Die Strahlenschutzkommission 2019). Specific CT protocols for TKA planning have been introduced, with the aim of a reducing the respective radiation dose (Henckel et al. 2006; Chauhan et al. 2004). Finally, regular CT and MRI systems only allow for imaging in supine position, which is detrimental with regard to the assessment of the joint space and/or interbone parameters. Specialized upright MRI, CT and orthopedic cone-beam computed tomography (CBCT) systems exist, but involve the disadvantage of an even lower availability (and - in case of upright MRI – image quality/resolution). Alternatively, the limitation of the supine position could be overcome when matching the detailed CT based bone models to X-ray images acquired in standing, wheight-bearing position. In conclusion, depending on the age of the patient, either CT imaging with specific TKA protocols for minimizing radiation or alternatively MRI (in younger patients) are adequate options for detailed 3D imaging of the knee. However, the benefits of the detailed imaging and planning must be weighed against the high costs associated with both imaging techniques and, in the case of CT, also against the induced radiation dose.

4.1.3 2D-3D reconstruction

Reconstructing surface models from individual radiographs is advantageous as it shares the benefits of conventional radiographs while potentially allowing for comprehensive 3D

assessment. However, adequate accuracy of the reconstruction would first have to be ensured. The EOS system (EOS imaging, Paris, France) enables the acquisition of biplanar imaging data of the entire body with low radiation dose (Guenoun et al. 2012). The images are taken in the weight-bearing position. In combination with the sterEOS software surface models of the bony structures can be created from the acquired image data (Illés and Somoskeöy 2012). The most relevant disadvantage of the EOS system is a lower resolution compared to CT. Therefore, the system is mainly suitable for the analysis of large body sections, but cannot replace CT, especially when detailed images of small body areas are required (Stein et al. 2019). Consequently, the relevance of EOS in the context of TKA has increased, with regard to measurement of leg alignment parameters (Corbett et al. 2023; Schlatterer et al. 2009), however the resolution to date is expected to be insufficient for the design of patient-specific instruments and implants of the knee.

Several other workflows and/or methodologies for X-ray based 2D-3D reconstruction have been reported in the literature. Studies reporting on the respective reconstruction accuracies are listed in **Table 4-3**. Methods applied for 2D-3D reconstruction include, for example, the use of statistical shape models (Baka et al. 2011; Cerveri et al. 2017; Wu and Mahfouz 2021; Zheng et al. 2018) and/or bone databases/atlases (ElHak et al. 2007; Messmer et al. 2001). The imaging data used included standard/calibrated radiographs, EOS^{TM}/fluoroscopy images or digitally reconstructed radiographs (DRRs). Studies using DRRs were classified as *in vivo* & *in silico* or *in vitro* & *in silico*, according to the data source (subjects/cadavers). Different error metrics were reported in the literature, including the mean absolute error (MAE), the root mean square error (RMSE) and the Hausdorff distance. Furthermore, different calculation methods were applied, such as point-to-point (P2P) and point-to-surface (P2S) distances. In addition, one group quantified normal/projected error vectors (Shetty et al. 2021). Errors were either computed unidirectionally, or no information regarding directionality was provided.

Table 4-3: Accuracy of 2D-3D reconstruction from a small number of X-ray images compared to 3D models from CT. Various different error metrics were used and often no specification regarding directionality and type of measurement (P2P/P2S) was given, which complicates the assessment and comparison of the studies' results. (MAE = Mean absolute error, MaxAE = Maximum abslute error, DRR = digitally reconstructed radiographs, CI = confidence interval, P2P = Point to Point, P2S = Point to Surface. * Evaluated at specific landmarks ** Evaluated normal to plane.)

Source	**Image type, number**	**Study type, n bones**	**Bone(s)**	**Accuracy [mm]**				**Specifics**	
				Error Metric 1		**Error Metric 2**		**Uni-/ bi-dir.**	**P2P / P2S**
(Chaibi et al. 2012)	EOS, 4	*in vitro*, 11	Tibia& Femur	MAE (CI 95%)	1.0 (2.4)	MaxAE	6.6	uni	P2S
(Mahfouz et al. 2006)	DRRs, 2	*in vivo/ in silico*, 1	Femur	MaxAE	0.46			/	P2S
(Zheng et al. 2018)	EOS (+ fixation device), 2	*in vivo*, n.a.	Femur	MAE ± SD	1.4 ± 0.3	Hausdorff dist. (One-Sided)	6.6 ± 1.6	uni	P2S
			Tibia	MAE ± SD	1.2 ± 0.3	Hausdorff dist. (One-Sided)	5.6 ± 1.7		
(ElHak et al. 2007)	X-rays biplanar 2	n.a.	Femur	MAE	1.9			/	P2P
			Tibia	MAE	1.82				
(Gamage et al. 2009)	X-rays, 2	*in vitro*, 6	Femur	MAE	0.86				
(Quijano et al. 2013)	DRRs, 2	*in vitro/ in silico*, 9	Femur	MAE (CI 95%)	1.3 (3.5)	MaxAE	8.2	/	P2S
			Tibia	MAE (CI 95%)	1.3 (3.2)	MaxAE	8.1		
			Distal Femur	MAE (CI 95%)	1.2 (3.1)	MaxAE	6.5		
			Proximal Tibia	MAE (CI 95%)	1.3 (3.2)	MaxAE	8.1		
(Schmutz et al. 2008)	X-rays Calibrated, 2	*in vitro*, 7	Distal Femur	MAE	1.21	MaxAE	5.81	/	P2P
(Laporte et al. 2003)	X-rays Calibrated, 2	*in vitro*, 8	Distal Femur	MAE	1.0	RMSE	1.4	uni	P2S
(Baka et al. 2011)	X-rays Calibrated, 5	*in vivo*, 30	Distal Femur	RMSE ± SD	1.68 ± 0.35			uni	P2S
(Cerveri et al. 2017)	DRRs, 3	*in vivo/ in silico*, n.a.	Distal Femur	RMSE	0.75	Hausdorff distance	1.5	/	/
(Tchinde Fotsin et al. 2019)	DRRs (orthogonal), 2	*in vivo/ in silico*, 109	Distal Femur	RMSE	0.72	Max. RMSE	1.38	/	/
			Proximal Tibia	RMSE	0.99	Max. RMSE	1.81		
(Messmer et al. 2001)	X-rays (+ fixation device) 2	*in vitro*, 1	Tibia (condyles)	MAE ± SD	2.4 ± 0.82	MaxAE	4.5	/	/
(Shetty et al. 2021)	Xrays Calibrated, 2	*in vivo*, 45	Distal Femur	MAE ± SD	1.0 ± 0.9	MaxAE	1.7	uni	P2S**
			Proximal Tibia	MAE ± SD	1.1 ± 1.0	MaxAE	1.7		
(Wu and Mahfouz 2021)	Fluoroscopy, 1	*in vivo*, 5	Distal Femur	RMSE ± SD	1.19 ± 0.36	/		/	/
			Proximal Tibia	RMSE ± SD	1.15 ± 0.17				
	Fluoroscopy and standard Xray, 2	*in vivo*, 5	Distal Femur	RMSE ± SD	1.04 ± 0.33				
			Proximal Tibia	RMSE ± SD	1.03 ± 0.19				

In conclusion, few methods for 2D-3D reconstruction showed MAE or RMSE in the submillimeter range and maximum absolute errors below three millimeters. In addition, the respective studies solely included *in silico* analyses, based on DRRs. One *in vivo* study reported a normal maximum absolute error of 1.7 mm (Shetty et al. 2021). The projection of the error vectors may be the reason for the comparably low maximum absolute error. Other *in vitro* studies showed maximum absolute (P2S/ P2P) errors of ~5-6 mm, and hence do not reach the required accuracy, defined in the introduction (**Chapter 4.1**). In addition, most studies required image calibration or EOS images, limiting their availability. The small study populations constitute a further limitation. Therefore, the accuracy of *in vivo* reconstruction of knees of different morphotypes, ethnicities, etc. may be significantly lower than reported in the literature. For these reasons, 2D-3D reconstruction is a promising option to allow for more comprehensive analyses, solely on the basis of (conventional) radiographs. However, maximum errors reported are still too high for a fit assessment in TKA.

4.1.4 3D freehand/ robotic ultrasound

Ultrasound (US) imaging is widely available, there is no harming radiation involved and costs are comparable to standard radiography, with an estimated cost of 50.28$ in the study of Saini et al. (Saini et al. 2000). Limitations of US images involve a low signal to noise ratio and that tissue types cannot be mapped to specific gray values as is the case with radiographs or CT, which complicates US interpretation and (automated) segmentation. The application of convolutional neural networks to the segmentation task have increased segmentation accuracy and resulted in a minimal RMSE of 0.64 mm (SD = 1.66 mm) in the study of Pandey et al. (Pandey et al. 2022). Respectively segmented point clouds from US images can be completed to 3D models using statistical shape models, which led to a mean surface distance error of 0.96 mm (1.24 mm) for the articulating area of the distal femoral (proximal tibial) bone surface in an *in vivo* study of 10 subjects by Hohlmann et al. (Hohlmann et al. 2023). Analyses of larger control groups and of OA patients are pending. Instead of freehand guidance of the US probe, more recently robotic assistance has been applied for the purpose of automation, to reduce the need for sonography specialists (Phlippen et al. 2023). Remaining limitations include relevant maximum errors (Hausdorff distance ~3mm), a limited robustness (Phlippen et

al. 2023), and pending evaluations in standing position with potentially required compensation of motion artefacts. In conclusion, a high potential for the application of 3D freehand and robotic US imaging in the context of knee implant fit assessment has been found, while the listed limitations first have to be overcome.

4.1.5 Conclusion

In the previous sub-chapters, available imaging modalities considered for the use in knee implant fit assessment were discussed and evaluated with respect to previously defined criteria. A summary of the evaluation is given in **Table 4-4**.

Table 4-4: Evaluation of imaging modalities and processing methods regarding suitability for implant fit assessment. **Sources:** Radiation dose (Henckel et al. 2006; Chauhan et al. 2004; Dartus et al. 2021), Availability (Wenham et al. 2014), Cost (Saini et al. 2000), Accuracy (Zheng et al. 2018; McPherson et al. 2005; Dartus et al. 2021). Imaging modalities and processing methods used for the two concepts proposed are highlighted by a black box.

	Radiation dose (effect. Dose)	**Contra-indications**	**Availability**	**Cost**	**Accuracy**	**3D**	**Upright**
X-ray (2D)						x	✓
X-ray (2D-3D)						✓	✓
US (3D)						✓	
CT						✓	x
CT Perth Protocol						✓	x
CT Imperial Protocol						✓	x
CT Imperial Protocol + **EOS** match.						✓	✓
MRI						✓	x
Upright CT						✓	✓
Upright MRI						✓	✓
Cone beam CT						✓	✓

Ideal case (example: no radiation) : ■ | Undesirable case (example: highest radiation dose in this comparison) : ■. Gradations in between are color-coded accordingly.

Based on the information collected, two concepts were developed, using either **(1)** X-rays & CT or **(2)** 3D freehand/ robotic US imaging. The respective workflows of the two concepts are displayed in **Figure 4-1**. The first workflow begins with a basic fit assessment based on conventional X-rays, which are regularly available for diagnosis and preoperative planning in TKA. Reliable parameter definitions from **Chapter 4.1.1** can be used to preliminarily assess the fit of standard implants. Consecutively, a decision for an OTS and 2D planning or for further analysis via CT can be made. To minimize the radiation dose, adequate methods or protocols specific to TKA planning should be used

(Henckel et al. 2006; Chauhan et al. 2004; van Sint Jan et al. 2006). A matching with biplanar x-ray or EOS images respectively enables the assessment of morpho-functional interbone parameters in weight bearing position. With the CT analysis, a detailed fit assessment is enabled, which can be used for a profound decision-making between a standard and a customized implant. With the second workflow, 3D freehand/ robotic US imaging is used to directly derive a surface model and enable the detailed fit assessment. This concept includes the advantages of a chairside fit assessment and patient information. The respective workflows of the two concepts are displayed in **Figure 4-1**.

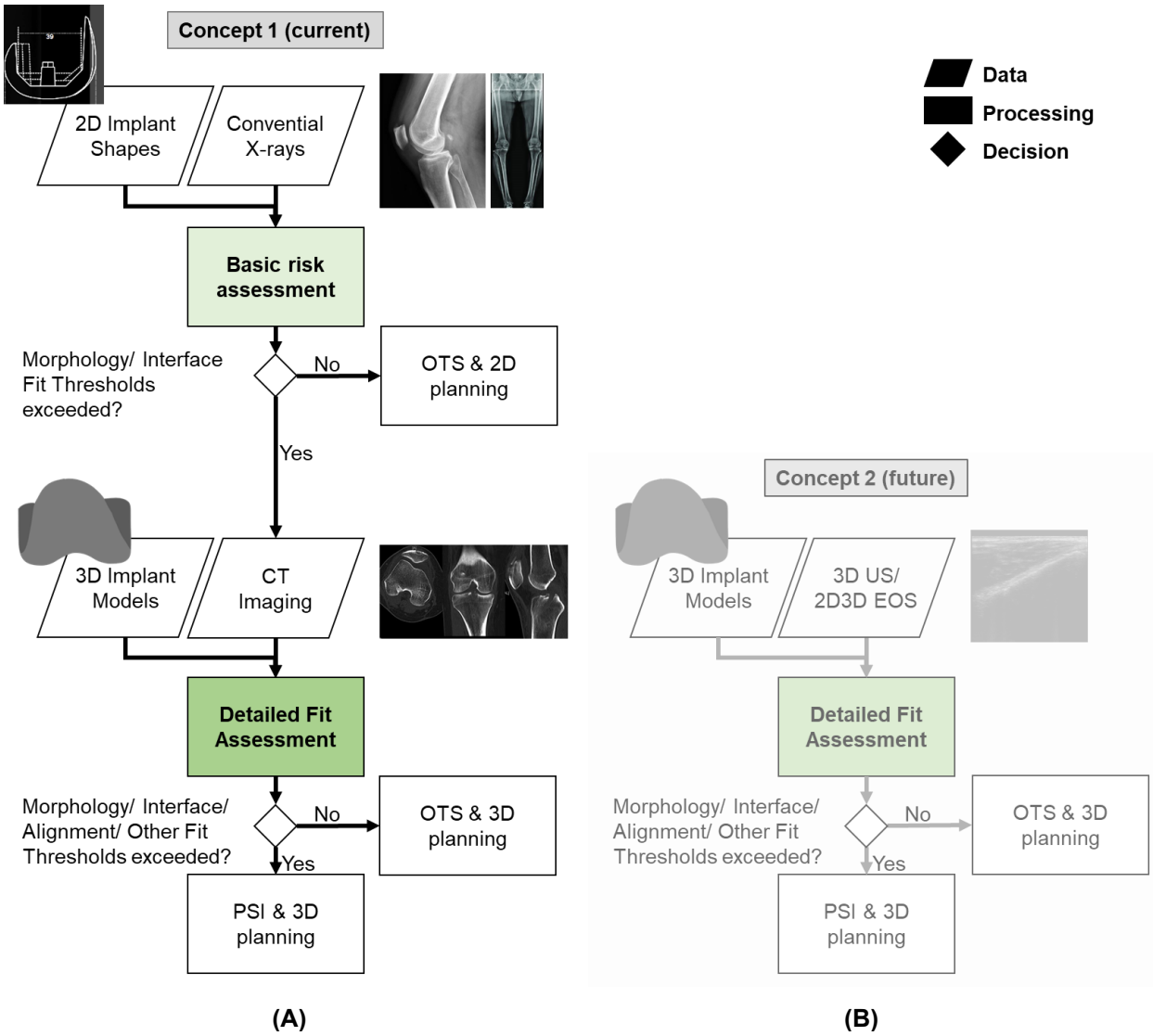

Figure 4-1: Two concepts for implant fit assessment. **(A)** Concept 1: current concept with an initial basic fit assessment based on conventional radiographs and if required additional comprehensive fit assessment based on CT imaging. **(B)** Concept 2: future concept with direct detailed fit assessment based on surface models from 3D freehand/ robotic US imaging or 2D3D reconstruction from biplanar X-rays. Workflow visualization according to DIN 66001 (DIN DIN 66001).

The central aspect of both concepts (current/ future) is the detailed 3D fit assessment. In the future, any method for the derivation of 3D bone surfaces with sufficient accuracy can be used and the results applied to the frameworks developed, independent of their origin.

4.2 Criteria for implant fit assessment

Work in this chapter has been presented in parts in:

S. Grothues & K. Radermacher: Criteria for Implant Fit Assessment in Total Knee Arthroplasty – A Review. Current Directions in Biomedical Engineering, 8(2), 2022, pp. 165-168 [DOI: 10.1515/cdbme-2022-1043]

4.2.1 Introduction

With the imaging data specified, criteria for implant fit assessment are to be identified. In clinical practice, only a limited assessment of the implant fit is performed, regularly restricted to the matching of the AP and ML size of the bone and the implant component. For an optimal selection of implant size and design during preoperative planning, further criteria with relevance for patient satisfaction and functional outcome should be considered. Hence, the goal of this review was to identify and structure relevant criteria for an implant fit evaluation for cruciate retaining TKA.

The research question addressed in this chapter is the following:

> *RQ4: Are objective criteria available for patient-specific morphological and functional implant fit evaluation?*

4.2.2 Literature Research

Methods

A literature review was performed in PubMed. As keywords “Implant”, “Design”, “Knee” and “Fit” were used. The reference lists of the articles included were also scanned for further articles. Implant fit was considered not only as matching of interface, size and shape, but also to include the implant’s (rotational) alignment, as proposed by Dai et al.

(Dai et al. 2014a). The (rotational) component alignment is determined by the surgeon during implant positioning. However, many authors have described compromises being required between the rotational alignment, bony coverage and implant overhang (Dai et al. 2014a; Hirakawa et al. 2017; Martin et al. 2014). Hence, a fit evaluation should account for such a compromise as it reflects the compatibility of the implant design with the patient's anatomy.

Several exclusion and inclusion criteria were defined for the review. Inclusion criteria were a patient-specific fit evaluation of the geometry of knee implant components (uni-, bi- or tri-compartimental (ISO ISO 7207-1)). Further inclusion criteria were a comprehensible motivation for the fit criterion including a description of the (potential) relationship to the postoperative outcome, and a clear measurement description. Criteria regarding the constraint level and type of fixation were excluded, as CR implants are focused on. In addition, criteria with only one literature reference were excluded.

In order to structure the results, the fit criteria were assigned to the following categories: morphology, alignment, interface, other. Morphologic criteria were defined as metrics for the restoration of individual morphologic parameters, such as the posterior condylar offset. The category of alignment criteria was defined to include goals regarding overall limb alignment and implant component positioning. Interface criteria were defined as metrics of the bone-implant interface. All parameters that could not be classified were assigned to the category other criteria.

Results

Overall, 64 studies reporting on 151 criteria for implant fit evaluation were found, that met the inclusion criteria. An overview of the number of studies in the different categories is displayed in **Figure 4-2**. Studies identifying a statistically significant relationship between a fit criterion and an outcome measure are listed in **Table 4-5**. In each study, only few of the summarized criteria were evaluated. An exception represents the study of Dai et al. (Dai et al. 2014a), who have analyzed implant fit for the tibia comprehensively, including an assessment of the interface, morphology and the alignment fit. Criteria of the different categories are discussed in more detail in the following paragraphs.

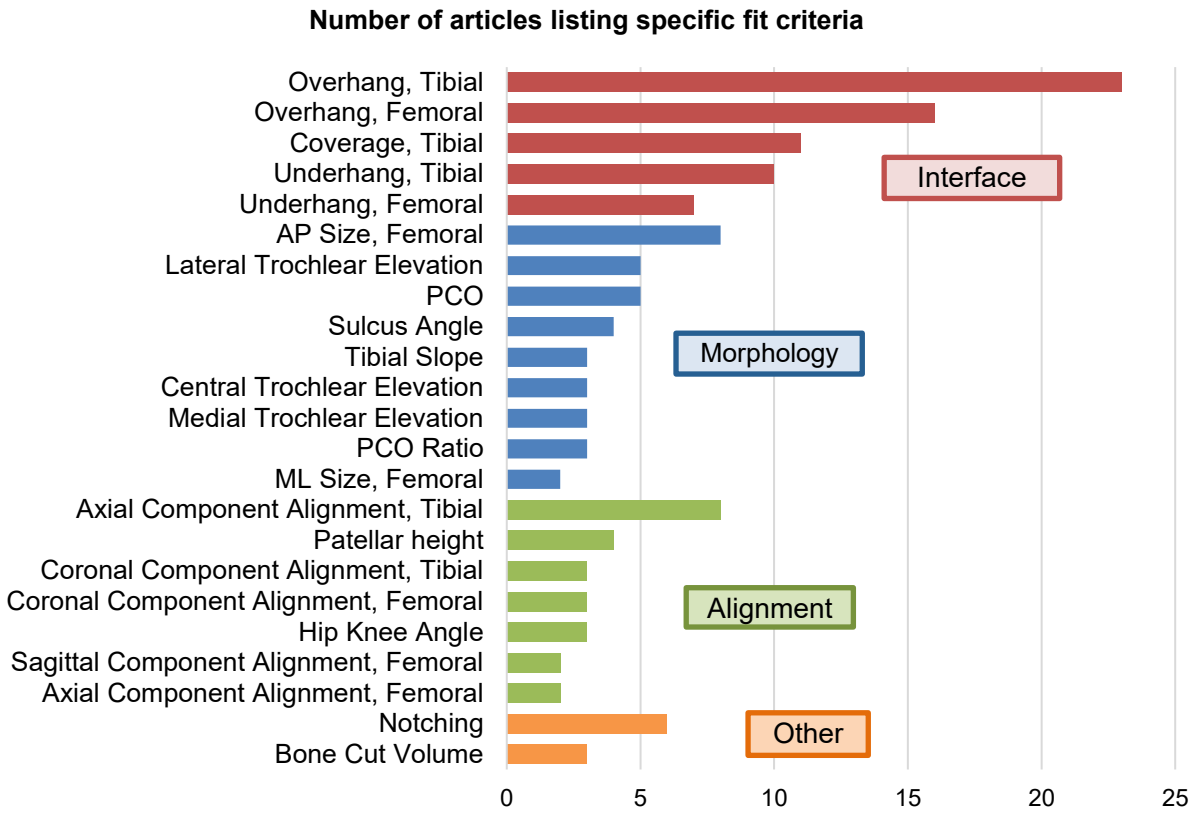

Figure 4-2: Quantitative results of the literature review.

Table 4-5: Implant fit criteria for which a relationship with an outcome measure is indicated based on statistical analysis. ROM: Range of motion. VAS: Visual Analog Scale, -P: Pain sub-score, -F: Function sub-score. Filling indicates the category of the criteria: interface (red), morphology (blue), alignment (green).

Fit Criterion	Data Basis	Outcome Measure	Source
Overhang, Femoral	Image (CT)	KOOS-P, Flexion ROM	(Bonnin et al. 2013)
	Intraoperative measurement	Pain (standardized telephone interview)	(Mahoney and Kinsey 2010)
	Image (Xray)	Flexion ROM	(Chung et al. 2015)
Overhang, Tibial	Image (CT)	Flexion ROM	(Bonnin et al. 2013)
	Image (Xray)	KSS & WOMAC-P (for medial overhang)	(Liu et al. 2021)
	Image (CT)	KSS, KSS-F and WOMAC-P	(Simsek et al. 2018)
	Image (Xray)	OKS & OKS-P (5 years postop)	(Chau et al. 2009)
	Image (CT)	KOOS Score	(Klasan et al. 2020)
Underhang, Tibial	Image (Xray)	Tibial bone resorption (for medial & lateral underhang)	(Liu et al. 2021)
	Image (Xray)	Tibial bone resorption	(Gu et al. 2019)
Coverage, Tibial	Image (CT)	KOOS Score	(Klasan et al. 2020)
Posterior Condylar Offset	Image (Xray)	Flexion ROM	(Bellemans et al. 2002)
Axial Component Alignment, Femoral	Image (CT)	KSS-P	(Nicoll and Rowley 2010)
Axial Component Alignment, Tibial	Image (CT)	Anterior Knee Pain (VAS)	(Barrack et al. 2001)
	Image (CT)	Patellofemoral complications requiring revision	(Berger et al. 1998)
	Image (CT)	KSS-P	(Nicoll and Rowley 2010)
Axial Component Alignment, Combined	Image (CT)	Patellofemoral complications requiring revision	(Berger et al. 1998)
	Image (CT)	KSS-P	(Nicoll and Rowley 2010)
	Image (CT)	Anterior Knee Pain (VAS)	(Barrack et al. 2001)
Coronal Component Alignment, Tibial	Image (Xray)	Implant failure rate	(Ritter et al. 2011)
	Image (Xray)	KSS-F	(Rassir et al. 2021)
Coronal Component Alignment, Femoral	Image (Xray)	Implant failure rate	(Ritter et al. 2011)
Sagittal Component Alignment, Femoral	Image (Xray)	Flexion contracture >10°	(Okamoto et al. 2019)
Hip Knee Angle	Image (Xray)	Implant failure rate	(Ritter et al. 2011)
Patellar Height	Image (Xray)	OKS	(Rassir et al. 2021)

Interface criteria

The evaluation of interface criteria was the focus in TKA fit assessment reported in the literature. Overhang was assessed the most, followed by underhang and the tibial (cortical rim) coverage. Most authors performed a 3D analysis (femur: 80%, tibia: 67%). With the 3D evaluation, overhang and underhang was evaluated in different zones. Exemplary zones from the literature are summarized in **Figure 4-3**. Coverage can either be evaluated over the entire interface, in similar zones as defined for overhang and

underhang, or solely at the cortical rim (Fitzpatrick et al. 2007; Carpenter et al. 2014). With the specification to the cortical rim the authors aimed to quantify the risk for subsidence of the implant, which is expected to be higher when the implant is not positioned at the cortical rim and instead in the inner area, with higher levels of spongiotic, less durable bone. The evaluation of interface criteria during the planning process is partly realized in modern 3D planning software, for example an analysis of implant overhang in the SurgiCase Knee Planner, Version 3.4 (Materialise, Leuven, Belgium). However, such planning is currently not part of the clinical routine.

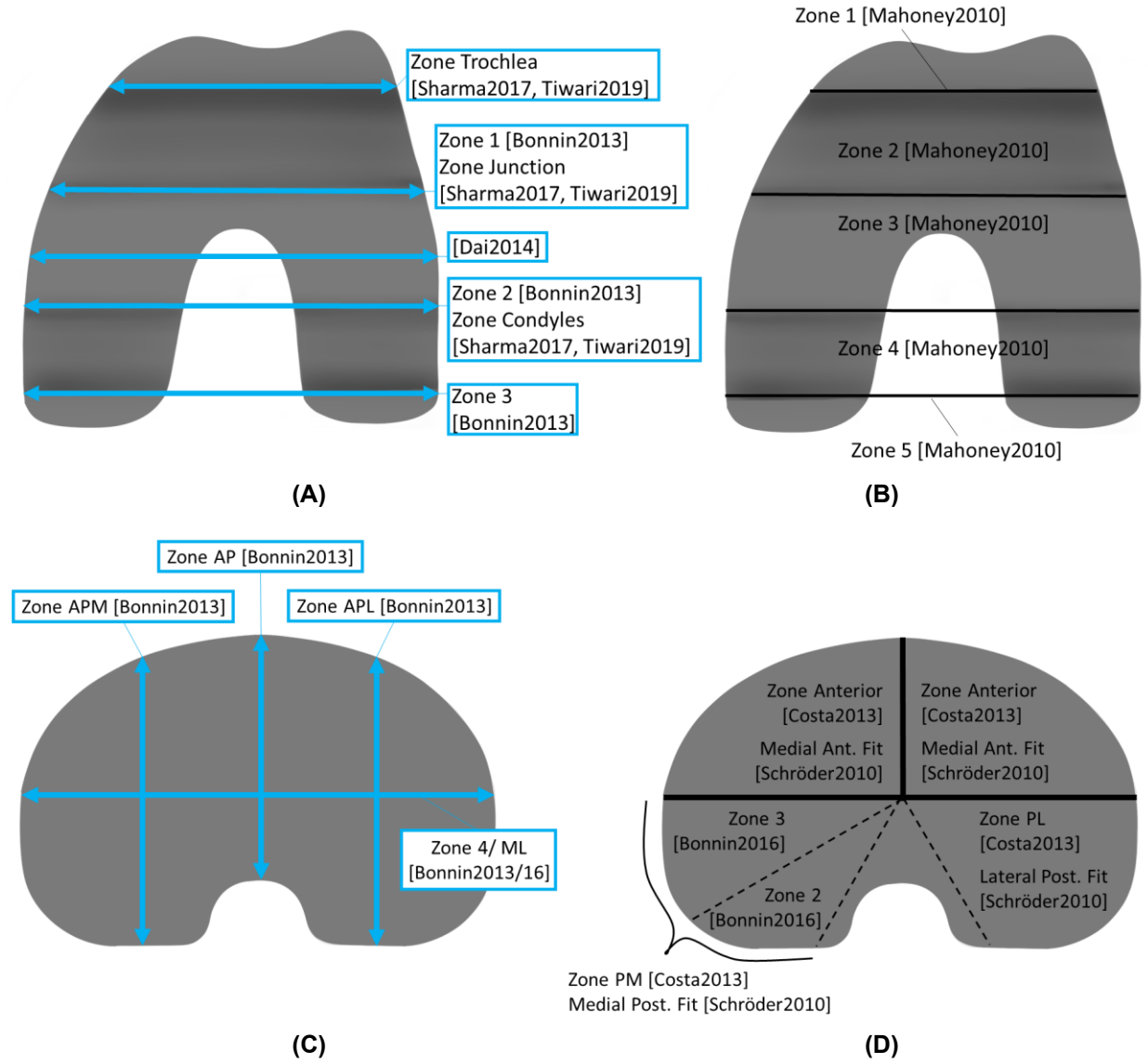

Figure 4-3: Exemplary anatomical zones for the evaluation of over-/ underhang in TKA for the femoral and tibial component. (A) Femoral ML over-/ underhang measurements at specific anatomical lines. (B) Femoral medial/lateral over-/ underhang measurements in specific anatomical zones. (C) Tibial over-/ underhang measurements at specific anatomical lines. (D) Tibial over-/ underhang measurements in specific anatomical zones.

Morphological criteria

The matching of specific morphological parameters was the second most frequently assessed type of criterion. Bellemans et al. (Bellemans et al. 2002) reported a statistically significant correlation between a decreased PCO and a decreased postoperative flexion range of motion. Other criteria identified relate to parameters of the femoral trochlea, such as the sulcus angle and the trochlear elevations, motivated by a potential relationship with patella tracking and stability (Itou et al. 2021; Asseln 2019; Asseln et al. 2021). The restoration of the native knee morphology is further motivated by the relevance for preserving physiological proprioception, among others, by restoring preoperative strain of the ligaments.

One must consider that respective morphological fit criteria cannot directly be applied to the preoperative knee shape in the case of severe deformities such as trochlear dysplasia. Respective deformities may have contributed to a pathological loading and contact pressure of the articulating surfaces and thereby to OA. Hence, in these cases a deformity correction is required, before the evaluation of morphological criteria.

Alignment criteria

Physiological limb alignment is one main aspect which is restored or achieved with TKA (**Chapter 2.2.1**). Several alignment criteria are routinely assessed in TKA, both pre- and postoperatively. However, they are regularly not connected to an implant (fit) evaluation. In addition, for the detailed alignment of the components for example, the tibial component IE rotation, different targets and different safe zones are reported. Dai et al. (Dai et al. 2014a) proposed the accuracy in rotational alignment as a fit criterion for the tibial component. This inclusion was motivated by the often-required compromise between coverage, overhang, and alignment. Similar compromises may be necessary for the positioning of the femoral component (Chen et al. 2017b; Okamoto et al. 2019). In general, axial alignment of both the femoral and the tibial components has proven to be a relevant influence factor for postoperative pain scores (**Table 4-5**). For coronal component alignment, Ritter et al. (Ritter et al. 2011) have reported a statically significant relationship with implant failure rates. Lee et al. (Lee et al. 2018) have reported femoral component varus malpositioning to be the primary source of overall varus outliers (> 3°)

and an independent risk factor for aseptic loosening. Sagittal alignment targets have been motivated by adverse effects on stability, range of motion, wear and ligament stress, with changes in the preoperative vs. postoperative tibial slope (Ahmad et al. 2016).

More recently, parameters describing bone relative position have been discussed in the context of TKA (Hochreiter et al. 2019). Those “interbone” parameters include for example the TT-TG distance and the patellar height. In the literature, the assessment of patellar height was motivated e.g., by a relationship with the OKS (Rassir et al. 2021). The TT-TG distance is expected to influence patellofemoral kinematics, such as patellar tilt after TKA (Nakamura et al. 2019). Interbone parameters are often influenced by many factors, such as the effective TT-TG distance by the position of the TT point, the ASIS, the trochlea shape and orientation, and the patella shape. In TKA, an altered trochlea shape or orientation can thus potentially be compensated by an adjusted patella component geometry, and thus also maintain a physiological TT-TG distance (= functional compatibility). This functional compatibility with the patient’s anatomy can thus be partially captured by interbone parameters. In conclusion, the relevance of alignment criteria has been motivated by impact on pain, function and implant survivorship and exemplary targets were identified. The list of interbone (alignment) criteria is limited, and should be extended, due to their potential as indicators for functional compatibility.

Other criteria

Other fit criteria reported in the literature include femoral notching and the bone cut volume. Notching represents an over-resection of the anterior femoral shield and is classified regarding severity, depending on the depth of the resection cut in the femoral diaphysis (Gujarathi et al. 2009). Several authors have reported a relationship between the presence of femoral notching and of periprosthetic fractures (Culp et al. 1987; Aaron and Scott 1987), which has been attributed to a weakening of the anterior cortex (Lesh et al. 2000). A recent meta-analysis has found an increased risk for supracondylar periprosthetic femoral fractures after TKA with an anterior femoral notching of ≥ 3 mm. In contrast, other studies have found no relationship between notching and fractures (Gujarathi et al. 2009). As periprosthetic fractures are dramatic and require complex

revision surgeries (Kuzyk et al. 2017), any potential risk factor should be avoided, including femoral notching.

The bone cut volume (Kurtz et al. 2016; Pugh et al. 2013) is an outcome measure in itself, as bone preservation is of relevance for revision surgeries. A normalization is to be aimed at, to adequately compare the individual amounts of bone cut volume.

4.2.3 Evaluation and weighting of the criteria

Introduction

Several objective criteria for implant fit assessment in TKA have been identified in the previous chapter. To allow for a fast comparison of different implant systems with respect to the criteria analyzed, the combination of all criteria into a single score is favorable. To the best of the author's knowledge, no equivalent scoring system for TKA planning has been presented in the literature to date. However, several scores for biomechanical evaluation of THA planning have been presented.

Elkins et al. (Elkins et al. 2015) developed a score, incorporating both criteria for wear and component stability. Respective criteria are based on parameter measurements mapped to a scoring system. For example, the inverse average femoral subluxation was normalized to result in a score between 0 (maximum instability) and 100 (minimum instability), with interpolation of intermediate score values. The two sub-scores for stability and wear were added with equal weighting to define the final "THA Performance Score". Babisch et al. (Babisch et al. 2001) presented a scoring system which includes six biomechanical parameters of the hip derived from a 2D biomechanical model presented by Blumentritt (Blumentritt 1988). The parameters are calculated both preoperatively and for the surgical planning. The results are evaluated with regard to standard and limit ranges or "safe zones". Per parameter 0-2 points are given, resulting in an overall score of 0-12 points.

As a first step to combining all knee implant fit criteria identified into one score, the method for criteria evaluation and the factors to be considered with respect to weighting of the knee implant fit criteria are described in the following. In addition, an initial weighting for each parameter (0-1) is defined.

Evaluation of criteria

To enable the scoring of individual criteria, for each criterion and respective parameter measure, a start, end, and threshold value are set. On the basis of the actual parameter values as well as the start and end value, an individual score is calculated as a rating between 0-1. Start values are theoretical, ideal target values, for example a maximum overhang of 0 mm (≙ no overhang). End values are defined as the percentiles from the database analysis. The threshold values are inspired by the approach of Babisch et al. (Babisch et al. 2001), which penalizes values outside specific ranges. In the framework presented, if the threshold is exceeded, the respective score value is halved and the implant analyzed is rated to have an inadequate fit in the context of the respective criterion. As different thresholds are reported in the literature, the surgeon can select those thresholds, which are listed together with the respective literature reference, or define individual thresholds based on her/his clinical experience. An overview of the start, end and threshold values, including respective literature references, is given in **Table 4-6**. The combined score is calculated as a mean, while considering the individual weighting of the criteria, which is discussed in the following.

Table 4-6: Start, end, and threshold values for the individual fit criteria, listed with the respective sources. Values for the morphological parameters are given as preop vs. postop deviation. Values for the alignment parameters are given as deviation from target alignment. **Abbreviations:** P95: 95% percentile, calculated for the database analyzed. (*) Patellar thickness analyzed, translated to over-/ understuffing and hence to the trochlear parameters. The selected threshold values used in **Chapter 6** are highlighted in blue.

Category	Parameter	Start	End	Threshold	Explanation Threshold	Sources
Interface	Overhang	0mm	P95	3 mm	Increased risk for clinically significant pain at 2 years postoperative.	(Mahoney and Kinsey 2010)
				4 mm	Decreased flexion range of motion	(Chung et al. 2015)
				0 mm	Negative impact on function and pain scores	(Bonnin et al. 2013)
Morpho-logy	J-Curve distance measures	0mm	P95	0.5-1.2 mm	Relationship with increased ligament tension and resultant forces	(Delport et al. 2013)
				1-2 mm	Theoretical relationship with increased ligament tension and resultant forces, as well as negative impact on proprioception.	(Grothues and Radermacher 2021)
	Trochlea distance measures	0mm	P95	8 mm	Decreased passive knee flexion after TKA (-1.2° per 2 mm increase) (stat. sign.)	(Bracey et al. 2015)*
				4 mm	Increased stretch and tension of the MPFL and the ITB-patellar band	(Ghosh et al. 2009)*
Alignment	Femoral Sagittal Alignment	0°	15°	3.5°	Increased risk for mild flexion contracture, 1 year postop	(Lustig et al. 2012)
				3.0°	Increased risk for failure/ revision	(Kim et al. 2014)
	Femoral Coronal Alignment	0°	15°	Range: 0°-7° valgus)	Increased risk for implant failure	(Slevin et al. 2022)
				Range: 2°-8.0° valgus	Increased risk for failure/ revision	(Kim et al. 2014)
	Tibial Coronal Alignment	0°	15°	0°	Increased risk for failure/ revision	(Kim et al. 2014)
				3.0° (range: 3° varus – 3° valgus)	Increased risk for medial bone collapse/ Increased wear/ Implant failure	(Slevin et al. 2022)
	Femoral Rotational Alignment	0°	15°	5° (range: 2-5° ext.)	Increased risk for failure/ revision	(Kim et al. 2014)
				3° (abs: 3° int-6° ext.)	Risk for: patellar subluxation, Abnormal stress on the patellar implant, Anterior knee pain, Implant failure	(Slevin et al. 2022)
	Tibial Rotational Alignment	0°	15°	Range: 2-5° external	Increased risk for failure/ revision	(Kim et al. 2014)
				Range: 0°-7° external	Risk for: Patellar tracking complications, Anterior knee pain, Decreased ROM, Implant failure	(Slevin et al. 2022)
Other	Notching (distance to cortex)	0mm	Gr.4 (50% depth)	3 mm	Increased risk for supracondylar periprosthetic fracture	(Stamiris et al. 2022) Grade 4: (Gujarathi et al. 2009)
	Bone Cut Volume	P5	P95	P50	/	/

Weighting of fit criteria

Apart from a scoring system for evaluation, a system for weighting of the criteria is required. In this context, various patient-specific factors, surgeon preferences, and general ranking of the criteria's relevance for clinical outcome should be considered.

A reasonable start for the criteria weighting would be a general ranking depending on the clinical relevance (i.e., influence on clinical scores), which can later on be adjusted based on more individual factors. However, the comparison of different clinical scores used in the literature is difficult and especially for the PROMs scores, various modifiers have to be considered and accounted for. For respective analysis, larger PROM databases including comprehensive information about modifiers are required. The impact of fit criteria on CROMs and especially on measurements such as range of motion, is less affected by modifiers. In addition, the functional impact of the criteria may also be assessed by (patient-specific) morpho-functional simulation analyses. Previous simulation studies on the relationship between TKA shape and function reported the highest impact for the femoral sagittal radii, the tibial slopes and the lateral trochlear elevation (Asseln et al. 2021; Fitzpatrick et al. 2012b). Similarly for alignment parameters, their functional consequences can be compared, based on *in silico* (Innocenti et al. 2016), *in vitro* or *in vivo* analyses (Lee et al. 2018). Innocenti et al. (Innocenti et al. 2016) identified a higher relevance of adequate tibial compared to femoral component alignment. Consequently, parameters that show high relevance in sensitivity analyses and in terms of functional scores should be ranked and weighted highest, while the remaining may be weighted lower.

Starting from this general criterion ranking, patient-specific factors should be considered to individualize the weighting. One example criterion for individualization is the bone cut volume. As bone preservation is of relevance for revision surgeries, this criterion should be weighted higher in younger patients, which may require several TKA revision surgeries in their lifetime (Klug et al. 2021; Kurtz et al. 2009). In contrast, the weighting could be reduced in older patients in whom revision surgery is not expected in view of the durability of the implant. Regarding morphological criteria, the ability for adaption of the muscular and ligamentous apparatus should be considered. Hence, in older patients

with focus on pain relief, the restoration of all morphological parameters may be weighted highest and further the deformity correction performed cautiously.

Likewise, the surgeon may choose to increase the weighting of individual criteria, based on her/his clinical experience together with information on the individual patient e.g., from anamnesis and functional tests. For example, she/he may increase the weighting of all trochlear parameters (after deformity correction) in the case of a preoperatively unstable patella, to ensure adequate bony guidance. In contrast, when an ACL retaining implant is used, the surgeon may prioritize the morphological parameters linked to ACL rupture (Pfeiffer et al. 2018; Pfeiffer et al. 2019). An exemplary initial weighting of the different criteria is given in **Table 4-7** based on the factors discussed, to be adapted for the individual patient.

Table 4-7: Exemplary initial weighting of the fit criteria, to be adapted for the individual patient. Criteria with broader indication for individualization are highlighted in blue.

Category	Criteria	Weighting	Explanation
Interface	Overhang	1	Relationship with pain and function outcome scores (Bonnin et al. 2013; Mahoney and Kinsey 2010; Chung et al. 2015).
	Underhang	0.75	Relationship with the tibial bone resorption (Gu et al. 2019; Liu et al. 2021).
	Coverage	0.75	
	Cort. Rim Coverage	0.75	Potential relevance for avoiding implant subsidence.
Morphology	Size parameters	0.75	Functional relevance of the AP size. Relationships with other morphological parameters (Mensch and Amstutz 1975).
	J-Curve parameters	1	Relevance for tibiofemoral kinematics (Asseln et al. 2021; Ardestani et al. 2015; Kessler et al. 2007).
	Trochlea parameters	1	Relevance for patellofemoral kinematics (Leichtle et al. 2017; Asseln et al. 2021; Itou et al. 2021).
	Notch	0-1	Relevance for cruciate ligament preservation (Kızılgöz et al. 2018). Relevance depending on the implant system used (CR/PS).
Alignment	Tibial Sagittal Alignment	1	Relevance for physiological knee kinematics and resulting stability, for the extensor mechanism function, and to prevent tibial component subsidence (Ahmad et al. 2016).
	Femoral Sagittal Alignment	1	Flexed component positions were associated with increased risk for persistent flexion contracture (Okamoto et al. 2019)
	Tibial Coronal Alignment	1	Relevance for implant survivorship in the context of aseptic loosening (Ritter et al. 2011) and scores (Rassir et al. 2021). Higher functional relevance of tibial compared to femoral alignment (Innocenti et al. 2016).
	Femoral Coronal Alignment	0.75	
	Tibial Axial Alignment	1	Relationship with pain outcome scores (Nicoll and Rowley 2010; Barrack et al. 2001).
	Femoral Axial Alignment	0.75	
Other	Bone Cut Volume	0-1	Preservation of bone stock. Relevance depending on age.
	Notching	1	(Potential) relationship with periprosthetic fractures.

4.2.4 Discussion

To date, the focus of implant fit evaluation in the literature is the assessment of the bone-implant interface. However, many other criteria regarding morphology or alignment are coming into focus. The majority of the studies evaluated implant fit based on intraoperative measurements or postoperative imaging. However, several authors showed that an evaluation based on preoperative data is possible (Rivière et al. 2018a; Dai et al. 2014a; Itou et al. 2021). In addition, with a standardized, virtual positioning of the implant components, the evaluation of the implant size and design is independent of the surgical technique or potential errors (Dai et al. 2014a). In most of the studies, the measurements were performed manually, which is time-consuming and adds variability (intra-/ interrater). Automation could solve this limitation and also enable the processing of large databases. To easily compare the fit of different implant designs, a combined score is aimed at. Factors for evaluation and weighting of the sub-scores as well was for the interpretation of the combined score have been identified and discussed.

In conclusion, the research question addressed in this chapter can be answered as follows:

> *There are objective criteria for the assessment of implant fit in TKA, of which a relevant share is directly linked to outcome measures. The criteria were classified into the categories interface, morphology, alignment, and other. Relevant interface parameters include implant over-/ underhang as well as bony or cortical rim coverage. Morphological parameters considered for knee implant fit evaluation describe the overall size, the trochlea, as well as the J-Curve. A link with the postoperative range of motion was found for the posterior condylar offset. Alignment criteria linked to the clinical outcome describe the sagittal, axial, and coronal rotational alignment of both tibia and femur. Other criteria include the bone cut volume and femoral notching. An initial weighting can be defined based on the criteria's impact on function and pain (scores), patient-specific factors, and surgeon preferences. As the morphological criteria identified are defined for the healthy knee, a method for deformity checks and optional correction has to be applied.*

4.3 Correction of morphologic deformities

Work in this chapter has been presented in parts in:

S. Grothues, A.-K. Becker, B. Hohlmann & K. Radermacher: Parameter-based patient-specific restoration of physiological knee morphology for optimized implant design and matching. Biomedical Engineering / Biomedizinische Technik, 2023, 68(5), pp. 537-544 [DOI: 10.1515/bmt-2023-0017]

4.3.1 Introduction

Various morphological criteria for implant fit evaluation were presented in the previous chapter. Prior to their assessment, the presence of bony deformities such as trochlear dysplasia has to be evaluated for the individual patient. Such deformities would be reproduced, if the implant for TKA is designed solely on the basis of native knee morphology. Many current OTS implant systems feature a dysplastic trochlear shape (Dejour et al. 2014) and thereby a clinically relevant deformity. Hence, instead of a patient's native, deformed knee morphology, the equivalent (reconstructed) physiological knee morphology should be used for detailed three-dimensional preoperative planning and the implant design process. This is especially the case for the patient-specific implant design process, which provides more flexibility to adapt to patient-specific correction needs (Slamin and Parsley 2012; Zingde and Slamin 2017). In addition, the knowledge and correction of deformities is also of relevance with regard to implant component alignment as surgical reference axes may be affected (Matsuda et al. 2004).

Related research

To the best of the author's knowledge, there is only one study presenting a method for identifying equivalent physiological parameter values for a set of pathological parameter values, using an unsupervised neural network, by van den Heever et al. (van den Heever et al. 2011). The respective self-organizing map was trained with data from 35 physiological knee joints. Nine morphologic parameters were evaluated for every knee. They were categorized depending on whether or not they are affected by OA. Those parameters affected were defined as the lateral and medial condyle radius, the posterior

medial and lateral radius, and the resected posterior condyle. Remaining, unaffected parameters were the AP and ML size, the AP box and the sulcus length. Limitations of the study include the small set of morphological parameters considered, and both a small training and test dataset. In addition, the neural network was not compared to other prediction methods, such as regression. Finally, the method for the classification of "affected" parameters was not specified.

To enable a parametric deformity correction, the following chapter covers the analysis of parametric deformity definition. Further chapters cover the development, evaluation and comparison of methods for:

1. The classification of (un)affected morphologic parameters of the knee for a specific deformity.
2. The parameter-based deformity correction of respective affected parameters.

The research question addressed in this chapter is the following:

> *RQ5: In the case of deformities, can those be clearly identified and adequately corrected by a parameter-based, data-driven approach?*

4.3.2 Parametric deformity definition

Bony deformities in the knee can originate from genetic factors, trauma, or diseases such as OA. This section presents relevant knee deformities along with their corresponding parameter definitions. Additionally, the parameters used to quantify these deformities are listed, including any available cut-off values, hereafter referred to as "deformity parameters".

Osteoarthritis-related deformities

OA may be associated with several knee deformities. First, there are deformities which may predispose a patient to developing OA. As discussed in **Chapter 2.1.2**, OA is presumed to result from an imbalance of load and repair processes, with various risk factors contributing to its development and progression (Doherty 2001). One prominent risk factor for OA progression is pathological lower limb alignment (Sharma et al. 2001). In addition, specific features of knee morphology, such as the small medial femoral

condyle knee morphotype, have been linked to a higher risk of medial compartment OA (Grammens et al. 2021).

Second, OA itself can alter the shape of the knee through the formation of osteophytes or deformities of the subchondral bone in late stages of OA (Kellgren-Lawrence Scale: 4, (Kellgren and Lawrence 1957)). Osteophytes typically form at the outer boundaries of the knee's articulating surfaces, in random distribution (Pap and Meinecke 2011). Because of their complex shape, osteophytes affect various morphological parameters and hence should be removed prior to 3D TKA planning. Existing SSM-based approaches can be applied for this purpose (Hänisch and Radermacher 2016) or the osteophytes can be directly excluded during segmentation. Other OA-related defects mostly are located in the contact area of the affected compartment including the plateaus and condyles, and generally involve the flattening of the respective surfaces (Buckland-Wright 2004). Analyzing and comparing these deformities in varus, valgus and control knees allows to establish reference ranges and cut-off-values.

Several studies have compared varus and valgus knees and found, for example, statistically significant differences for the angle between the posterior condylar line and the transepicondylar axis (Cohen et al. 2019; Choi et al. 2022). Others have compared valgus and/or varus against control knees (Matsuda et al. 2004; Lee et al. 2021; Chang et al. 2018). Matsuda et al. (Matsuda et al. 2004) evaluated 30 varus, 30 valgus and 30 control knees and found significant distortion and hypoplasia of the lateral condyle in valgus knees. These studies identified statistically significant differences in the lateral condylar depth and in the angles of the transepicondylar axis and transverse axis with the posterior condylar tangent. In addition, respective studies highlight more extensive parameter effects in valgus knees than in varus knees.

Correcting these deformities benefits both cases: The OA-predisposing deformities should be corrected, to achieve adequate loading and thereby minimizing wear. Deformities developed during OA, such as the flattening of condyles, should be corrected to achieve native, pre-arthritic joint kinematics. As a first step to the correction, those knees with OA-related deformities need to be identified, for example, on the basis of parameter cut-off values. To date, literature lacks established parameter cut-off values to differentiate between varus, valgus and physiological knee morphology. To address

this knowledge gap, a parameter analysis of a database with over 800 knees was performed. For this purpose, an existing framework for bone-specific morphological parameter analysis (Asseln et al. 2018; Asseln 2019) was extended to include interbone parameters such as the hip-knee-ankle-angle (HKA) (Grothues et al. 2022). On the basis of the respective HKA, the individual knee parameter sets were classified as neutral (HKA: 177°-183°), varus (HKA: <177°), or valgus (HKA: >183°). After normalization, the varus, valgus and neutral group were evaluated regarding equal means using the t-test or welch test, depending on the results of the Levene test performed (significance level: 5%). In case of statistically significant differences in the normalized mean with relevant effect sizes, which are also supported by the literature, the parameter was classified as a deformity parameter. Cut-off values were defined by the 5% and 95% percentiles of the neutrally aligned knees. Although a previous study by our group presented by Asseln et al. (Asseln et al. 2018) found minimal sex differences after appropriate normalization, we provide gender-specific boundaries here because the distance measures analyzed were not part of the previous study. A more detailed description of the methodology and the respective verification can be found in **Appendix B)** and of the database analysis in **Appendix C)**.

Table 4-8: Parameters with statistically different normalized mean values in the individual varus and valgus in comparison with the neutrally aligned sub-populations, by paired t-test or welch test analysis. Effect sizes are highlighted and the color code is given below. The given upper and lower cut-off values are defined by the 5% and 95% percentiles of the neutral sub-population (not normalized).

Bone	Aspect	Parameter name	Varus vs. neutral	Valgus vs. neutral	Upper Cut-Off value		Lower Cut-Off value	
					Female	Male	Female	Male
Femur	J-Curve	Distal Condylar Offset	0.57	0.83	7.01	7.01	0.81	1.18
		PCO Lateral	0.14	0.91	28.11	30.00	21.81	22.16
	Alignment	Posterior Condylar Angle	1.52	2.05	3.69	3.04	-0.99	-1.83
Tibia	Alignment	Coronal Tibial Slope	1.41	1.34	5.87	6.34	-0.42	-0.11
Interbone	Alignment	TT-TG	0.91	0.61	21.21	23.25	7.21	5.48

Color code: Medium effect size= 0.5-0.8: ■ | Large effect size > 0.8: ■ (Cohen 1988)

Congenital deformities

Apart from OA-related deformities, one must consider bony congenital deformities with functional relevance. Examples include, trochlear dysplasia, which is associated with symptomatic patellar instability (Dejour et al. 1994) and patellofemoral OA (Jungmann et al. 2013). Further reported risk factors for these symptoms include patella alta and an

increased TT-TG distance (Steensen et al. 2015). Morphological risk factors for (anterior) cruciate ligament injuries include a reduced notch width (van Diek et al. 2014; van Kuijk et al. 2019), an increased lateral condylar offset ratio (Pfeiffer et al. 2018) and an increased medial tibial sagittal slope (Bayer et al. 2020). Those deformities of course are primarily relevant for CR implant systems and can be neglected in posterior-stabilized PS systems.

Even preoperatively asymptomatic congenital deformities may lead to complications after TKA. For instance, patellar bony guidance may decrease dramatically, when using an undersized femoral implant component implanted in slight external rotation (as previously recommended (Anouchi et al. 1993; Rhoads et al. 1990)), combined with implant designs often featuring a dysplastic trochlear shape (Dejour et al. 2014). Additional aspects of TKA which may worsen patellar tracking and stability, include changes in tibiofemoral internal-external rotation due to J-Curve changes and ligament mal-balancing based on passive kinematics. In cases where patellar stability was already limited prior to TKA, this preoperative situation could result in clinically significant instability and/or (anterior) knee pain postoperatively. The exemplary congenital deformities discussed are listed in **Table 4-10** (risk factors for patellar instability) and in **Table 4-10** (risk factors for ACL injury), together with respective deformity parameters and cut-off values.

Table 4-9: Congenital deformities associated with patellar instability, respective deformity parameters and cut-off values from the literature.

Deformities	Deformity parameters	Cut-off values	Imaging	Source
trochlear dysplasia	Trochlear depth Trochlear Facet Asymmetry	≤ 3 mm ≤ 40%	MRI	(Pfirrmann et al. 2000)
Patella alta	Insall Salvati Index	IS Index > 1.3	Lateral Xray	(Steensen et al. 2015)
Pathological TT-TG dist.	TT-TG distance	> 20 mm	MRI	(Steensen et al. 2015)

Table 4-10: Congenital deformities associated with ACL injury, respective deformity parameters and cut-off values from the literature. Of note, the relevance of the respective deformity correction depends on the implant system used (CR vs. PS).

Deformities	Deformity parameters	Cut-off values	Imaging	Source
Reduced notch width	Intercondylar Notch Width	females < 18 mm males < 20 mm	MRI	(Kızılgöz et al. 2018)
Pathological tibial slope	Medial Sagittal Tibial Slope	males > 4.3 mm females > 4.5 mm	MRI	(Kızılgöz et al. 2018)
Increased lateral condyle ratio	Lateral Condylar Offset Ratio	> 63%	Lateral Xray	(Pfeiffer et al. 2018)

4.3.3 Concept for parametric deformity correction

With the parametric deformity definition and cut-off derived, a parameter-based deformity correction can be addressed. First the parameters used for prediction have to be identified, meaning the distinction between affected (i.e., pathologic/ deformed) and unaffected (i.e., “healthy”/undeformed) parameters. Second, the methods for prediction have to be determined and applied. Third, the model variants have to be evaluated and compared, to identify the one best-suited for the deformity considered.

Classification of (un)affected parameters

The deformities considered are characterized not only by the defining parameters (**Table 4-9**-**Table 4-10**) but also by various others, which are, hence, also “affected” by the respective deformity and must, therefore, be taken into account for the correction. Trochlear dysplasia, for example, is characterized not only by a low trochlear depth, but also by a high sulcus angle. In addition, when correcting the sulcus angle to a physiological value, other parameters of the femoral trochlea, such as the trochlear elevations, also need to be adapted. The trochlear shape before and after trochlearplasty and the corresponding morphological parameters are schematically shown in **Figure 4-4**. In this figure, it becomes apparent that an isolated change of a specific deformity parameter is not possible, but that several other parameters are always changed as well (affected). The physiological equivalents of those affected parameters have to be predicted by the unaffected parameters. Therefore, a method to distinguish between parameters affected or unaffected by a specific deformity (correction) is required. Consequently, a trade-off may be involved between prediction accuracy and a sufficient parameter correction. The prediction accuracy will potentially increase with a high number of predicting (unaffected) parameters. However, the parameters may not be corrected to a physiological range when too many parameters are used for the prediction. In this case, affected parameters may falsely be classified as unaffected parameters.

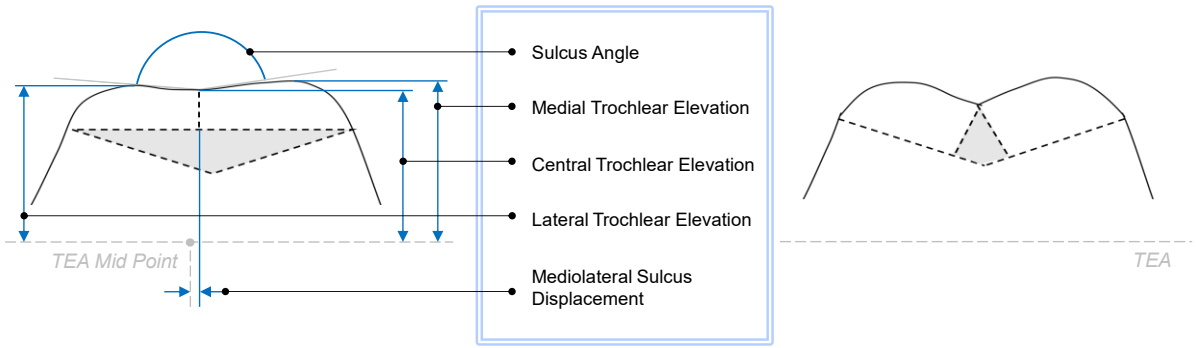

Figure 4-4: Femoral trochlear dysplasia both before and after correction surgery (trochlearplasty according to the Lyon's procedure (Dejour and Saggin 2010)). **Left:** Femoral anterior region with trochlear dysplasia and denoted parameter values. **Right:** Femoral trochlea after trochlearplasty.

Both a "clinical" and a "mathematical" classification approach for defining the parameters as affected or unaffected were considered (**Figure 4-5 Step 2**). Using the clinical classification approach, those parameters which are changed in a respective correction surgery (e.g., trochlearplasty or notchplasty) were defined as affected. For the notchplasty (deformity parameter: notch width) these include the medial and lateral condylar width. It has to be noted that the knee's shape in a conventional trochlearplasty or notchplasty is changed according to generic targets and not in an individualized approach as proposed here. Taking the mathematical classification approach, the parameters were sorted according to their correlation with the deformity parameter. Parameters with the highest correlations were defined as affected. Instead of defining a limit for the correlation coefficient, the number of affected parameters for every deformity parameter was varied, depending on the model's capability of predicting physiological parameter values. The minimum was set to 95 % of the pathological data points corrected to physiological parameter values (**Figure 4-5 Step 8**). For the example of the notch width, these parameters included again the medial and lateral condylar width, as well as several parameters of the distal and posterior condylar shape.

Model variants

Three different methods were used to predict physiological parameter values: regression, nearest neighbor search and neural networks. Different model variants were considered for each method, which are listed in **Table 4-11**. Regarding the nearest neighbor search, different variants of the Minkowski distance measure were used to

identify a physiological data point with the closest parameter values to the respective pathological data point analyzed. On the basis of the performance in a previous study (Chomboon et al. 2015), the Euclidian, Chebyshev and Cityblock distance measures were chosen. The regression model predicts the affected parameters through a linear combination of the unaffected (predicting) parameters. The following regression model variants were considered: the ordinary least squares regression and different types of regularizations which optimize regression coefficients and aim to remove irrelevant or redundant predictors (Zou and Hastie 2005). As regularizations, the ridge (Hoerl and Kennard 1970), lasso (Tibshirani 1996) and elastic nets regularization were considered (Zou and Hastie 2005). A neural network is inspired by the learning behavior of the human brain. After training (**Figure 4-5 Step 5**), the network predicts the affected parameters based on adapted node weights. In contrast to regression models, nonlinear relationships can be represented with neural networks. The networks were built and trained using the built-in MATLAB functions *fitnet* and *train* (MathWorks, Inc., Natick, MA, US). The optimal network architectures were defined empirically. Hence, model variants of the neural networks were defined by different architectures: the number of hidden layers and the number of neurons per layer. A frequent problem is overfitting, which describes the effect that the model has been trained to a point where it learns the output desired by memory (Uzair and Jamil 2020). In order to counteract overfitting, it is recommended to reduce the quantity of neurons in each layer to a minimum. Dogan et al. (Dogan et al. 2009) identified an optimal network architecture of one hidden layer with three neurons for the prediction of one output by eight input parameters with eleven data points. Because of a (slightly) higher number of input parameters and a higher number of data points in the present study, architectures with one to two hidden layers and two to four neurons per layer were chosen. The number of epochs was set to 100.

Table 4-11: Model variants of the methods for prediction of physiological parameter values for given pathological parameter values, including the nearest neighbor search, regression and neural networks.

Nearest Neighbor Search k=number of unaffected parameters x_{ij}=value of the unaffected parameter j of the data point i x_{tj} =value of the unaffected parameter j of the neighbor t	A	Euclidean (p=2)	$d_{it} = \sqrt{\sum_{j=1}^{k} \left\lvert x_{ij} - x_{tj} \right\rvert^2}$
	B	Chebyshev (p=∞)	$d_{it} = \max_j \left\lvert x_{ij} - x_{tj} \right\rvert$
	C	Cityblock (p=1)	$d_{it} = \sum_{j=1}^{k} \left\lvert x_{ij} - x_{tj} \right\rvert$
Regression k=number of unaffected parameters n=number of data points x_{ij}=value of the unaffected parameter j of the data point i y_i=affected parameter values of the data point i	A	OLS	$\hat{\beta}^{OLS} = \underset{\beta_0 \beta}{\operatorname{argmin}} \sum_{i=1}^{n} (y_i - \beta_0 - \sum_{j=1}^{k} x_{ij}\beta_j)^2$
	B	Ridge	$\hat{\beta}^{ridge} = \underset{\beta_0 \beta}{\operatorname{argmin}} (\frac{1}{n} \sum_{i=1}^{n} (y_i - \beta_0 - \sum_{j=1}^{k} x_{ij}\beta_j)^2 + \lambda \sum_{j=1}^{k} \beta_j^2)$
	C	Elastic nets C1: α=0.25 C2: α=0.5 C3: α=0.75	$\hat{\beta}^{EN} = \underset{\beta_0 \beta}{\operatorname{argmin}} (\frac{1}{2n} \sum_{i=1}^{n} (y_i - \beta_0 - \sum_{j=1}^{k} x_{ij}\beta_j)^2 + \lambda \sum_{j=1}^{k} (\frac{1-a}{2} {\beta_j}^2 + \alpha \left\lvert \beta_j \right\rvert))$
	D	Lasso	$\hat{\beta}^{lasso} = \underset{\beta_0 \beta}{\operatorname{argmin}} (\frac{1}{2n} \sum_{i=1}^{n} (y_i - \beta_0 - \sum_{j=1}^{k} x_{ij}\beta_j)^2 + \lambda \sum_{j=1}^{k} \left\lvert \beta_j \right\rvert)$
Neural networks (architecture) MATLAB (*fitnet*)		Hidden layers	Neurons each layer
	A B C D	h = 1 h = 1 h = 2 h = 2	k = 5 k = 10 k = 2 k = 5

Evaluation of model variants

An important aspect of this topic is the prediction accuracy required. Such accuracy would have to be determined individually per parameter, for example, based on morpho functional *in vitro/in silico* studies. The deviation in notch width represents over-/ underhang in the intercondylar area, therefore, existing limits for the clinical significance of ML over-/ underhang could be considered. Those limits range from 0 mm (Bonnin et al. 2013) to 3 mm (Mahoney and Kinsey 2010). Morpho-functional studies on the trochlear elevations could be considered for the trochlear depth. The study by Leichtle et al. (Leichtle et al. 2017) e.g. reports on the statistically significant impact on patellofemoral kinematics and contact pressure with combined changes of medial and lateral trochlear height of 1 to 2 mm.

The combined methodology, with the clinical/mathematical classification approach and the different model variants, was evaluated using both pathological and physiological datasets. Regarding the test dataset (only physiological data points), the accuracy of prediction was evaluated by calculating the mean squared error (MSE) over all affected parameters, the mean absolute error (MAE) and the coefficient of determination (R^2) for the specific deformity parameter (**Figure 4-5 Step 6**). The MSE was used to identify the best-fitting model variant for the individual deformity. Concerning the pathological dataset, the correction to physiological parameter values was assessed. Hence, whether or not the corrected value is above the cut-off value from the literature. The workflow describing the methodology developed is displayed in **Figure 4-5**.

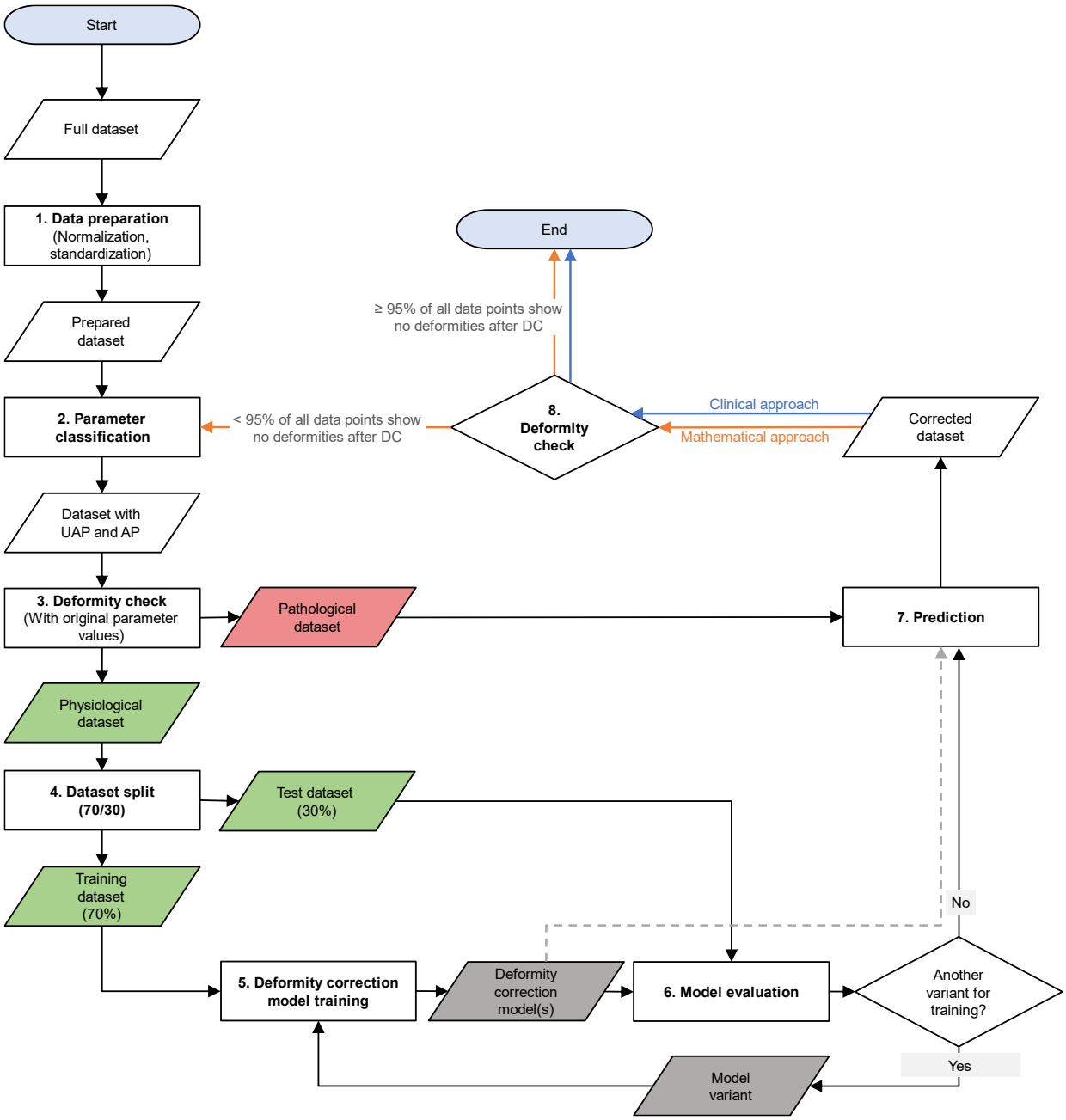

Figure 4-5: Workflow for training and evaluation of the different model variants. AP = Affected Parameter, UAP = Unaffected Parameter, DC = Deformity Correction.

4.3.4 Concept evaluation

The concept developed is subsequently applied to a large database, to evaluate and compare the methods developed. For the present concept evaluation, the congenital deformities trochlear dysplasia, characterized by a low Trochlear Depth and low Trochlear Facet Asymmetry (Diederichs and Scheffler 2013; Pfirrmann et al. 2000), as

well as a reduced notch width were focused on. Those parameters are denoted as deformity parameter from hereon.

Database

A parametric database of 673 knees, each described by 36 femoral parameter values, was used for the study. According to the common nomenclature of machine learning applications (Badillo et al. 2020; Greener et al. 2022), each knee in the database is referred to as a "data point" in the following. The parameter values were determined using a framework for automated morphological analysis, presented by Asseln et al. (Asseln et al. 2018). In addition to the existing parameters, the deformity parameters Trochlear depth and Trochlear Facet Asymmetry were integrated (Diederichs and Scheffler 2013; Pfirrmann et al. 2000). The sex distribution was 318 female and 355 male knees. The surface models were derived from computed tomography. The segmentation and an osteophyte removal were performed semi-automatically. For each deformity, all data points were classified as pathological (deformed) or physiological, based on the cut-off values derived from literature (**Table 4-10**) or based on the physiological boundaries derived in a database analysis (**Table 4-8**). Applying the cut-off values to the database led to 17 pathological data points for Trochlear Depth, 52 for Trochlear Facet Asymmetry, and 135 for the Notch Width. A total of 486 data points were without any deformity and, therefore, defined as physiological data points. Normalized values were used, to overcome the impact height- and gender-related factors have on the morphology of the knee joint (Asseln et al. 2018). Data points used for machine learning pipelines need to be standardized, so that all parameters have an equivalent impact on the distance measure, independent of their mean and variance. Hence, a z score normalization was performed as a first step of the workflow (**Figure 4-5**). The physiological data points were split into training and test dataset, with a data split of 70:30, respectively (**Figure 4-5 Step 4**). The pathological data points could not be used as training or test data because no physiological values for the deformity parameter and, accordingly, no ground truth are available for them. Therefore, the training and test dataset consisted solely of physiological data points. The physiological values for the affected parameters represent the ground truth. Because of the limited size of the dataset and the focus on the comparison of different methods, no hyperparameter

optimization with a validation dataset was performed (e.g., number of epochs) but instead the test dataset was applied directly.

Results: Classification of (un)affected parameters

Utilizing the clinical classification approach, an average of only half of the pathological parameter values were corrected to physiological values. This limitation can be seen in **Figure 4-6** in the example of the correction of the deformity parameter trochlear facet asymmetry using the lasso regression model variant. Half of the new parameter values defined by the clinical classification approach (blue) are below the cut-off-value. It can be seen in the example case (highlighted by circles) that the parameter is corrected in the direction of the cut-off value. However, the amount of correction is insufficient. Taking the mathematical classification approach, the percentage of cases corrected to physiological parameter values increased with the number of affected parameters, however, with a decreasing gradient. As described in the methods section, boundaries were set such that 95% of the pathological data points were corrected to physiological parameter values. This threshold led to a number of four to nine affected parameters, depending on the deformity parameter. It can be seen in **Figure 4-6** that the majority of pathological data points are corrected to a physiological trochlear facet asymmetry. As this target and, therefore, the aim of this study could not be reached with the clinical classification approach, only the mathematical classification approach was considered from here on.

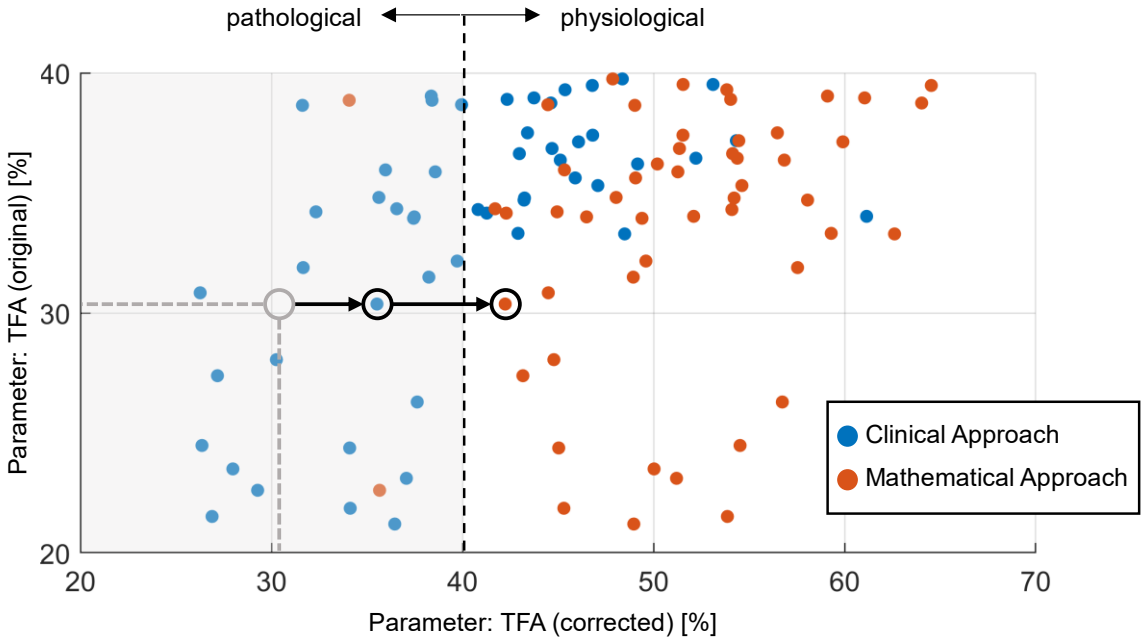

Figure 4-6: Comparison of the clinical and the mathematical approach for selection of (un)affected parameters as a basis for deformity correction, in the example of the *Trochlear Facet Asymmetry* using the lasso regression model variant. The number of affected parameters was six for the clinical and nine for the mathematical classification approach. It can be seen for the highlighted example case that using the clinical classification approach, the parameter value is corrected towards the physiological area, but is still below the cut-off value. Utilizing the mathematical classification approach, the parameter value is corrected to above the cut-off value.

Results: Evaluation of model variants

The resulting MSE for the different model variants is given in **Table 4-12**. For all methods, the chosen model variant resulted in a prediction error below the parameters' standard deviation, while the regression yielded the lowest errors. The following results on prediction (accuracy) were found: MAE = 0.78 mm (Trochlear depth)/ 8.07 % (Trochlear Facet Asymmetry)/ 1.17 mm (Notch Width); R^2 = 0.32 (Trochlear depth)/ 0.41 (Trochlear Facet Asymmetry)/ 0.19 (Notch Width).

Table 4-12: Evaluation of the model variants with the test dataset (only physiological data points) using the mathematical classification approach. Mean squared errors (MSE) are displayed in a standardized form. The best-performing model variants, which are selected for the prediction, are highlighted in green.

Deformity parameter	Twin Search			Regression						Neural Network			
	Euclidean	Chebyshev	Cityblock	OLS	Ridge	Elastic nets α=0.25	Elastic nets α=0.5	Elastic nets α=0.75	Lasso	1 HL, 5 Neurons	1HL, 10 Neurons	2 HL, 2 Neurons	2 HL, 5 Neurons
Trochlear depth	1.25	1.51	1.25	0.51	0.51	0.53	0.53	0.53	0.53	0.74	0.89	0.76	1.16
Trochlear Facet Asymmetry	1.04	1.19	1.10	0.32	0.31	0.28	0.28	0.28	0.28	0.47	0.31	0.47	0.32
Notch Width	1.56	1.81	1.66	0.82	0.77	0.79	0.79	0.79	0.79	0.91	1.13	0.91	1.13

4.3.5 Verification

The deformities considered for verification were selected according to their individual functional relevance (**Table 4-10**). Hence, different goals are pursued with the individual deformity corrections. With the correction of trochlear dysplasia, the aim is an improved bony guidance of the patella in the femoral trochlea, which is reflected in enhanced patella tracking and reduced risk of dislocation or subluxation (Ntagiopoulos et al. 2013). To verify whether the aim of the deformity correction is achieved, a multi-body simulation study is performed. Respective analyses are described in the following.

Materials and methods

The patient-specific simulation model used for the verification study was based on a model of TKA, previously presented by Asseln et al. (Asseln 2019). The model was written in the AnyBody Modeling System™ (AnyBody Technology A/S, Aalborg, Denmark). A validation with both *in vitro* and *in vivo* data was performed for the kinematic and kinetic simulation results (Asseln 2019; Asseln et al. 2021). The model was thus adopted to enable the simulation of the native knee joint. The model includes the femoral, tibial and patellar segment, incorporating the patient-specific bony surface models, the major extensor (quadriceps femoris) and flexor (biceps femoris & semimembranosus) muscles of the knee, and the main ligamentous structures including collateral and cruciate ligaments. A visualization of the model is displayed in **Table 4-7**.

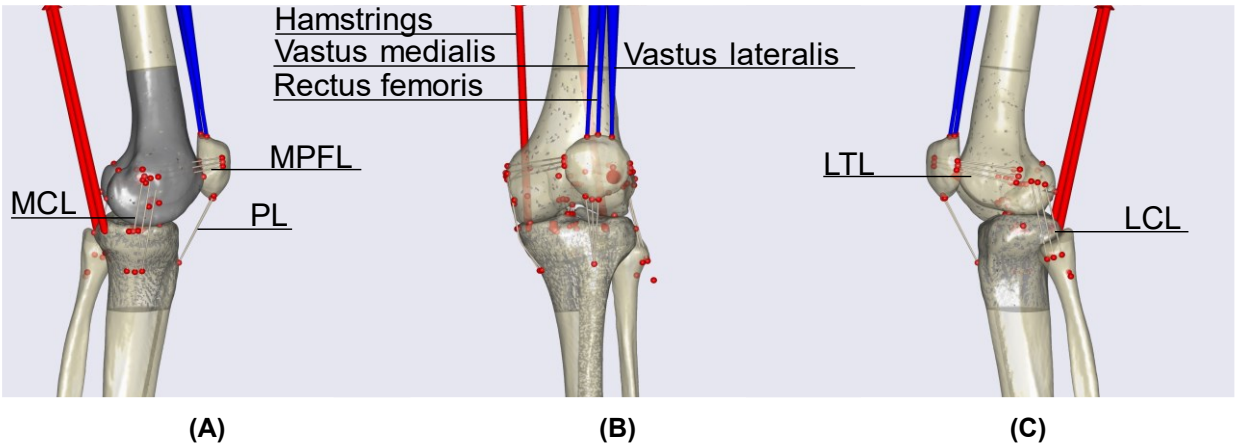

Figure 4-7: Exemplary, patient-specific, native knee model used for the verification study in **(A)** medial, **(B)** anterior, and **(C)** posterior view. The model is individualized using the surface models of the respective patients, individual landmarks derived using an atlas-method, and the patient's weight.

For the verification of the deformity correction approach, a random subset of ten knees was selected from the cases with trochlear dysplasia classified by a trochlear depth below 3 mm. The subset consisted of four right and six left knees, from eight female and two male patients. The surface models of the bones were adjusted according to the corrected parameter values. The corrections of the three different approaches (regression, neural networks, twin search) were considered. Subsequently, an existing tool for parameter-based surface modification, specific to the distal femur (Asseln et al. 2015; Asseln 2019), was applied. Thereby the parameterized data were transformed into surface models. Subsequently, two individualized models were built for each patient, one prior and one after the deformity correction, using the newly generated surfaces. A deep knee bend simulation was performed with both models and the resulting kinematics were compared for each patient.

Results

Distinct differences between the simulation results for the model prior and the model after deformity correction were seen for the patellar medial-lateral tilt and the patellar anterior-posterior translation. After deformity correction, a more central tilt position and a more posterior position of the patella with respect to the femur was found for all cases analyzed. **Figure 4-8** displays respective results for an example case.

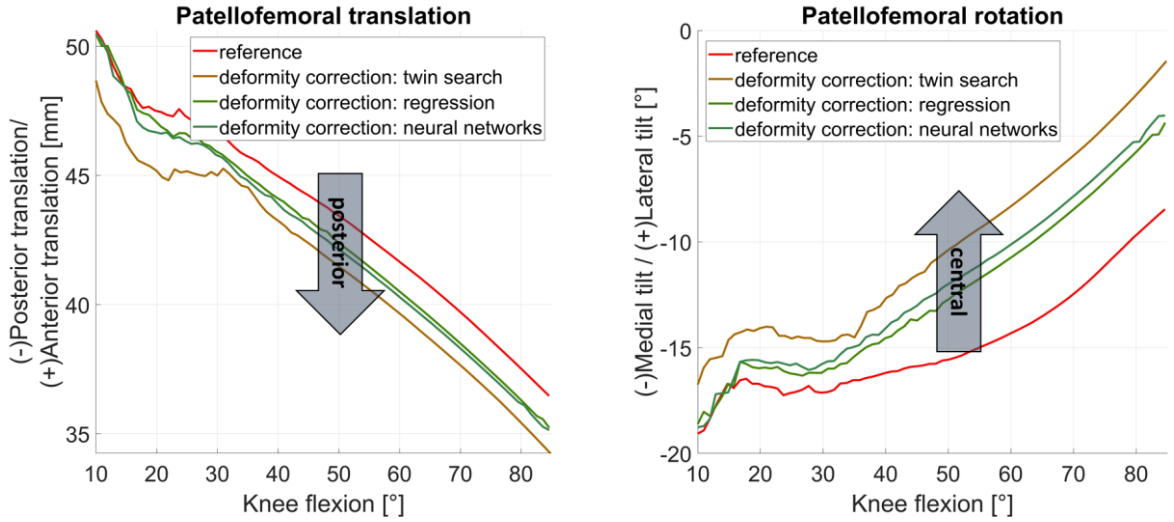

(A) **(B)**

Figure 4-8: Exemplary simulation results of the verification study of deformity correction: Patellofemoral kinematics before (red) and after deformity corrections, using twin search (beige), regression (green) and neural networks (turquoise). **(A)** Patellofemoral anterior-posterior translation. **(B)** Patellofemoral medial-lateral tilt.

Discussion

The results of the functional analyses show a deeper and more central tilt position of the patella in the femoral trochlea after correction of trochlear dysplasia by deepening the femoral trochlea. These differences suggest a better guidance of the patella by the femoral trochlea. It can thus be concluded, that the parameter-based deformity correction of trochlear dysplasia demonstrated the desired enhanced bony guidance of the patella in a multi-body simulation analysis of ten example knees.

4.3.6 Discussion and conclusion

The methodology for deformity corrections including the parameter classification, the model variants, as well as the respective evaluation and verification studies are discussed in the following.

Classification of (un)affected parameters

The clinical classification approach could not achieve sufficient correction of the pathological parameter values in the present application. While this approach was originally favored because of its compact and conservative parameter selection, it

proved to be inadequate. This can be illustrated using the example of the notch width. With the clinical approach, only the medial and lateral condylar widths are classified as affected, as these are potentially adjusted during a corrective surgery (notchplasty). In contrast, the mathematical approach also includes parameters such as the distal and posterior mediolateral condylar width as affected parameters. This is reasonable, as femora with a larger notch width are expected to have a correspondingly different condylar shape.

Therefore, the mathematical classification approach was used in the following. With this approach, the parameters with the highest linear correlation and, thus, the best predictors for the deformity parameter are classified as affected. A selection based on high correlation may often be reasonable, because of an actual link to the deformity. However, the affected parameters should always be reviewed to prevent parameters with high predictive power and no direct link to the deformity being included in the prediction. Regarding the deformities studied, the parameters determined by the clinical classification approach were mainly a subset of those determined by the mathematical classification approach, which already represents a partial verification of the two approaches. A weak and indirect relationship with the deformity was identified for the remaining (additional) affected parameters of the mathematical classification approach. In the future, for other deformities, such a verification should be integrated, representing a combination of the mathematical and the clinical classification approach.

Model variants

No clear superiority of one model variant was found for the regression models and the neural networks. By contrast, the Chebyshev distance measure led to the highest MSE for all deformity parameters for the twin search. One possible explanation is that the Chebyshev distance only considers the highest error and neglects all others. In the present application, the minimal MSE regarding all affected parameters was used to identify the best model variant. Therefore, prioritizing the highest error proved to be unsuitable.

Evaluation of model variants

A relevant limitation of the present study is the absence of a validation dataset, which was not included because of the comparably small database and the focus on method comparison. A validation dataset would be required with which to optimize, for example, the number of epochs, and for an accurate assessment of the prediction accuracy. Nevertheless, all prediction models developed estimate equivalent physiological parameter values for given unaffected parameters with a mean error below one standard deviation. The accuracy is comparable with a previous study using a neural network (van den Heever et al. 2011), while the regression models outperformed the neural networks in the present study. Some of the predicted parameters in this study are geometrically related, thus, their compatibility must be checked or subsequently established. The percentage of variance accounted for by the models is comparably low, which could be due to various possible reasons. In the context of machine learning, the database presented is considered small. Larger databases are expected to improve the prediction, especially for the nearest neighbor search. In addition, knee morphology is highly individual. No clusters could be found after normalization based on the ML and AP size in a previous study on knee morphotypes (Hohlmann et al. 2022). Hence, high interindividual differences may explain the comparably low share of parameter variance explained by the data-based models.

The MAE of 0.78 mm regarding the Trochlear depth is below changes in trochlear elevations of 1 to 2 mm analyzed in *in vitro/in silico* studies (Leichtle et al. 2017; Asseln et al. 2021). When assuming a linear morpho-functional relationship, maximum deviations are assumed to be below 1° and 1 mm even for the kinematic parameters most-affected (Leichtle et al. 2017; Asseln et al. 2021). Regarding the Notch Width, an MAE of 1.17 mm was found, which is below the limit of 3 mm for overhang defined by Mahoney et al. (Mahoney and Kinsey 2010). However, Bonnin et al. (Bonnin et al. 2013) have found all errors above 0 mm to have a negative influence on outcome scores. Hence, an increase in the prediction accuracy would be favorable (for example: a maximum error < 1 mm). To the best of the author's knowledge, there are no morpho-functional analyses of the Trochlear Facet Asymmetry. When applying the predictions to the (patient-specific) implant design, the influence of the local cartilage thickness on the morphological parameters must be taken into account. However, patient-specific implant design is regularly based on computed tomography imaging. Therefore, the

cartilage impact must be considered by default. Average cartilage maps of physiological (control) subjects are available (Favre et al. 2017; Lösch et al. 1997; Carballido-Gamio et al. 2008) and can be used for this task.

As an outlook, the analyses should be repeated for a larger database and include a validation dataset. Subsequently, the effects on the prediction accuracy should be quantified. Finally, similar studies could be performed for other deformities, and additionally for the tibia and patella.

Verification

In addition to the parameter-based deformity correction, an evaluation of the respective functional consequences was performed, using a multi-body simulation. With the simulation model, an improved patellar tracking was demonstrated after correction of the trochlear depth to a physiological parameter range. It was thus shown that the desired functional effects of deformity correction were achieved with the parameter-based approach.

The research question addressed in this chapter can be answered as follows:

> *Morphological knee deformities can be corrected by a data-driven approach, with an estimated error below one standard deviation for the morphological parameters analyzed. When considering available in silico and/or in vitro analyses, the respective error is expected to have no clinically relevant impact on knee kinematics. In the example of trochlear dysplasia correction, respective surface modifications for pathological cases have the desired consequences of a more stable patellar tracking in a multi-body simulation.*

5. Proposed workflow and implementation

Work in this chapter has been presented in parts in:

S. Grothues & K. Radermacher: X-ray based morphological analysis of the knee - a review. In: F. Rodriguez Y Baena, J.W. Giles & E. Stindel (ed.): Proceedings of The 20th Annual Meeting of the International Society for Computer Assisted Orthopaedic Surgery, 5, 2022, pp. 89-98 [DOI: 10.29007/sqcb]

S. Grothues & K. Radermacher: Automated analysis of femoral over-/underhang and bone coverage of OTS TKA implants. In: J.W. Giles (ed.): Proceedings of The 22nd Annual Meeting of the International Society for Computer Assisted Orthopaedic Surgery, 2023, pp. 26-30 [DOI: 10.29007/5636]

5.1 General workflow

In the previous chapters, the concept for an implant fit evaluation has been presented, including specific criteria and methods for their evaluation and weighting. The implementation of the current concept of the implant fit evaluation with available imaging technology is presented below, using MATLAB. The implantation is restricted to femur and tibia. This is because no fit criteria have been found for the patella and also because the patella is regularly not resurfaced in Germany (Lützner et al. 2023). Depending on the accessibility of the parameters the following criteria are evaluated, which were identified as relevant for function and/or outcome in **Chapter 4.2**. **Interface:** implant overhang, implant underhang, bone coverage, cortical rim coverage. **Morphology:** femoral size, femoral J-Curve, femoral trochlea, femoral notch, tibial size, tibial slope. **Alignment:** coronal, sagittal and transverse alignment, as well as interbone parameters. **Other:** bone cut volume, (notching).

The implementation and subsequent evaluation are performed in two levels, according to the concepts developed in **Chapter 4.1** (concept 1 (current), concept 2 (future)). First a fit assessment based on biplanar X-ray images is performed (2D). Afterwards the optional, comprehensive evaluation based on CT data (3D) is presented, which in the

future can be applied to data for example from 3D freehand/robotic US imaging. Both assessments include the following steps:

1) Pre-processing of the bone data
2) Transformation to a bone-specific coordinate system
3) Positioning of implant contours/ meshes
4) Evaluation of interface and other criteria
5) Evaluation of morphological and alignment parameters, with potential deformity correction and consideration of cartilage
6) Comparison of implant and (corrected) bone measures
7) Visualization of the results, with the option to adapt each sub-score weighting.

The respective workflow is depicted in **Figure 5-1**. Detailed steps for both the 2D and the 3D assessment are presented in the following.

The research question addressed in this chapter is the following:

Can the proposed implant fit evaluation be integrated in the clinical workflow?

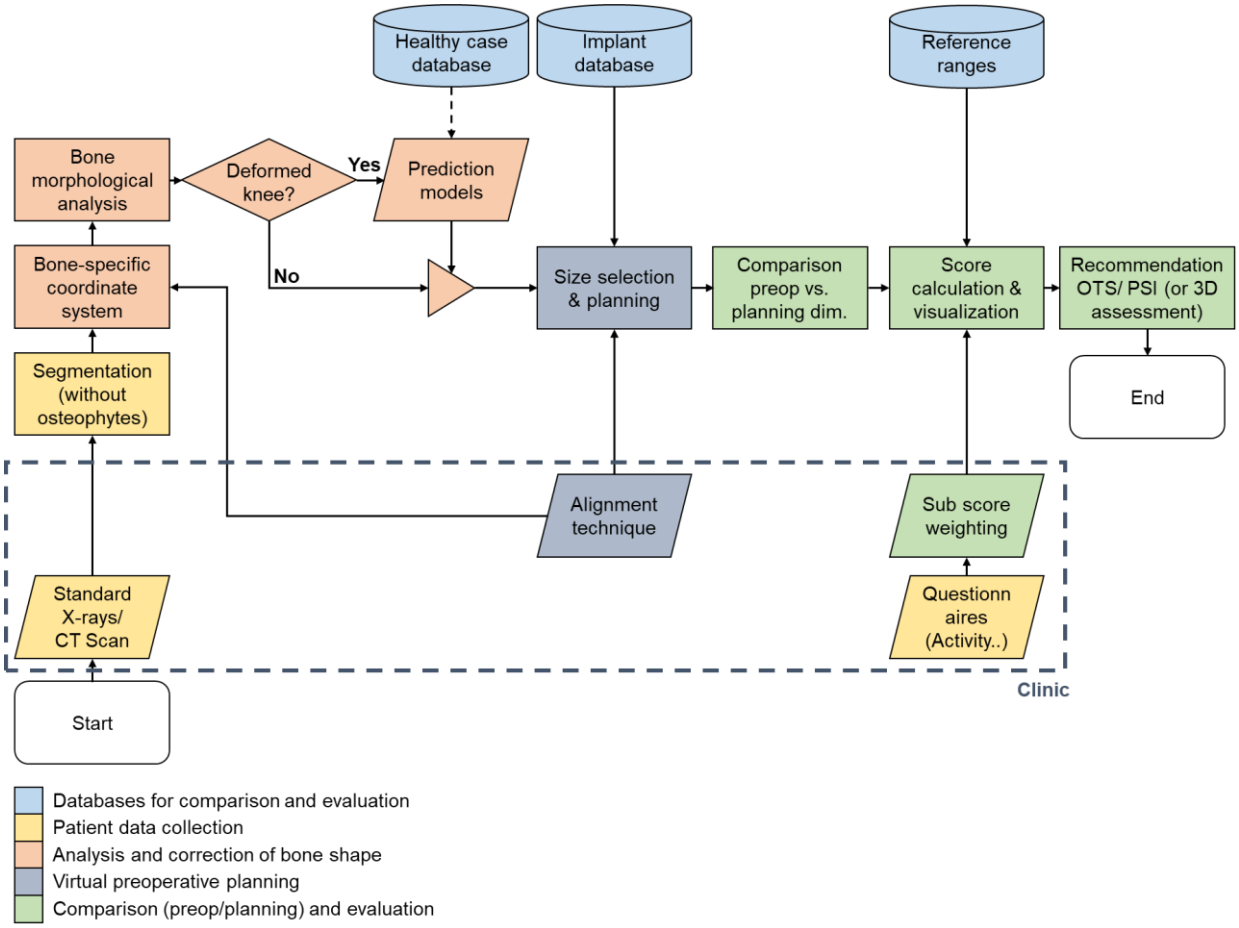

Figure 5-1: General workflow of the implant fit assessment, for both the basic 2D fit assessment and the detailed 3D fit assessment.

5.2 Preliminary fit assessment

After standard TKA imaging, the biplanar radiographs are processed to derive the bone contours required. This step can be automated, for example using a convolutional neural network, while several options are available (Wu and Mahfouz 2016; Dong and Zheng 2008; Chen et al. 2014; Lindner et al. 2013). The labels should be osteophyte-free. A differentiation between the medial and lateral condylar contour is required, such as implemented by Serrurier et al. (Serrurier et al. 2012), to enable an assessment of both structures. Before further processing, all data points including the contours are scaled based on the known dimensions of the scaling object in the radiograph.

Bone- and alignment-specific coordinate system

Bony landmarks are required for bone contour orientation, for the implant positioning as well as for the morphological analysis. To derive respective landmarks, both the frontal and lateral bone contours are repositioned. The mechanical axis of femur and tibia are identified in the lateral view by using a PCA. The first mode of shape variation represents the respective mechanical axis, while for the tibial contours a refinement based on the proximal and distal diaphysis points is required. After orientation of the bone contours along their mechanical axis, further landmarks can be determined. In the frontal view, the same procedure can be applied to the tibia. For the femoral frontal contour, the mechanical axis can only roughly be identified by PCA. For this reason, the actual mechanical axis has subsequently to be defined, by identification of the femoral head center and the distal condylar points.

The femoral head center is determined using a method similar to the one presented by Kuiper et al. (Kuiper et al. 2023) for 3D analysis. Relevant landmarks in the proximal femur region are used to define the femoral head points, which are the input for a circle fit analysis (Circle Fit (Pratt method), MATLAB Central File Exchange, Nikolai Chernov, version 1.0). The mean between medial and lateral most distal condylar point defines the center of the frontal femoral coordinate system. The process is depicted in **Figure 5-2**.

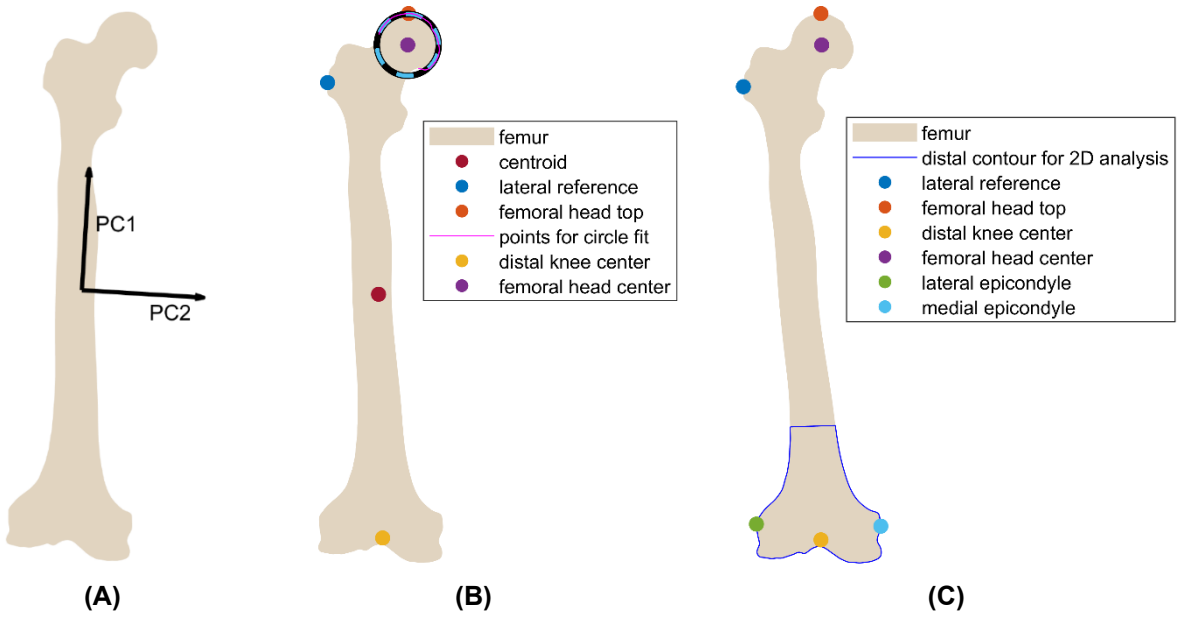

Figure 5-2: Pre-processing of the femoral frontal contour information. **(A)** Femoral contour with principal components 1-2. **(B)** Femoral contour oriented along principal components 1-2, with landmarks. **(C)** Femoral contour oriented along mechanical axis, with further landmarks and the distal contour for 2D fit analysis.

Size selection and planning

The bone contours are transformed according to the alignment selected by the surgeon. In the case of mechanical alignment, no further transformation is required. Afterwards, a morphological analysis is performed. For this purpose, further landmarks are identified based on geometrical relations. The overall size of the bone in ML and AP direction is measured. On the basis of respective measurements, the closest matching implant size is selected, analogue to the size selection in **Chapter 3.1**. Hence the AP fit is prioritized, under consideration of 2 mm estimated cartilage thickness (**Table 5-4**). For the ML fit, only a maximum deviation of 6 mm is defined. The tibial components are rotated according to the slope selected by the surgeon, which may either be generic or personalized. The centroid of the respective bone contour is chosen as an initial position for the contours of the selected implant components. Afterwards the implant contours are shifted with respect to the bone contours, based on previously defined reference landmarks. For the femoral lateral contour, those landmarks include a reference point on the anterior cortex and the most distal and most posterior condylar points. The positioning landmarks for the frontal contour include the medial and lateral most distal condylar points as well as the medial and lateral outer contour points at half of the notch depth in proximodistal direction. For the tibial lateral contour, those landmarks include the most anterior and most posterior plateau points. For the tibial frontal contour, those landmarks include the most medial and most lateral plateau points and the intercondylar eminentia. Afterwards the contours are combined, to define the postoperative knee contours.

Parameter evaluation

Consecutively, accessible (morphological) parameters are evaluated for the native knee and for the individual TKA planning. The accessibility and accuracy of the morphological parameters has been reviewed in **Chapter 4.1.1** and the ones selected for evaluation are listed in **Table 5-1**. A visualization of the preoperative morphological analysis for the sagittal femoral contour is given in **Figure 5-3**. Afterwards a plausibility check of the parameter values is performed, using values from the literature as described by Asseln et al. (Asseln et al. 2018). For plausible parameter values, the boundaries for physiological parameter values from **Chapter 4.3.2** are applied. The previously

presented methodology for deformity correction can be applied, however, respectively large databases of 2D radiographs would be required. Hence, for the given implementation, deformed cases are highlighted and respective morphological fit criteria are excluded from the fit score evaluation. Subsequently, a mean cartilage thickness is added to specific parameters, for which details are given in **Table 5-4**.

Table 5-1: Femoral and tibial morphological parameters to be evaluated in 2D on Frontal and Lateral radiographs. (*) image requirements of the original source. (+) originally defined only for the combined contour. (x) originally defined as the mean between both medial and lateral measurements.

Bone	Image	Aspect	Parameter	Description
Femur	Frontal	Size	Condylar Mediolateral Width	(Mahfouz et al. 2007) (projected)
			Mediolateral Spacing	(Kurosawa et al. 1985)
		Alignment	Anatomical lateral distal femur angle	(Springer et al. 2020)
			Mechanical lateral distal femur angle	(Springer et al. 2020)
		J-Curve	Distal Condylar Offset	(Meier et al. 2019) (projected)
	Lateral	Size	Anteroposterior Size	(Pfeiffer et al. 2018)*
		J-Curve	Posterior Condylar Offset Lateral	(Bellemans et al. 2002; Johal et al. 2012)*+
			Posterior Condylar Offset Medial	(Bellemans et al. 2002; Johal et al. 2012)*+
			Posterior Condylar Offset Ratio Lateral	(Johal et al. 2012)*+
			Posterior Condylar Offset Ratio Medial	(Johal et al. 2012)*+
			Condyle Ratio Lateral	(Pfeiffer et al. 2018)*+
			Condyle Ratio Medial	(Pfeiffer et al. 2018)*+
			Posterior Sagittal Radius Lateral	(Li et al. 2010) (projected)
			Posterior Sagittal Radius Medial	(Li et al. 2010) (projected)
Tibia	Lateral	Size	Anteroposterior depth	(Zhang et al. 2018)
		Alignment	Posterior slope	(Zhang et al. 2018)
	Frontal	Size	Mediolateral width	(Zhang et al. 2018)
		Alignment	Medial proximal tibial angle	(Springer et al. 2020)

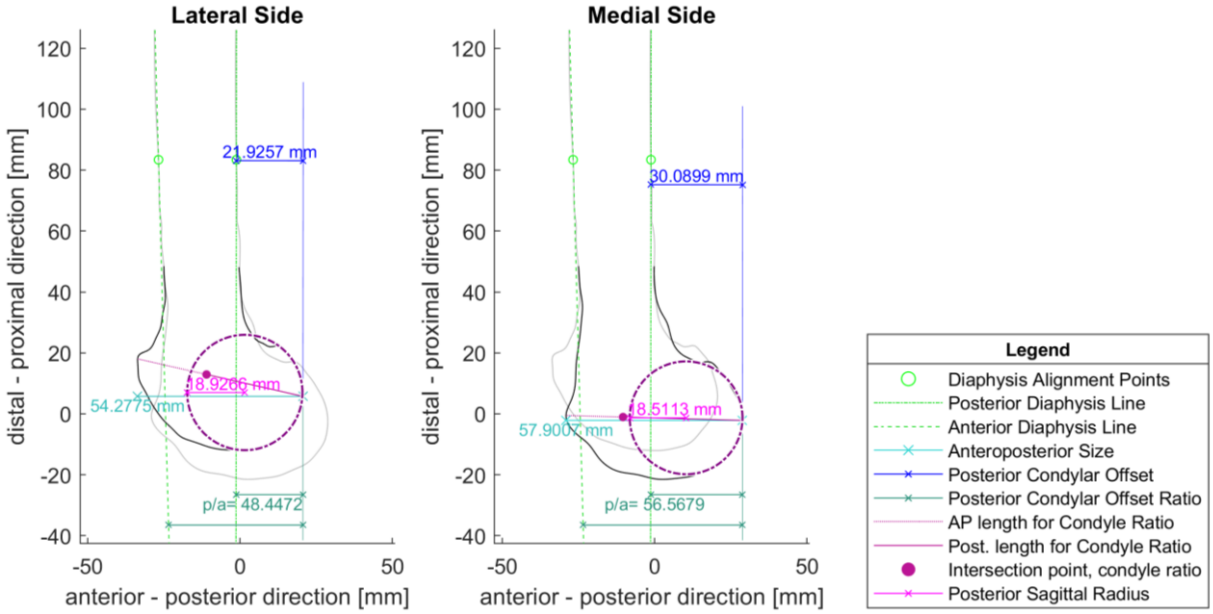

Figure 5-3: Overview of the morphological parameters evaluated in lateral view for the native femur.

The morphological analysis is repeated with the postoperative knee shapes. Finally, all plausible, non-deformed and cartilage-corrected morphological parameter values of the bones are compared with those of the implant, and deviations are reported. The comparison is visualized in form of a bar chart, for which an example can be found in **Figure 5-4**. In addition, a detailed comparison of the preoperative and postoperative J-Curve contour regarding over-/ undersizing is performed, for which an exemplary visualization is given **Figure 5-5**.

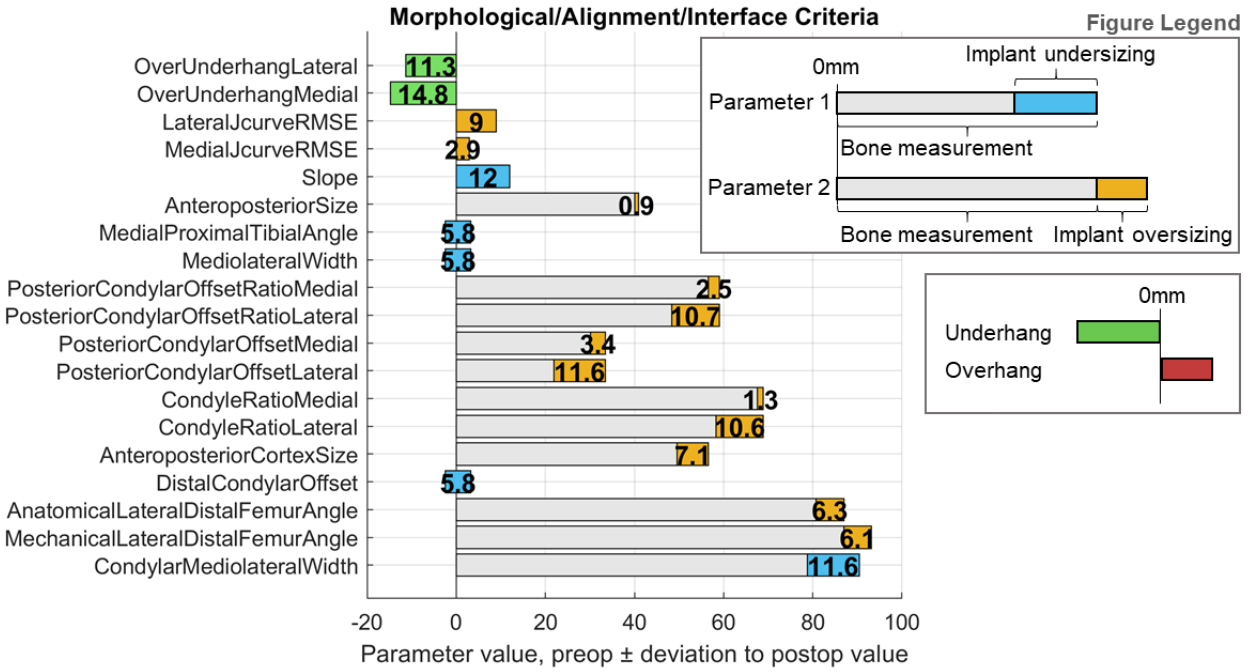

Figure 5-4: Visualization of the patient-specific femoral implant fit with regard to the frontal and sagittal morphological and alignment parameters as well as the projected ML implant over-/ underhang from the 2D analysis. For the morphological parameters, the patient's individual parameter values are given as bars, with the amount of undersize (blue) or oversize (orange) caused by the implant.

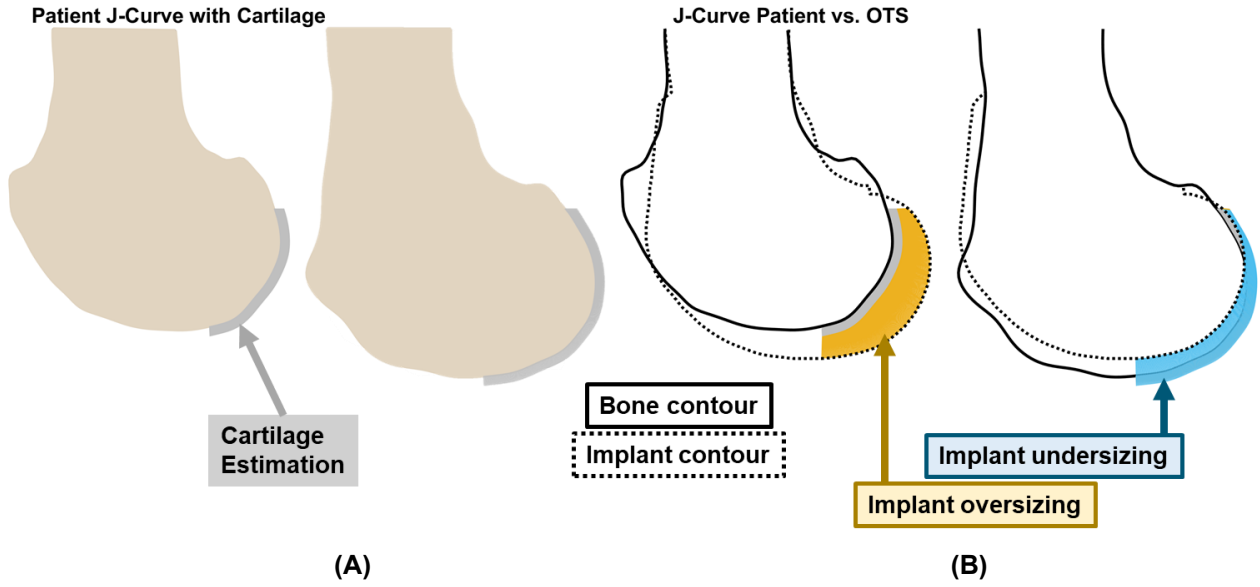

Figure 5-5: Results of the preoperative to postoperative J-Curve comparison. **(A)** Native medial and lateral sagittal bone contours, with estimated cartilage thickness in the functionally relevant J-Curve area. **(B)** Comparison of the native and the postoperative J-Curve shape in the functionally relevant J-Curve area. Offsets are highlighted in blue for undersizing and in yellow for oversizing.

In addition to the morphological and alignment criteria, the projected implant over-/ underhang is assessed. The projection represents an extensive restriction, compared to a comprehensive contour evaluation in 3D. In 2D only the local offset

between bone contour cut, and implant contour in one specific plane including errors through projection is evaluated. Nevertheless, the 2D evaluation may give early insight into the general extent of the full implant over-/ underhang. For the respective evaluation, the ML distance of the virtually resected bone contour and implant contour is calculated on the frontal image. Implant over-/ underhang at the medial and lateral side are reported separately.

Score

For the score calculation, the evaluation and weighting of the morphological parameters and of the projected implant over-/ underhang is performed as described in **Chapter 4.2.3**. In this step, the surgeon can select from different thresholds from the literature or define own thresholds, and also individualize the weighting based on his/her experience or based on patient-specific factors (age, ligament status, etc.). Subsequently, for each case and each implant component analyzed, a summary of the individual implant fit rating is provided in form of a spider plot. An exemplary spider plot with highlighting of the individual scoring, the start and threshold values, as well as the risk and safe zone(s) can be found in **Figure 5-6**. An assignment of the presented criteria or (sub-)scores to the categories interface, morphology, alignment and other can be found in **Figure 5-7**.

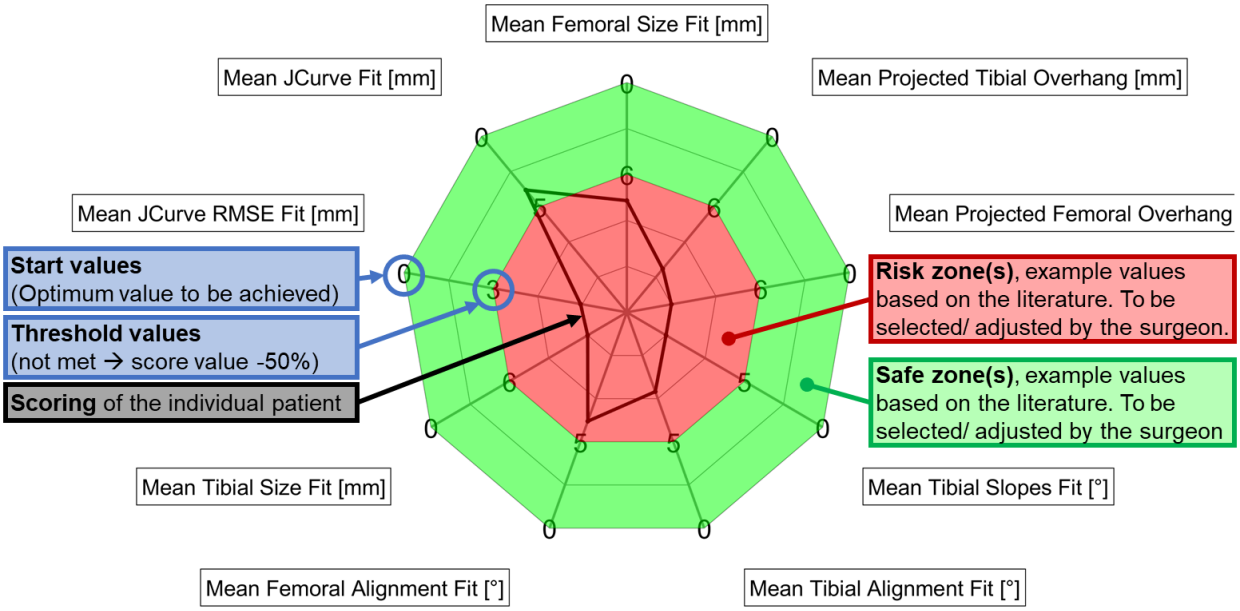

Figure 5-6: Exemplary spider plot visualization of the basic, initial 2D fit evaluation. The individual scoring, start and threshold values as well as exemplary risk and safe zones(s) are highlighted.

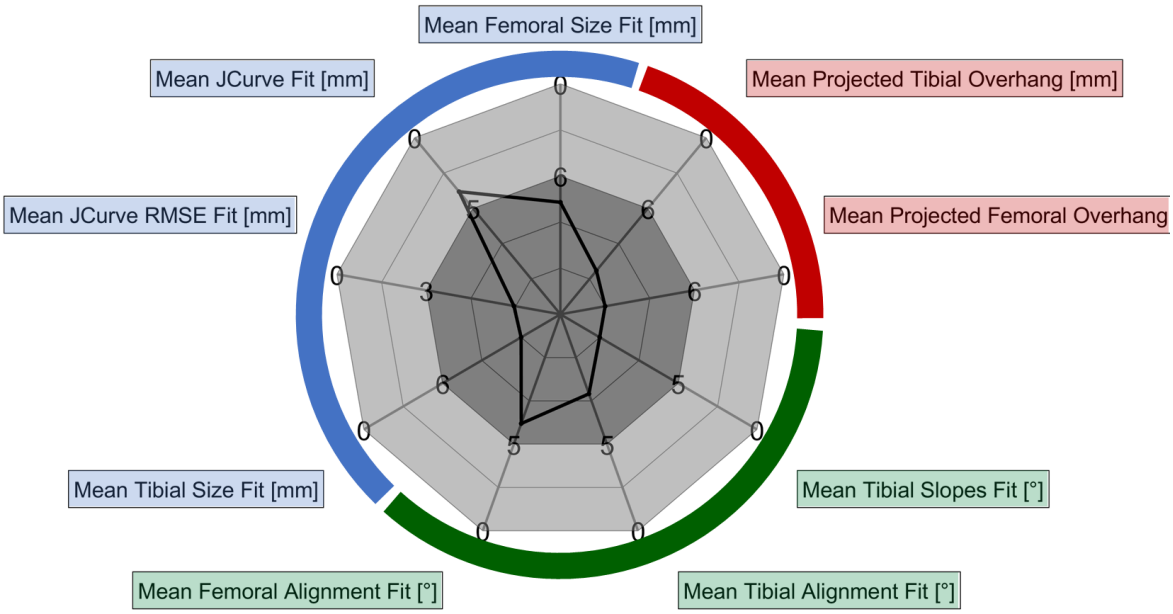

Figure 5-7: Exemplary spider plot visualization of the basic, initial 2D fit evaluation. The correspondence of individual scores to the different categories of criteria is given.

As described in **Chapter 4.1.5** (**Figure 4-5**), the interpretation of the score depends on the dimensionality of assessment, with the 2D evaluation providing a preliminary, basic fit assessment. With the visualizations and the combined score resulting from the 2D evaluation, an initial evaluation and comparison of the best-matching sizes of implant systems from different manufacturers are possible. A subsequent detailed 3D fit analysis may be recommended in the following cases:

1. The surgeon wants to analyze **further fit criteria** (e.g., the posterolateral tibial posterolateral overhang or interbone parameters such as the TT-TG distance)
2. **Remaining uncertainty** about the adequacy of the fit (e.g., based on the X-ray analysis it is unclear whether the mediolateral overhang exceeds the recommended 3 mm threshold and/or if the tibial coverage is sufficient)
3. The surgeon deems the achieved **fit inadequate** (hence a detailed evaluation and potentially a comparison with a customized implant is indicated)

5.3 Detailed 3D fit assessment

The first step of the detailed fit assessment is 3D imaging (CT/MRI). Afterwards, segmentation and osteophyte removal are required. Both can be performed semi-automatically. CNN-based tools are available for the segmentation process (Minnema et al. 2018), including ones specifically designed for image segmentation of osteoarthritic knees (Marsilio et al. 2022). Ideally, the bones are segmented without osteophytes. Alternatively, the osteophyte removal can be performed afterwards, for example based on an SSM (Hänisch and Radermacher 2016). A pre-processing including uniform mesh resampling and shape preserving smoothing (Taubin Smooth, Meshlab, Visual Computing Lab, ISTI-CNR) (Cignoni et al. 2008) is performed.

5.3.1 3D TKA Planning

The 3D TKA planning is described exemplarily for the Sigma PFC implant system (Depuy Synthes, Raynham, MA, US). For the exemplary description and subsequent database analysis the femoral size 5 and the tibial tray size 4 (revision system) (D'Lima et al. 2006) were used, which were provided in the scope of the fourth grand challenge competition, presented by Fregly et al. (Fregly et al. 2012). The implant surface models were processed and analyzed regarding respective cutting planes, and the outer contour was determined. The description of the automated virtual implantation is given in the following, individually for the femur and tibia. An exemplary documentation of the respective 3D TKA planning results is provided in **Appendix D)**.

Femur

As a first step of 3D TKA planning, the surface model of the distal femur is roughly oriented in the CT coordinate system (RAS) and then transformed into a unified sagittal plane as described by Li et al. (Li et al. 2010). Subsequently, the femoral epicondyles are identified. Depending on the selected alignment technique, bone and implant meshes are transformed accordingly. For the mechanical alignment, the femur is transformed so that the z-Axis coincides with the bone's mechanical axis. The x- and y-axes are defined by using the femoral epicondyles (**Figure 5-8**). The sizing is performed as described for the cadaver knees in **Chapter 3.1.2**, by measuring the bone's AP height

and condylar ML width. To measure the AP height, the distance between the anterior cortex and the most posterior point in AP direction is determined (Du et al. 2017; Dai et al. 2014b). For the sizing, two millimeters of estimated cartilage thickness at the posterior condyles are added (Omoumi et al. 2015; Wernecke et al. 2016) with the goal of recreating the physiological articulating morphology. The condylar ML width is measured 10 mm above the most distal point of the condyles, as an estimate for the distal femoral resection cut. The with was then defined as the distance of the most medial and most lateral condylar point in ML direction. The bone's size is then compared with the implant size information. The AP size fit is prioritized, because of its high functional relevance. Maximum deviation in AP is set to 3 mm overall. With regard to ML fit, solely a maximum deviation of 6 mm is set, to limit maximum overhang on each side to 3 mm, as suggested by Mahoney et al. (Mahoney and Kinsey 2010). Maximum deviation in AP is set to 3 mm overall. For the analysis of the bone-implant interface match, the implant is first translated and rotated to match the positioning landmarks on implant and femur, resulting in imitation of an anterior referencing technique. Respective landmarks include the anterior cortex point as well as the distal condylar points. After positioning, the femur is virtually resected following the implant's cutting planes.

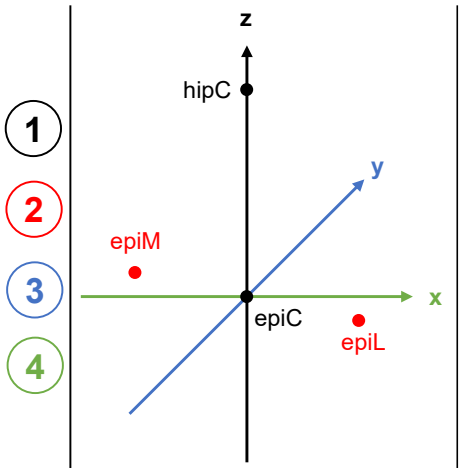

Figure 5-8: Definition of the femoral coordinate system for mechanical alignment. The numbers represent the order of steps with respect to the bone transformations. Legend: hipC= hip joint center, epiL= lateral epicondyle, epiM= medial epicondyle, epiC= midpoint between epiM and epiL.

Tibia

As for the femur, the segmented surface model of the proximal tibia is roughly oriented in the CT coordinate system (RAS). The plateau centers are determined and iteratively

optimized according to the definition by Cobb et al. (Cobb et al. 2008) and the implementation by Asseln et al. (Asseln et al. 2017). For the final COS, the tibia is rotated so that the z-axis coincides with the bone's mechanical axis. The y-axis is defined perpendicular to the z-axis and the connecting line of the final (optimized) tibial plateau centers. The x-axis is defined as orthogonal to the y- and z-axis. The resection cut is set at 15 mm below the lowest plateau point. The resection is adjusted to the example implant system used, which has a tray plateau height of 14 mm and an insert contact point height of ~3 mm (above the tray's outer rim). With an estimated cartilage thickness of 2 mm at the tibial articulating surface, a cut depth of 15 mm is required (*14 mm (tray plateau) + 3 mm (insert) - 2 mm (cartilage) = 15 mm*). Recommendations for the posterior slope range from 0-7° (Dai et al. 2014a; Kim et al. 2014). Slopes from 5-7° lead to an inadequate stem position with penetration of the tibial diaphysis surface. Hence, a posterior slope of 4° is used. Then, the ML width and AP height are measured at the resection cut level (Dai et al. 2014a). The ML width is defined as the distance of the most medial to the most lateral point in x-direction. The AP height is defined as the distance of the most anterior to the most posterior point in the z-y-plane. The measurements are compared with those of the implant systems' tibial trays. For the size choice, AP and ML are equally weighted. With regard to both, a maximum deviation of 6 mm is set, to avoid clinically relevant overhang. Subsequently, the implant is positioned with regard to the tibia based on bony landmarks and the implant equivalents. Those include the most anterior and posterior as well as most medial and lateral plateau points.

5.3.2 Interface criteria

For the evaluation of interface criteria, the outer contour of bone and implant at the interface level are determined. Respective data points are identified on the basis of the normal vectors of the cutting planes. The assignment to the individual cutting planes is saved. The contours are post-processed, including interpolation with equal distances. Exemplary contours are given in **Figure 5-9**, with a color code for the five cutting planes of the respective implant component. The contours are also displayed in a developed view in 2D, which provides a better overview of the implant over-/ underhang along the entire bone contour.

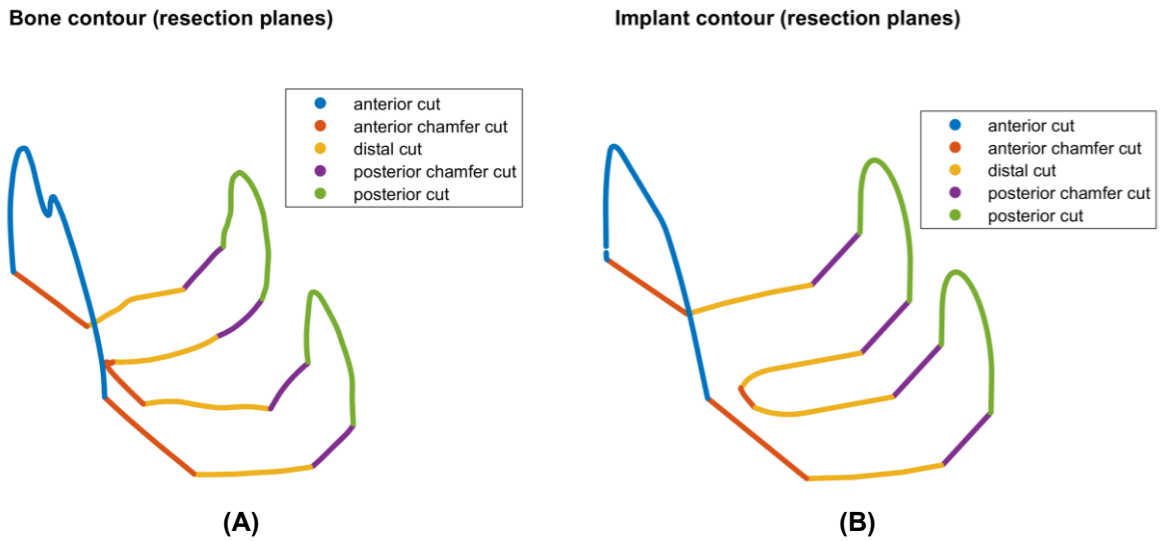

Figure 5-9: Processed contours of **(A)** an exemplary femoral bone and **(B)** the femoral implant component analyzed. The assignment to specific cutting planes is visualized.

First, implant over-/ underhang is evaluated over the entire interface area, however, excluding the posterior notch analogous to Schroeder et al. (Schroeder and Martin 2019) and Dai et al. (Dai et al. 2014a). Over-/ underhang is calculated as point-to-line error, normal to the implant contour. Second, over-/ underhang is evaluated in specific zones, defined by Bonnin et al. (Bonnin et al. 2013) and by Dai et al. (Dai et al. 2014b). Thereby, a literature-based verification of the results is enabled. In addition, bony coverage is evaluated over the entire interface and at the cortical rim, defined by a 1.5 mm thick area from the outer contour, according to Fitzpatrick et al. (Fitzpatrick et al. 2007) and Carpenter et al. (Carpenter et al. 2014). Visualizations of an example case are given in **Figure 5-10**-**Figure 5-11** for the femur and in **Figure 5-12** for the tibia.

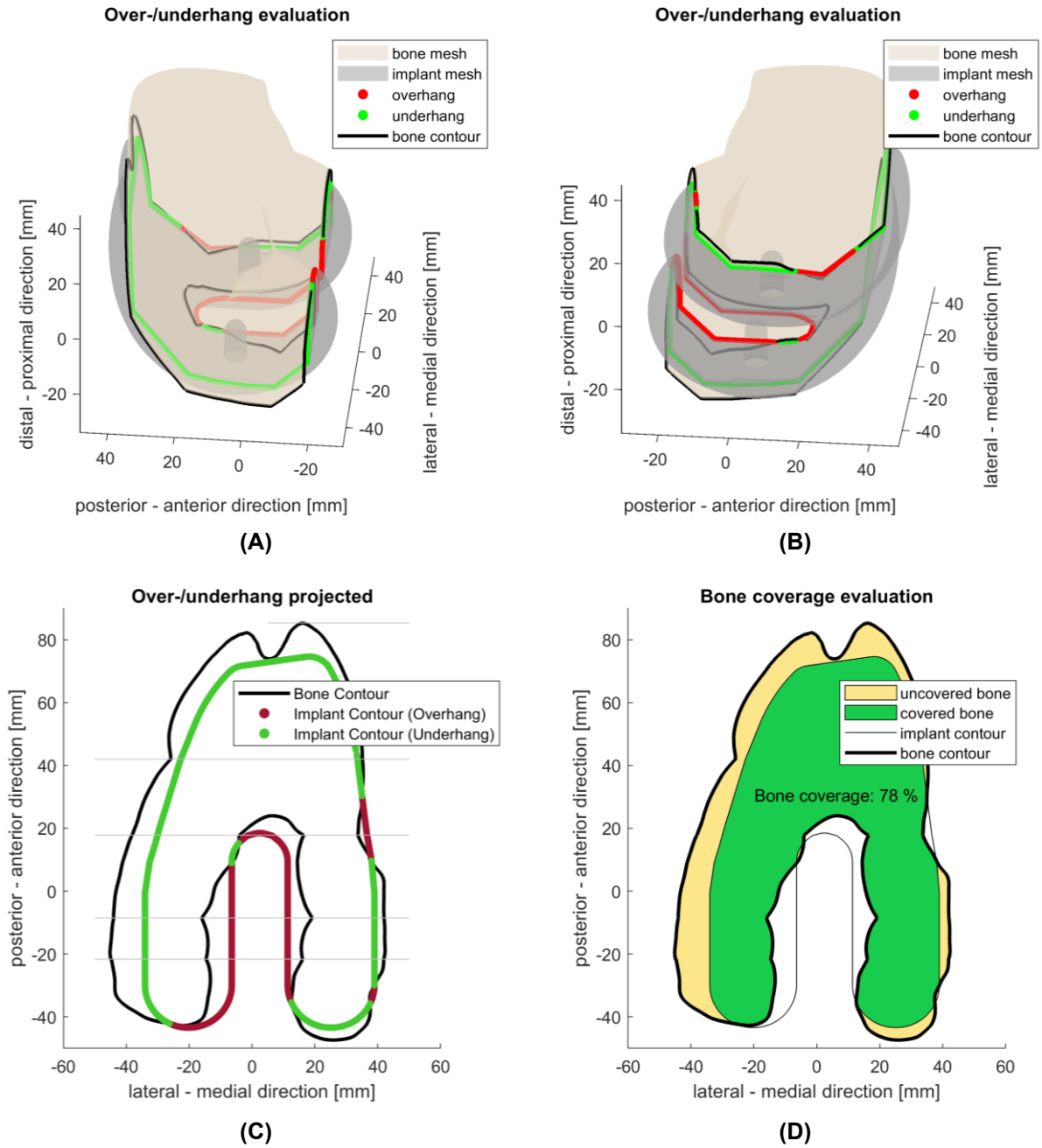

Figure 5-10: Results of the femoral interface fit evaluation. Femoral over-/ underhang evaluation in 3D, together with the implant and bone surface models **(A)** in anteromedial-posterolateral view and **(B)** in posteromedial-anterolateral view. **(C)** Femoral over-/ underhang and **(D)** coverage evaluation in developed view. Overhang is visualized in red, underhang is visualized in green. The covered bony surface at the interface level is highlighted in green, the uncovered are is highlighted in yellow. The coverage is given in percentage.

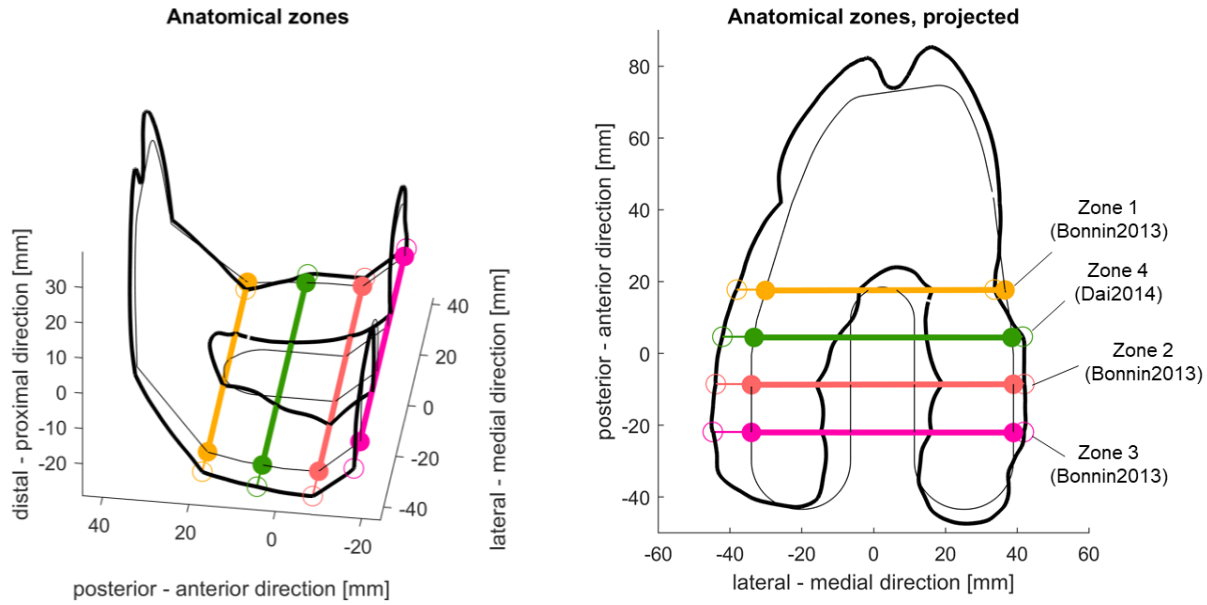

(E) **(F)**

Figure 5-11: Anatomical zones defined in the literature for over-/ underhang evaluation. **(A)** 3D view. **(B)** Projected contours.

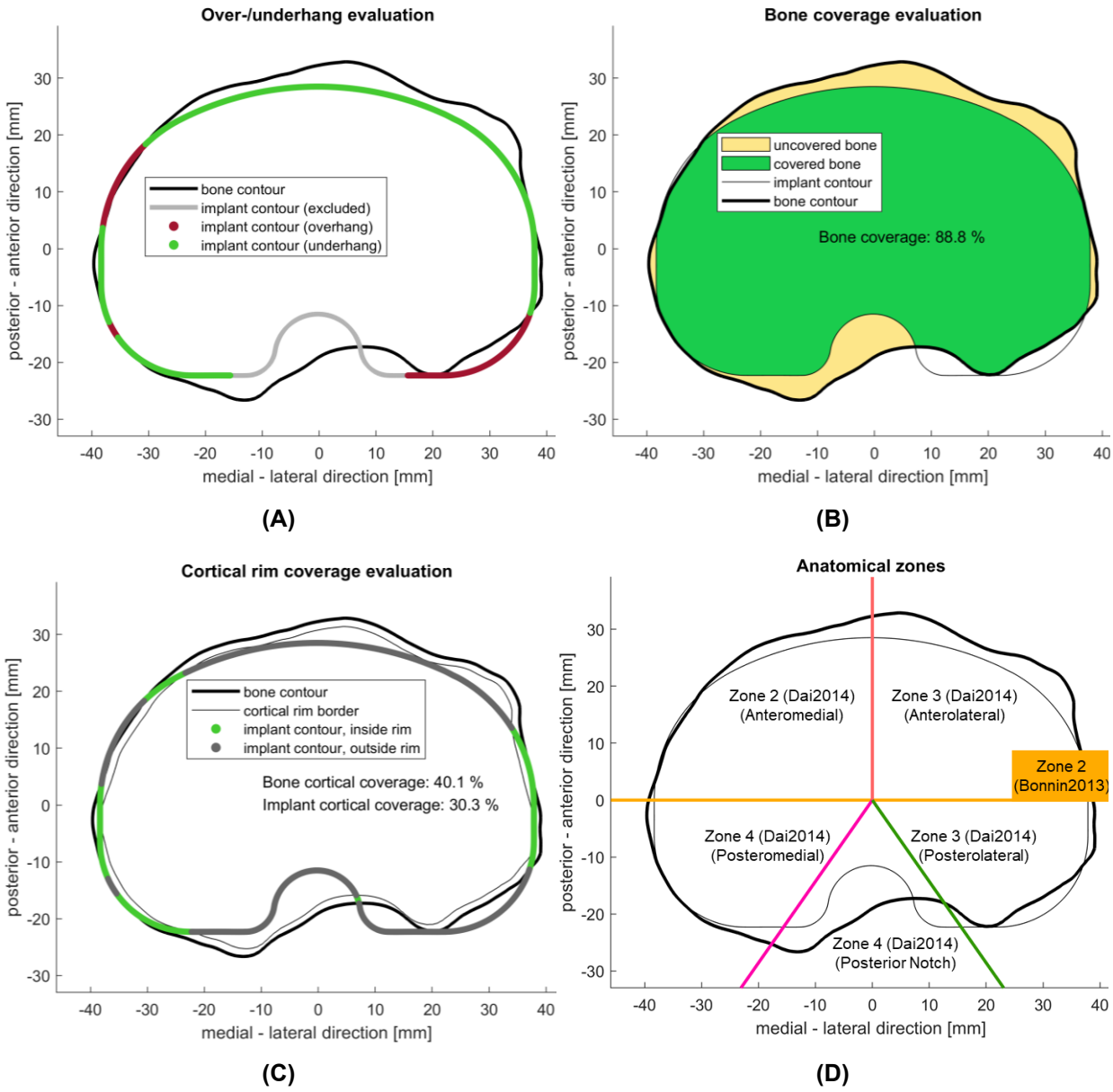

Figure 5-12: Results of the tibial interface fit evaluation (all images in superior view). **(A)** Tibial over-/ underhang evaluation. Implant overhang is visualized in red, underhang is visualized in green. **(B)** Tibial coverage evaluation. The covered bony surface at the interface level is highlighted in green, the uncovered area is highlighted in yellow. **(C)** Implant cortical bone coverage evaluation according to Fitzpatrick et al. (Fitzpatrick et al. 2007). The outer implant contour points at the interface level are highlighted in green, if located in the cortical rim area. In addition, the cortical rim coverage of the bone is given in percentage. **(D)** Anatomical zones defined in the literature for over-/ underhang and coverage evaluation according to Dai et al. (Dai et al. 2014a) and Bonnin et al. (Bonnin et al. 2013).

5.3.3 Morphological and alignment criteria

A morphological analysis of both surface models of the native knee and those of the merged postoperative shape of implant and bone is performed, to evaluate morphological and alignment criteria. The consequences of implant component

(mal-) alignment can be assessed both by the corresponding angular measures, including the tibial sagittal slopes, the tibial coronal slope and the mechanical LDFA, as well as by the resulting impact on morphological parameters. For example, external rotation of the femoral component rotation regularly decreases lateral trochlear height and shifts the trochlea groove laterally (Dejour et al. 2014), leading to changes in TT-TG distance, patellar shift, and others.

To evaluate respective parameters, the framework for morphological analysis developed by Asseln et al. (Asseln et al. 2018; Asseln 2019) was adapted to also allow for the analysis of the postoperative shape. In addition to the existing parameters, the analysis of specifically listed morphological fit parameters (**Chapter 4.2.2**), of interbone parameters (**Appendix B)**) as well as of the 3D J-Curve RMSE (preoperative compared to postoperative) was integrated in the framework. The list of morphological parameters considered for fit evaluation is given in **Table 5-2**.

Table 5-2: Femoral and tibial morphological parameters to be evaluated on 3D bone models. (*) originally defined for 2D analyses. (x) originally defined for manual measurement. (+) adapted, using the mechanical axis instead of the cortex or anatomical axis lines as reference lines.

Bone	Aspect	Parameter	Literature reference
Femur	Sizing	Condylar ML Width	(Mahfouz et al. 2007)
		Overall AP Length	(Mahfouz et al. 2007)
		Lateral Condylar Depth	(Mahfouz et al. 2007)
		Medial Condylar Depth	(Mahfouz et al. 2007)
	Trochlea	Anterior ML Width	(Mahfouz et al. 2007)
		Lateral Trochlear Elevation	(Varadarajan et al. 2011)
		Medial Trochlear Elevation	(Varadarajan et al. 2011)
		Central Trochlear Elevation	(Varadarajan et al. 2011)
		Trochlear Depth	(Pfirrmann et al. 2000)
		Mediolateral Sulcus Displacement	(Varadarajan et al. 2011)
	J-Curve	Mediolateral Spacing	(Bellemans et al. 2005)
		Posterior Mediolateral Width	(Mahfouz et al. 2007)
		Distal Condylar Offset	(Meier et al. 2019)
		PCO Lateral	(Bellemans et al. 2002; Johal et al. 2012)*+
		PCO Medial	(Bellemans et al. 2002; Johal et al. 2012)*+
		Lateral Distal Sagittal Radius	(Ardestani et al. 2015)
		Medial Distal Sagittal Radius	(Ardestani et al. 2015)
		Lateral Posterior Sagittal Radius	(Li et al. 2010)
		Medial Posterior Sagittal Radius	(Li et al. 2010)
		PCO Ratio Lateral	(Johal et al. 2012)*+
		PCO Ratio Medial	(Johal et al. 2012)*+
		Condyle Ratio	(Pfeiffer et al. 2018)*
	Alignment	Mechanical LDFA	(Springer et al. 2020)*
		Posterior Condylar Angle	(Berger et al. 1993)
Tibia	Sizing	ML Width	(Zhang et al. 2018)
		AP Height	(Zhang et al. 2018)
	Alignment	Medial Sagittal Tibial Slope	(Zhang et al. 2018)
		Lateral Sagittal Tibial Slope	(Springer et al. 2020)
		Coronal Tibial Slope	(Hashemi et al. 2008)
		Tuberositas Tibiae Angle	(Mahfouz et al. 2012)
Inter-bone	Alignment	Patella Tilt	(Davies et al. 2000)
		Patella Shift	(Chia et al. 2009)
		TTTG Distance	(Schoettle et al. 2006)
		Joint Rotation	(Seitlinger et al. 2012)
		Insall Salvati Index 3D	(Insall and Salvati 1971; Fürmetz et al. 2021)

As a first step, the **preoperative morphology** is analyzed with the framework for morphological analysis described. Subsequently, both a plausibility (Asseln et al. 2018) and a deformity check are performed for the preoperative parameter values. If a parameter value is identified as “deformed”, an equivalent healthy parameter value is estimated by using regression models. The regression models were defined according to the methods developed in **Chapter 4.3**. The accuracy in this case is significantly higher as in the 2D evaluation, as more parameters from the 3D evaluation can be used

for prediction. Information about the prediction models used for the specific deformity parameters and related affected parameters are given in **Table 5-3**. If the share of 95% of case correction was not reached, instead of applying the regression model, the gender-specific mean value of the physiological cases was used for the individual deformity parameter. In this context, the medial tibial slope's cut-off values reported in the literature were identified to be incompatible with the parametric database used, as the mean values of the healthy population exceeded these boundaries. Hence, this parameter was not considered as a deformity parameter in the implementation presented.

Table 5-3: Prediction models used for individual deformity parameters. The number (n) of not affected parameters (NAP) was empirically defined. Note: Only regression models were considered as prediction models in this exemplary implementation. **Err:** Regression model did not yield 95% corrected cases. Hence the minimum number of AP yielding the maximum percentage of corrected cases is provided. Respective parameters are highlighted in grey. **Note:** The training and test data split is randomized, hence when repeating the data preparation and using the new datasets for training, differences in the required NAP, the prediction models and the resulting accuracy can occur.

Origin	Bone	Aspect	Deformity parameter	Nr AP	Prediction model	Specifics	Max
Con-genital	Femur	Trochlea	Trochlear depth	13	Regression	Elastic Nets α=.25	
			Trochlear Facet Asymmetry	20	Regression	Elastic Nets α=.25	
		Notch	Intercondylar Width	14	Regression	Ridge	
	Tibia	Slopes	Medial Sagittal Tibial Slope	1	Regression	Ridge	3.4%
OA-related	Femur	J-Curve	Distal Condylar Offset	9	Regression	Elastic Nets α=.25	
			PCO Lateral	25	Regression	Lasso	94%
		Alignment	Posterior Condylar Angle	31	Regression	Elastic Nets α=.25	
	Tibia	Alignment	Coronal Tibial Slope	7	Regression	Elastic Nets α=.25	
	Interbone	Alignment	TT-TG	1	Regression	Ridge	

In addition to the parameter-based deformity correction, an estimated cartilage thickness is considered with specific parameters (see **Table 5-4**). Of note, individual cartilage defects or the general severity of the cartilage degeneration of the patient are irrelevant because the pre-arthritic, healthy shape of the articulating surfaces is targeted.

Table 5-4: Estimated cartilage thickness added to individual femoral parameters.

Aspect	Parameter	∆Cartilage	Source(s)
Sizing	Overall AP Length	4.5 mm	(Favre et al. 2017; Wernecke et al. 2016; Omoumi et al. 2015)
	Lateral Condylar Depth	4.5 mm	
	Medial Condylar Depth	4.5 mm	
J-Curve	Posterior Condylar Offset	2 mm	(Favre et al. 2017; Wernecke et al. 2016; Omoumi et al. 2015)
	Posterior Condylar Offset	2 mm	
	Lateral Distal Sagittal Radius	2 mm	(Favre et al. 2017)
	Medial Distal Sagittal Radius	2 mm	
	Lateral Posterior Sagittal Radius	2 mm	(Wernecke et al. 2016; Omoumi et al. 2015)
	Medial Posterior Sagittal Radius	2 mm	
Trochlea	Central Trochlear Elevation	4 mm	(Favre et al. 2017)
	Medial Trochlear Elevation	2.5 mm	
	Lateral Trochlear Elevation	2.5 mm	
	Trochlear depth	-1.5 mm	

As a next step the **postoperative morphology** is analyzed. For this purpose, the shape of the implant components and that of the resected bones are merged and a combined surface is generated by using the gptoolbox from the MATLAB Central File Exchange (gptoolbox, MATLAB Central File Exchange, Alec Jacobson, version 1.0.0.0). In this way, all aspects of the planning process, including the alignment and referencing, are taken into account. The previously identified bone-specific coordinate system is used to orient the merged meshes. The relative orientation of the bones is approximated by joining the estimated contact areas of the articulating surfaces in extension. For patella positioning, medial and lateral contact with the implant's trochlea is targeted, with a distance of 4.0 mm, to account for patellar cartilage (Sittek et al. 1996; Draper et al. 2006). An exemplary visualization of the postoperative mesh orientation process is given in **Figure 5-13**, with which the morphological analysis is repeated. Respective measurements are then compared with the native bone's parameter values, after the previously described correction of potential deformities and consideration of cartilage.

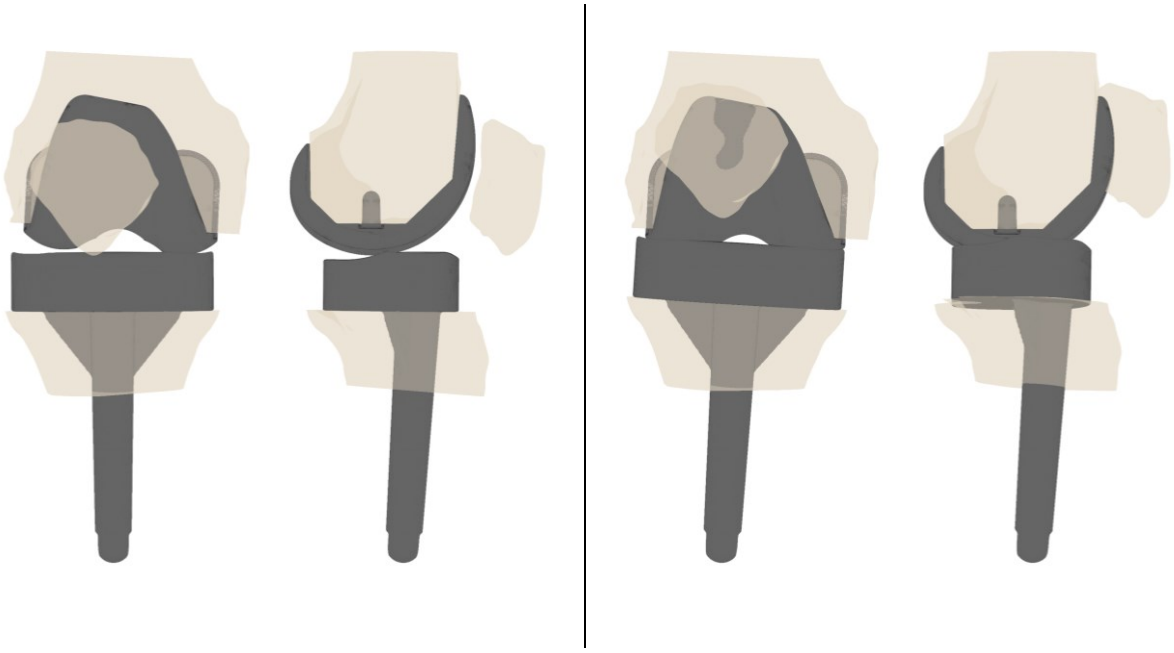

Figure 5-13: Orientation of the bone and implant merged surfaces for interbone morphological analyses. **(A)** Merged meshes of femur and tibia with the native patella before alignment and **(B)** after alignment via joining estimated contact points.

An exemplary visualization of the morphological and alignment fit results are given in **Figure 5-16 A-B**. In the bar charts, the parameter values of the native knee are given, and the amount of undersizing (oversizing) by the implant is highlighted in blue (orange). Because of the high relevance of the J-Curve, an additional detailed RMSE calculation is performed and the respective plot is provided, for which an example can be found in **Figure 5-16 C-D**. Further, shape deviations are visualized over the whole surface in **Figure 5-15**, similar as presented by Akbari Shandiz et al. (Akbari Shandiz et al. 2018).

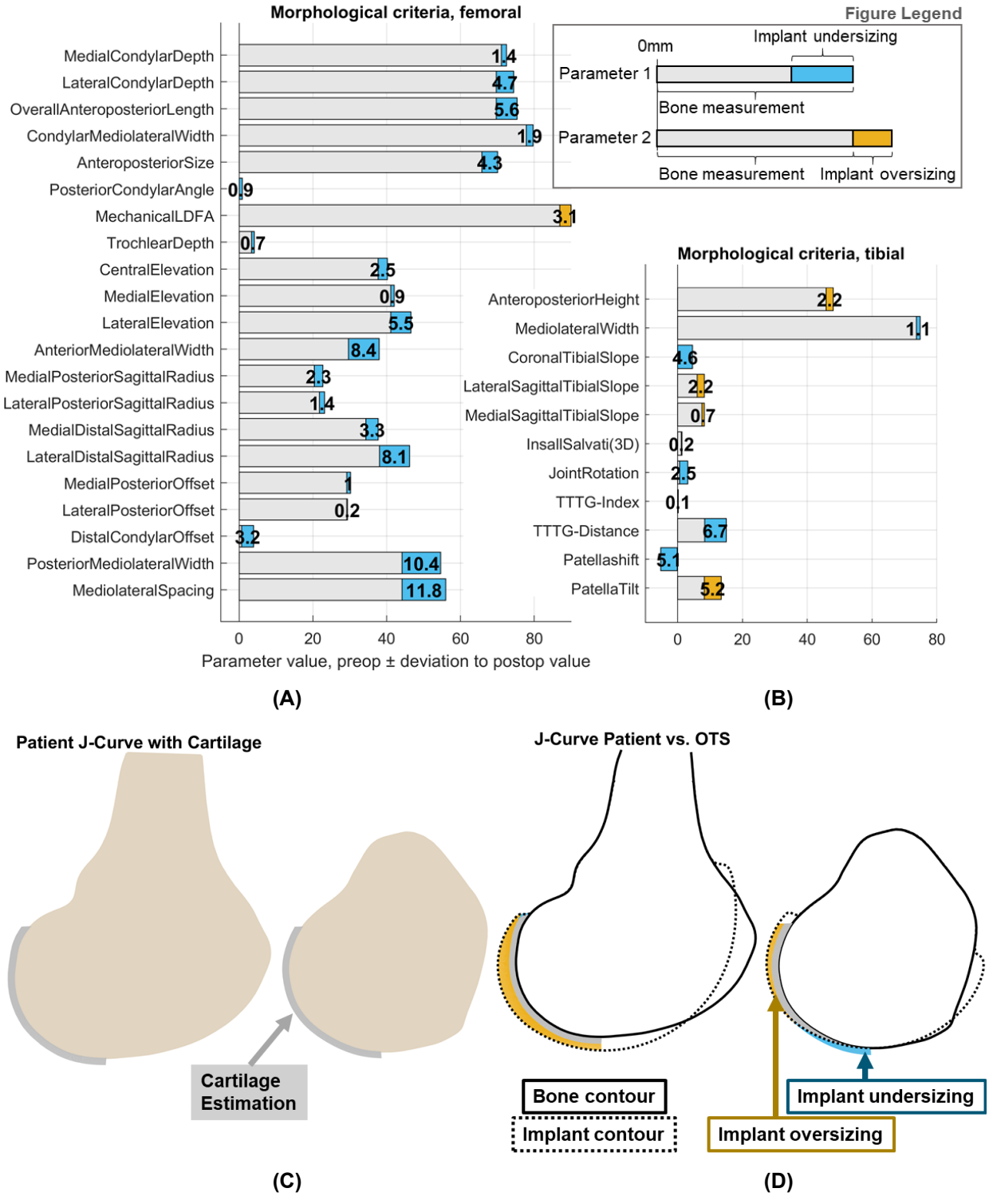

Figure 5-14: Results of the detailed morphological and alignment fit evaluation for an exemplary case. **(A)** Bar chart of femoral morphological/ alignment parameters. **(B)** Bar chart of tibial morphological/ alignment parameters. **(E)** Native medial and lateral sagittal bone contours, with estimated cartilage thickness in the functionally relevant J-Curve area. **(F)** Comparison of the native and the postoperative J-Curve shape in the functionally relevant J-Curve area. Offsets are highlighted in blue for undersizing and in yellow for oversizing.

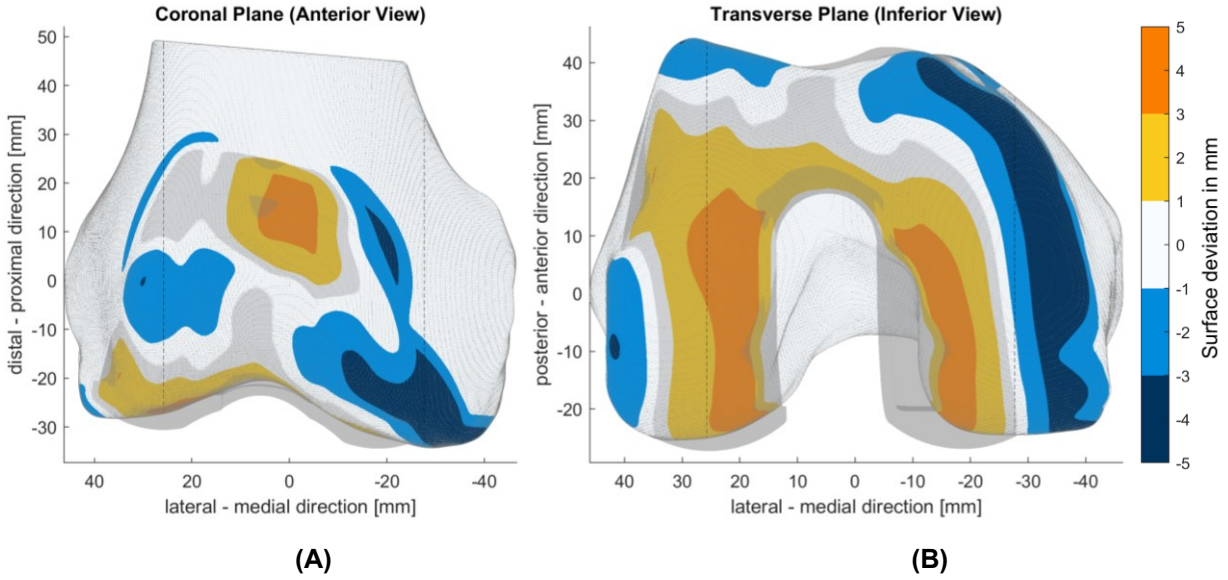

Figure 5-15: Results of the detailed fit evaluation for an exemplary cadaver case for which the available implant size was selected. **(A)** Surface deviation visualized in anterior-posterior view and **(B)** in distal-proximal view. **Note:** in the case of deformities in the articulating areas, a deformity correction and subsequent surface modification by methods for surface parametrization is required, such as presented by Asseln et al. (Asseln et al. 2015; Asseln et al. 2017; Asseln 2019). Implant surface model: Sigma femoral component size 5 (Depuy Synthes, Raynham, MA, US) (Fregly et al. 2012).

5.3.4 Other criteria

The bone cut volume is calculated using the meshboolean function from the gptoolbox of the MATLAB Central File Exchange (gptoolbox, MATLAB Central File Exchange, Alec Jacobson, version 1.0.0.0). The visualization of the femoral and tibial bone cut volume for an exemplary case is given in **Figure 5-16**.

Notching is ruled out in this workflow by using anterior referencing, whereas it should be considered when using posterior referencing or other referencing techniques. A grading based on existing classification systems (Gujarathi et al. 2009) or cut-off values (Stamiris et al. 2022) could directly be used as a fit score component.

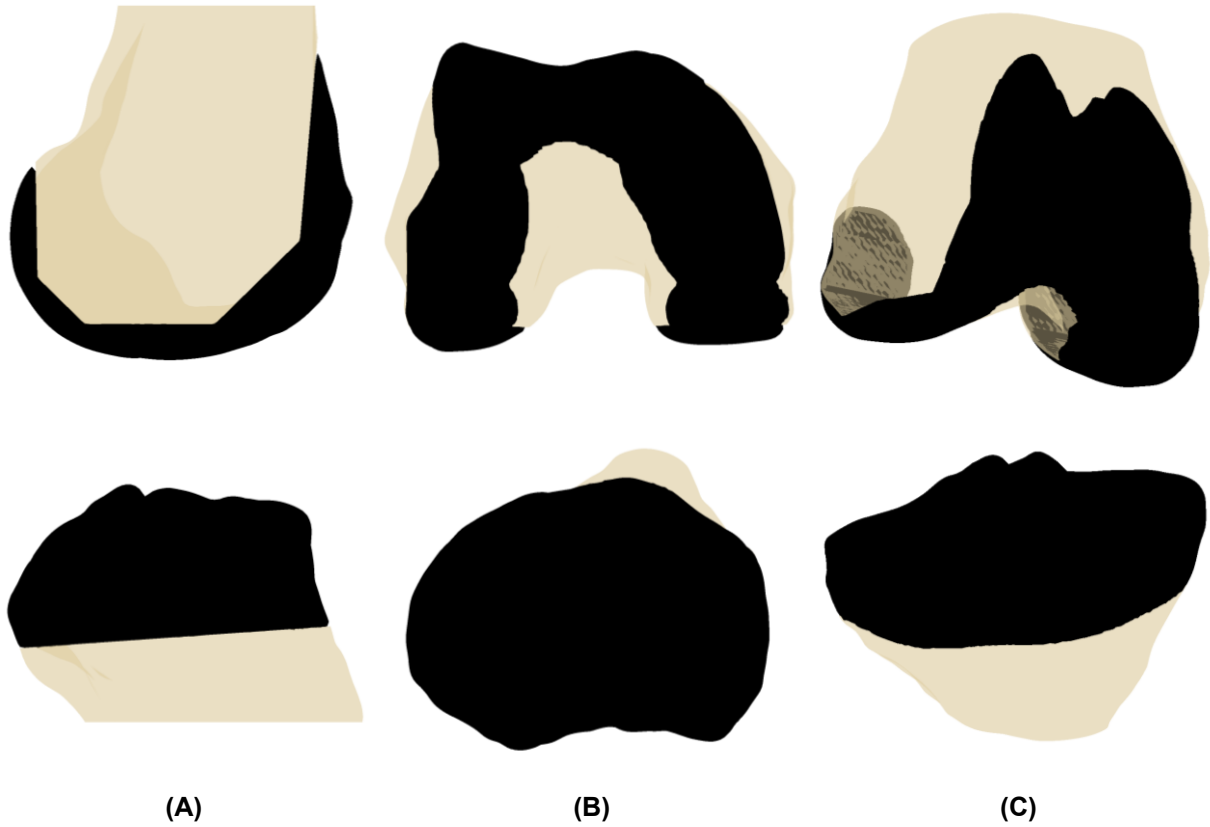

Figure 5-16: Visualization of the bone cut volume in black of the femur and tibia of one example case, in **(A)** medial-lateral view, **(B)** inferior-superior view, and **(C)** anterolateral-posteromedial view.

5.3.5 Score and visualization

For the score calculation, the evaluation and weighting of the individual parameters is performed as described in **Chapter 4.2.3**. For the evaluation, the surgeon selects from the provided thresholds derived from the literature, or defines individual thresholds her/him-self. The surgeon can adapt all weights, both of the individual criteria as well as of the sub-score rating e.g., based on patient-specific factors. For each implant component analyzed, visualizations are given. The combined score is visualized in a spider plot, whereby the surgeon can easily assess the fit regarding the individual sub-scores of the categories developed (interface, morphology, alignment, other). An exemplary spider plot with highlighting of the individual scoring, the start and threshold values, as well as the risk and safe zone(s) can be found in **Figure 5-17**. An assignment of the presented criteria or (sub-)scores to the categories interface, morphology, alignment and other can be found in **Figure 5-18**.

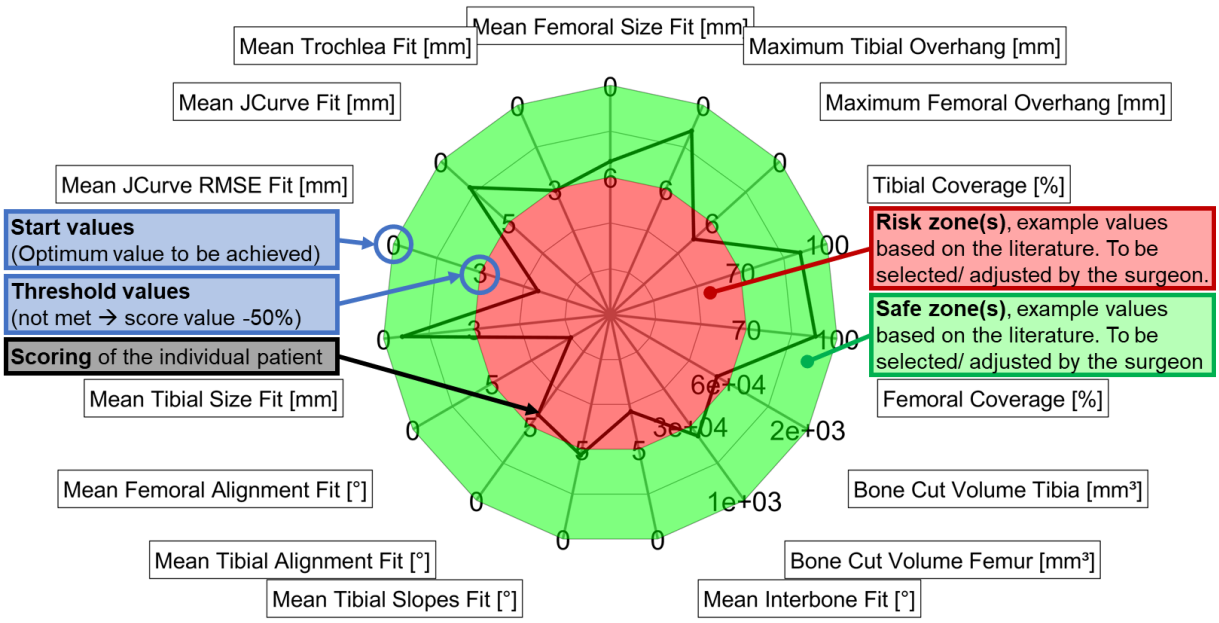

Figure 5-17: Exemplary spider plot visualization of the (patient-specific) detailed 3D fit evaluation. The individual scoring, start and threshold values, and exemplary risk and safe zones(s) are highlighted.

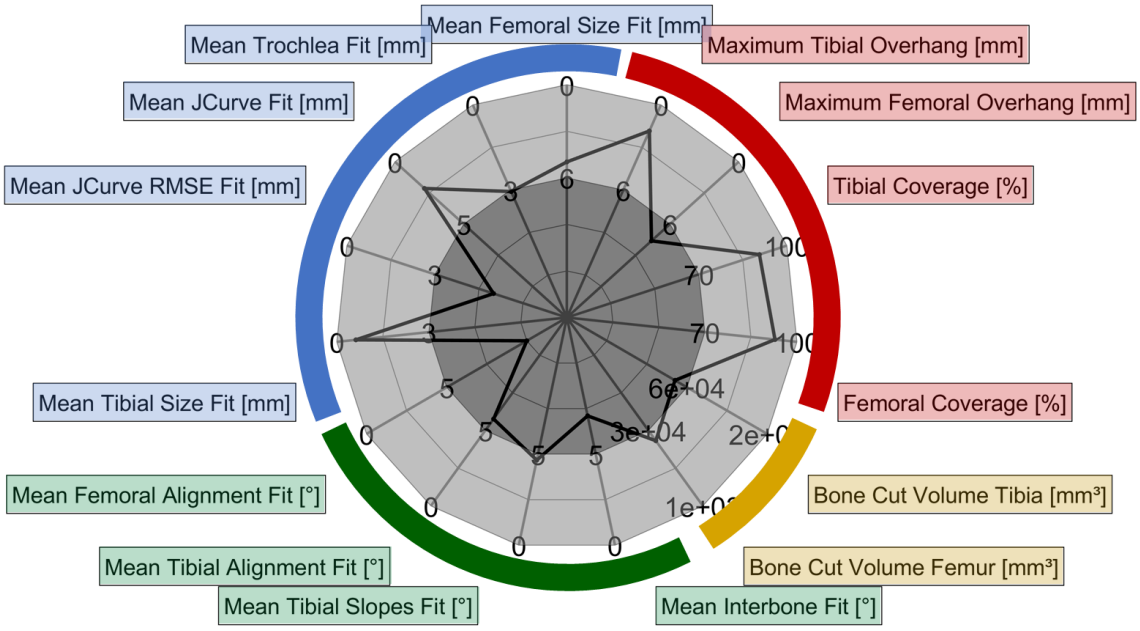

Figure 5-18: Exemplary spider plot visualization of the (patient-specific) detailed 3D fit evaluation. The correspondence of individual scores to the different categories of criteria is given.

Score Interpretation

With the 3D evaluation, a recommendation regarding the surgical planning and/or the implant choice is aimed at. In the study of Elkins et al. (Elkins et al. 2015), the definition

of an adequate score (“landing zone”) has been theoretically proposed as a trade-off between highest performance and realistically achievable clinical targets and arbitrarily defined to above 90 points (out of 100). In the framework presented, the surgeon decides about the suitability of the score on an individual level. The final score evaluates the overall 3D TKA planning which is dependent on patient-specific factors, surgical parameters, and implant sizing or design. Consequently, the surgeon decides which aspects to address. If the surgeon deems some of the surgical parameters as modifiable, he/she may vary those to explore the influence on the score. In the case of an inadequate 3D score and fixed surgical parameters, a change in the implant system or the use of a customized implant would be recommended.

5.4 Database analyses

In the following, the framework presented in the previous chapter is applied to a large database of 3D surface models of the knee. The results are described individually for the different categories of criteria.

Materials and methods

The proposed workflow has been implemented semi-automatedly. Hence, the processing of large databases is possible. A respective database of 3D data was available for testing of the workflow. Surface data, coordinates of hip and ankle joint center as well as side information were available for 421 cadaver knees. The data was provided by Conformis (Conformis Inc., Billerica, MA, USA). The same implant data was used, as for the exemplary 3D TKA planning described in **Chapter 5.3.1**. Additionally, the sizing of other implant sizes from the implant system was considered.

The previously described framework for implant fit evaluation was applied to the database. First step was the virtual implantation, including bone resection and implant positioning (**Chapter 5.3.1**). Second, the detailed interface fit evaluation was performed as described in **Chapter 5.3.2**. After the analysis, a visual inspection of the automated implant size determination, implant positioning and over-/ underhang evaluation of all processed cases was performed. The documentation of an exemplary virtual

implantation is provided in **Appendix D)**. The workflow for detailed morphological and alignment fit evaluation described in **Chapter 5.3.3** was subsequently applied to the database. As with the interface fit assessment, a visual inspection of the results for each morphological parameter was performed. The use of anterior referencing in the presented workflow prevents the occurrence of notching. Hence, with regard to other criteria solely the bone cut volume is evaluated. Therefore, the process described in **Chapter 5.4.3** is applied to the database.

5.4.1 Results on interface criteria

For 118 femora (28.0%), and for 125 tibiae (29.7%), the implant size with surface data available was selected. The virtual implantation was successful for all femora and for all tibiae. Three femora were excluded based on visual inspection. The interface fit analysis was successful for 109 femora and 121 tibiae. For those cases, implant positioning, bone resection and interface fit assessment were approved by an expert. Quantitative results of the over-/ underhang analysis are given in **Table 5-5**. The mean contour deviation of the entire contour was 0.2 mm overhang for the femur and 1.0 mm of underhang for the tibia. The mean absolute contour deviation for the entire contour was 3.7 mm for the femur and 2.0 mm for the tibia. Maximum femoral underhang in the zones ranged from 7.8 mm to 15.9 mm. Maximum femoral overhang ranged from 6.3 mm to 11.8 mm. For the tibia, a maximum overhang of 2.3 mm and a maximum underhang of 5.6 mm was found in the zone defined by Bonnin et al. (Bonnin et al. 2013). A mean femoral bone coverage of 87.3% (range: 75.8% -98.3%) was found. For the tibia it was 87.6% (range: 78.4% - 95.5%). The mean tibial rim coverage was 39.6% (range: 10.3% - 74.0%). Regarding tibial anatomical zones, the anterolateral and posteromedial areas showed the lowest implant coverage.

Table 5-5: Quantitative results of the automated over-/ underhang analysis. A visualization of the zones can be found in **Figure 5-11**.

	Zone 1 Bonnin2013	**Zone 2** Bonnin2013	**Zone 3** Bonnin2013	**Zone 4** Bonnin2013	**Zone** Dai2014
Overall mean contour deviation	0.4 mm **overhang**	5.7 mm underhang	5.0 mm underhang	1.2 mm underhang	4.7 mm underhang
Range: maximum underhang	7.8 mm	13.0 mm	15.9 mm	5.6 mm	12.1 mm
Range: maximum overhang	11.8 mm	6.3 mm	8.2 mm	2.3 mm	8.2 mm
Values from literature (manual measurements)					
Overall mean contour deviation	2.2 mm **overhang**	2.2 mm underhang	3.2 mm underhang	0.9 mm **overhang**	~4.0 mm underhang
Range: maximum underhang	13-14 mm	13-14 mm	13-14 mm	8-9 mm	~12.0 mm
Range: maximum overhang	12-13 mm	8-9 mm	6-7 mm	7-8 mm	~3.0 mm

5.4.2 Results on morphological and alignment criteria

A preoperative and postoperative shape analysis was performed for all cases, for which the available implant sizes were selected, which are described above. The success rates of the analysis of morphology and alignment parameters, as well as proportions of non-plausible and deformed bone values are displayed in **Table 5-6**.

Table 5-6: Success rates of the analysis of morphology and alignment parameters, as well as proportions of non-plausible and deformed bone values. **Note:** No fit evaluation is performed for the patella, hence also no deformity correction and plausibility check are performed for the patella. Interbone parameters were only evaluated, if the bone-specific analysis results were evaluated as plausible. No further plausibility check was incorporated afterwards.

	Preoperative Shape			**Postoperative Shape**		
	Femur (n=421)	Tibia (n=421)	Interbone (417)	Femur (115)	Tibia (125)	Interbone (57)
Failed Cases (%)	0.0%	1.0%	0.0%	0.0%	1.0%	0.0%
Failed Cases (n)	0	4	0	0	2	0
Implausible Cases (%)	10.2%	11.0%		7.0%	6.5%	
Implausible Cases (n)	43	46		8	8	
Deformed Cases (%)	51.3%	14.4%	14.6%			
Deformed Cases (n)	216	60	61			
Excluded Cases (%)	23.3%	0.7%	0.5%			
Excluded Cases (n)	97	3	2			

The deviations of the cartilage- and deformity-corrected preoperative parameter values with the postoperative parameter are presented in **Table 5-7** in terms of mean values and standard deviations. In addition, the result of the t-test/ Welch test and the effect sizes are given.

Of the 34 parameters analyzed, 30 parameters showed statistically significant differences in the preoperative compared to the postoperative mean values, evaluated in a paired t-test analysis or welch test analysis. Effect sizes were rated as high for 24

parameters, as moderate for 6 parameters, and as low for 2 parameters (Cohen 1988). Parameters solely influenced by implantation technique and/or implant design showed none to minimal variability in the postop measures, which is plausible. The minimal standard deviations observed (≤ 0.2 mm/0.5°) may be explained by minimal inaccuracies of the implant landmark estimation. With the mechanical alignment and fixed tibial slope, those parameters solely defined by implantation technique and/or implant design included the following:

- Condylar mediolateral width
- Overall anteroposterior length
- Medial and lateral condylar depth
- Trochlear depth
- Mediolateral spacing
- Posterior mediolateral width
- Mechanical lateral distal femoral angle
- Posterior condylar angle
- Medial and lateral tibial slopes
- Coronal tibial slope

Those values would vary with different alignment techniques, such as with kinematic or anatomical alignment, as well as with different (asymmetric) implant design.

Table 5-7: Comparison of preoperative with postoperative morphological and alignment parameter values. Preoperative values were checked for plausibility and deformities, optionally corrected, and estimated cartilage thickness was added. Medium and large effect sizes according to Cohen et al. (Cohen 1988) are highlighted (color code below). Statistically significant differences in the means according to the results of the paired t-tests or welch test are highlighted in bold font. LDFA= lateral distal femoral angle. PCO= posterior condylar offset. ML= Mediolateral. AO= Anteroposterior.

Bone	**Aspect**	**Parameter**	**preop** (deformity & cartilage corrected)		**postop** (bone and implant merged)		**mean deviation**		**mean absolute deviation**		**Effect size**
			mean	sd	mean	sd	mean	sd	mean	sd	
Femur	Sizing	Condylar ML Width	**80.8**	**2.7**	**73.1**	**0**	**7.7**	**2.7**	**7.7**	**2.7**	**4.1**
		Overall AP Length	**74.2**	**1.7**	**69.7**	**0**	**4.5**	**1.7**	**4.5**	**1.7**	**3.9**
		Lateral Condylar Depth	**73.5**	**1.7**	**69.7**	**0**	**3.7**	**1.7**	**3.7**	**1.7**	**3.6**
		Medial Condylar Depth	**72.4**	**2.4**	**71.1**	**0.1**	**1.4**	**2.4**	**2.1**	**1.7**	**1.3**
	Trochlea	Anterior ML Width	**38.9**	**2.2**	**29.7**	**0.3**	**9.2**	**2.2**	**9.2**	**2.2**	**6.2**
		Lateral Trochlear Elevation	**46.6**	**2.2**	**41.9**	**1.8**	**4.8**	**1.7**	**4.8**	**1.7**	**2.5**
		Medial Trochlear Elevation	**43.3**	**2.6**	**41.9**	**1.8**	**1.4**	**1.7**	**1.8**	**1.2**	**0.8**
		Central Trochlear Elevation	**40.5**	**2.8**	**38.5**	**1.8**	**2**	**2**	**2.4**	**1.5**	**1.2**
		Trochlear depth	**4.5**	**1.1**	**3.4**	**0**	**1.1**	**1.1**	**1.2**	**0.9**	**1.5**
		ML Sulcus Displacement	**2.1**	**2**	**7.5**	**1.3**	**-5.4**	**2.3**	**5.4**	**2.3**	**4.4**
	J-Curve	Mediolateral Spacing	**56.6**	**4.5**	**44.2**	**0.2**	**12.4**	**4.5**	**12.4**	**4.5**	**4.4**
		Posterior Mediolateral Width	**55.7**	**3.9**	**44.2**	**0.2**	**11.5**	**3.9**	**11.5**	**3.9**	**1.9**
		Distal Condylar Offset	**4.4**	**1.1**	**0.8**	**1.4**	**3.6**	**1.5**	**3.6**	**1.5**	**0.1**
		PCO Lateral	28.6	1.6	28.3	1.7	0.3	1.5	1.3	0.8	0.3
		PCO Medial	**29.3**	**2**	**28.3**	**1.7**	**1**	**1.6**	**1.5**	**1.0**	**1.8**
		Lateral Distal Sagittal Rad.	**45.6**	**6.5**	**38.1**	**0.4**	**7.5**	**6.5**	**7.5**	**6.5**	**1.8**
		Medial Distal Sagittal Rad.	**37.6**	**2.8**	**33.6**	**1.8**	**4**	**3.4**	**4.4**	**2.9**	**1.3**
		Lateral Posterior Sagittal Rad.	**23.2**	**1.5**	**21.8**	**0.8**	**1.4**	**1.4**	**1.6**	**1.1**	**2.0**
		Medial Posterior Sagittal Rad.	**22.6**	**1.2**	**20.2**	**0.9**	**2.3**	**1.4**	**2.4**	**1.3**	**0.5**
		PCO Ratio Lateral	42.6	2.3	43.7	2.6	-1.2	1.7	1.6	1.2	0.3
		PCO Ratio Medial	43.2	2.5	43.8	2.6	-0.6	1.5	1.3	0.9	1.3
		Condyle Ratio	63.6	2.7	66	1.6	-2.5	2.6	3.1	1.8	2.3
	Alignment	Mechanical LDFA	**86.6**	**1.7**	**90**	**0**	**-3.4**	**1.7**	**3.4**	**1.7**	**0.5**
		Posterior Condylar Angle	**0.7**	**1.2**	**0.1**	**0.2**	**0.6**	**1.2**	**1.1**	**0.8**	**1.3**
Tibia	Sizing	ML Width	**75.7**	**1.9**	**73.5**	**1**	**2.3**	**2.2**	**2.5**	**1.9**	**0.7**
		AP Height	**45**	**2**	**47**	**3.6**	**-2**	**3.5**	**2.8**	**2.8**	**0.5**
	Alignment	Medial Sagittal Tibial Slope	**6.9**	**3.3**	**8.2**	**0.2**	**-1.3**	**3.4**	**3**	**2.0**	**1.3**
		Lateral Sagittal Tibial Slope	**5**	**2.8**	**8.2**	**0.2**	**-3.2**	**2.8**	**3.5**	**2.3**	**3.8**
		Coronal Tibial Slope	**3.8**	**1.4**	**-0.1**	**0.5**	**3.9**	**1.4**	**3.9**	**1.4**	**0.2**
Inter-bone	Alignment	Patellar Tilt	10.4	5.4	11.4	8.5	-1.1	8.7	6.6	5.6	0.9
		Patellar Shift	**1.3**	**6.8**	**-4.7**	**5.7**	**5.6**	**3.3**	**5.6**	**3.3**	**1.5**
		TT-TG Distance	**15.7**	**4.2**	**8.4**	**4**	**7.3**	**3.6**	**7.4**	**3.5**	**1.5**
		Joint Rotation	**3.6**	**4.1**	**1.6**	**2.3**	**2**	**4.5**	**3.7**	**3.1**	**0.4**
		Insall Salvati Index 3D	**1.1**	**0.3**	**1.3**	**0.2**	**-0.2**	**0.2**	**0.3**	**0.2**	**0.4**

Color code: medium effect size= 0.5-0.8: □ | Large effect size > 0.8: ■

5.4.3 Results on other criteria

The bone cut volume was successfully calculated for all tibiae and femora with prior successful virtual implantation. Quantitative results are given in **Table 5-8**. The tibial size available was selected only for male knees. This fact can be explained by the comparably larger implant size which matches the larger knees in the male patient population. The mean femoral (tibial) bone cut volume in the database was 29.6 cm³ ± 4.7 cm³ (67.9 cm³ ± 7.3 cm³). The mean normalized femoral (tibial) bone cut volume in the database was 16.3 ± 1.7 (56.2 ± 8.4).

Table 5-8: Quantitative results of the bone cut volume evaluation.

	Femur, combined (n=115)	**Femur,** female (n=12)	**Femur,** male (n=103)	**Tibia,** male (n=125)
Mean bone cut volume (Standard deviation)	29.6 cm³ (±4.7 cm³)	23.0 cm³ (±1.8 cm³)	30.3 cm³ (±4.3 cm³)	67.9 cm³ (±7.3 cm³)
Normalized mean bone cut volume (Standard deviation)	16.3 (±1.7)	16.3 (±1.1)	16.2 (±1.7)	56.2 (±8.4)

5.5 Discussion and conclusion

In the following chapters, the individual aspects of the proposed workflow and exemplary implementation of the knee fit score concept are discussed.

5.5.1 Preliminary fit assessment

The preliminary fit assessment enables the assessment of 16 femoral and 4 tibial morphological parameters both pre- and postoperatively. The morphological parameters evaluated were selected based on intra- and interobserver reliability. In terms of interface criteria, the local, projected over-/ underhang is calculated in the framework. The results of the morphological and interface assessment are combined in an initial fit score, which can be compared against scores of previous planning or if available against scores from research databases. Previous studies on implant fit evaluation in 2D have considered less parameters and were mostly based on manual measurements in the TKA planning software used (Liu et al. 2021; Gu et al. 2019; Clarke and Hentz 2008). The assessment presented provides a more comprehensive evaluation of the patient-specific 2D implant fit, an increased automation, and a consolidation in one score.

5.5.2 Detailed fit assessment

The detailed, 3D fit assessment presented enables a complex assessment of the implant fit, regarding interface, morphological, alignment, and other criteria. In contrast to previous studies evaluating partial aspects of implant fit (Dai et al. 2014a; Dai et al. 2014b; Chen et al. 2017a; Du et al. 2017), the virtual implantation in the framework presented is completely automated. The interface fit evaluation incorporated includes the assessment of the entire bone contour, whereas previous studies have focused solely on specific zones (Dai et al. 2014b; Bonnin et al. 2013). The morphological and alignment implant fit evaluation includes 24 femoral, 5 tibial and 5 interbone parameters. If a deformity is detected, respective affected parameters are identified and an individual prediction model is used to identify equivalent physiological parameter values. In addition, the impact of cartilage on morphological parameters is compensated. Furthermore, both the tibial and femoral bone cut volume are evaluated. Similar as for the 2D assessment, in comparison to previous studies, an increase in the number of parameters assessed, an increase in process automation, and a consolidation in one score was realized.

In the clinical scenario, the surgeon receives a comprehensive visualization of the fit score evaluation as well as a ranking of the current planning in relation to all preoperative planning of a representative database. In addition, if available, the clinical outcomes of age- and gender-matched patients receiving a respectively rated fit score can be integrated. Thereby, the surgeon is supported in interpreting the results and in the subsequent informed decision-making.

The prediction of TKA outcomes based on a priori information has previously been applied to patient selection. An example is the probabilistic prediction tool of TKA outcome, presented by Twiggs et al. (Twiggs et al. 2019). The predictions are based on preoperative variables such as demographic data and preoperative scores, but the model does not consider individual knee shape or the preoperative planning. The model has been validated in a retrospective analysis and was able to identify patients at risk for poor outcomes, with those showing a 27% chance of not improving after TKA compared to a 1.4% chance in the improvement group. Hence the tool showed potential for risk assessment and patient selection, however, it does not provide indications of

possible surgical or implant-related causes of the risk and therefore also no support for an individual adjustment of the preoperative planning. This restriction to patient selection is also the case for other outcome prediction tools (Houserman et al. 2022; Greiwe et al. 2019). In contrast, the framework presented in this study provides an indication of the source(s) of incompatibility and thus of the factors that need to be addressed to resolve it.

5.5.3 Database analyses

Interface criteria

In the present database analysis on the knee interface fit, wide ranges of contour deviation per zone were seen, ranging from 15.9 mm underhang to 11.8 mm overhang. These results are in agreement with the literature, reporting exemplary ranges of 14 mm underhang to 13 mm overhang (Bonnin et al. 2013) and of ~15 mm underhang to ~7 mm overhang (Dai et al. 2014b). Bonnin et al. (Bonnin et al. 2013) reported a mean contour deviation of 2.2 mm and 0.9 mm overhang in zone 1 and 4 and of 2.2 and 3.2 mm underhang in zone 2 and 3. In the analysis presented, slightly lower mean overhang in zone 1 (0.4 mm), and higher levels of underhang in zone 2 (5.7 mm), zone 3 (5.0 mm) and zone 4 (1.2 mm) were found. The differences may be explained by the different aspect ratio of the two implant systems used. Bonnin et al. used the HLS Noetos implant components (Tornier SA, Montbonnot, France) whereas in the analysis presented surface information from the Sigma implant system (Depuy Synthes, Raynham, MA, US) (Fregly et al. 2012) was used. The HLS Noetos femoral component has a mean aspect ratio (ML/AP) of 1.11, whereas for the Sigma it is 1.05. This difference in design seems to have led to higher underhang in the present study. Dai et al. (Dai et al. 2014b) analyzed different implant systems and found that the Sigma and the Triathlon implant systems exhibited the highest amounts of underhang. For the size, which was also analyzed in the present study, a mean contour deviation of ~4 mm underhang and a range of ~12 mm underhang to ~3 mm overhang was reported by the authors. Similar results however with higher maximum overhang were seen in the present study (mean: 4.7 mm underhang, range: 12.1 mm underhang to 8.2 mm overhang).

In the interface fit study presented in this thesis, on average, more than 10% of the femoral and tibial bone surface was not covered by the implant, although adequate sizing was ensured with a maximum deviation of 3 mm in AP and of 6 mm in ML. Even slightly lower tibial coverage was found in the literature (Clary et al. 2014; Shao et al. 2020). Shao et al. (Shao et al. 2020), performed virtual TKA planning for 103 knees of healthy volunteers and analyzed tibial coverage for four different baseplate designs. They reported a mean tibial bone coverage of 85.62%, across subjects and implants. Clary et al. (Clary et al. 2014) found coverage ranging from 80.2% to 83.8%, for two different designs in the same population. To the best of the author's knowledge, there are no studies reporting femoral bone coverage in TKA.

Fitzpatrick et al. (Fitzpatrick et al. 2007) investigated different uni-compartmental tibial implant design based on morphological data of 34 tibiae. They targeted the cortical bone coverage and reached 66.7% with a theoretical, symmetric implant system with five sizes (simple scaling). In the present study, the mean cortical rim coverage was lower (39.6%). The deviation is plausible, as the results of Fitzpatrick et al. represent a theoretical optimum for the 34 tibiae analyzed, which does not account for the large variability in the patient population as well as for technical restrictions in implant design.

In conclusion, the results of the database analyses are in agreement with the literature. With regard to the interface fit of the implant design analyzed, an inadequate relation of the femoral aspect ratios in anterior, distal and posterior region was found with respect to the study population. To address ML underhang, an increase of the aspect ratio in zone 2-3 of the femoral component could be considered. For the tibia, an increase in anterolateral and posteromedial plateau coverage could be targeted with a more asymmetric design.

Morphological and alignment criteria

Statistically significant differences in preoperative versus postoperative mean were found for 88% of the morphological and alignment parameters analyzed. For femoral **implant sizing**, the AP cortex length was targeted as proposed in literature (Du et al. 2017; Dai et al. 2014b), leading to a minimal mean deviation of 0.2 mm with regard to this measure. The deviation of 4.5 mm with respect to the overall AP length (high effect

size) may be explained by a change in lateral trochlear elevation, which is of similar extent (4.8 mm). During the size selection, the femoral ML fit was only restricted with respect to a maximum overhang of 3 mm on each side (overall 6 mm oversizing), which led to a decrease in condylar ML width by 7.7 mm after TKA (high effect size). For tibial sizing, ML and AP mismatch were not differentiated, resulting in almost the same magnitude of deviation with a mean undersizing of 2.3 mm in ML and a mean oversizing of 2.0 mm in AP. These results are in agreement with those of the interface fit evaluation, regarding an inadequate aspect ratio of the implant system analyzed with respect to the study population.

Furthermore, high effect sizes (d>0.8) were seen for the following **trochlear parameters**: lateral trochlear elevation, central trochlear elevation, anterior ML width, trochlear depth, mediolateral sulcus displacement. The decrease in lateral trochlear elevation and trochlear depth are consistent with the literature, as several implant systems have been reported to feature a shallow, dysplastic trochlea shape (Dejour et al. 2014). A decrease in the lateral trochlear elevation with TKA was also reported by Akbari-Shandiz (Akbari Shandiz et al. 2018), who compared the preoperative and postoperative knee shape in 9 TKA patients. The change in mediolateral sulcus displacement, with a lateralization of the trochlear groove, may partially explain the statistically significant decrease in TT-TG distance, which is of similar extent. The comprehensive changes in preoperative to postoperative trochlear shape, may have induced the changes in patellar shift (high effect size). Further, in the present study, several high effect sizes were seen for parameters of the **femoral J-Curve**. This is in agreement with the high variability in J-Curve shape identified in **Chapter 3.2**, which is not reflected by standard OTS implants, especially for the example with symmetric condyles. Akbari Shandiz et al. (Akbari Shandiz et al. 2018) also analyzed changes in knee condylar shape and reported on prosthesis-bone distances in the full posterior condylar region of 2.7 mm medially and 0.6 mm laterally. Taking into account an estimated cartilage thickness of 2 mm (= medial: 4.7 mm, lateral: 2.6 mm), the reported lateral prosthesis-bone distances are in a comparable range to the mean absolute deviations in PCO found in the present study. However, the medial deviations found by Akbari Shandiz et al. are notably higher (Δ=3.2 mm). This deviation may be due to different segmentation and post-processing. In the present study osteophyte-free labels

were used and a deformity correction was performed if required. In contrast, the preoperative surface models of Akbari Shandiz et al. showed significant osteophytes, often located in the posterior region of the medial condyle, which should not be restored by TKA. Hence, the presence of osteophytes may explain the higher prosthesis-bone distances in the study of Akbari Shandiz et al. compared to the present study. Regarding **alignment**, the generic tibial slope of four degrees in combination with the built-in slope of the tibial insert led to significant deviations with regard to the lateral tibial slope (high effect size). Further, the mechanical alignment caused relevant deviations with high effect sizes in the coronal tibial slope and mechanical LDFA. In the literature, a phenomenon of (pseudo-) patella baja after TKA has been reported (Lum et al. 2020; Bugelli et al. 2018), with different explanations including an elevation of the joint line (Grelsamer 2002). In contrast, in the present study, a slight increase in patellar height in terms of Insall Salvati Index was found after virtual TKA.

In conclusion, the automated analysis of morphological and alignment parameter enabled a comprehensive comparison of the preoperative with the postoperative knee shape. The mean parameter differences represent potential changes in standard implant shape required for this specific population, after consideration of technical restrictions in knee implant design. The mean deviations show a wide range both for distances (-5.4 mm - 12.4 mm) and angular measurements (-3.2° - 3.9°). In general, the observed standard deviations also showed a wide range. This observation supports the hypothesis of individual differences to represent a relevant source for implant-bone shape mismatch and further motivates the patient-specific fit evaluation.

Bone cut volume

Several authors have reported on the bone resection volume in the intercondylar area with posterior-stabilized implant systems, ranging from 3.6 cm³ to 13.5 cm³ depending on the implant size and design (Bozkurt et al. 2017; Haas et al. 2000; Pugh et al. 2013). However, to the author’s knowledge, the full bone cut volume has not been reported in the literature so far. Hence only the plausibility of the results can be discussed.

The higher tibial compared to the femoral resection volume, both in absolute and normalized measures, is reasonable as only one cut is performed. Increasing the

number of bone cuts may be desirable to limit the bone cut volume both for tibia and femur. An example for an implant system with additional femoral cuts represents the iTotal implant system from Conformis Inc. (Conformis Inc, Billerica, MA, US). Kurtz et al. reported on 12-49% more bone cut volume in TKA with standard OTS implant components compared to with the iTotal implant system (Kurtz et al. 2016).

Limitations

The study involved limitations. For the initial fit assessment, the 2D implant contours were derived from images of a TKA planning software (mediCAD Hectec, Altdorf, Germany). Deviations may be involved in the display accuracy and in the contour derivation by thresholding. However, size measurements of the implant components match well with those reported by the manufacturers. Hence, the deviations are expected to be minimal and of no relevance.

For the detailed 3D fit assessment, a 3D surface model of the OTS implant was only available for one implant size. This meant that only the knees that fitted this size could be analyzed, resulting in a smaller database. Further, the robustness of the method with regard to other sizes and implant systems could not be tested.

Further, surgical plans are not always exactly met, for example, because of required intraoperative adjustments. Hence, the virtual planning is theoretical. Actual implant position and resulting over-/ underhang and coverage may slightly differ from the one calculated during planning. However, for an objective evaluation of different implant system designs, an automated virtual planning has the advantage of being more time-saving and having less unknown variation. Finally, the automated planning was only reviewed by the author.

Limitations in the assessment of morphological and alignment criteria can be found with regard to the measurement of interbone parameters. Preoperative measurements were based on CT imaging taken in supine position and not in an active weight-bearing position. This limitation however is present in most of the previous studies on interbone parameters (Fürmetz et al. 2021; Hochreiter et al. 2019). Further, an automated positioning of the postoperative shapes was performed. The native patella was positioned with respect to the femoral trochlear groove based on a medial and lateral

reference point, neglecting the restriction of the patellar tendon. This estimation may have led to the contrasting results regarding patellar height, in comparison with the literature. This limitation may be addressed in the future, by 3D-2D matching with EOS images, if respective imaging is part of the clinical routine. A corresponding 3D-2D matching has been presented by Akbari Shandiz et al. (Akbari Shandiz et al. 2018) for estimating the actual postoperative joint line.

Overall, the database analyses demonstrated the robustness of the semi-automated workflow based on standard clinical imaging. The results for the different categories of fit criteria are consistent and give insight into optimization potential for implant design.

The research question addressed in this chapter can be answered as follows:

> *The proposed fit evaluation can potentially be integrated in the clinical workflow when 2D bone contours and adequate 3D surface data of the knee and of the respective implant components are available. The implementation was demonstrated exemplarily using MATLAB. To support an informed decision-making of the surgeon, a comprehensive visualization of the patient-specific fit assessment is provided. A subsequent evaluation of a large database showed the robustness of the approach and demonstrates its suitability for identifying optimization potential in existing implant systems. For a final positive assessment, an evaluation of the workflow together with clinicians (ideally in the clinical routine) is required.*

6. Discussion and outlook

6.1 Discussion

The aim of this thesis was to optimize the morpho-functional fit of OTS implants for each individual patient by developing **methods for implant sizing** as well as for **detailed implant fit evaluation** in TKA. This goal was motivated both by design limitations of existing implant systems and by increasing demands on TKA. Limitations of existing implant design include among others overall size and morphological mismatch, as well as pathological design features, such as a dysplastic trochlea. Increasing demands on TKA are placed by the increasing volume of primary and revision TKA, the broader indication to younger and more active patients, in combination with an increasing life expectancy. These developments necessitate increased implant functionality and survivorship, which can be addressed by implant design optimization.

Particle swarm optimization was successfully applied for an exemplary **optimization of femoral implant sizing** for TKA. The database used consisted of the sizes of over 85,000 patient-specific implants, which were found to be representative of the native knee size when compared with the sizes of 1049 patients and 386 cadaver knees. To the best of the author's knowledge, this database represents the largest database on knee size information presented in the literature to date. The database demonstrated a mixed-gaussian distribution with primarily small and narrow female knees and large and wide male knees. This observation is consistent with previous analyses of knee size distributions (Conley et al. 2007; Bellemans et al. 2010; Hitt et al. 2003). The resulting optimized sizing complies with the recommendation of Bellemans et al. (Bellemans et al. 2010) to offer wide large implants (male design) and small narrow implants (female design), instead of offering a comprehensive number of narrow and wide variants for each implant size. The numerical optimization proved to be better suited for the definition of implant sizing than the previously applied regression models, increasing patient population coverage by 19% to 26% compared to previous (regression) sizing. A logarithmic relationship of the patient population coverage with both sizing error bounds and the number of implant sizes was observed. This led to "saturation" effects when

increasing the number of implant sizes and suggests the use of customized implants for the remaining, uncovered cases.

The requirement for detailed fit evaluation apart from the first-addressed size fit was evaluated by analyzing inter-individual variation in knee morphology. The variability was demonstrated in the example of the femoral 2D and 3D J-Curves, by building an SSM and subsequently applying PCA. **Several shape variations apart from size** were observed, both for the 2D and 3D J-Curves. For the 3D J-Curves, the variation of size was primarily restricted to the first and third mode, accounting for 52.0% of shape variation, which is consistent with the literature (Fitzpatrick et al. 2008). Because of the missing shape variation observed in existing implant systems, implant-bone mismatch is expected and should be evaluated on an individual level.

The targeted fit evaluation requires knee imaging data, with several modalities showing potential for this application. On this basis, two concepts for implant fit evaluation were developed: The **current concept** involves a two-step procedure, with an initial basic fit assessment based on conventional radiographs (2D analysis) and - only if indicated - a subsequent analysis with CT (3D analysis). In contrast, with the **future concept**, a 3D analysis is performed directly based on radiation-free, 3D freehand/ robotic US imaging. The current concept is therefore motivated by cost, availability, and ease of integration into clinical routine. The future concept already provides an outlook for future setups. The two fit assessment approaches also take into account the different technical equipment of individual clinics, for example in low-resource environments.

As a basis for the implant fit evaluation, **fit criteria** presented in the literature were reviewed and summarized. Most of the studies considered focused on describing the femoral implant component fit, whereas only few criteria were defined for tibia and patella, especially regarding the morphological fit. Further, a discrepancy between the recommended 3D assessment and available 2D imaging in regular TKA planning was observed. In addition, the high number of studies relying on manual measurements do not coincide with the decreasing time available for TKA planning and decreasing reimbursement to clinics. With adequate imaging and the semi-automated framework presented, those issues can be overcome and fit criteria can be routinely evaluated. An initial weighting of the criteria identified was defined, which may be refined in the future

based on larger clinical studies enabling a systematic comparison of the individual criteria's impact on outcomes.

For an adequate assessment of the morphological fit criteria identified, a **parameter-based deformity correction** was developed and verified by multi-body simulation. The accuracy of the methodology was comparable to that of the only previous study (van den Heever et al. 2011) and is expected to improve with larger training datasets. The importance of deformity correction extends beyond the implant design process, as OA-related deformities often affect surgically relevant axes such as the posterior condylar line. Therefore, pre-operative planning in the orthopedic treatment of knees with severe OA will benefit greatly from an automated deformity correction.

The parameter-based deformity correction was integrated into the conceptualized workflow. Afterwards, the current concept for implant fit assessment was implemented exemplarily in MATLAB, including both the initial basic fit assessment as well as the detailed fit evaluation. In contrast to previous studies, the presented workflow and implementation shows a **high level of automation**. The interface fit assessment involves coverage and over/ underhang along the whole bone contours, as well as in specific (anatomical) zones reported in literature. Further advances, include the check and correction for osteophytes and potential congenital or OA-related deformities. The comparison of respectively corrected preoperative morphological parameters (target shape) with the equivalent postoperative parameters, enables an adequate evaluation of morphological and alignment fit criteria. Finally, the (normalized) femoral and tibial bone cut volume is assessed. Because of the high level of automation, analyses of large databases are enabled.

Implant fit analyses were performed with a representative implant model (Sigma PFC) for a database of 421 cadaver knees. **Optimization potential** of the implant design analyzed was found **regarding all fit categories**. For the interface fit of the femoral component, this included a change in aspect ratio, a wider notch and changes in condylar shape, especially on the medial side. For the tibia, the database analysis suggested a more asymmetric design for better coverage of the anterolateral and posteromedial areas. The morphological and alignment fit evaluation revealed high statistically significant deviations for ~90% of the parameters analyzed. High effect sizes

were found for parameters of the overall size, trochlea, J-Curves, coronal and sagittal alignment, and interbone parameters. Apart from the results of the patellar height, the results are consistent with the literature (Dejour et al. 2014; Akbari Shandiz et al. 2018). Limitations including the landmark-based positioning of the postoperative shapes have to be considered, and should be addressed with adequate databases including long leg radiographs or EOS imaging. Nevertheless, the deviations in TT-TG distance and patellar shift are plausible and of relevance for postoperative function and pain. In general, respective deviations in interbone parameters are an indication for missing compatibility with the patient's anatomy, as they describe changes in the relative position of the bones and hence also in ligament, tendon, and muscle paths and strains, as well as resulting alterations in terms of proprioception. The bone cut volume analysis showed higher bone resection at the tibia, both absolute and relative. For this reason, the addition of further resection levels and a corresponding change in tray design should be investigated. Apart from the indications for design optimization, the framework developed provides an objective assessment of the need for a customized implant at an individual level using thresholds derived from the literature.

For the individual patient, a detailed report on the fit assessment including a score ranking is provided for the surgeon to enable an informed decision-making regarding treatment. This data-driven approach enables the **integration of a priori information** of the clinic as well of research databases. In contrast to previous prediction models of TKA outcome (Twiggs et al. 2019; Greiwe et al. 2019; Houserman et al. 2022), the framework presented in this thesis gives detailed insight into potential morpho-functional causes of poor outcome predictions and identifies factors to be addressed with regard to implant positioning and/or design.

6.2 Outlook

An adequate patient specific design fit in TKA is expected to significantly increase the **cost-effectiveness** of the treatment. The optimized femoral sizing has significantly increased the proportion of patients who can be provided with an appropriately sized standard implant compared to existing implant systems. In an exemplary setup of

optimized sizes, only 15% of the patients would require a customized implant, compared to 27%-48% for existing implant systems. Hence, less patients would require the more expensive customized implant, reducing the overall costs. In addition, a **correct allocation of standard and customized implants** can be supported by the implant fit evaluation presented. Further potential for enhanced cost-effectiveness may be realized, when addressing specific conclusions from the analyses performed.

One example would be the offering of different **implant versions based on modes of shape variation**, presented exemplarily for the 3D J-Curve. These included different circularity, partially reflected in single- or multi-radius design of the femoral component, but not available in the scope of one implant system. In addition, differences in relative position of the medial and lateral J-Curve with respect to anatomical axes were seen. Most of the available implant systems offer a symmetric condyle design and hence do not account for the variability in offsets. In the light of requirements with regard to inventory management and shelf live, a **modularization** of the femoral component could be considered. With a junction of two modules at the intercondylar area, the fit of the medial and lateral condyle shape could be addressed and improved individually. A similar vision for modularization was proposed by Riviere et al. (Rivière et al. 2020), for the femoral trochlea. An industry example for such modularization are the individual lateral and medial tibial inserts in the iTotal implant system (Conformis Inc, Billerica, MA, US). Similarly, uni- or bicompartmental implant systems represent “modularization”, as artificial knee compartment replacements are combined with the preserved native joint compartments. With a combination of both tibial insert and femoral component trochlear and medial/lateral compartment modularization, the high individuality of knee morphology can be better accommodated while maintaining a limited number of implant components. Thereby, trade-offs between e.g., an adequate trochlear and medial/lateral condyle fit, could be avoided. The framework developed may further be used to verify the effectiveness of respective design changes addressing the optimization potential identified.

The fit assessment can also be extended to include **individualized biomechanical simulation analyses**, such as those performed in the deformity correction verification study. However, individual targets for kinematics and loading would be required. These

targets may be based on comprehensive analyses of native knee kinematics as well as ligament loading and contact force estimations from *in vitro/ in silico* sensitivity analyses of healthy control subjects. The simulated kinematics could further be used as an input for a collision detection, identifying possible bone-implant and implant-implant impingement.

In conclusion, the implant size optimization demonstrated the possibility for a significant increase in population coverage. A comprehensive set of methods for the assessment of knee implant fit was developed, enabling adequate implant allocation on an individual level. In addition, implant design changes with respect to a representative database were investigated. When implemented, such advances in implant sizing, design, and matching are expected to significantly increase the cost-effectiveness of TKA. Finally, because of similar targets in joint replacement surgeries, the methods for sizing optimization and the framework for fit evaluation could be applied to the prosthetic treatment of other joints.

References

Aaron, R.; Scott, R. (1987): Supracondylar Fracture of the Femur After Total Knee Arthroplasty. In *Clinical orthopaedics and related research* 219, 136-139. DOI: 10.1097/00003086-198706000-00020.

Ahmad, Riaz; Patel, Amit; Mandalia, Vipul; Toms, Andrew (2016): Posterior Tibial Slope: Effect on, and Interaction with, Knee Kinematics. In *JBJS reviews* 4 (4), 1–6. DOI: 10.2106/JBJS.RVW.O.00057.

Akbari Shandiz, Mohsen; Boulos, Paul; Saevarsson, Stefan Karl; Ramm, Heiko; Fu, Chun Kit Jack; Miller, Stephen et al. (2018): Changes in knee shape and geometry resulting from total knee arthroplasty. In *Proceedings of the Institution of Mechanical Engineers. Part H, Journal of engineering in medicine* 232 (1), pp. 67–79. DOI: 10.1177/0954411917743274.

Al Hares, Ghaith: MRI as a basis for patient-specific morphological and functional planning for computer-assisted knee surgery. Dissertation. Rheinisch-Westfälische Technische Hochschule Aachen; Shaker Verlag.

Alemparte, José; Ekdahl, Max; Burnier, Loreto; Hernández, Rodrigo; Cardemil, Ana; Cielo, Raúl; Danilla, Stefan (2007): Patellofemoral evaluation with radiographs and computed tomography scans in 60 knees of asymptomatic subjects. In *Arthroscopy : the journal of arthroscopic & related surgery : official publication of the Arthroscopy Association of North America and the International Arthroscopy Association* 23 (2), pp. 170–177. DOI: 10.1016/j.arthro.2006.08.022.

Altman, R.; Asch, E.; Bloch, D.; Bole, G.; Borenstein, D.; Brandt, K. et al. (1986): Development of criteria for the classification and reporting of osteoarthritis. Classification of osteoarthritis of the knee. Diagnostic and Therapeutic Criteria Committee of the American Rheumatism Association. In *Arthritis and rheumatism* 29 (8), pp. 1039–1049. DOI: 10.1002/art.1780290816.

Anouchi, Y. S.; Whiteside, L. A.; Kaiser, A. D.; Milliano, M. T. (1993): The effects of axial rotational alignment of the femoral component on knee stability and patellar

tracking in total knee arthroplasty demonstrated on autopsy specimens. In *Clinical orthopaedics and related research* (287), pp. 170–177.

Ardestani, Marzieh M.; Moazen, Mehran; Jin, Zhongmin (2015): Contribution of geometric design parameters to knee implant performance: Conflicting impact of conformity on kinematics and contact mechanics. In *The Knee* 22 (3), pp. 217–224. DOI: 10.1016/j.knee.2015.02.011.

Argenson, Jean-Noël A.; Komistek, Richard D.; Mahfouz, Mohamed; Walker, Scott A.; Aubaniac, Jean-Manuel; Dennis, Douglas A. (2004): A high flexion total knee arthroplasty design replicates healthy knee motion. In *Clinical orthopaedics and related research* (428), pp. 174–179. DOI: 10.1097/01.blo.0000148948.79128.76.

Asseln, Malte (2019): Morphological and Functional Analysis of the Knee Joint for Implant Design Optimization. In S. Leonhardt, K. Radermacher, T. Schmitz-Rode (Eds.): Aachener Beiträge zur Medizintechnik, vol. 57: Shaker Verlag.

Asseln, Malte; Fischer, Maximilian C. M.; Chan, Hao Yang; Meere, Patrick; Walker, Peter; Radermacher, Klaus (2019): Automatic standardized shape analysis of the sagittal profiles (J-Curves) of the femoral condyles based on three-dimensional (3D) surface data. In : CAOS 2019. The 19th Annual Meeting of the International Society for Computer Assisted Orthopaedic Surgery, 21-15.

Asseln, Malte; Fischer, Maximilian C. M.; Hänisch, Christoph; Radermacher, Klaus (2017): Automatic parameterization of the proximal tibia based on 3D surface data for morphological analysis and implant optimization. In : CAOS 2017. 17th Annual Meeting of the International Society for Computer Assisted Orthopaedic Surgery.

Asseln, Malte; Grothues, Sonja A. G. A.; Radermacher, Klaus (2021): Relationship between the form and function of implant design in total knee replacement. In *Journal of biomechanics* 119, p. 110296. DOI: 10.1016/j.jbiomech.2021.110296.

Asseln, Malte; Hänisch, Christoph; Al Hares, G.; Eschweiler, J.; Radermacher, Klaus (2015): Automatic Parameterisation of the Distal Femur Based on 3D Surface Data: A Novel Approach for Systematic Morphological Analysis and Optimisation. In :

Proceedings of The 15th Annual Meeting of the International Society for Computer Assisted Orthopaedic Surgery, p. 68.

Asseln, Malte; Hänisch, Christoph; Schick, Fabian; Radermacher, Klaus (2018): Gender differences in knee morphology and the prospects for implant design in total knee replacement. In *The Knee* 25 (4), pp. 545–558. DOI: 10.1016/j.knee.2018.04.005.

Aunan, Eirik; Alhaug, Eivind; Schuller, Siri G.; Rundfloen, Jan E. (2023): 3-dimensional computer tomography is more accurate than traditional long-leg radiographs in the planning and evaluation of coronal alignment in total knee arthroplasty: a prospective study on 121 knees. In *Acta orthopaedica* 94, pp. 530–536. DOI: 10.2340/17453674.2023.19695.

Ayers, David C. (2017): Implementation of Patient-reported Outcome Measures in Total Knee Arthroplasty. In *The Journal of the American Academy of Orthopaedic Surgeons* 25 Suppl 1, S48-S50. DOI: 10.5435/JAAOS-D-16-00631.

Babisch, J.; Layher, F.; Ritter, B.; Venbrocks, R.-A. (2001): Computergestützte biomechanisch fundierte zweidimensionale Operationsplanung hüftchirurgischer Eingriffe. In *Orthopädische Praxis* 37 (1), pp. 29–38.

Badillo, Solveig; Banfai, Balazs; Birzele, Fabian; Davydov, Iakov I.; Hutchinson, Lucy; Kam-Thong, Tony et al. (2020): An Introduction to Machine Learning. In *Clinical pharmacology and therapeutics* 107 (4), pp. 871–885. DOI: 10.1002/cpt.1796.

Baka, N.; Kaptein, B. L.; Bruijne, M. de; van Walsum, T.; Giphart, J. E.; Niessen, W. J.; Lelieveldt, B. P. F. (2011): 2D-3D shape reconstruction of the distal femur from stereo X-ray imaging using statistical shape models. In *Medical image analysis* 15 (6), pp. 840–850. DOI: 10.1016/j.media.2011.04.001.

Balcarek, Peter; Jung, Klaus; Frosch, Karl-Heinz; Stürmer, Klaus Michael (2011): Value of the tibial tuberosity-trochlear groove distance in patellar instability in the young athlete. In *The American journal of sports medicine* 39 (8), pp. 1756–1761. DOI: 10.1177/0363546511404883.

Banks, Scott A.; Hodge, W. Andrew (2004): Implant design affects knee arthroplasty kinematics during stair-stepping. In *Clinical orthopaedics and related research* (426), pp. 187–193. DOI: 10.1097/01.blo.0000138956.04316.ac.

Barrack, R. L.; Schrader, T.; Bertot, A. J.; Wolfe, M. W.; Myers, L. (2001): Component rotation and anterior knee pain after total knee arthroplasty. In *Clinical orthopaedics and related research* (392), pp. 46–55. DOI: 10.1097/00003086-200111000-00006.

Bayer, Steve; Meredith, Sean J.; Wilson, Kevin W.; Sa, Darren de; Pauyo, Thierry; Byrne, Kevin et al. (2020): Knee Morphological Risk Factors for Anterior Cruciate Ligament Injury: A Systematic Review. In *The Journal of bone and joint surgery. American volume* 102 (8), pp. 703–718. DOI: 10.2106/JBJS.19.00535.

Bellemans, J.; Banks, S.; Victor, J.; Vandenneucker, H.; Moemans, A. (2002): Fluoroscopic analysis of the kinematics of deep flexion in total knee arthroplasty. In *The Journal of Bone and Joint Surgery. British volume* 84-B (1), pp. 50–53. DOI: 10.1302/0301-620X.84B1.0840050.

Bellemans, J.; Ries, Michael D.; Victor, Jan M.K. (Eds.) (2005): Total Knee Arthroplasty. A Guide to Get Better Performance. Berlin, Heidelberg: Springer Berlin Heidelberg (SpringerLink Bücher).

Bellemans, Johan; Carpentier, Karel; Vandenneucker, Hilde; Vanlauwe, Johan; Victor, Jan (2010): The John Insall Award: Both morphotype and gender influence the shape of the knee in patients undergoing TKA. In *Clinical orthopaedics and related research* 468 (1), pp. 29–36. DOI: 10.1007/s11999-009-1016-2.

Berger, R. A.; Crossett, L. S.; Jacobs, J. J.; Rubash, H. E. (1998): Malrotation causing patellofemoral complications after total knee arthroplasty. In *Clinical orthopaedics and related research* (356), pp. 144–153. DOI: 10.1097/00003086-199811000-00021.

Berger, R. A.; Rubash, Harry E.; Seel, M. J.; Thompson, W. H.; Crossett, L. S. (1993): Determining the Rotational Alignment of the Femoral Component in Total Knee Arthroplasty Using the Epicondylar Axis. In *Clinical orthopaedics and related research* 286, 40???47. DOI: 10.1097/00003086-199301000-00008.

Bergmann, Georg; Bender, Alwina; Graichen, Friedmar; Dymke, Jörn; Rohlmann, Antonius; Trepczynski, Adam et al. (2014): Standardized loads acting in knee implants. In *PloS one* 9 (1), e86035. DOI: 10.1371/journal.pone.0086035.

Bijlsma, Johannes W. J.; Berenbaum, Francis; Lafeber, Floris P. J. G. (2011): Osteoarthritis: an update with relevance for clinical practice. In *Lancet (London, England)* 377 (9783), pp. 2115–2126. DOI: 10.1016/S0140-6736(11)60243-2.

Biscević, Mirza; Hebibović, Mujo; Smrke, Dragica (2005): Variations of femoral condyle shape. In *Collegium antropologicum* 29 (2), pp. 409–414.

Blumentritt, S. (1988): Biomechanische Bauprinzipien des menschlichen Hüftgelenkes in der Frontalebene. In *Gegenbaurs morphologisches Jahrbuch* 134 (2), pp. 221–240.

Bonnin, Michel; Selmi, Tarik Ait Si; Langlois, Jean (2022): Optimal Sizing of the Femoral, Tibial, and Patellofemoral Components in TKA. In Roland Becker, Michael T. Hirschmann, Nanne P. Kort (Eds.): Basics in Primary Knee Arthroplasty, vol. 57. Cham: Springer International Publishing, pp. 421–435.

Bonnin, Michel P.; Kok, Arnoud de; Verstraete, Matthias; van Hoof, Tom; van der Straten, Catherine; Saffarini, Mo; Victor, Jan (2017): Popliteus impingement after TKA may occur with well-sized prostheses. In *Knee surgery, sports traumatology, arthroscopy : official journal of the ESSKA* 25 (6), pp. 1720–1730. DOI: 10.1007/s00167-016-4330-8.

Bonnin, Michel P.; Schmidt, Axel; Basiglini, Luca; Bossard, Nadine; Dantony, Emmanuelle (2013): Mediolateral oversizing influences pain, function, and flexion after TKA. In *Knee surgery, sports traumatology, arthroscopy : official journal of the ESSKA* 21 (10), pp. 2314–2324. DOI: 10.1007/s00167-013-2443-x.

Bourne, Robert B.; Chesworth, Bert M.; Davis, Aileen M.; Mahomed, Nizar N.; Charron, Kory D. J. (2010): Patient satisfaction after total knee arthroplasty: who is satisfied and who is not? In *Clinical orthopaedics and related research* 468 (1), pp. 57–63. DOI: 10.1007/s11999-009-1119-9.

Bozic, Kevin J.; Kurtz, Steven M.; Lau, Edmund; Ong, Kevin; Chiu, Vanessa; Vail, Thomas P. et al. (2010): The epidemiology of revision total knee arthroplasty in the United States. In *Clinical orthopaedics and related research* 468 (1), pp. 45–51. DOI: 10.1007/s11999-009-0945-0.

Bozkurt, Murat; Tahta, Mesut; Gursoy, Safa; Akkaya, Mustafa (2017): Total and intercondylar notch bone resection in posterior stabilized knee arthroplasty: analysis of five manufacturer designs. In *Knee surgery, sports traumatology, arthroscopy : official journal of the ESSKA* 25 (6), pp. 1731–1735. DOI: 10.1007/s00167-015-3864-5.

Bracey, Daniel N.; Brown, Matthew L.; Beard, Hoyt R.; Mannava, Sandeep; Nazir, Omar F.; Seyler, Thorsten M.; Lang, Jason E. (2015): Effects of patellofemoral overstuffing on knee flexion and patellar kinematics following total knee arthroplasty: a cadaveric study. In *International orthopaedics* 39 (9), pp. 1715–1722. DOI: 10.1007/s00264-015-2715-9.

Bredbenner, Todd L.; Eliason, Travis D.; Potter, Ryan S.; Mason, Robert L.; Havill, Lorena M.; Nicolella, Daniel P. (2010): Statistical shape modeling describes variation in tibia and femur surface geometry between Control and Incidence groups from the osteoarthritis initiative database. In *Journal of biomechanics* 43 (9), pp. 1780–1786. DOI: 10.1016/j.jbiomech.2010.02.015.

Brembo, Espen Andreas; Kapstad, Heidi; van Dulmen, Sandra; Eide, Hilde (2017): Role of self-efficacy and social support in short-term recovery after total hip replacement: a prospective cohort study. In *Health and quality of life outcomes* 15 (1), p. 68. DOI: 10.1186/s12955-017-0649-1.

Bryan, Stirling; Goldsmith, Laurie J.; Davis, Jennifer C.; Hejazi, Samar; MacDonald, Valerie; McAllister, Patrick et al. (2018): Revisiting patient satisfaction following total knee arthroplasty: a longitudinal observational study. In *BMC musculoskeletal disorders* 19 (1), p. 423. DOI: 10.1186/s12891-018-2340-z.

Buckland-Wright, Christopher (2004): Subchondral bone changes in hand and knee osteoarthritis detected by radiography. In *Osteoarthritis and cartilage* 12 Suppl A, S10-9. DOI: 10.1016/j.joca.2003.09.007.

Buckwalter, Joseph A.; Saltzman, Charles; Brown, Thomas (2004): The impact of osteoarthritis: implications for research. In *Clinical orthopaedics and related research* (427 Suppl), S6-15. DOI: 10.1097/01.blo.0000143938.30681.9d.

Budhiparama, Nicolaas C.; Lumban-Gaol, Imelda; Ifran, Nadia Nastassia; Groot, Pieter C. J. de; Utomo, Dwikora Novembri; Nelissen, Rob G. H. H. (2021): Mismatched knee implants in Indonesian and Dutch patients: a need for increasing the size. In *Knee surgery, sports traumatology, arthroscopy : official journal of the ESSKA* 29 (2), pp. 358–369. DOI: 10.1007/s00167-020-05914-9.

Bugelli, Giulia; Ascione, Francesco; Cazzella, Niki; Franceschetti, Edoardo; Franceschi, Francesco; Dell'Osso, Giacomo et al. (2018): Pseudo-patella baja: a minor yet frequent complication of total knee arthroplasty. In *Knee surgery, sports traumatology, arthroscopy : official journal of the ESSKA* 26 (6), pp. 1831–1837. DOI: 10.1007/s00167-017-4828-8.

Busija, Lucy; Osborne, Richard H.; Nilsdotter, Anna; Buchbinder, Rachelle; Roos, Ewa M. (2008): Magnitude and meaningfulness of change in SF-36 scores in four types of orthopedic surgery. In *Health and quality of life outcomes* 6, p. 55. DOI: 10.1186/1477-7525-6-55.

Carballido-Gamio, Julio; Bauer, Jan S.; Stahl, Robert; Lee, Keh-Yang; Krause, Stefanie; Link, Thomas M.; Majumdar, Sharmila (2008): Inter-subject comparison of MRI knee cartilage thickness. In *Medical image analysis* 12 (2), pp. 120–135. DOI: 10.1016/j.media.2007.08.002.

Carpenter, Dylan P.; Holmberg, Rebecca R.; Quartulli, Marc J.; Barnes, C. Lowry (2014): Tibial plateau coverage in UKA: a comparison of patient specific and off-the-shelf implants. In *The Journal of arthroplasty* 29 (9), pp. 1694–1698. DOI: 10.1016/j.arth.2014.03.026.

Carr, Andrew J.; Robertsson, Otto; Graves, Stephen; Price, Andrew J.; Arden, Nigel K.; Judge, Andrew; Beard, David J. (2012): Knee replacement. In *Lancet (London, England)* 379 (9823), pp. 1331–1340. DOI: 10.1016/S0140-6736(11)60752-6.

Cerveri, Pietro; Sacco, Costanza; Olgiati, Gianluca; Manzotti, Alfonso; Baroni, Guido (2017): 2D/3D reconstruction of the distal femur using statistical shape models addressing personalized surgical instruments in knee arthroplasty: A feasibility analysis. In *The international journal of medical robotics + computer assisted surgery : MRCAS* 13 (4). DOI: 10.1002/rcs.1823.

Chaibi, Y.; Cresson, T.; Aubert, B.; Hausselle, J.; Neyret, P.; Hauger, O. et al. (2012): Fast 3D reconstruction of the lower limb using a parametric model and statistical inferences and clinical measurements calculation from biplanar X-rays. In *Computer methods in biomechanics and biomedical engineering* 15 (5), pp. 457–466. DOI: 10.1080/10255842.2010.540758.

Chang, Moon Jong; Jeong, Hyeon Jang; Kang, Seung-Baik; Chang, Chong Bum; Yoon, Chan; Shin, Joung Youp (2018): Relationship Between Coronal Alignment and Rotational Profile of Lower Extremity in Patients With Knee Osteoarthritis. In *The Journal of arthroplasty* 33 (12), pp. 3773–3777. DOI: 10.1016/j.arth.2018.07.022.

Charette, Ryan S.; Sheth, Neil P.; Boettner, Friedrich; Scuderi, Giles R.; Melnic, Christopher M. (2018): Femoral Component Sizing During Total Knee Arthroplasty: Anterior Versus Posterior Referencing. In *JBJS reviews* 6 (1), e4. DOI: 10.2106/JBJS.RVW.17.00051.

Chau, R.; Gulati, A.; Pandit, H.; Beard, D. J.; Price, A. J.; Dodd, C. A. F. et al. (2009): Tibial component overhang following unicompartmental knee replacement--does it matter? In *The Knee* 16 (5), pp. 310–313. DOI: 10.1016/j.knee.2008.12.017.

Chauhan, S. K.; Clark, G. W.; Lloyd, S.; Scott, R. G.; Breidahl, W.; Sikorski, J. M. (2004): Computer-assisted total knee replacement. A controlled cadaver study using a multi-parameter quantitative CT assessment of alignment (the Perth CT Protocol). In *The Journal of Bone and Joint Surgery. British volume* 86 (6), pp. 818–823. DOI: 10.1302/0301-620X.86B6.15456.

Chen, C.; Xie, W.; Franke, J.; Grutzner, P. A.; Nolte, L-P; Zheng, G. (2014): Automatic X-ray landmark detection and shape segmentation via data-driven joint estimation of

image displacements. In *Medical image analysis* 18 (3), pp. 487–499. DOI: 10.1016/j.media.2014.01.002.

Chen, Jiaxing; Li, Xinyi; Xu, Zijie; Yang, Haitao; Zhang, Hua; Zhang, Jian; Zhou, Aiguo (2022): Tibial tubercle-Roman arch (TT-RA) distance is superior to tibial tubercle-trochlear groove (TT-TG) distance when evaluating coronal malalignment in patients with knee osteoarthritis. In *European radiology* 32 (12), pp. 8404–8413. DOI: 10.1007/s00330-022-08924-y.

Chen, Shichang; Zeng, Yiming; Yan, Mengning; Yue, Bing; Zhang, Jun; Wang, You (2017a): Morphological evaluation of the sagittal plane femoral load-bearing surface in computer-simulated virtual total knee arthroplasty implantation at different flexion angles. In *Knee surgery, sports traumatology, arthroscopy : official journal of the ESSKA* 25 (9), pp. 2880–2886. DOI: 10.1007/s00167-016-3997-1.

Chen, Shi-Chang; Zeng, Yi-Ming; Yan, Meng-Ning; Yue, Bing; Zhang, Jun; Wang, You (2017b): Effect of Femoral Component Flexion Implantation on the Mediolateral Bone-prosthetic Fit in Total Knee Arthroplasty. In *Orthopaedic surgery* 9 (1), pp. 91–96. DOI: 10.1111/os.12319.

Chia, Shi-Lu; Merican, Azhar M.; Devadasan, Bernard; Strachan, Robin K.; Amis, Andrew A. (2009): Radiographic features predictive of patellar maltracking during total knee arthroplasty. In *Knee surgery, sports traumatology, arthroscopy : official journal of the ESSKA* 17 (10), pp. 1217–1224. DOI: 10.1007/s00167-009-0832-y.

Choi, Yun Seong; Kim, Tae Woo; Song, Seung Cheol; Kim, Sang Yoon; Chang, Moon Jong; Kang, Seung-Baik (2022): Asymmetric transepicondylar axis between varus and valgus osteoarthritic knees in windswept deformity can be predicted by hip-knee-ankle angle difference. In *Knee surgery, sports traumatology, arthroscopy : official journal of the ESSKA* 30 (9), pp. 3024–3031. DOI: 10.1007/s00167-021-06661-1.

Chomboon, Kittipong; Chujai, Pasapichi; Teerarassammee, Pongsakorn; Kerdprasop, Kittisak; Kerdprasop, Nittaya (2015): An Empirical Study of Distance Metrics for k-Nearest Neighbor Algorithm. In : The Proceedings of the 2nd International Conference on Industrial Application Engineering 2015, 28-31, March, 2015, pp. 280–285.

Chung, Byung June; Kang, Jong Yeal; Kang, Yeon Gwi; Kim, Sung Ju; Kim, Tae Kyun (2015): Clinical Implications of Femoral Anthropometrical Features for Total Knee Arthroplasty in Koreans. In *The Journal of arthroplasty* 30 (7), pp. 1220–1227. DOI: 10.1016/j.arth.2015.02.014.

Cicchetti, Domenic V. (1994): Guidelines, criteria, and rules of thumb for evaluating normed and standardized assessment instruments in psychology. In *Psychological Assessment* 6 (4), pp. 284–290. DOI: 10.1037/1040-3590.6.4.284.

Cignoni, Paolo; Callieri, Marco; Corsini, Massimiliano; Dellepiane, Matteo; Ganovelli, Fabio; Ranzuglia, Guido (2008): MeshLab: an Open-Source Mesh Processing Tool.

Clarke, Henry D.; Hentz, Joseph G. (2008): Restoration of femoral anatomy in TKA with unisex and gender-specific components. In *Clinical orthopaedics and related research* 466 (11), pp. 2711–2716. DOI: 10.1007/s11999-008-0454-6.

Clary, Chadd; Aram, Luke; Deffenbaugh, Daren; Heldreth, Mark (2014): Tibial base design and patient morphology affecting tibial coverage and rotational alignment after total knee arthroplasty. In *Knee surgery, sports traumatology, arthroscopy : official journal of the ESSKA* 22 (12), pp. 3012–3018. DOI: 10.1007/s00167-014-3402-x.

Clary, Chadd W.; Fitzpatrick, Clare K.; Maletsky, Lorin P.; Rullkoetter, Paul J. (2013): The influence of total knee arthroplasty geometry on mid-flexion stability: an experimental and finite element study. In *Journal of biomechanics* 46 (7), pp. 1351–1357. DOI: 10.1016/j.jbiomech.2013.01.025.

Clement, Nicholas D.; Hamilton, David F.; Burnett, Richard (2014): A technique of predicting radiographic joint line and posterior femoral condylar offset of the knee. In *Arthritis* 2014, p. 121069. DOI: 10.1155/2014/121069.

Cobb, J. P.; Dixon, H.; Dandachli, W.; Iranpour, F. (2008): The anatomical tibial axis: reliable rotational orientation in knee replacement. In *The Journal of Bone and Joint Surgery. British volume* 90 (8), pp. 1032–1038. DOI: 10.1302/0301-620X.90B8.19905.

Cohen, Daniel A.; Gursel, Ali C.; Low, Adrian K. (2019): How coronal alignment affects distal femoral anatomy: an MRI-based comparison of varus and valgus knees. In

Journal of orthopaedic surgery and research 14 (1), p. 92. DOI: 10.1186/s13018-019-1133-x.

Cohen, Jacob (1988): Statistical power analysis for the behavioral sciences. 2nd ed. Hillsdale, N.J.: L. Erlbaum Associates. Available online at https://permalink.obvsg.at/.

Conley, Sheryl; Rosenberg, Aaron; Crowninshield, Roy (2007): The female knee: anatomic variations. In *The Journal of the American Academy of Orthopaedic Surgeons* 15 Suppl 1, S31-6. DOI: 10.5435/00124635-200700001-00009.

Corbett, James; Tai, Jeffrey; Salmon, Lucy; Roe, Justin (2023): Comparison of CT and EOS in assessing coronal lower limb alignment when planning total knee arthroplasty. In *The Knee* 42, pp. 400–408. DOI: 10.1016/j.knee.2023.04.010.

Creamer, P.; Hochberg, M. C. (1997): Osteoarthritis. In *Lancet (London, England)* 350 (9076), pp. 503–508. DOI: 10.1016/S0140-6736(97)07226-7.

Cui, Aiyong; Li, Huizi; Wang, Dawei; Zhong, Junlong; Chen, Yufeng; Lu, Huading (2020): Global, regional prevalence, incidence and risk factors of knee osteoarthritis in population-based studies. In *EClinicalMedicine* 29-30, p. 100587. DOI: 10.1016/j.eclinm.2020.100587.

Culler, Steven D.; Martin, Greg M.; Swearingen, Alyssa (2017): Comparison of adverse events rates and hospital cost between customized individually made implants and standard off-the-shelf implants for total knee arthroplasty. In *Arthroplasty today* 3 (4), pp. 257–263. DOI: 10.1016/j.artd.2017.05.001.

Culp, R. W.; Schmidt, R. G.; Hanks, G.; Mak, A.; Esterhai, J. L.; Heppenstall, R. B. (1987): Supracondylar fracture of the femur following prosthetic knee arthroplasty. In *Clinical orthopaedics and related research* (222), pp. 212–222.

Dai, Yifei; Cross, Michael B.; Angibaud, Laurent D.; Hamad, Cyril; Jung, Amaury; Jenny, Jean-Yves (2018): Posterior tibial slope impacts intraoperatively measured mid-flexion anteroposterior kinematics during cruciate-retaining total knee arthroplasty. In *Knee surgery, sports traumatology, arthroscopy : official journal of the ESSKA* 26 (11), pp. 3325–3332. DOI: 10.1007/s00167-018-4877-7.

Dai, Yifei; Scuderi, Giles R.; Bischoff, Jeffrey E.; Bertin, Kim; Tarabichi, Samih; Rajgopal, Ashok (2014a): Anatomic tibial component design can increase tibial coverage and rotational alignment accuracy: a comparison of six contemporary designs. In *Knee surgery, sports traumatology, arthroscopy : official journal of the ESSKA* 22 (12), pp. 2911–2923. DOI: 10.1007/s00167-014-3282-0.

Dai, Yifei; Scuderi, Giles R.; Penninger, Charles; Bischoff, Jeffrey E.; Rosenberg, Aaron (2014b): Increased shape and size offerings of femoral components improve fit during total knee arthroplasty. In *Knee surgery, sports traumatology, arthroscopy : official journal of the ESSKA* 22 (12), pp. 2931–2940. DOI: 10.1007/s00167-014-3163-6.

Dalury, David F.; Pomeroy, Donald L.; Gorab, Robert S.; Adams, Mary Jo (2013): Why are total knee arthroplasties being revised? In *The Journal of arthroplasty* 28 (8 Suppl), pp. 120–121. DOI: 10.1016/j.arth.2013.04.051.

Dartus, Julien; Jacques, Thibaut; Martinot, Pierre; Pasquier, Gilles; Cotten, Anne; Migaud, Henri et al. (2021): The advantages of cone-beam computerised tomography (CT) in pain management following total knee arthroplasty, in comparison with conventional multi-detector CT. In *Orthopaedics & traumatology, surgery & research : OTSR* 107 (3), p. 102874. DOI: 10.1016/j.otsr.2021.102874.

Davies, A. P.; Costa, M. L.; Shepstone, L.; Glasgow, M. M.; Donell, S. (2000): The sulcus angle and malalignment of the extensor mechanism of the knee. In *The Journal of Bone and Joint Surgery. British volume* 82 (8), pp. 1162–1166. DOI: 10.1302/0301-620x.82b8.10833.

Dejour, David; Ntagiopoulos, Panagiotis G.; Saffarini, Mohammed (2014): Evidence of trochlear dysplasia in femoral component designs. In *Knee surgery, sports traumatology, arthroscopy : official journal of the ESSKA* 22 (11), pp. 2599–2607. DOI: 10.1007/s00167-012-2268-z.

Dejour, David; Saggin, Paulo (2010): The sulcus deepening trochleoplasty-the Lyon's procedure. In *International orthopaedics* 34 (2), pp. 311–316. DOI: 10.1007/s00264-009-0933-8.

Dejour, H.; Walch, G.; Nove-Josserand, L.; Guier, C. (1994): Factors of patellar instability: an anatomic radiographic study. In *Knee surgery, sports traumatology, arthroscopy : official journal of the ESSKA* 2 (1), pp. 19–26. DOI: 10.1007/BF01552649.

Delanois, Ronald E.; Mistry, Jaydev B.; Gwam, Chukwuweike U.; Mohamed, Nequesha S.; Choksi, Ujval S.; Mont, Michael A. (2017): Current Epidemiology of Revision Total Knee Arthroplasty in the United States. In *The Journal of arthroplasty* 32 (9), pp. 2663–2668. DOI: 10.1016/j.arth.2017.03.066.

Delfosse, Daniel; Saladin, Stefan; Becker, Roland (2022): TKA Component Design: What Do Engineers Need to Know? In Roland Becker, Michael T. Hirschmann, Nanne P. Kort (Eds.): Basics in Primary Knee Arthroplasty, vol. 24. Cham: Springer International Publishing, pp. 193–205.

Delport, Hendrik; Labey, Luc; Corte, Ronny de; Innocenti, Bernardo; Vander Sloten, Jos; Bellemans, Johan (2013): Collateral ligament strains during knee joint laxity evaluation before and after TKA. In *Clinical biomechanics (Bristol, Avon)* 28 (7), pp. 777–782. DOI: 10.1016/j.clinbiomech.2013.06.006.

Dennis, D. A.; Komistek, R. D.; Walker, S. A.; Cheal, E. J.; Stiehl, J. B. (2001): Femoral condylar lift-off in vivo in total knee arthroplasty. In *The Journal of Bone and Joint Surgery. British volume* 83-B (1), pp. 33–39. DOI: 10.1302/0301-620X.83B1.0830033.

Dennis, Douglas A.; Komistek, Richard D.; Mahfouz, Mohamed R.; Haas, Brian D.; Stiehl, James B. (2003): Multicenter determination of in vivo kinematics after total knee arthroplasty. In *Clinical orthopaedics and related research* (416), pp. 37–57. DOI: 10.1097/01.blo.0000092986.12414.b5.

Desio, S. M.; Burks, R. T.; Bachus, K. N. (1998): Soft tissue restraints to lateral patellar translation in the human knee. In *The American journal of sports medicine* 26 (1), pp. 59–65. DOI: 10.1177/03635465980260012701.

Die Strahlenschutzkommission (2019): Orientierungshilfe für bildgebende Verfahren. 3. überarbeitete Auflage. Available online at www.ssk.de.

Diederichs, G.; Scheffler, S. (2013): MRT nach Patellaluxation: Quantifizierung der Risikofaktoren und Beschreibung der Folgeschäden. In *RoFo : Fortschritte auf dem Gebiete der Rontgenstrahlen und der Nuklearmedizin* 185 (7), pp. 611–620. DOI: 10.1055/s-0032-1330690.

D'Lima, Darryl D.; Patil, Shantanu; Steklov, Nikolai; Slamin, John E.; Colwell, Clifford W. (2006): Tibial forces measured in vivo after total knee arthroplasty. In *The Journal of arthroplasty* 21 (2), pp. 255–262. DOI: 10.1016/j.arth.2005.07.011.

Dogan, Emrah; Sengorur, Bülent; Koklu, Rabia (2009): Modeling biological oxygen demand of the Melen River in Turkey using an artificial neural network technique. In *Journal of environmental management* 90 (2), pp. 1229–1235. DOI: 10.1016/j.jenvman.2008.06.004.

Doherty, M. (2001): Risk factors for progression of knee osteoarthritis. In *Lancet (London, England)* 358 (9284), pp. 775–776. DOI: 10.1016/S0140-6736(01)06006-8.

Dong, Xiao; Zheng, Guoyan (2008): Automatic extraction of femur contours from calibrated x-ray images: A Bayesian inference approach. In : 2008 5th IEEE International Symposium on Biomedical Imaging: From Nano to Macro. Paris, France, 2008: IEEE, pp. 57–60.

Draper, C. E.; Besier, T. F.; Gold, G. E.; Fredericson, M.; Fiene, A.; Beaupre, G. S.; Delp, S. L. (2006): Is cartilage thickness different in young subjects with and without patellofemoral pain? In *Osteoarthritis and cartilage* 14 (9), pp. 931–937. DOI: 10.1016/j.joca.2006.03.006.

Du, Zhe; Chen, Shichang; Yan, Mengning; Yue, Bing; Wang, You (2017): Differences between native and prosthetic knees in terms of cross-sectional morphology of the femoral trochlea: a study based on three-dimensional models and virtual total knee arthroplasty. In *BMC musculoskeletal disorders* 18 (1), p. 166. DOI: 10.1186/s12891-017-1529-x.

Dumic, Emil; Duarte, Carlos Rafael; da Silva Cruz, Luis A. (2018): Subjective evaluation and objective measures for point clouds — State of the art. In : 2018 First

International Colloquium on Smart Grid Metrology (SmaGriMet). Split, 24.04.2018 - 27.04.2018: IEEE, pp. 1–5.

Dürselen, L.; Freutel, M. (2015): Biomechanik des Meniskus. In *Orthopädie und Unfallchirurgie up2date* 10 (03), pp. 215–227. DOI: 10.1055/s-0041-101820.

ElHak, E.; Fatah, E. E. Abdel; Mahfouz, M. R.; Eldakhakhni, H.; Tadross, R. (2007): 3D Reconstruction of Patient Specific Bone Utilizing Biplanar X-Ray Images and Sex Specific Atlases. In : 6th Combined Meeting of the Orthopaedic Research Societies. Honolulu, HI, October 20-24.

Eliasziw, M.; Young, S. L.; Woodbury, M. G.; Fryday-Field, K. (1994): Statistical methodology for the concurrent assessment of interrater and intrarater reliability: using goniometric measurements as an example. In *Physical Therapy* 74 (8), pp. 777–788. DOI: 10.1093/ptj/74.8.777.

Elkins, Jacob M.; Callaghan, John J.; Brown, Thomas D. (2015): The 2014 Frank Stinchfield Award: The 'landing zone' for wear and stability in total hip arthroplasty is smaller than we thought: a computational analysis. In *Clinical orthopaedics and related research* 473 (2), pp. 441–452. DOI: 10.1007/s11999-014-3818-0.

Essner, Aaron; Herrera, Lizeth; Hughes, Phillip; Kester, Mark (2011): The influence of material and design on total knee replacement wear. In *The journal of knee surgery* 24 (1), pp. 9–17. DOI: 10.1055/s-0031-1275390.

Fantozzi, Silvia; Catani, Fabio; Ensini, Andrea; Leardini, Alberto; Giannini, Sandro (2006): Femoral rollback of cruciate-retaining and posterior-stabilized total knee replacements: in vivo fluoroscopic analysis during activities of daily living. In *Journal of orthopaedic research : official publication of the Orthopaedic Research Society* 24 (12), pp. 2222–2229. DOI: 10.1002/jor.20306.

Favre, Julien; Erhart-Hledik, Jennifer C.; Blazek, Katerina; Fasel, Benedikt; Gold, Garry E.; Andriacchi, Thomas P. (2017): Anatomically Standardized Maps Reveal Distinct Patterns of Cartilage Thickness With Increasing Severity of Medial Compartment Knee Osteoarthritis. In *Journal of orthopaedic research : official*

publication of the Orthopaedic Research Society 35 (11), pp. 2442–2451. DOI: 10.1002/jor.23548.

Felson, D. T. (2013): Osteoarthritis as a disease of mechanics. In *Osteoarthritis and cartilage* 21 (1), pp. 10–15. DOI: 10.1016/j.joca.2012.09.012.

Fitzpatrick, C. K.; FitzPatrick, D. P.; Auger, D. D. (2008): Size and shape of the resection surface geometry of the osteoarthritic knee in relation to total knee replacement design. In *Proceedings of the Institution of Mechanical Engineers. Part H, Journal of engineering in medicine* 222 (6), pp. 923–932. DOI: 10.1243/09544119JEIM332.

Fitzpatrick, Clare; FitzPatrick, David; Lee, Jordan; Auger, Daniel (2007): Statistical design of unicompartmental tibial implants and comparison with current devices. In *The Knee* 14 (2), pp. 138–144. DOI: 10.1016/j.knee.2006.11.005.

Fitzpatrick, Clare K.; Clary, Chadd W.; Laz, Peter J.; Rullkoetter, Paul J. (2012a): Relative contributions of design, alignment, and loading variability in knee replacement mechanics. In *Journal of orthopaedic research : official publication of the Orthopaedic Research Society* 30 (12), pp. 2015–2024. DOI: 10.1002/jor.22169.

Fitzpatrick, Clare K.; Clary, Chadd W.; Rullkoetter, Paul J. (2012b): The role of patient, surgical, and implant design variation in total knee replacement performance. In *Journal of biomechanics* 45 (12), pp. 2092–2102. DOI: 10.1016/j.jbiomech.2012.05.035.

Freeman, M. A. R.; Pinskerova, V. (2005): The movement of the normal tibio-femoral joint. In *Journal of biomechanics* 38 (2), pp. 197–208. DOI: 10.1016/j.jbiomech.2004.02.006.

Fregly, Benjamin J.; Besier, Thor F.; Lloyd, David G.; Delp, Scott L.; Banks, Scott A.; Pandy, Marcus G.; D'Lima, Darryl D. (2012): Grand challenge competition to predict in vivo knee loads. In *Journal of orthopaedic research : official publication of the Orthopaedic Research Society* 30 (4), pp. 503–513. DOI: 10.1002/jor.22023.

Fridén, T.; Jonsson, A.; Erlandsson, T.; Jonsson, K.; Lindstrand, A. (1993): Effect of femoral condyle configuration on disability after an anterior cruciate ligament rupture. 100 patients followed for 5 years. In *Acta orthopaedica Scandinavica* 64 (5), pp. 571–574. DOI: 10.3109/17453679308993695.

Fürmetz, J.; Daniel, T.; Sass, J.; Bergsträßer, M.; Degen, N.; Suero, E. et al. (2021): Three-dimensional assessment of patellofemoral anatomy: Reliability and reference ranges. In *The Knee* 29, pp. 271–279. DOI: 10.1016/j.knee.2021.02.016.

Gamage, P.; Xie, S. Q.; Delmas, P.; Xu, P. (2009): 3D Reconstruction of Patient Specific Bone Models from 2D Radiographs for Image Guided Orthopedic Surgery. In : 2009 Digital Image Computing: Techniques and Applications. Melbourne, Australia, 01.12.2009 - 03.12.2009: IEEE, pp. 212–216.

Gao, Fuqiang; Guo, Wanshou; Sun, Wei; Li, Zirong; Wang, Weiguo; Wang, Bailiang et al. (2014): Correlation between the coverage percentage of prosthesis and postoperative hidden blood loss in primary total knee arthroplasty. In *Chinese medical journal* 127 (12), pp. 2265–2269.

Ghosh, K. M.; Merican, A. M.; Iranpour, F.; Deehan, D. J.; Amis, Andrew A. (2009): The effect of overstuffing the patellofemoral joint on the extensor retinaculum of the knee. In *Knee surgery, sports traumatology, arthroscopy : official journal of the ESSKA* 17 (10), pp. 1211–1216. DOI: 10.1007/s00167-009-0830-0.

Giesinger, K.; Hamilton, D. F.; Jost, B.; Holzner, B.; Giesinger, J. M. (2014): Comparative responsiveness of outcome measures for total knee arthroplasty. In *Osteoarthritis and cartilage* 22 (2), pp. 184–189. DOI: 10.1016/j.joca.2013.11.001.

Grammens, Jonas; van Haver, Annemieke; Danckaers, Femke; Booth, Brian; Sijbers, Jan; Verdonk, Peter (2021): Small medial femoral condyle morphotype is associated with medial compartment degeneration and distinct morphological characteristics: a comparative pilot study. In *Knee surgery, sports traumatology, arthroscopy : official journal of the ESSKA* 29 (6), pp. 1777–1789. DOI: 10.1007/s00167-020-06218-8.

Gray, Alastair M.; Clarke, Philip M.; Wolstenholme, Jane L.; Wordsworth, Sarah (2011): Applied methods of cost-effectiveness analysis in health care. Oxford: Oxford

University Press (Handbooks in health economic evaluation series). Available online at https://search.ebscohost.com/login.aspx?direct=true&scope=site&db=nlebk&db=nlabk&AN=467577.

Greener, Joe G.; Kandathil, Shaun M.; Moffat, Lewis; Jones, David T. (2022): A guide to machine learning for biologists. In *Nature reviews. Molecular cell biology* 23 (1), pp. 40–55. DOI: 10.1038/s41580-021-00407-0.

Greiwe, Raymond M.; Spanyer, Jonathon M.; Nolan, Joseph R.; Rodgers, Renée N.; Hill, Misti A.; Harm, Richard G. (2019): Improving Orthopedic Patient Outcomes: A Model to Predict 30-Day and 90-Day Readmission Rates Following Total Joint Arthroplasty. In *The Journal of arthroplasty* 34 (11), pp. 2544–2548. DOI: 10.1016/j.arth.2019.05.051.

Grelsamer, Ronald P. (2002): Patella baja after total knee arthroplasty: is it really patella baja? In *The Journal of arthroplasty* 17 (1), pp. 66–69. DOI: 10.1054/arth.2002.28728.

Grimberg, Alexander; Jansson, Volkmar; Lützner, Jörg; Melsheimer, Oliver; Morlock, Michael; Steinbrück, Arnd (2021): EPRD- Jahresbericht 2021. Mit Sicherheit mehr Qualität. Berlin: EPRD Deutsche Endoprothesenregister.

Grimberg, Alexander; Lützner, Jörg; Melsheimer, Oliver; Morlock, Michael; Steinbrück, Arnd (2022): EPRD- Jahresbericht 2022. Mit Sicherheit mehr Qualität. 2022. Auflage. Berlin: EPRD Deutsche Endoprothesenregister.

Grimberg, Alexander; Lützner, Jörg; Melsheimer, Oliver; Morlock, Michael; Steinbrück, Arnd (2023): EPRD- Jahresbericht 2023. Mit Sicherheit mehr Qualität. Berlin: EPRD Deutsche Endoprothesenregister.

Grosso, Matthew J.; Courtney, P. Maxwell; Kerr, Joshua M.; Della Valle, Craig J.; Huddleston, James I. (2020): Surgeons' Preoperative Work Burden Has Increased Before Total Joint Arthroplasty: A Survey of AAHKS Members. In *The Journal of arthroplasty* 35 (6), pp. 1453–1457. DOI: 10.1016/j.arth.2020.01.079.

Grothues, Sonja; Berger, Luisa; Radermacher, Klaus (2022): Automated analysis of morpho-functional interbone parameters of the knee based on three dimensional (3D) surface data. In : Proceedings of The 20th Annual Meeting of the International Society for Computer Assisted Orthopaedic Surgery, 81-72.

Grothues, Sonja A. G. A.; Radermacher, Klaus (2021): Variation of the Three-Dimensional Femoral J-Curve in the Native Knee. In *Journal of personalized medicine* 11 (7). DOI: 10.3390/jpm11070592.

Gu, ShiZhong; Kuriyama, Shinichi; Nakamura, Shinichiro; Nishitani, Kohei; Ito, Hiromu; Matsuda, Shuichi (2019): Underhang of the tibial component increases tibial bone resorption after total knee arthroplasty. In *Knee surgery, sports traumatology, arthroscopy : official journal of the ESSKA* 27 (4), pp. 1270–1279. DOI: 10.1007/s00167-018-5309-4.

Gu, Wei; Pandy, Marcus G. (2020): Direct Validation of Human Knee-Joint Contact Mechanics Derived From Subject-Specific Finite-Element Models of the Tibiofemoral and Patellofemoral Joints. In *Journal of biomechanical engineering* 142 (7). DOI: 10.1115/1.4045594.

Guenoun, B.; Zadegan, F.; Aim, F.; Hannouche, D.; Nizard, R. (2012): Reliability of a new method for lower-extremity measurements based on stereoradiographic three-dimensional reconstruction. In *Orthopaedics & traumatology, surgery & research : OTSR* 98 (5), pp. 506–513. DOI: 10.1016/j.otsr.2012.03.014.

Gujarathi, Narendra; Putti, Amit B.; Abboud, Rami J.; MacLean, James G. B.; Espley, Arthur J.; Kellett, Catherine F. (2009): Risk of periprosthetic fracture after anterior femoral notching. In *Acta orthopaedica* 80 (5), pp. 553–556. DOI: 10.3109/17453670903350099.

Guy, S. P.; Farndon, M. A.; Sidhom, S.; Al-Lami, M.; Bennett, C.; London, N. J. (2012): Gender differences in distal femoral morphology and the role of gender specific implants in total knee replacement: a prospective clinical study. In *The Knee* 19 (1), pp. 28–31. DOI: 10.1016/j.knee.2010.12.005.

Haas, Steven B.; Nelson, Charles L.; Laskin, Richard S. (2000): Posterior stabilized knee arthroplasty: an assessment of bone resection. In *The Knee* 7 (1), pp. 25–29. DOI: 10.1016/S0968-0160(99)00038-1.

Haasper, C.; Kendoff, D.; Gebauer, M.; Gehrke, T.; Klauser, W. (2012): Oberflächenersatzwechsel in der Knieendoprothetik - eine intraoperative Ursachenanalyse. In *Zeitschrift fur Orthopadie und Unfallchirurgie* 150 (3), pp. 290–295. DOI: 10.1055/s-0031-1298529.

Halder, A. M.; Köhler, S. (2011): Indikation, Untersuchungen, Aufklärung und Planung der Knieendoprothese. In Dieter Christian Wirtz (Ed.): AE-Manual der Endoprothetik: Springer, Berlin, Heidelberg, pp. 85–108.

Hänisch, Christoph; Radermacher, Klaus (2016): Automatic osteophyte removal from distal femur surfaces obtained from CT scans. In : CAOS 2016. 16th Annual Meeting of the International Society for Computer Assisted Orthopaedic Surgery. Osaka, Japan, 2016-06-08 - 2016-06-11.

Harrysson, Ola L. A.; Robertsson, Otto; Nayfeh, Jamal F. (2004): Higher cumulative revision rate of knee arthroplasties in younger patients with osteoarthritis. In *Clinical orthopaedics and related research* (421), pp. 162–168. DOI: 10.1097/01.blo.0000127115.05754.ce.

Hashemi, Javad; Chandrashekar, Naveen; Gill, Brian; Beynnon, Bruce D.; Slauterbeck, James R.; Schutt, Robert C. et al. (2008): The geometry of the tibial plateau and its influence on the biomechanics of the tibiofemoral joint. In *The Journal of bone and joint surgery. American volume* 90 (12), pp. 2724–2734. DOI: 10.2106/JBJS.G.01358.

Henckel, J.; Richards, R.; Lozhkin, K.; Harris, S.; Rodriguez y Baena, F. M.; Barrett, A. R. W.; Cobb, J. P. (2006): Very low-dose computed tomography for planning and outcome measurement in knee replacement. The imperial knee protocol. In *The Journal of Bone and Joint Surgery. British volume* 88 (11), pp. 1513–1518. DOI: 10.1302/0301-620X.88B11.17986.

Hess, Silvan; Hirschmann, Michael T. (2022): 3D Planning of Total Knee Arthroplasty: Why and How? In Roland Becker, Michael T. Hirschmann, Nanne P. Kort (Eds.): Basics in Primary Knee Arthroplasty. Cham: Springer International Publishing, pp. 233–248.

Higano, Yukimasa; Hayami, Tadashi; Omori, Go; Koga, Yoshio; Endo, Kazuo; Endo, Naoto (2016): The varus alignment and morphologic alterations of proximal tibia affect the onset of medial knee osteoarthritis in rural Japanese women: Case control study from the longitudinal evaluation of Matsudai Knee Osteoarthritis Survey. In *Journal of orthopaedic science : official journal of the Japanese Orthopaedic Association* 21 (2), pp. 166–171. DOI: 10.1016/j.jos.2015.12.002.

Hingelbaum, Swen; Best, Raymond; Huth, Jochen; Wagner, Daniel; Bauer, Gerhard; Mauch, Frieder (2014): The TT-TG Index: a new knee size adjusted measure method to determine the TT-TG distance. In *Knee surgery, sports traumatology, arthroscopy : official journal of the ESSKA* 22 (10), pp. 2388–2395. DOI: 10.1007/s00167-014-3204-1.

Hirakawa, Masashi; Miyazaki, Masashi; Ikeda, Shinichi; Matsumoto, Yoshiki; Kondo, Makoto; Tsumura, Hiroshi (2017): Evaluation of the rotational alignment of the tibial component in total knee arthroplasty: position prioritizing maximum coverage. In *European journal of orthopaedic surgery & traumatology : orthopedie traumatologie* 27 (1), pp. 119–124. DOI: 10.1007/s00590-016-1850-3.

Hirschmann, Michael T.; Hess, Silvan; Behrend, Henrik; Amsler, Felix; Leclercq, Vincent; Moser, Lukas B. (2019a): Phenotyping of hip-knee-ankle angle in young non-osteoarthritic knees provides better understanding of native alignment variability. In *Knee surgery, sports traumatology, arthroscopy : official journal of the ESSKA* 27 (5), pp. 1378–1384. DOI: 10.1007/s00167-019-05507-1.

Hirschmann, Michael T.; Moser, Lukas B.; Amsler, Felix; Behrend, Henrik; Leclerq, Vincent; Hess, Silvan (2019b): Functional knee phenotypes: a novel classification for phenotyping the coronal lower limb alignment based on the native alignment in young non-osteoarthritic patients. In *Knee surgery, sports traumatology, arthroscopy : official journal of the ESSKA* 27 (5), pp. 1394–1402. DOI: 10.1007/s00167-019-05509-z.

Hiss, E.; Schwerbrock, B. (1980): Untersuchungen zur räumlichen Form der Femurkondylen. In *Zeitschrift fur Orthopadie und ihre Grenzgebiete* 118 (3), pp. 396–404. DOI: 10.1055/s-2008-1053523.

Hitt, Kirby; Shurman, John R.; Greene, Kenneth; McCarthy, Joseph; Moskal, Joseph; Hoeman, Tim; Mont, Michael A. (2003): Anthropometric measurements of the human knee: correlation to the sizing of current knee arthroplasty systems. In *The Journal of bone and joint surgery. American volume* 85-A Suppl 4, pp. 115–122.

Hochreiter, Bettina; Hirschmann, Michael T.; Amsler, Felix; Behrend, Henrik (2019): Highly variable tibial tubercle-trochlear groove distance (TT-TG) in osteoarthritic knees should be considered when performing TKA. In *Knee surgery, sports traumatology, arthroscopy : official journal of the ESSKA* 27 (5), pp. 1403–1409. DOI: 10.1007/s00167-018-5141-x.

Hodel, Sandro; Postolka, Barbara; Flury, Andreas; Schütz, Pascal; Taylor, William R.; Vlachopoulos, Lazaros; Fucentese, Sandro F. (2022): Influence of Bone Morphology on In Vivo Tibio-Femoral Kinematics in Healthy Knees during Gait Activities. In *Journal of clinical medicine* 11 (17). DOI: 10.3390/jcm11175082.

Hodges, Nicholas A.; Sussman, Eric M.; Stegemann, Jan P. (2021): Aseptic and septic prosthetic joint loosening: Impact of biomaterial wear on immune cell function, inflammation, and infection. In *Biomaterials* 278, p. 121127. DOI: 10.1016/j.biomaterials.2021.121127.

Hoerl, Arthur E.; Kennard, Robert W. (1970): Ridge Regression: Biased Estimation for Nonorthogonal Problems. In *Technometrics* 12 (1), pp. 55–67. DOI: 10.1080/00401706.1970.10488634.

Hohlmann, Benjamin; Asseln, Malte; Xu, Jiacheng; Radermacher, Klaus (2022): Investigation of morphotypes of the knee using cluster analysis. In *The Knee* 35, pp. 157–163. DOI: 10.1016/j.knee.2022.03.006.

Hohlmann, Benjamin; Brossner, Peter; Phlippen, Lovis; Rohde, Thorsten; Radermacher, Klaus (2023): Knee Bone Models from Ultrasound. In *IEEE transactions*

on ultrasonics, ferroelectrics, and frequency control PP. DOI: 10.1109/TUFFC.2023.3286287.

Holme, T. J.; Henckel, J.; Cobb, J.; Hart, A. J. (2011): Quantification of the difference between 3D CT and plain radiograph for measurement of the position of medial unicompartmental knee replacements. In *The Knee* 18 (5), pp. 300–305. DOI: 10.1016/j.knee.2010.07.010.

Houserman, David J.; Berend, Keith R.; Lombardi, Adolph V.; Duhaime, Erik P.; Jain, Anant; Crawford, David A. (2022): The Viability of an Artificial Intelligence/Machine Learning Prediction Model to Determine Candidates for Knee Arthroplasty. In *The Journal of arthroplasty*. DOI: 10.1016/j.arth.2022.04.003.

Howell, Stephen M.; Howell, Stacey J.; Hull, Maury L. (2010): Assessment of the radii of the medial and lateral femoral condyles in varus and valgus knees with osteoarthritis. In *The Journal of bone and joint surgery. American volume* 92 (1), pp. 98–104. DOI: 10.2106/JBJS.H.01566.

Illés, Tamás; Somoskeöy, Szabolcs (2012): The EOS™ imaging system and its uses in daily orthopaedic practice. In *International orthopaedics* 36 (7), pp. 1325–1331. DOI: 10.1007/s00264-012-1512-y.

ISO ISO 7207-1, 2007-02: Implants for surgery - Components for partial and total knee joint prostheses - Part 1: Classification, definitions and designation of dimensions.

DIN DIN 66001, 1983-12: Informationsverarbeitung - Sinnbilder und ihre Anwendung.

Innocenti, Bernardo; Bellemans, Johan; Catani, Fabio (2016): Deviations From Optimal Alignment in TKA: Is There a Biomechanical Difference Between Femoral or Tibial Component Alignment? In *The Journal of arthroplasty* 31 (1), pp. 295–301. DOI: 10.1016/j.arth.2015.07.038.

Insall, J.; Salvati, E. (1971): Patella position in the normal knee joint. In *Radiology* 101 (1), pp. 101–104. DOI: 10.1148/101.1.101.

Itou, Junya; Kuwashima, Umito; Itoh, Masafumi; Okazaki, Ken (2021): Anterior prominence of the femoral condyle varies among prosthesis designs and surgical

techniques in total knee arthroplasty. In *BMC musculoskeletal disorders* 22 (1), p. 784. DOI: 10.1186/s12891-021-04670-2.

Jacobs, Cale A.; Christensen, Christian P. (2014): Factors influencing patient satisfaction two to five years after primary total knee arthroplasty. In *The Journal of arthroplasty* 29 (6), pp. 1189–1191. DOI: 10.1016/j.arth.2014.01.008.

Jagodzinski, M.; Müller, W.; Friederich, N. (2016): Kinematik und angewandte Physiologie und Pathophysiologie der Ligamente. In Michael Jagodzinski, Niklaus Friederich, Werner Müller (Eds.): Das Knie, vol. 27. Berlin, Heidelberg: Springer Berlin Heidelberg, pp. 15–57.

Jennings, L. M.; Bell, C. I.; Ingham, E.; Komistek, R. D.; Stone, M. H.; Fisher, J. (2007): The influence of femoral condylar lift-off on the wear of artificial knee joints. In *Proceedings of the Institution of Mechanical Engineers. Part H, Journal of engineering in medicine* 221 (3), pp. 305–314. DOI: 10.1243/09544119JEIM215.

Jo, Ah-Reum; Song, Eun-Kyoo; Lee, Keun-Bae; Seo, Hyoung-Yeon; Kim, Sung-Kyu; Seon, Jong-Keun (2014): A comparison of stability and clinical outcomes in single-radius versus multi-radius femoral design for total knee arthroplasty. In *The Journal of arthroplasty* 29 (12), pp. 2402–2406. DOI: 10.1016/j.arth.2014.03.033.

Johal, Parm; Hassaballa, Mohammed A.; Eldridge, Jonathan D.; Porteous, Andrew J. (2012): The Posterior Condylar Offset Ratio. In *The Knee* 19 (6), pp. 843–845. DOI: 10.1016/j.knee.2012.03.017.

Johansson, H. (1991): Role of knee ligaments in proprioception and regulation of muscle stiffness. In *Journal of electromyography and kinesiology : official journal of the International Society of Electrophysiological Kinesiology* 1 (3), pp. 158–179. DOI: 10.1016/1050-6411(91)90032-Z.

Jud, Lukas; Roth, Tabitha; Fürnstahl, Philipp; Vlachopoulos, Lazaros; Sutter, Reto; Fucentese, Sandro F. (2020): The impact of limb loading and the measurement modality (2D versus 3D) on the measurement of the limb loading dependent lower extremity parameters. In *BMC musculoskeletal disorders* 21 (1), p. 418. DOI: 10.1186/s12891-020-03449-1.

Jungmann, Pia M.; Tham, Seng-Choe; Liebl, Hans; Nevitt, Michael C.; McCulloch, Charles E.; Lynch, John; Link, Thomas M. (2013): Association of trochlear dysplasia with degenerative abnormalities in the knee: data from the Osteoarthritis Initiative. In *Skeletal radiology* 42 (10), pp. 1383–1392. DOI: 10.1007/s00256-013-1664-x.

Kasahara, Yasuhiko; Majima, Tokifumi; Kimura, Shoichi; Nishiike, Osamu; Uchida, Jun (2013): What are the causes of revision total knee arthroplasty in Japan? In *Clinical orthopaedics and related research* 471 (5), pp. 1533–1538. DOI: 10.1007/s11999-013-2820-2.

Katchburian, Marcos V.; Bull, Anthony M. J.; Shih, Yi-Fen; Heatley, Frederick W.; Amis, Andrew A. (2003): Measurement of patellar tracking: assessment and analysis of the literature. In *Clinical orthopaedics and related research* (412), pp. 241–259. DOI: 10.1097/01.blo.0000068767.86536.9a.

Kawahara, S.; Matsuda, S.; Fukagawa, S.; Mitsuyasu, H.; Nakahara, H.; Higaki, H. et al. (2012): Upsizing the femoral component increases patellofemoral contact force in total knee replacement. In *The Journal of Bone and Joint Surgery. British volume* 94 (1), pp. 56–61. DOI: 10.1302/0301-620X.94B1.27514.

Kayaalp, Mahmut Enes; Becker, Roland (2022): The Optimal Indication for Total Knee Arthroplasty. In Roland Becker, Michael T. Hirschmann, Nanne P. Kort (Eds.): Basics in Primary Knee Arthroplasty, vol. 35. Cham: Springer International Publishing, pp. 107–113.

Kellgren, J. H.; Lawrence, J. S. (1957): Radiological assessment of osteo-arthrosis. In *Annals of the rheumatic diseases* 16 (4), pp. 494–502. DOI: 10.1136/ard.16.4.494.

Kennedy, J.; Eberhart, R. (1995): Particle swarm optimization. In : Proceedings of ICNN'95 - International Conference on Neural Networks. Perth, WA, Australia, 27 Nov.-1 Dec. 1995: IEEE, pp. 1942–1948.

Kessler, Oliver; Dürselen, Lutz; Banks, Scott; Mannel, Henrich; Marin, Frédéric (2007): Sagittal curvature of total knee replacements predicts in vivo kinematics. In *Clinical biomechanics (Bristol, Avon)* 22 (1), pp. 52–58. DOI: 10.1016/j.clinbiomech.2006.07.011.

Kim, T. K.; Phillips, Mark; Bhandari, Mohit; Watson, John; Malhotra, Rajesh (2017): What Differences in Morphologic Features of the Knee Exist Among Patients of Various Races? A Systematic Review. In *Clinical orthopaedics and related research* 475 (1), pp. 170–182. DOI: 10.1007/s11999-016-5097-4.

Kim, Y-H; Choi, Y.; Kim, J-S (2010): Comparison of standard and gender-specific posterior-cruciate-retaining high-flexion total knee replacements: a prospective, randomised study. In *The Journal of Bone and Joint Surgery. British volume* 92 (5), pp. 639–645. DOI: 10.1302/0301-620X.92B5.24129.

Kim, Young-Hoo; Park, Jang-Won; Kim, Jun-Shik; Park, Sang-Doo (2014): The relationship between the survival of total knee arthroplasty and postoperative coronal, sagittal and rotational alignment of knee prosthesis. In *International orthopaedics* 38 (2), pp. 379–385. DOI: 10.1007/s00264-013-2097-9.

Kızılgöz, Volkan; Sivrioğlu, Ali Kemal; Ulusoy, Gökhan Ragıp; Aydın, Hasan; Karayol, Sunay Sibel; Menderes, Utku (2018): Analysis of the risk factors for anterior cruciate ligament injury: an investigation of structural tendencies. In *Clinical imaging* 50, pp. 20–30. DOI: 10.1016/j.clinimag.2017.12.004.

Klasan, Antonio; Twiggs, Joshua G.; Fritsch, Brett A.; Miles, Brad P.; Heyse, Thomas J.; Solomon, Michael; Parker, David A. (2020): Correlation of tibial component size and rotation with outcomes after total knee arthroplasty. In *Archives of orthopaedic and trauma surgery* 140 (11), pp. 1819–1824. DOI: 10.1007/s00402-020-03550-z.

Klein, Paul; Sommerfeld, Peter (2012): Biomechanik der menschlichen Gelenke. Grundlagen, Becken, untere Extremität. 1. Aufl. München: Elsevier Urban & Fischer. Available online at http://www.blickinsbuch.de/item/425e4736262e991bd9ce5e8ade1f8790.

Klit, Jakob; Jacobsen, Steffen; Rosenlund, Signe; Sonne-Holm, Stig; Troelsen, Anders (2014): Total knee arthroplasty in younger patients evaluated by alternative outcome measures. In *The Journal of arthroplasty* 29 (5), pp. 912–917. DOI: 10.1016/j.arth.2013.09.035.

Kloth, Jost Karsten; Neumann, Regina; Stillfried, Eva von; Stiller, Wolfram; Kauczor, Hans-Ulrich; Ewerbeck, Volker; Weber, Marc-André (2015): Quality-controlled dose reduction of full-leg radiography in patients with knee malalignment. In *Skeletal radiology* 44 (3), pp. 423–429. DOI: 10.1007/s00256-014-2004-5.

Klug, Alexander; Gramlich, Yves; Rudert, Maximilian; Drees, Philipp; Hoffmann, Reinhard; Weißenberger, Manuel; Kutzner, Karl Philipp (2021): The projected volume of primary and revision total knee arthroplasty will place an immense burden on future health care systems over the next 30 years. In *Knee surgery, sports traumatology, arthroscopy : official journal of the ESSKA* 29 (10), pp. 3287–3298. DOI: 10.1007/s00167-020-06154-7.

Koch, P. P.; Müller, D.; Pisan, M.; Fucentese, S. F. (2013): Radiographic accuracy in TKA with a CT-based patient-specific cutting block technique. In *Knee surgery, sports traumatology, arthroscopy : official journal of the ESSKA* 21 (10), pp. 2200–2205. DOI: 10.1007/s00167-013-2625-6.

Koh, In Jun; Cho, Woo-Shin; Choi, Nam Yong; Kim, Tae Kyun (2014): Causes, risk factors, and trends in failures after TKA in Korea over the past 5 years: a multicenter study. In *Clinical orthopaedics and related research* 472 (1), pp. 316–326. DOI: 10.1007/s11999-013-3252-8.

Koo, Terry K.; Li, Mae Y. (2016): A Guideline of Selecting and Reporting Intraclass Correlation Coefficients for Reliability Research. In *Journal of chiropractic medicine* 15 (2), pp. 155–163. DOI: 10.1016/j.jcm.2016.02.012.

Krueger, Chad A.; Austin, Matthew S.; Levicoff, Eric A.; Saxena, Arjun; Nazarian, David G.; Courtney, P. Maxwell (2020): Substantial Preoperative Work Is Unaccounted for in Total Hip and Knee Arthroplasty. In *The Journal of arthroplasty* 35 (9), pp. 2318–2322. DOI: 10.1016/j.arth.2020.04.066.

Kuiper, Ruurd J. A.; Seevinck, Peter R.; Viergever, Max A.; Weinans, Harrie; Sakkers, Ralph J. B. (2023): Automatic Assessment of Lower-Limb Alignment from Computed Tomography. In *The Journal of bone and joint surgery. American volume*. DOI: 10.2106/JBJS.22.00890.

Kuo, Alexander W.; Chen, Darren B.; Wood, Jil; MacDessi, Samuel J. (2020): Modern total knee arthroplasty designs do not reliably replicate anterior femoral morphology. In *Knee surgery, sports traumatology, arthroscopy : official journal of the ESSKA* 28 (9), pp. 2808–2815. DOI: 10.1007/s00167-019-05610-3.

Kurosawa, H.; Walker, P. S.; Abe, S.; Garg, A.; Hunter, T. (1985): Geometry and motion of the knee for implant and orthotic design. In *Journal of biomechanics* 18 (7), pp. 487–499. DOI: 10.1016/0021-9290(85)90663-3.

Kurtz, Steven M.; Lau, Edmund; Ong, Kevin; Zhao, Ke; Kelly, Michael; Bozic, Kevin J. (2009): Future young patient demand for primary and revision joint replacement: national projections from 2010 to 2030. In *Clinical orthopaedics and related research* 467 (10), pp. 2606–2612. DOI: 10.1007/s11999-009-0834-6.

Kurtz, Steven M.; Ong, Kevin L.; Lau, Edmund; Widmer, Marcel; Maravic, Milka; Gómez-Barrena, Enrique et al. (2011): International survey of primary and revision total knee replacement. In *International orthopaedics* 35 (12), pp. 1783–1789. DOI: 10.1007/s00264-011-1235-5.

Kurtz, William B.; Slamin, John E.; Doody, Scott W. (2016): Bone Preservation in a Novel Patient Specific Total Knee Replacement. In *ReconRev* 6 (1). DOI: 10.15438/rr.6.1.133.

Kuzyk, Paul R. T.; Watts, Evan; Backstein, David (2017): Revision Total Knee Arthroplasty for the Management of Periprosthetic Fractures. In *The Journal of the American Academy of Orthopaedic Surgeons* 25 (9), pp. 624–633. DOI: 10.5435/JAAOS-D-15-00680.

Lan, Roy H.; Bell, Jack W.; Samuel, Linsen T.; Kamath, Atul F. (2020): Evolving Outcome Measures in Total Knee Arthroplasty: Trends and Utilization Rates Over the Past 15 Years. In *The Journal of arthroplasty* 35 (11), pp. 3375–3382. DOI: 10.1016/j.arth.2020.06.036.

Laporte, S.; Skalli, W.; Guise, J. A. de; Lavaste, F.; Mitton, D. (2003): A biplanar reconstruction method based on 2D and 3D contours: application to the distal femur. In

Computer methods in biomechanics and biomedical engineering 6 (1), pp. 1–6. DOI: 10.1080/1025584031000065956.

Laurin, C. A.; Lévesque, H. P.; Dussault, R.; Labelle, H.; Peides, J. P. (1978): The abnormal lateral patellofemoral angle: a diagnostic roentgenographic sign of recurrent patellar subluxation. In *The Journal of bone and joint surgery. American volume* 60 (1), pp. 55–60.

Le Stum, Mathieu; Gicquel, Thomas; Dardenne, Guillaume; Le Goff-Pronost, Myriam; Stindel, Eric; Clavé, Arnaud (2023): Total knee arthroplasty in France: Male-driven rise in procedures in 2009-2019 and projections for 2050. In *Orthopaedics & traumatology, surgery & research : OTSR* 109 (5), p. 103463. DOI: 10.1016/j.otsr.2022.103463.

Lee, Bum-Sik; Cho, Hyun-Ik; Bin, Seong-Il; Kim, Jong-Min; Jo, Byeong-Kyu (2018): Femoral Component Varus Malposition is Associated with Tibial Aseptic Loosening After TKA. In *Clinical orthopaedics and related research* 476 (2), pp. 400–407. DOI: 10.1007/s11999.0000000000000012.

Lee, O-Sung; Lee, Jangyun; Lee, Myung Chul; Han, Hyuk-Soo (2021): Changes in the femoral varus and rotational profiles are correlated in women with varus osteoarthritic lower limbs. In *Archives of orthopaedic and trauma surgery*. DOI: 10.1007/s00402-021-04094-6/.

Leichtle, Ulf G.; Lange, Barbara; Herzog, Yvonne; Schnauffer, Peter; Leichtle, Carmen I.; Wülker, Nikolaus; Lorenz, Andrea (2017): Influence of Different Patellofemoral Design Variations Based on Genesis II Total Knee Endoprosthesis on Patellofemoral Pressure and Kinematics. In *Applied bionics and biomechanics* 2017, p. 5492383. DOI: 10.1155/2017/5492383.

Leonard, Hollie J.; Ewen, Alistair, M.; Dwarakanathan, Hariharan T.; Deep, Kamal (2023): Are Patient Reported Outcome Measures Sensitive Enough: Making the Case for Functional Biomechanical Assessment of Navigated Total Hip Arthroplasty Patients. In Press. In : Proceedings of The 21th Annual Meeting of the International Society for Computer Assisted Orthopaedic Surgery.

Lesh, M. L.; Schneider, D. J.; Deol, G.; Davis, B.; Jacobs, C. R.; Pellegrini, V. D. (2000): The consequences of anterior femoral notching in total knee arthroplasty. A biomechanical study. In *The Journal of bone and joint surgery. American volume* 82 (8), pp. 1096–1101. DOI: 10.2106/00004623-200008000-00005.

Li, Kang; Langdale, Evan; Tashman, Scott; Harner, Christopher; Zhang, Xudong (2012): Gender and condylar differences in distal femur morphometry clarified by automated computer analyses. In *Journal of orthopaedic research : official publication of the Orthopaedic Research Society* 30 (5), pp. 686–692. DOI: 10.1002/jor.21575.

Li, Kang; Tashman, Scott; Fu, Freddie; Harner, Christopher; Zhang, Xudong (2010): Automating analyses of the distal femur articular geometry based on three-dimensional surface data. In *Annals of biomedical engineering* 38 (9), pp. 2928–2936. DOI: 10.1007/s10439-010-0064-9.

Lindner, C.; Thiagarajah, S.; Wilkinson, J. M.; Wallis, G. A.; Cootes, T. F. (2013): Fully automatic segmentation of the proximal femur using random forest regression voting. In *IEEE transactions on medical imaging* 32 (8), pp. 1462–1472. DOI: 10.1109/TMI.2013.2258030.

Liu, Changquan; Zhao, Guanglei; Chen, Kangming; Lyu, Jinyang; Chen, Jie; Shi, Jingsheng et al. (2021): Tibial component coverage affects tibial bone resorption and patient-reported outcome measures for patients following total knee arthroplasty. In *Journal of orthopaedic surgery and research* 16 (1), p. 134. DOI: 10.1186/s13018-021-02250-7.

Lombardi, Adolph V.; Nunley, Ryan M.; Berend, Keith R.; Ruh, Erin L.; Clohisy, John C.; Hamilton, William G. et al. (2014): Do patients return to work after total knee arthroplasty? In *Clinical orthopaedics and related research* 472 (1), pp. 138–146. DOI: 10.1007/s11999-013-3099-z.

Lösch, A.; Eckstein, F.; Haubner, M.; Englmeier, K. H. (1997): A non-invasive technique for 3-dimensional assessment of articular cartilage thickness based on MRI. Part 1: Development of a computational method. In *Magnetic resonance imaging* 15 (7), pp. 795–804. DOI: 10.1016/S0730-725X(97)00012-X.

Losina, Elena; Walensky, Rochelle P.; Kessler, Courtenay L.; Emrani, Parastu S.; Reichmann, William M.; Wright, Elizabeth A. et al. (2009): Cost-effectiveness of total knee arthroplasty in the United States: patient risk and hospital volume. In *Archives of internal medicine* 169 (12), 1113-21; discussion 1121-2. DOI: 10.1001/archinternmed.2009.136.

Lum, Zachary C.; Saiz, Augustine M.; Pereira, Gavin C.; Meehan, John P. (2020): Patella Baja in Total Knee Arthroplasty. In *The Journal of the American Academy of Orthopaedic Surgeons* 28 (8), pp. 316–323. DOI: 10.5435/JAAOS-D-19-00422.

Lustig, Sebastien; Scholes, Corey J.; Stegeman, Tim J.; Oussedik, Sam; Coolican, Myles R. J.; Parker, David A. (2012): Sagittal placement of the femoral component in total knee arthroplasty predicts knee flexion contracture at one-year follow-up. In *International orthopaedics* 36 (9), pp. 1835–1839. DOI: 10.1007/s00264-012-1580-z.

Lützner, Cornelia; Lange, Toni; Lützner, Jörg (2022): How to Assess Outcome After Partial or Total Knee Arthroplasty—Measuring Results that Really Matter! In Roland Becker, Michael T. Hirschmann, Nanne P. Kort (Eds.): Basics in Primary Knee Arthroplasty, vol. 43. Cham: Springer International Publishing, pp. 601–621.

Lützner, Jörg; Kirschner, Stephan (2017): SOP Primäre Endoprothetik am Kniegelenk. In *Orthopädie und Unfallchirurgie up2date* 12 (04), pp. 345–349. DOI: 10.1055/s-0043-109037.

Lützner, Jörg; Melsheimer, Oliver; Morlock, Michael; Steinbrück, Arnd (2023): Annual Report 2022. Edited by Alexander Grimberg. Berlin: EPRD Deutsche Endoprothesenregister.

MacDessi, Samuel J.; Griffiths-Jones, William; Harris, Ian A.; Bellemans, Johan; Chen, Darren B. (2021): Coronal Plane Alignment of the Knee (CPAK) classification. In *The bone & joint journal* 103-B (2), pp. 329–337. DOI: 10.1302/0301-620X.103B2.BJJ-2020-1050.R1.

Maffiuletti, Nicola A.; Bizzini, Mario; Widler, Katharina; Munzinger, Urs (2010): Asymmetry in quadriceps rate of force development as a functional outcome measure

in TKA. In *Clinical orthopaedics and related research* 468 (1), pp. 191–198. DOI: 10.1007/s11999-009-0978-4.

Mahfouz, M. R.; Badawi, Ahmed; Fatah, E. E. Abdel; Kuhn, Michael; Merkl, Brandon (2006): Reconstruction of 3D Patient-Specific Bone Models From Biplanar X-Ray Images Utilizing Morphometric Measurements. In : Proceedings of the 2006 International Conference on Image Processing, Computer Vision, & Pattern Recognition. Las Vegas, Nevada, USA, June 26-29. Volume 2.

Mahfouz, M. R.; Merkl, B. C.; Fatah, E. E. Abdel; Booth, R.; Argenson, J. N. (2007): Automatic methods for characterization of sexual dimorphism of adult femora: distal femur. In *Computer methods in biomechanics and biomedical engineering* 10 (6), pp. 447–456. DOI: 10.1080/10255840701552093.

Mahfouz, Mohamed; Abdel Fatah, Emam Elhak; Bowers, Lyndsay Smith; Scuderi, Giles (2012): Three-dimensional morphology of the knee reveals ethnic differences. In *Clinical orthopaedics and related research* 470 (1), pp. 172–185. DOI: 10.1007/s11999-011-2089-2.

Mahoney, Ormonde M.; Kinsey, Tracy (2010): Overhang of the femoral component in total knee arthroplasty: risk factors and clinical consequences. In *The Journal of bone and joint surgery. American volume* 92 (5), pp. 1115–1121. DOI: 10.2106/JBJS.H.00434.

Marsilio, Luca; Faglia, Alberto; Rossi, Matteo; Mainardi, Luca; Manzotti, Alfonso; Cerveri, Pietro (2022): CEL-Unet: a novel CNN architecture for 3D Segmentation of Knee Bones affected by Severe Osteoarthritis for PSI-Based Surgical Planning. In *Annual International Conference of the IEEE Engineering in Medicine and Biology Society. IEEE Engineering in Medicine and Biology Society. Annual International Conference* 2022, pp. 5039–5042. DOI: 10.1109/EMBC48229.2022.9871953.

Martelli, S.; Pinskerova, V. (2002): The shapes of the tibial and femoral articular surfaces in relation to tibiofemoral movement. In *The Journal of Bone and Joint Surgery. British volume* 84-B (4), pp. 607–613. DOI: 10.1302/0301-620X.84B4.0840607.

Martin, Stacey; Saurez, Alex; Ismaily, Sabir; Ashfaq, Kashif; Noble, Philip; Incavo, Stephen J. (2014): Maximizing tibial coverage is detrimental to proper rotational alignment. In *Clinical orthopaedics and related research* 472 (1), pp. 121–125. DOI: 10.1007/s11999-013-3047-y.

Mason, J. J.; Leszko, F.; Johnson, T.; Komistek, R. D. (2008): Patellofemoral joint forces. In *Journal of biomechanics* 41 (11), pp. 2337–2348. DOI: 10.1016/j.jbiomech.2008.04.039.

Matsuda, Shuichi; Miura, Hiromasa; Nagamine, Ryuji; Mawatari, Taro; Tokunaga, Masami; Nabeyama, Ryotaro; Iwamoto, Yukihide (2004): Anatomical analysis of the femoral condyle in normal and osteoarthritic knees. In *Journal of orthopaedic research : official publication of the Orthopaedic Research Society* 22 (1), pp. 104–109. DOI: 10.1016/S0736-0266(03)00134-7.

Mattiassich, G.; Hochreiter, J. (2022): Standard Approaches to the Knee. In Roland Becker, Michael T. Hirschmann, Nanne P. Kort (Eds.): Basics in Primary Knee Arthroplasty, vol. 16. Cham: Springer International Publishing, pp. 291–297.

McPherson, A.; Kärrholm, J.; Pinskerova, V.; Sosna, A.; Martelli, S. (2005): Imaging knee position using MRI, RSA/CT and 3D digitisation. In *Journal of biomechanics* 38 (2), pp. 263–268. DOI: 10.1016/j.jbiomech.2004.02.007.

Meier, Malin; Zingde, Sumesh; Steinert, André; Kurtz, William; Koeck, Franz; Beckmann, Johannes (2019): What Is the Possible Impact of High Variability of Distal Femoral Geometry on TKA? A CT Data Analysis of 24,042 Knees. In *Clinical orthopaedics and related research* 477 (3), pp. 561–570. DOI: 10.1097/CORR.0000000000000611.

Mensch, J. S.; Amstutz, H. C. (1975): Knee morphology as a guide to knee replacement. In *Clinical orthopaedics and related research* (112), pp. 231–241.

Meric, Gokhan; Gracitelli, Guilherme C.; Aram, Luke J.; Swank, Michael L.; Bugbee, William D. (2015): Variability in Distal Femoral Anatomy in Patients Undergoing Total Knee Arthroplasty: Measurements on 13,546 Computed Tomography Scans. In *The Journal of arthroplasty* 30 (10), pp. 1835–1838. DOI: 10.1016/j.arth.2015.04.024.

Merle, C.; Herre, J.; Aldinger, P. R. (2012): 7 Endoprothetik des Kniegelenkes. In Manfred Georg Krukemeyer, Gunnar Möllenhoff (Eds.): Endoprothetik: DE GRUYTER, pp. 129–162.

Messmer, P.; Long, G.; Suhm, N.; Regazzoni, P.; Jacob, A. L. (2001): Volumetric model determination of the tibia based on 2D radiographs using a 2D/3D database. In *Computer aided surgery : official journal of the International Society for Computer Aided Surgery* 6 (4), pp. 183–194. DOI: 10.1002/igs.10009.

Meyer, H.; Heller, K.-D.; Becker, Roland (2022): Surgical 2D Planning of Total Knee Arthroplasty. In Roland Becker, Michael T. Hirschmann, Nanne P. Kort (Eds.): Basics in Primary Knee Arthroplasty, vol. 248. Cham: Springer International Publishing, pp. 217–232.

Mihalko, William M.; Saleh, Khaled J.; Krackow, Kenneth A.; Whiteside, Leo A. (2009): Soft-tissue balancing during total knee arthroplasty in the varus knee. In *The Journal of the American Academy of Orthopaedic Surgeons* 17 (12), pp. 766–774. DOI: 10.5435/00124635-200912000-00005.

Minami, Takao; Koga, Hideyuki; Sekiya, Ichiro; Watanabe, Toshifumi; Horie, Masafumi; Katagiri, Hiroki et al. (2018): Posteriorly inserted anterior cruciate ligament in knees with discoid lateral meniscus corresponding to bony morphological characteristics of femoral lateral condyle. In *Journal of orthopaedic science : official journal of the Japanese Orthopaedic Association* 23 (2), pp. 350–355. DOI: 10.1016/j.jos.2017.10.003.

Minnema, Jordi; van Eijnatten, Maureen; Kouw, Wouter; Diblen, Faruk; Mendrik, Adriënne; Wolff, Jan (2018): CT image segmentation of bone for medical additive manufacturing using a convolutional neural network. In *Computers in biology and medicine* 103, pp. 130–139. DOI: 10.1016/j.compbiomed.2018.10.012.

Mueller, John Kyle P.; Wentorf, Fred A.; Moore, Richard E. (2014): Femoral and tibial insert downsizing increases the laxity envelope in TKA. In *Knee surgery, sports traumatology, arthroscopy : official journal of the ESSKA* 22 (12), pp. 3003–3011. DOI: 10.1007/s00167-014-3339-0.

Müller, Jacobus H.; Liebensteiner, Michael; Kort, Nanne; Stirling, Patrick; Pilot, Peter; Demey, Guillaume (2023): No significant difference in early clinical outcomes of custom versus off-the-shelf total knee arthroplasty: a systematic review and meta-analysis. In *Knee surgery, sports traumatology, arthroscopy : official journal of the ESSKA* 31 (4), pp. 1230–1246. DOI: 10.1007/s00167-021-06678-6.

Müller, R. T.; Schürmann, N. (2001): Kostenanalyse von Hüft- und Knieprothesen als Grundlage einer Kosten-Nutzen-Bilanz. In *Zentralblatt fur Chirurgie* 126 (1), pp. 55–61. DOI: 10.1055/s-2001-11722.

Nakamura, Shinichiro; Shima, Koichiro; Kuriyama, Shinichi; Nishitani, Kohei; Ito, Hiromu; Matsuda, Shuichi (2019): Tibial Tubercle-Trochlear Groove Distance Influences Patellar Tilt After Total Knee Arthroplasty. In *The Journal of arthroplasty* 34 (12), pp. 3080–3087. DOI: 10.1016/j.arth.2019.07.038.

Namin, Amir T.; Jalali, Mohammad S.; Vahdat, Vahab; Bedair, Hany S.; O'Connor, Mary I.; Kamarthi, Sagar; Isaacs, Jacqueline A. (2019): Adoption of New Medical Technologies: The Case of Customized Individually Made Knee Implants. In *Value in health : the journal of the International Society for Pharmacoeconomics and Outcomes Research* 22 (4), pp. 423–430. DOI: 10.1016/j.jval.2019.01.008.

Neogi, Tuhina; Bowes, Michael A.; Niu, Jingbo; Souza, Kevin M. de; Vincent, Graham R.; Goggins, Joyce et al. (2013): Magnetic resonance imaging-based three-dimensional bone shape of the knee predicts onset of knee osteoarthritis: data from the osteoarthritis initiative. In *Arthritis and rheumatism* 65 (8), pp. 2048–2058. DOI: 10.1002/art.37987.

Nicoll, D.; Rowley, D. I. (2010): Internal rotational error of the tibial component is a major cause of pain after total knee replacement. In *The Journal of Bone and Joint Surgery. British volume* 92 (9), pp. 1238–1244. DOI: 10.1302/0301-620X.92B9.23516.

Nishikawa, Kazutaka; Okazaki, Ken; Matsuda, Shuichi; Tashiro, Yasutaka; Kawahara, Shinya; Nakahara, Hiroyuki et al. (2014): Improved design decreases wear in total knee arthroplasty with varus malalignment. In *Knee surgery, sports traumatology,*

arthroscopy : official journal of the ESSKA 22 (11), pp. 2635–2640. DOI: 10.1007/s00167-013-2506-z.

Noble, Philip C.; Conditt, Michael A.; Cook, Karon F.; Mathis, Kenneth B. (2006): The John Insall Award: Patient expectations affect satisfaction with total knee arthroplasty. In *Clinical orthopaedics and related research* 452, pp. 35–43. DOI: 10.1097/01.blo.0000238825.63648.1e.

Noble, Philip C.; Scuderi, Giles R.; Brekke, Adam C.; Sikorskii, Alla; Benjamin, James B.; Lonner, Jess H. et al. (2012): Development of a new Knee Society scoring system. In *Clinical orthopaedics and related research* 470 (1), pp. 20–32. DOI: 10.1007/s11999-011-2152-z.

Ntagiopoulos, Panagiotis G.; Byn, Pieter; Dejour, David (2013): Midterm results of comprehensive surgical reconstruction including sulcus-deepening trochleoplasty in recurrent patellar dislocations with high-grade trochlear dysplasia. In *The American journal of sports medicine* 41 (5), pp. 998–1004. DOI: 10.1177/0363546513482302.

Nuño, N.; Ahmed, A. M. (2001): Sagittal profile of the femoral condyles and its application to femorotibial contact analysis. In *Journal of biomechanical engineering* 123 (1), pp. 18–26. DOI: 10.1115/1.1339819.

Okamoto, Yoshinori; Otsuki, Shuhei; Nakajima, Mikio; Jotoku, Tsuyoshi; Wakama, Hitoshi; Neo, Masashi (2019): Sagittal Alignment of the Femoral Component and Patient Height Are Associated With Persisting Flexion Contracture After Primary Total Knee Arthroplasty. In *The Journal of arthroplasty* 34 (7), pp. 1476–1482. DOI: 10.1016/j.arth.2019.02.051.

Omoumi, P.; Michoux, N.; Roemer, F. W.; Thienpont, E.; Vande Berg, B. C. (2015): Cartilage thickness at the posterior medial femoral condyle is increased in femorotibial knee osteoarthritis: a cross-sectional CT arthrography study (Part 2). In *Osteoarthritis and cartilage* 23 (2), pp. 224–231. DOI: 10.1016/j.joca.2014.08.017.

Pandey, Prashant; Hohlmann, Benjamin; Brößner, Peter; Hacihaliloglu, Ilker; Barr, Keiran; Ungi, Tamas et al. (2022): Standardized Evaluation of Current Ultrasound Bone Segmentation Algorithms on Multiple Datasets. In : Proceedings of The 20th

Annual Meeting of the International Society for Computer Assisted Orthopaedic Surgery, 148-141.

Pap, G.; Meinecke, I. (2011): Ätiologie und Pathogenese der Gonarthrose. In Dieter Christian Wirtz (Ed.): AE-Manual der Endoprothetik: Springer, Berlin, Heidelberg, pp. 33–46.

Petersen, Wolf; Rembitzki, Ingo Volker; Brüggemann, Gerd-Peter; Ellermann, Andree; Best, Raymond; Koppenburg, Andreas Gösele; Liebau, Christian (2014): Anterior knee pain after total knee arthroplasty: a narrative review. In *International orthopaedics* 38 (2), pp. 319–328. DOI: 10.1007/S00264-013-2081-4.

Pfeiffer, Thomas R.; Burnham, Jeremy M.; Hughes, Jonathan D.; Kanakamedala, Ajay C.; Herbst, Elmar; Popchak, Adam et al. (2018): An Increased Lateral Femoral Condyle Ratio Is a Risk Factor for Anterior Cruciate Ligament Injury. In *The Journal of bone and joint surgery. American volume* 100 (10), pp. 857–864. DOI: 10.2106/JBJS.17.01011.

Pfeiffer, Thomas R.; Burnham, Jeremy M.; Kanakamedala, Ajay C.; Hughes, Jonathan D.; Zlotnicki, Jason; Popchak, Adam et al. (2019): Distal femur morphology affects rotatory knee instability in patients with anterior cruciate ligament ruptures. In *Knee surgery, sports traumatology, arthroscopy : official journal of the ESSKA* 27 (5), pp. 1514–1519. DOI: 10.1007/s00167-018-5269-8.

Pfirrmann, C. W.; Zanetti, M.; Romero, J.; Hodler, J. (2000): Femoral trochlear dysplasia: MR findings. In *Radiology* 216 (3), pp. 858–864. DOI: 10.1148/radiology.216.3.r00se38858.

Pfitzner, Tilman; Moewis, Philippe; Stein, Patrick; Boeth, Heide; Trepczynski, Adam; Roth, Philipp von; Duda, Georg N. (2018): Modifications of femoral component design in multi-radius total knee arthroplasty lead to higher lateral posterior femoro-tibial translation. In *Knee surgery, sports traumatology, arthroscopy : official journal of the ESSKA* 26 (6), pp. 1645–1655. DOI: 10.1007/s00167-017-4622-7.

Phlippen, Lovis; Hohlmann, Benjamin; Radermacher, Klaus (2023): 3D Reconstruction of Femur using Ultrasound - Hand Guided Evaluation and Autonomous Robotic

Approach. In Press. In : Proceedings of The 21th Annual Meeting of the International Society for Computer Assisted Orthopaedic Surgery.

Pogonke, M.-A. (2012): 2 DRG-Fallpauschalen in der Endoprothetik. In Manfred Georg Krukemeyer, Gunnar Möllenhoff (Eds.): Endoprothetik: DE GRUYTER, pp. 19–32.

Postler, Anne; Lützner, Cornelia; Beyer, Franziska; Tille, Eric; Lützner, Jörg (2018): Analysis of Total Knee Arthroplasty revision causes. In *BMC musculoskeletal disorders* 19 (1), p. 55. DOI: 10.1186/s12891-018-1977-y.

Powers, Christopher M. (2000): Patellar Kinematics, Part II: The Influence of the Depth of the Trochlear Groove in Subjects With and Without Patellofemoral Pain. In *Physical Therapy* 80 (10), pp. 965–973. DOI: 10.1093/ptj/80.10.965.

Provenzano, Paolo P.; Heisey, Dennis; Hayashi, Kei; Lakes, Roderic; Vanderby, Ray (2002): Subfailure damage in ligament: a structural and cellular evaluation. In *Journal of applied physiology (Bethesda, Md. : 1985)* 92 (1), pp. 362–371. DOI: 10.1152/jappl.2002.92.1.362.

Pugh, Luke; Ruel, Allison; Lipman, Joseph; Wright, Timothy; Gessell, Mark; Westrich, Geoffrey (2013): Reduction in bone volume resection with a newer posterior stabilized total knee arthroplasty design. In *HSS journal : the musculoskeletal journal of Hospital for Special Surgery* 9 (2), pp. 157–160. DOI: 10.1007/s11420-013-9340-1.

Quijano, S.; Serrurier, A.; Aubert, B.; Laporte, S.; Thoreux, P.; Skalli, W. (2013): Three-dimensional reconstruction of the lower limb from biplanar calibrated radiographs. In *Medical engineering & physics* 35 (12), pp. 1703–1712. DOI: 10.1016/j.medengphy.2013.07.002.

Rabenberg, Martina (2013): Arthrose. Berlin: Robert Koch-Inst (Gesundheitsberichterstattung des Bundes, 54). Available online at https://www.gbe-bund.de/pdf/Arthrose.pdf.

Radtke, Kerstin; Becher, Christoph; Noll, Yvonne; Ostermeier, Sven (2010): Effect of limb rotation on radiographic alignment in total knee arthroplasties. In *Archives of*

orthopaedic and trauma surgery 130 (4), pp. 451–457. DOI: 10.1007/s00402-009-0999-1.

Rassir, Rachid; Sierevelt, Inger N.; Schager, Marjolein; Nolte, Peter A. (2021): Design and rationale of the ATtune Knee Outcome Study (ATKOS): multicenter prospective evaluation of a novel uncemented rotating platform knee system. In *BMC musculoskeletal disorders* 22 (1), p. 622. DOI: 10.1186/s12891-021-04493-1.

Rathnayaka, Kanchana; Momot, Konstantin I.; Noser, Hansrudi; Volp, Andrew; Schuetz, Michael A.; Sahama, Tony; Schmutz, Beat (2012): Quantification of the accuracy of MRI generated 3D models of long bones compared to CT generated 3D models. In *Medical engineering & physics* 34 (3), pp. 357–363. DOI: 10.1016/j.medengphy.2011.07.027.

Reichel, H. (2005): 13.6 Alloarthroplastik. In C. J. Wirth, L. Zichner, D. Kohn (Eds.): Knie. 67 Tabellen. Stuttgart: Thieme (Orthopädie und orthopädische Chirurgie).

Rhoads, D.; Noble, Philip C.; Reuben, J. D.; Mahoney, Ormonde M.; Tullos, H. (1990): The Effect of Femoral Component Position on Patellar Tracking After Total Knee Arthroplasty. In *Clinical orthopaedics and related research* 260 (&NA;), 43???51. DOI: 10.1097/00003086-199011000-00009.

Ringnér, Markus (2008): What is principal component analysis? In *Nature biotechnology* 26 (3), pp. 303–304. DOI: 10.1038/nbt0308-303.

Ritter, Merrill A.; Davis, Kenneth E.; Meding, John B.; Pierson, Jeffery L.; Berend, Michael E.; Malinzak, Robert A. (2011): The effect of alignment and BMI on failure of total knee replacement. In *The Journal of bone and joint surgery. American volume* 93 (17), pp. 1588–1596. DOI: 10.2106/JBJS.J.00772.

Rivière, C.; Iranpour, F.; Harris, S.; Auvinet, E.; Aframian, A.; Parratte, S.; Cobb, J. (2018a): Differences in trochlear parameters between native and prosthetic kinematically or mechanically aligned knees. In *Orthopaedics & traumatology, surgery & research : OTSR* 104 (2), pp. 165–170. DOI: 10.1016/j.otsr.2017.10.009.

Rivière, Charles; Harman, Ciara; Boughton, Oliver; Cobb, Justin (2020): Personalized Hip and Knee Joint Replacement. The Kinematic Alignment Technique for Total Knee Arthroplasty. Edited by Charles Rivière, Pascal-André Vendittoli. Cham (CH).

Rivière, Charles; Lazic, Stefan; Boughton, Oliver; Wiart, Yann; Vïllet, Loic; Cobb, Justin (2018b): Current concepts for aligning knee implants: patient-specific or systematic? In *EFORT open reviews* 3 (1), pp. 1–6. DOI: 10.1302/2058-5241.3.170021.

Robertsson, O.; Knutson, K.; Lewold, S.; Lidgren, L. (2001): The Swedish Knee Arthroplasty Register 1975-1997: an update with special emphasis on 41,223 knees operated on in 1988-1997. In *Acta orthopaedica Scandinavica* 72 (5), pp. 503–513. DOI: 10.1080/000164701753532853.

Rodriguez-Merchan, E. Carlos (2011): Instability following total knee arthroplasty. In *HSS journal : the musculoskeletal journal of Hospital for Special Surgery* 7 (3), pp. 273–278. DOI: 10.1007/s11420-011-9217-0.

Röhrig, H. (2011): Operation der Kniegelenksendoprothese. In Dieter Christian Wirtz (Ed.): AE-Manual der Endoprothetik: Springer, Berlin, Heidelberg, pp. 127–141.

Roos, E. M.; Roos, H. P.; Lohmander, L. S.; Ekdahl, C.; Beynnon, B. D. (1998): Knee Injury and Osteoarthritis Outcome Score (KOOS)--development of a self-administered outcome measure. In *The Journal of orthopaedic and sports physical therapy* 28 (2), pp. 88–96. DOI: 10.2519/jospt.1998.28.2.88.

Rosa, Sergio Barroso; Hazratwala, Kaushik; Wilkinson, Matthew P. R. (2023): Mismatch between trochlear coronal alignment of arthritic knees and currently available prosthesis: a morphological analysis of 4116 knees and 45 implant designs. In *Knee surgery, sports traumatology, arthroscopy : official journal of the ESSKA* 31 (8), pp. 3116–3123. DOI: 10.1007/s00167-022-07251-5.

Ruiz, David; Koenig, Lane; Dall, Timothy M.; Gallo, Paul; Narzikul, Alexa; Parvizi, Javad; Tongue, John (2013): The direct and indirect costs to society of treatment for end-stage knee osteoarthritis. In *The Journal of bone and joint surgery. American volume* 95 (16), pp. 1473–1480. DOI: 10.2106/JBJS.L.01488.

Saffarini, Mo; Hirschmann, Michael T.; Bonnin, Michel (2023): Personalisation and customisation in total knee arthroplasty: the paradox of custom knee implants. In *Knee surgery, sports traumatology, arthroscopy : official journal of the ESSKA* 31 (4), pp. 1193–1195. DOI: 10.1007/s00167-023-07385-0.

Saffarini, Mo; Ntagiopoulos, Panagiotis G.; Demey, Guillaume; Le Negaret, Benoit; Dejour, David H. (2014): Evidence of trochlear dysplasia in patellofemoral arthroplasty designs. In *Knee surgery, sports traumatology, arthroscopy : official journal of the ESSKA* 22 (10), pp. 2574–2581. DOI: 10.1007/s00167-014-2967-8.

Saini, S.; Seltzer, S. E.; Bramson, R. T.; Levine, L. A.; Kelly, P.; Jordan, P. F. et al. (2000): Technical cost of radiologic examinations: analysis across imaging modalities. In *Radiology* 216 (1), pp. 269–272. DOI: 10.1148/radiology.216.1.r00jl18269.

Schlatterer, B.; Suedhoff, I.; Bonnet, X.; Catonne, Y.; Maestro, M.; Skalli, W. (2009): Skeletal landmarks for TKR implantations: evaluation of their accuracy using EOS imaging acquisition system. In *Orthopaedics & traumatology, surgery & research : OTSR* 95 (1), pp. 2–11. DOI: 10.1016/j.otsr.2008.05.001.

Schmutz, B.; Reynolds, K. J.; Slavotinek, J. P. (2008): Customization of a generic 3D model of the distal femur using diagnostic radiographs. In *Journal of medical engineering & technology* 32 (2), pp. 156–161. DOI: 10.1080/03091900701234390.

Schoettle, Philip B.; Zanetti, Marco; Seifert, Burkart; Pfirrmann, Christian W. A.; Fucentese, Sandro F.; Romero, Jose (2006): The tibial tuberosity-trochlear groove distance; a comparative study between CT and MRI scanning. In *The Knee* 13 (1), pp. 26–31. DOI: 10.1016/j.knee.2005.06.003.

Schotanus, Martijn G. M.; Kort, Nanne P. (2022): Patient-Specific Instrumentation in TKA. In Roland Becker, Michael T. Hirschmann, Nanne P. Kort (Eds.): Basics in Primary Knee Arthroplasty, vol. 463. Cham: Springer International Publishing, pp. 385–390.

Schroeder, Lennart; Dunaway, Andrew; Dunaway, Daniel (2022): A Comparison of Clinical Outcomes and Implant Preference of Patients with Bilateral TKA: One Knee

with a Patient-Specific and One Knee with an Off-the-Shelf Implant. In *JBJS reviews* 10 (2). DOI: 10.2106/JBJS.RVW.20.00182.

Schroeder, Lennart; Martin, Gregory (2019): In Vivo Tibial Fit and Rotational Analysis of a Customized, Patient-Specific TKA versus Off-the-Shelf TKA. In *The journal of knee surgery* 32 (6), pp. 499–505. DOI: 10.1055/s-0038-1653966.

Schroer, William C.; Berend, Keith R.; Lombardi, Adolph V.; Barnes, C. Lowry; Bolognesi, Michael P.; Berend, Michael E. et al. (2013): Why are total knees failing today? Etiology of total knee revision in 2010 and 2011. In *The Journal of arthroplasty* 28 (8 Suppl), pp. 116–119. DOI: 10.1016/j.arth.2013.04.056.

Schwarzkopf, Ran; Scott, Richard D.; Carlson, Evan M.; Currier, John H. (2015): Does increased topside conformity in modular total knee arthroplasty lead to increased backside wear? In *Clinical orthopaedics and related research* 473 (1), pp. 220–225. DOI: 10.1007/s11999-014-3648-0.

Scott, C. E. H.; Howie, C. R.; MacDonald, D.; Biant, L. C. (2010): Predicting dissatisfaction following total knee replacement: a prospective study of 1217 patients. In *The Journal of Bone and Joint Surgery. British volume* 92 (9), pp. 1253–1258. DOI: 10.1302/0301-620X.92B9.24394.

Scuderi, Giles R.; Bourne, Robert B.; Noble, Philip C.; Benjamin, James B.; Lonner, Jess H.; Scott, W. N. (2012): The new Knee Society Knee Scoring System. In *Clinical orthopaedics and related research* 470 (1), pp. 3–19. DOI: 10.1007/s11999-011-2135-0.

Seitlinger, Gerd; Scheurecker, Georg; Högler, Richard; Labey, Luc; Innocenti, Bernardo; Hofmann, Siegfried (2012): Tibial tubercle-posterior cruciate ligament distance: a new measurement to define the position of the tibial tubercle in patients with patellar dislocation. In *The American journal of sports medicine* 40 (5), pp. 1119–1125. DOI: 10.1177/0363546512438762.

Serbin, Philip A.; Do, Dang-Huy; Hinkle, Andrew; Wukich, Dane; Huo, Michael; Sambandam, Senthil (2023): Comparative Analysis of Unicompartmental Total Knee Arthroplasty and High Tibial Osteotomy: Time to Total Knee Arthroplasty and Other

Outcome Measures. In *Arthroplasty today* 20, p. 101107. DOI: 10.1016/j.artd.2023.101107.

Serrurier, Antoine; Quijano, Sergio; Nizard, Remy; Skalli, Wafa (2012): Robust femur condyle disambiguation on biplanar X-rays. In *Medical engineering & physics* 34 (10), pp. 1433–1440. DOI: 10.1016/j.medengphy.2012.01.008.

Seuser, A. (2011): Postoperative Maßnahmen. In Dieter Christian Wirtz (Ed.): AE-Manual der Endoprothetik: Springer, Berlin, Heidelberg, pp. 165–194.

Shao, Long; Wu, Xiang-Dong; Wang, Ting; Liu, Xiao-Kang; Xu, Wei; Huang, Wei; Zeng, Zhi-Min (2020): Approximating the maximum tibial coverage in total knee arthroplasty does not necessarily result in implant malrotation. In *Scientific reports* 10 (1), p. 10529. DOI: 10.1038/s41598-020-67613-2.

Sharkey, Peter F.; Lichstein, Paul M.; Shen, Chao; Tokarski, Anthony T.; Parvizi, Javad (2014): Why are total knee arthroplasties failing today--has anything changed after 10 years? In *The Journal of arthroplasty* 29 (9), pp. 1774–1778. DOI: 10.1016/j.arth.2013.07.024.

Sharma, Gaurav; Liu, David; Malhotra, Rajesh; Zhou, Yi Xin; Akagi, Masao; Kim, T. K. (2017): Availability of Additional Mediolateral Implant Option During Total Knee Arthroplasty Improves Femoral Component Fit Across Ethnicities: Results of a Multicenter Study. In *JB & JS open access* 2 (2), e0014. DOI: 10.2106/JBJS.OA.16.00014.

Sharma, L.; Song, J.; Felson, D. T.; Cahue, S.; Shamiyeh, E.; Dunlop, D. D. (2001): The role of knee alignment in disease progression and functional decline in knee osteoarthritis. In *JAMA* 286 (2), pp. 188–195. DOI: 10.1001/jama.286.2.188.

Shetty, Vivek; Wagh, Yash; Karade, Vikas; Maurya, Amit; Parihar, Mangal; Shekhar, Sajeev; Tandel, Jignesh (2021): CT-Based 3D Reconstruction of Lower Limb Versus X-Ray-Based 3D Reconstruction: A Comparative Analysis and Application for a Safe and Cost-Effective Modality in TKA. In *Indian journal of orthopaedics* 55 (5), pp. 1150–1157. DOI: 10.1007/s43465-021-00456-9.

Shi, Xiaojun; Zhou, Zongke; Shen, Bin; Yang, Jing; Kang, Pengde; Pei, Fuxing (2015): Variations in morphological characteristics of prostheses for total knee arthroplasty leading to kinematic differences. In *The Knee* 22 (1), pp. 18–23. DOI: 10.1016/j.knee.2014.10.013.

Shlens, J. (2005): A Tutorial on Principal Component Analysis. Systems Neurobiology Laboratory, Salk Insitute for Biological Studies La Jolla, CA 92037 and Institute for Nonlinear Science, University of California, San Diego La Jolla. Available online at https://www.cs.cmu.edu/~elaw/papers/pca.pdf, checked on 1/14/2020.

Simsek, Mehmet Emin; Akkaya, Mustafa; Gursoy, Safa; Isik, Cetin; Zahar, Akos; Tarabichi, Samih; Bozkurt, Murat (2018): Posterolateral overhang affects patient quality of life after total knee arthroplasty. In *Archives of orthopaedic and trauma surgery* 138 (3), pp. 409–418. DOI: 10.1007/s00402-017-2850-4.

Simsek, Mehmet Emin; Gursoy, Safa; Akkaya, Mustafa; Kapicioglu, M. I. Safa; Bozkurt, Murat (2020): Radiographs are not sufficient for evaluation of component fit in subtle knee pain after total knee arthroplasty. In *Knee surgery, sports traumatology, arthroscopy : official journal of the ESSKA* 28 (6), pp. 2015–2022. DOI: 10.1007/s00167-020-05940-7.

Singh, Jasvinder A.; Lewallen, David G. (2013): Medical and psychological comorbidity predicts poor pain outcomes after total knee arthroplasty. In *Rheumatology (Oxford, England)* 52 (5), pp. 916–923. DOI: 10.1093/rheumatology/kes402.

Singh, Vivek; Fiedler, Benjamin; Sicat, Chelsea Sue; Bi, Andrew S.; Slover, James D.; Long, William J.; Schwarzkopf, Ran (2023): Impact of preoperative opioid use on patient-reported outcomes following primary total knee arthroplasty. In *European journal of orthopaedic surgery & traumatology : orthopedie traumatologie* 33 (4), pp. 1283–1290. DOI: 10.1007/s00590-022-03297-w.

Sittek, H.; Eckstein, F.; Gavazzeni, A.; Milz, S.; Kiefer, B.; Schulte, E.; Reiser, M. (1996): Assessment of normal patellar cartilage volume and thickness using MRI: an analysis of currently available pulse sequences. In *Skeletal radiology* 25 (1), pp. 55–62. DOI: 10.1007/s002560050032.

Slamin, John; Parsley, Brian (2012): Evolution of customization design for total knee arthroplasty. In *Current reviews in musculoskeletal medicine* 5 (4), pp. 290–295. DOI: 10.1007/s12178-012-9141-z.

Slevin, Omer; Moser, Lukas B.; Hirschmann, Michael T. (2022): Is There an Optimal TKA Component Position? In Roland Becker, Michael T. Hirschmann, Nanne P. Kort (Eds.): Basics in Primary Knee Arthroplasty, vol. 82. Cham: Springer International Publishing, pp. 299–309.

Sojka, P.; Sjölander, P.; Johansson, H.; Djupsjöbacka, M. (1991): Influence from stretch-sensitive receptors in the collateral ligaments of the knee joint on the gamma-muscle-spindle systems of flexor and extensor muscles. In *Neuroscience research* 11 (1), pp. 55–62. DOI: 10.1016/0168-0102(91)90066-8.

Spahn, Gunter; Hofmann, Gunther O.; Engelhardt, Lars Victor von; Li, Mengxia; Neubauer, Henning; Klinger, Hans Michael (2013): The impact of a high tibial valgus osteotomy and unicondylar medial arthroplasty on the treatment for knee osteoarthritis: a meta-analysis. In *Knee surgery, sports traumatology, arthroscopy : official journal of the ESSKA* 21 (1), pp. 96–112. DOI: 10.1007/s00167-011-1751-2.

Springer, Bernhard; Bechler, Ulrich; Waldstein, Wenzel; Rueckl, Kilian; Boettner, Cosima S.; Boettner, Friedrich (2020): The influence of femoral and tibial bony anatomy on valgus OA of the knee. In *Knee surgery, sports traumatology, arthroscopy : official journal of the ESSKA* 28 (9), pp. 2998–3006. DOI: 10.1007/s00167-019-05734-6.

Stamiris, Dimitrios; Gkekas, Nifon K.; Asteriadis, Konstantinos; Stamiris, Stavros; Anagnostis, Panagiotis; Poultsides, Lazaros et al. (2022): Anterior femoral notching ≥ 3 mm is associated with increased risk for supracondylar periprosthetic femoral fracture after total knee arthroplasty: a systematic review and meta-analysis. In *European journal of orthopaedic surgery & traumatology : orthopedie traumatologie* 32 (3), pp. 383–393. DOI: 10.1007/s00590-021-02989-z.

Statistisches Bundesamt (2019): Fallpauschalenbezogene Krankenhausstatistik (DRG-Statistik). Operationen und Prozeduren der vollstationären Patientinnen und Patienten in Krankenhäusern (4-Steller).

Statistisches Bundesamt (2020): Fallpauschalenbezogene Krankenhausstatistik (DRG-Statistik). Operationen und Prozeduren der vollstationären Patientinnen und Patienten in Krankenhäusern (4-Steller).

Statistisches Bundesamt (2021): Fallpauschalenbezogene Krankenhausstatistik (DRG-Statistik). Operationen und Prozeduren der vollstationären Patientinnen und Patienten in Krankenhäusern (4-Steller).

Statistisches Bundesamt (2022): Fallpauschalenbezogene Krankenhausstatistik (DRG-Statistik). Operationen und Prozeduren der vollstationären Patientinnen und Patienten in Krankenhäusern (4-Steller).

Steensen, Robert N.; Bentley, Jared C.; Trinh, Thai Q.; Backes, Jeffrey R.; Wiltfong, Roger E. (2015): The prevalence and combined prevalences of anatomic factors associated with recurrent patellar dislocation: a magnetic resonance imaging study. In *The American journal of sports medicine* 43 (4), pp. 921–927. DOI: 10.1177/0363546514563904.

Stegmann, Mikkel B.; Gomez, David Delgado (2002): A Brief Introduction to Statistical Shape Analysis. Informatics and Mathematical Modelling, Technical University of Denmark. Available online at http://www2.imm.dtu.dk/pubdb/edoc/imm403.pdf, checked on 5/31/2021.

Stein, Gregor; Eysel, Peer; Scheyerer, Max Joseph (Eds.) (2019): Expertise Orthopädie und Unfallchirurgie Wirbelsäule. 1. Auflage. Stuttgart: Thieme. Available online at http://nbn-resolving.org/urn:nbn:de:bsz:24-epflicht-1929831.

Stephen, Joanna M.; Calder, James Df; Williams, Andy; El Daou, Hadi (2021): Comparative accuracy of lower limb bone geometry determined using MRI, CT, and direct bone 3D models. In *Journal of orthopaedic research : official publication of the Orthopaedic Research Society* 39 (9), pp. 1870–1876. DOI: 10.1002/jor.24923.

Tanzer, Michael; Makhdom, Asim M. (2016): Preoperative Planning in Primary Total Knee Arthroplasty. In *The Journal of the American Academy of Orthopaedic Surgeons* 24 (4), pp. 220–230. DOI: 10.5435/JAAOS-D-14-00332.

Tchinde Fotsin, Ted Julien; Vazquez, Carlos; Cresson, Thierry; Guise, Jacques de (2019): Shape, Pose and Density Statistical Model for 3D Reconstruction of Articulated Structures from X-Ray Images. In *Annual International Conference of the IEEE Engineering in Medicine and Biology Society. IEEE Engineering in Medicine and Biology Society. Annual International Conference* 2019, pp. 2748–2751. DOI: 10.1109/EMBC.2019.8857699.

Tensho, Keiji; Akaoka, Yusuke; Shimodaira, Hiroki; Takanashi, Seiji; Ikegami, Shota; Kato, Hiroyuki; Saito, Naoto (2015): What Components Comprise the Measurement of the Tibial Tuberosity-Trochlear Groove Distance in a Patellar Dislocation Population? In *The Journal of bone and joint surgery. American volume* 97 (17), pp. 1441–1448. DOI: 10.2106/JBJS.N.01313.

Tew, Michelle; Dalziel, Kim; Clarke, Philip; Smith, Anne; Choong, Peter F.; Dowsey, Michelle (2020): Patient-reported outcome measures (PROMs): can they be used to guide patient-centered care and optimize outcomes in total knee replacement? In *Quality of life research : an international journal of quality of life aspects of treatment, care and rehabilitation* 29 (12), pp. 3273–3283. DOI: 10.1007/s11136-020-02577-4.

Theiss, Mark M.; Ellison, Michael W.; Tea, Christine G.; Warner, Julia F.; Silver, Renee M.; Murphy, Valerie J. (2011): The connection between strong social support and joint replacement outcomes. In *Orthopedics* 34 (5), p. 357. DOI: 10.3928/01477447-20110317-02.

Thiele, Kathi; Perka, Carsten; Matziolis, Georg; Mayr, Hermann Otto; Sostheim, Michael; Hube, Robert (2015): Current failure mechanisms after knee arthroplasty have changed: polyethylene wear is less common in revision surgery. In *The Journal of bone and joint surgery. American volume* 97 (9), pp. 715–720. DOI: 10.2106/JBJS.M.01534.

Tibshirani, Robert (1996): Regression Shrinkage and Selection Via the Lasso. In *Journal of the Royal Statistical Society: Series B (Methodological)* 58 (1), pp. 267–288. DOI: 10.1111/j.2517-6161.1996.tb02080.x.

Tuecking, Lars-René; Savov, Peter; Ettinger, Max (2020): Moderne Alignmentphilosophien unter Verwendung robotergestützter Systeme in der Knieendoprothetik. In *Knie J.* 2 (4), pp. 254–260. DOI: 10.1007/s43205-020-00083-8.

Twiggs, Joshua G.; Wakelin, Edgar A.; Fritsch, Brett A.; Liu, David W.; Solomon, Michael I.; Parker, David A. et al. (2019): Clinical and Statistical Validation of a Probabilistic Prediction Tool of Total Knee Arthroplasty Outcome. In *The Journal of arthroplasty* 34 (11), pp. 2624–2631. DOI: 10.1016/j.arth.2019.06.007.

Uzair, Muhammad; Jamil, Noreen (2020): Effects of Hidden Layers on the Efficiency of Neural networks. In : 2020 IEEE 23rd International Multitopic Conference (INMIC). Bahawalpur, Pakistan: IEEE, pp. 1–6.

van den Heever, Dawie; Scheffer, Cornie; Erasmus, Pieter; Dillon, Edwin (2011): Method for selection of femoral component in total knee arthroplasty (tka). In *Australasian physical & engineering sciences in medicine* 34 (1), pp. 23–30. DOI: 10.1007/s13246-011-0053-9.

van Diek, Floor M.; Wolf, Megan R.; Murawski, Christopher D.; van Eck, Carola F.; Fu, Freddie H. (2014): Knee morphology and risk factors for developing an anterior cruciate ligament rupture: an MRI comparison between ACL-ruptured and non-injured knees. In *Knee surgery, sports traumatology, arthroscopy : official journal of the ESSKA* 22 (5), pp. 987–994. DOI: 10.1007/s00167-013-2588-7.

van Kuijk, K. S. R.; Reijman, M.; Bierma-Zeinstra, S. M. A.; Waarsing, J. H.; Meuffels, D. E. (2019): Posterior cruciate ligament injury is influenced by intercondylar shape and size of tibial eminence. In *The bone & joint journal* 101-B (9), pp. 1058–1062. DOI: 10.1302/0301-620X.101B9.BJJ-2018-1567.R1.

van Sint Jan, Serge; Sobzack, Stéphane; Dugailly, Pierre-Michel; Feipel, Véronique; Lefèvre, Philippe; Lufimpadio, Jean-Louis et al. (2006): Low-dose computed tomography: a solution for in vivo medical imaging and accurate patient-specific 3D

bone modeling? In *Clinical biomechanics (Bristol, Avon)* 21 (9), pp. 992–998. DOI: 10.1016/j.clinbiomech.2006.05.007.

Varadarajan, Kartik M.; Rubash, Harry E.; Li, Guoan (2011): Are current total knee arthroplasty implants designed to restore normal trochlear groove anatomy? In *The Journal of arthroplasty* 26 (2), pp. 274–281. DOI: 10.1016/j.arth.2009.12.009.

Völlner, Florian; Weber, Tim; Weber, Markus; Renkawitz, Tobias; Dendorfer, Sebastian; Grifka, Joachim; Craiovan, Benjamin (2019): A simple method for determining ligament stiffness during total knee arthroplasty in vivo. In *Scientific reports* 9 (1), p. 5261. DOI: 10.1038/s41598-019-41732-x.

Walker, P. S. (2005): Bearing Surfaces for Motion Control in Total Knee Arthroplasty. In J. Bellemans, Michael D. Ries, Jan M.K. Victor (Eds.): Total Knee Arthroplasty. A Guide to Get Better Performance, vol. 82. Berlin, Heidelberg: Springer Berlin Heidelberg (SpringerLink Bücher), pp. 295–302.

Walker, P. S.; Garg, A. (1991): Range of motion in total knee arthroplasty. A computer analysis. In *Clinical orthopaedics and related research* (262), pp. 227–235.

Wasterlain, Amy S.; Courtney, P. Maxwell; Yayac, Michael F.; Nazarian, David G.; Austin, Matthew S. (2019): Quantifying the Perioperative Work Associated With Total Hip and Knee Arthroplasty: The Burden Has Increased With Contemporary Care Pathways. In *The Journal of arthroplasty* 34 (11), pp. 2528–2531. DOI: 10.1016/j.arth.2019.06.039.

Weber, Patrick; Schröder, Christian; Laubender, Rüdiger Paul; Baur-Melnyk, Andrea; Schulze Pellengahr, Christoph von; Jansson, Volkmar; Müller, Peter E. (2013): Joint line reconstruction in medial unicompartmental knee arthroplasty: development and validation of a measurement method. In *Knee surgery, sports traumatology, arthroscopy : official journal of the ESSKA* 21 (11), pp. 2468–2473. DOI: 10.1007/s00167-013-2617-6.

Weir, David J.; Becker, Roland; Deehan, David J. (2022): Principles of Total Knee Arthroplasty. In Roland Becker, Michael T. Hirschmann, Nanne P. Kort (Eds.): Basics in Primary Knee Arthroplasty. Cham: Springer International Publishing, pp. 173–185.

Welch, B. L. (1947): The generalisation of student's problems when several different population variances are involved. In *Biometrika* 34 (1-2), pp. 28–35. DOI: 10.1093/biomet/34.1-2.28.

Wenham, C. Y. J.; Grainger, A. J.; Conaghan, P. G. (2014): The role of imaging modalities in the diagnosis, differential diagnosis and clinical assessment of peripheral joint osteoarthritis. In *Osteoarthritis and cartilage* 22 (10), pp. 1692–1702. DOI: 10.1016/j.joca.2014.06.005.

Wernecke, G. C.; Seeto, B. G.; Chen, D. B.; MacDessi, S. J. (2016): Posterior condylar cartilage thickness and posterior condylar offset of the femur: a magnetic resonance imaging study. In *Journal of orthopaedic surgery (Hong Kong)* 24 (1), pp. 12–15. DOI: 10.1177/230949901602400105.

Whittaker, John-Paul; Dwyer, Kimberly A.; Howard, James; Huey, Verdonna; Lesko, James; Nunley, Ryan M.; Verdonk, Peter (2018): Learning curve with a new primary total knee arthroplasty implant: a multicenter perspective with more than 2000 patients. In *Arthroplasty today* 4 (3), pp. 348–353. DOI: 10.1016/j.artd.2018.05.004.

Wieland, Heike A.; Michaelis, Martin; Kirschbaum, Bernhard J.; Rudolphi, Karl A. (2005): Osteoarthritis - an untreatable disease? In *Nature reviews. Drug discovery* 4 (4), pp. 331–344. DOI: 10.1038/nrd1693.

Willing, Ryan; Kim, Il Yong (2011): Design optimization of a total knee replacement for improved constraint and flexion kinematics. In *Journal of biomechanics* 44 (6), pp. 1014–1020. DOI: 10.1016/j.jbiomech.2011.02.009.

Wilson, Ira B.; Cleary, Paul D. (1995): Linking Clinical Variables With Health-Related Quality of Life. In *JAMA* 273 (1), p. 59. DOI: 10.1001/jama.1995.03520250075037.

Wilson, William T.; Deakin, Angela H.; Payne, Anthony P.; Picard, Frederic; Wearing, Scott C. (2012): Comparative analysis of the structural properties of the collateral ligaments of the human knee. In *The Journal of orthopaedic and sports physical therapy* 42 (4), pp. 345–351. DOI: 10.2519/jospt.2012.3919.

Wirtz, Dieter Christian (2011): AE-Manual der Endoprothetik. Knie. Berlin, Heidelberg: Arbeitsgemeinschaft Endoprothetik. Available online at http://dx.doi.org/10.1007/978-3-642-12889-9.

Wu, Jing; Mahfouz, Mohamed R. (2016): Robust x-ray image segmentation by spectral clustering and active shape model. In *Journal of medical imaging (Bellingham, Wash.)* 3 (3), p. 34005. DOI: 10.1117/1.JMI.3.3.034005.

Wu, Jing; Mahfouz, Mohamed R. (2021): Reconstruction of knee anatomy from single-plane fluoroscopic x-ray based on a nonlinear statistical shape model. In *Journal of medical imaging (Bellingham, Wash.)* 8 (1), p. 16001. DOI: 10.1117/1.JMI.8.1.016001.

Young, Simon W.; Clarke, Henry D.; Graves, Stephen E.; Liu, Yen-Liang; Steiger, Richard N. de (2015): Higher Rate of Revision in PFC Sigma Primary Total Knee Arthroplasty With Mismatch of Femoro-Tibial Component Sizes. In *The Journal of arthroplasty* 30 (5), pp. 813–817. DOI: 10.1016/j.arth.2014.11.035.

Yue, Bing; Wang, Jun; Wang, You; Yan, Mengning; Zhang, Jun; Zeng, Yiming (2014): How the gender or morphological specific TKA prosthesis improves the component fit in the Chinese population? In *The Journal of arthroplasty* 29 (1), pp. 71–74. DOI: 10.1016/j.arth.2013.04.038.

Zhang, Xi; Eyles, Jillian P.; Makovey, Joanna; Williams, Matthew J.; Hunter, David J. (2017): Is the effectiveness of patellofemoral bracing modified by patellofemoral alignment and trochlear morphology? In *BMC musculoskeletal disorders* 18 (1), p. 168. DOI: 10.1186/s12891-017-1524-2.

Zhang, Yijie; Chen, Yanxi; Qiang, Minfei; Zhang, Kun; Li, Haobo; Jiang, Yuchen; Jia, Xiaoyang (2018): Comparison between three-dimensional CT and conventional radiography in proximal tibia morphology. In *Medicine* 97 (30), e11632. DOI: 10.1097/MD.0000000000011632.

Zheng, Guoyan; Hommel, Hagen; Akcoltekin, Alper; Thelen, Benedikt; Stifter, Jan; Peersman, Geert (2018): A novel technology for 3D knee prosthesis planning and treatment evaluation using 2D X-ray radiographs: a clinical evaluation. In *International*

journal of computer assisted radiology and surgery 13 (8), pp. 1151–1158. DOI: 10.1007/s11548-018-1789-4.

Zhou, Sijia; Maleitzke, Tazio; Geissler, Sven; Hildebrandt, Alexander; Fleckenstein, Florian Nima; Niemann, Marcel et al. (2022): Source and hub of inflammation: The infrapatellar fat pad and its interactions with articular tissues during knee osteoarthritis. In *Journal of orthopaedic research : official publication of the Orthopaedic Research Society* 40 (7), pp. 1492–1504. DOI: 10.1002/jor.25347.

Zingde, Sumesh M.; Slamin, John (2017): Biomechanics of the knee joint, as they relate to arthroplasty. In *Orthopaedics and Trauma* 31 (1), pp. 1–7. DOI: 10.1016/j.mporth.2016.10.001.

Zou, Hui; Hastie, Trevor (2005): Regularization and variable selection via the elastic net. In *J Royal Statistical Soc B* 67 (2), pp. 301–320. DOI: 10.1111/j.1467-9868.2005.00503.x.

Author contributions

The results presented in this thesis were presented in parts in previous publications. The publications and my contributions are listed below:

S. Grothues, B. Hohlmann, S.M. Zingde & K. Radermacher: Potential for femoral size optimization for off-the-shelf implants: A CT derived implant database analysis. Journal of Orthopaedic Research, 2023, 41(6), pp. 1198-1205 [DOI: 10.1002/jor.25464]

I designed the study with all the other authors. I performed all analyses with Benjamin Hohlmann. I analyzed and interpreted the results with Benjamin Hohlmann. I drafted the paper with Benjamin Hohlmann.

S.A.G.A. Grothues & K. Radermacher: Variation of the Three-Dimensional Femoral J-Curve in the Native Knee. Journal of Personalized Medicine, 2021, 11(7), pp. 592 [DOI: 10.3390/jpm11070592]

I co-designed the study with Klaus Radermacher. I performed all analyses. I analyzed and interpreted the results. I drafted the paper.

S.A.G.A. Grothues, M. Asseln & K. Radermacher: Variation of the femoral J-Curve in the native knee. In: F. Rodriguez Y Baena & F. Tatti (ed.): CAOS 2020. The 20th Annual Meeting of the International Society for Computer Assisted Orthopaedic Surgery, 4, 2020, pp. 86-91 [DOI: 10.29007/5k32]

I designed the study with all the other authors. I performed all analyses. I analyzed and interpreted the results. I drafted the paper.

S. Grothues & K. Radermacher: X-ray based morphological analysis of the knee - a review. In: F. Rodriguez Y Baena, J.W. Giles & E. Stindel (ed.): Proceedings of The 20th Annual Meeting of the International Society for Computer Assisted Orthopaedic Surgery, 5, 2022, pp. 89-98 [DOI: 10.29007/sqcb]

I co-designed the study with Klaus Radermacher. I performed all analyses. I analyzed and interpreted the results. I drafted the paper.

S. Grothues & K. Radermacher: Criteria for Implant Fit Assessment in Total Knee Arthroplasty – A Review. Current Directions in Biomedical Engineering, 8(2), 2022, pp. 165-168 [DOI: 10.1515/cdbme-2022-1043]

I co-designed the study with Klaus Radermacher. I performed all analyses. I analyzed and interpreted the results. I drafted the paper.

S. Grothues, A.-K. Becker, B. Hohlmann & K. Radermacher: Parameter-based patient-specific restoration of physiological knee morphology for optimized implant design and matching. Biomedical Engineering / Biomedizinische Technik, 2023, 68(5), pp. 537-544 [DOI: 10.1515/bmt-2023-0017]

I designed the study with all the other authors. I performed all analyses with Ann-Kristin Becker. I analyzed and interpreted the results with Ann-Kristin Becker. I drafted the paper.

S. Grothues & K. Radermacher: Automated analysis of femoral over-/underhang and bone coverage of OTS TKA implants. In: J.W. Giles (ed.): Proceedings of The 22nd Annual Meeting of the International Society for Computer Assisted Orthopaedic Surgery, 2023, pp. 26-30 [DOI: 10.29007/5636]

I co-designed the study with Klaus Radermacher. I performed all analyses. I analyzed and interpreted the results. I drafted the paper.

S. Grothues, L. Berger & K. Radermacher: Automated analysis of morpho-functional interbone parameters of the knee based on three-dimensional (3D) surface data. In: F. Rodriguez Y Baena, J.W. Giles & E. Stindel (ed.): Proceedings of The 20th Annual Meeting of the International Society for Computer Assisted Orthopaedic Surgery, 5, 2022, pp. 81-88 [DOI: 10.29007/8nb5]

I designed the study with all the other authors. I performed all analyses with Luisa Berger. I analyzed and interpreted the results with Luisa Berger. I drafted the paper.

Associated student theses

The results presented are partly based on results obtained in the course of final theses at the RWTH Aachen University at the Chair of Medical Engineering under the supervision of Univ.-Prof. Dr.-Ing. Klaus Radermacher and under the supervision of the author of this thesis as well as knowledge and know-how available at the Chair of Medical Engineering. These works are:

Master Thesis, Luisa Berger, Analyse von Knochenrelativparametern des nativen Kniegelenks im Kontext des künstlichen Kniegelenkersatzes, 2022

Master Thesis, Ann-Kristin Becker, Reconstruction of knee morphology in the presence of deformities and analysis of the impact on knee joint mechanics in the context of knee arthroplasty, 2022

Master Thesis, Sophie Gerbe, Identifikation und statistische Auswertung nativer tibiofemoraler und patellofemoraler 3D Kontaktverläufe und zugehöriger Konturlinien, 2021

Bachelor Thesis, Sabrina Hörmann, Development and evaluation of a workflow for patient-specific fit evaluation for different knee prostheses designs, 2020

List of Figures

List of Tables

Appendix

A) Error metrics for surface reconstruction

Work in this chapter has been presented in parts in:

S. Grothues & K. Radermacher: X-ray based morphological analysis of the knee - a review. In: F. Rodriguez Y Baena, J.W. Giles & E. Stindel (ed.): Proceedings of The 20th Annual Meeting of the International Society for Computer Assisted Orthopaedic Surgery, 5, 2022, pp. 89-98 [DOI: 10.29007/sqcb]

There are a wide range of error metrics used for the evaluation of the surface reconstruction accuracy. With regard to surface reconstruction of the knee, there are several studies reporting on methods for 2D-3D reconstruction and the accuracy achieved. The characteristics of the different error metrics (MAE/ RMSE /Hausdorff) and calculation methods used (P2P/P2S, uni/bidirectional) have to be considered when comparing the reported accuracies, thus they are visualized exemplarily in **Figure 6-1** and discussed in the following.
Unidirectional errors measure distances either from the reconstructed mesh to the ground truth or vice versa. Hence the focus of the former is to quantify offsets and of the latter to evaluate for missing surface areas. Bidirectional errors are the combined unidirectional errors, both from and to the reconstructed mesh. A unidirectional P2P error is defined as the distance between a mesh point and its nearest neighbor in the respective other mesh (reconstruction/ ground truth). In contrast, a unidirectional P2S error is defined as the minimal distance between a mesh point to the surface of the respective other mesh (Dumic et al. 2018). Hence, a P2S is lower compared to a P2P error for the same reconstruction. Furthermore, one has to differentiate normal absolute errors or projected errors. Those quantify the length of a projection of the error along the normal direction, hence resulting again in lower errors. The Hausdorff distance measures the overall highest distance between two point sets bidirectional, and is therefore equivalent to the maximum bidirectional absolute error. Consequently, the

One-Sided Hausdorff distance is equivalent to the maximum unidirectional absolute error.

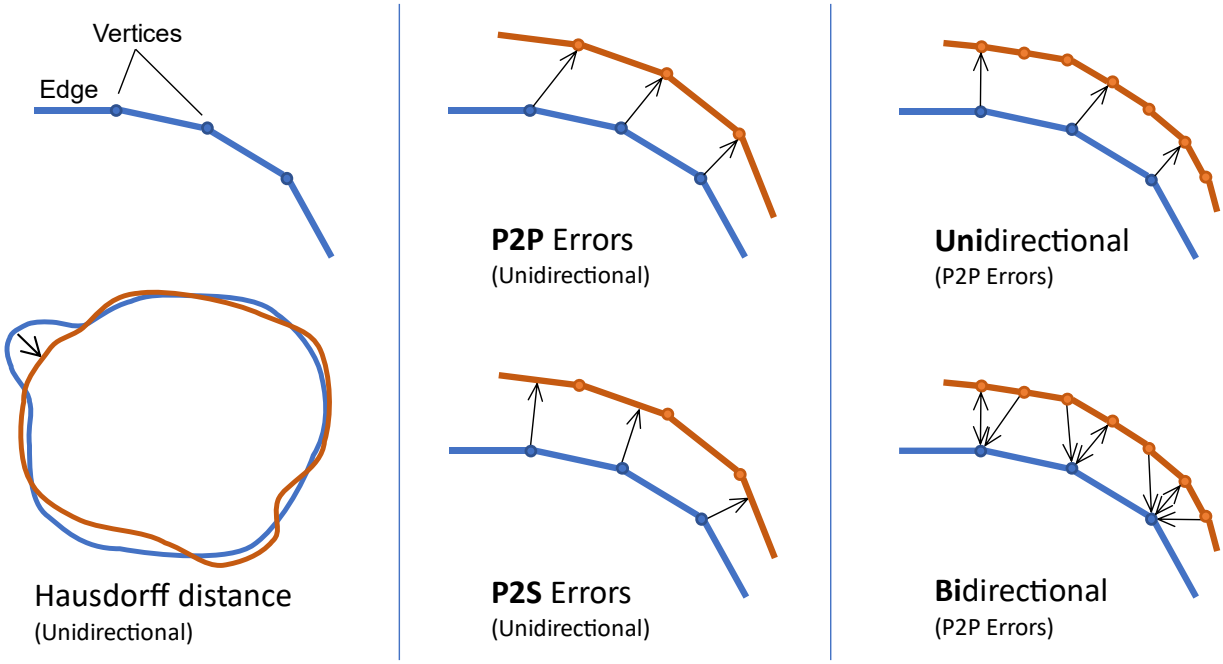

Figure 6-1: Differences in error metrics complicating the assessment and comparison of study results on 2D 3D reconstruction accuracy of the knee surfaces. P2P: point-to-point, P2S: point-to-surface.

B) Interbone morphological analysis and verification

Work in this chapter has been presented in parts in:

S. Grothues, L. Berger & K. Radermacher: Automated analysis of morpho-functional interbone parameters of the knee based on three-dimensional (3D) surface data. In: F. Rodriguez Y Baena, J.W. Giles & E. Stindel (ed.): Proceedings of The 20th Annual Meeting of the International Society for Computer Assisted Orthopaedic Surgery, 5, 2022, pp. 81-88 [DOI: 10.29007/8nb5]

Introduction

In this chapter, the extension of an existing framework for morphological analysis of the distal femur, the proximal tibia, and the patella (Asseln et al. 2018; Asseln 2019) is extended by the analysis of interbone parameters is presented. In addition, a literature-based verification is performed.

Interbone parameters of the knee, such as the tibial tuberosity to trochlear groove (TT-TG) distance, are frequently used in clinical practice in order to assess the functional anatomy of the individual patient. They can also be used as indicators for functional disorders, such as patellar instability (Dejour et al. 1994; Steensen et al. 2015). With 3D surface data of the knee, derived e.g., from CT, a comprehensive analysis regarding various interbone parameters is possible (Fürmetz et al. 2021). However, the identification of landmarks is mostly done manually and the parameter calculation is often not automated, which leads to a time-consuming process. To enable comprehensive database analyses, an automation of the interbone parameter analysis with 3D surface models is aimed at.

Materials and methods

A dataset of 414 knees from patients scheduled for TKA was available for the analysis, of which 164 were male and 248 were female. For two knees, no gender information was present. The database was provided by Conformis (Conformis Inc., Billerica, MA, USA). For each case, surface models of femur, tibia and patella and the coordinates of the hip and ankle joint center were available. The surface models were derived previously from CT images, with the patient in supine position. This is a relevant limitation, since the relative position of the bones may differ significantly between the weight-bearing and non-weight-bearing situation. However, CT is the gold standard for the measurement of bone morphology and some authors question whether the limitation of a non-weight-bearing measurement is of clinical relevance (Hirschmann et al. 2019a). In the future, the impact of weight-bearing on knee interbone parameter measurements should be evaluated e.g., through 3D2D referencing of the surface models with EOS images. The presented automated interbone analysis can be applied either way, both with and without prior referencing.

In a literature research, 8 interbone parameters of the knee were identified, which can be evaluated based on CT data: the patellar tilt and shift, the congruence angle, the TT TG distance both absolute and relative, the joint rotation, the hip knee angle and the Insall Salvati index.

The existing framework for the evaluation of individual bone morphology of femur, tibia and patella was extended for the calculation of respective interbone parameters. The workflow is initialized with meta-information about the patient before the morphological analysis. First, the morphology of each bone is analyzed individually as described in previous studies (Asseln et al. 2018; Asseln et al. 2015). During the process, the bone's polygon mesh is imported and transformed into a bone specific coordinate system (COS) and morphologic parameters are derived. Relevant landmarks as well as the transformations from the CT to the bone-specific COS are saved. After completion of the bone-specific morphological analyses, the interbone analysis is performed, as this meant that already defined landmarks of the bones could be used. Since the meshes and landmarks are stored in their specific COS, for the calculation of each interbone parameter the meshes and landmarks required must be transformed into a specific COS. For example, the femoral COS is selected for the TT-TG distance calculation, so the tibial mesh and the coordinates of the tibial tuberosity are transformed from the tibial COS to the femoral COS. Reference points and reference lines used for the calculation of the interbone parameters are presented **Figure 6-2**.

The plausibility of the bone-specific parameters is evaluated based on values from literature, as described in a previous study (Asseln et al. 2018). Since the interbone parameters depend on landmarks derived in the bone-specific morphological analyses, they are also evaluated as implausible if any of the bone-specific parameter sets is evaluated as such. In addition, the plausibility of the interbone parameters is evaluated, based on a box plot outlier assessment.

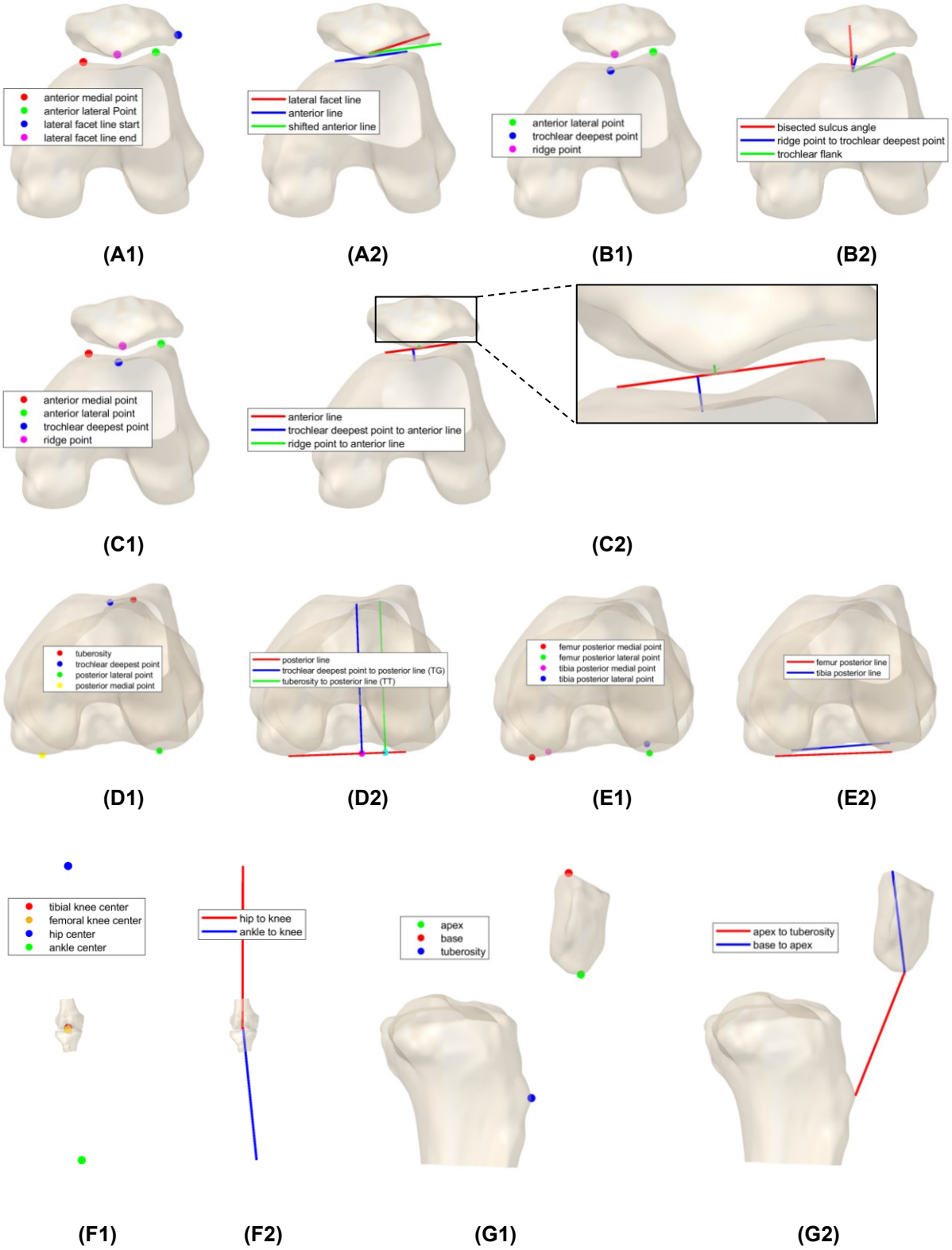

Figure 6-2: Reference points (1) and reference lines (2) for the calculation of interbone parameters as implemented in the automated morphological analysis. **(A)** Patellar tilt. **(B)** Congruence angle. **(C)** Patellar shift. **(D)** TT-TG distance. **(E)** Joint rotation. **(F)** Hip knee angle. **(G)** Insall Salvati index.

Results

411 (99.3%) femora, 409 (98.8%) tibiae and all patellae (100%) could be processed without error. The interbone workflow succeeded for 405 (98.3%) cases. 380 (92.5%) femora, 347 (84.8%) tibiae and 410 (99.0%) patellae passed the plausibility check. After the exclusion of implausible cases, either because of exceeding of bone specific parameter ranges or because of classification as outliers in the box plot assessment, 373 cases remained (225 female, 147 male, 1 without gender information), which were used for statistical evaluation. Respective results are listed in Table 1.

Table 6-1: Results of the statistical analysis of interbone parameters from 373 cases.

Parameter	**Mean ± SD**		
	Combined	**Female**	**Male**
Patellar tilt	4.82° ± 6.50°	4.80° ± 6.90°	4.85° ± 5.90°
Patellar shift	3.72 mm ± 3.11 mm	3.39 mm ± 3.03 mm	4.25 mm ± 3.17 mm
Congruence angle	20.21° ± 18.82°	19.69° ± 20.28°	21.13° ± 16.36°
TT-TG	12.19 mm ± 5.46 mm	11.91 mm ± 5.31 mm	12.64 mm ± 5.70 mm
Relative TT-TG	0.15 ± 0.07	0.15 ± 0.07	0.14 ± 0.07
Joint rotation	2.67° ± 3.91°	2.71° ± 3.764°	2.63° ± 4.15°
Hip knee angle	175.7° ± 5.1°	176.5° ± 5.0°	174.4° ± 5.0°
Insall Salvati index (3D)	1.35 ± 0.22	1.34 ± 0.22	1.36 ± 0.23

Discussion

The workflow demonstrated to be feasible for the automated analysis of a large dataset of knee surface models. For verification purposes, the results of the analysis presented are compared with those of studies with a similar patient population (OA/TKA patients), imaging technique (CT) and parameter definition, if available.

Alemparte et al. (Alemparte et al. 2007) analyzed asymptomatic knees regarding the patellar tilt according to the definition of Laurin et al. (Laurin et al. 1978)/ Davies et al. (Davies et al. 2000) and found a mean value of 8.1° ± 14.5° for CT data. The mean value in the present study was smaller (combined: 4.82°) and the standard deviation was much reduced (combined: 6.50°). The difference in mean value and standard deviation could be due to the different study populations (control vs. OA). In the case of isolated lateral patellofemoral OA, the patellar tilt could be reduced. This could explain the lower mean patellar tilt in the present study of OA patients. A second explanation for the difference

in standard deviation could be the difference in landmark detection, which was automated in the presented workflow and manual in the study of Alemparte et al. (Alemparte et al. 2007).

In the study presented, the patellar shift definition described by Chia et al. (Chia et al. 2009) was applied, which was also used by Zhang et al. (Zhang et al. 2017). Zhang et al. found a mean patellar tilt of 3.2 mm ± 3.8 mm for knees with patellofemoral OA based on radiographs. Chia et al. (Chia et al. 2009) found a mean patellar shift of 5.7 mm ± 4.6 mm in patients scheduled for TKA measured on radiographs. In the present study, a patellar shift of 3.72 mm ± 3.11 mm was found for the combined population, which is in agreement with the previous studies.

Zhang et al. (Zhang et al. 2017) investigated the congruence angle of OA patients and found a mean value of 27.9° ± 29.9°. In the analysis presented, a mean congruence angle of 20.21° ± 18.82° was found. An explanation for this difference may be found in the imaging technique. Zhang et al. (Zhang et al. 2017) used standard radiographs for their evaluation, while the analysis presented was based on surface models derived from CT. In the patella skyline view, the deepest point of the sulcus may be obscured due to projection (**Figure 6-2-B1**), whereby the deepest point would be estimated to be closer to the patellar ridge. For the same anatomy, this would lead to the higher congruence angle.

Various groups have reported mean values for the TT-TG distance (Balcarek et al. 2011; Dejour et al. 1994). Hochreiter et al. (Hochreiter et al. 2019) also analyzed patients scheduled for TKA and found a mean TT-TG of 12.9 mm ± 5.6 mm based on CT data. In the study presented, a mean value of 12.19 mm ± 5.46 mm was found, which is in good agreement with the results of Hochreiter et al., regarding both mean value and standard deviation.

Balcarek et al. (Balcarek et al. 2011) calculated the relative TT-TG distance in a control group, and found a mean value of 0.14 ± 0.05. In this thesis, a mean value for the combined population of 0.15 ± 0.07 was found, which is in agreement with the results of Balcarek et al. (Balcarek et al. 2011).

Tensho et al. (Tensho et al. 2015) found a mean joint rotation of 4.0° ± 3.7° in a control group analyzed by CT. Seitlinger et al. (Seitlinger et al. 2012) also analyzed a control group in their study, and found a mean joint rotation of 2.632° ± 3.143° based on MRI images. The results of the present study regarding the joint rotation are comparable (combined: 2.67° ± 3.91°), despite the different study populations.

Fürmetz et al. (Fürmetz et al. 2021) evaluated the Insall Salvati index in 3D based on CT data from healthy subjects. They determined a reference range of 1.0 - 1.4. The mean values found in the present study are within the given reference range, however, at its upper limit.

The mean leg alignment of patients undergoing TKA is reported to be slightly varus (HKA < 180°) (Hirschmann et al. 2019a; Seitlinger et al. 2012). With a mean HKA below 180° for all groups, this was supported by the results of the present study. In the present study, the hip knee angle was higher for female compared to male cases, which is also consistent with the literature (Hirschmann et al. 2019a). Summarizing the comparison with the literature, similar interbone parameter values were derived in the scope of this study, especially for studies on TKA patients. In conclusion, the interbone analysis was successfully verified by manual measurements from the literature.

C) Database analysis for parametric definition of osteoarthritis

Work in this chapter has been presented in parts in:

S. Grothues, L. Berger & K. Radermacher: Automated analysis of morpho-functional interbone parameters of the knee based on three dimensional (3D) surface data. In: F. Rodriguez Y Baena, J.W. Giles & E. Stindel (ed.): Proceedings of The 20th Annual Meeting of the International Society for Computer Assisted Orthopaedic Surgery, 5, 2022, pp. 81-88 [DOI: 10.29007/8nb5]

Introduction

This chapter describes the parametric definition of osteoarthritis, to be used for a parameter-based deformity correction in the context of TKA implant design. With the

parameter-based deformity correction, the definition of the pre-arthritic, healthy native knee morphology is aimed at, which would enable an adequate assessment of the implant morphological fit.

Materials and methods

The identification of deformity parameters of osteoarthritis was based on a database analysis. A dataset of 414 knees from patients scheduled for TKA was used, which has been the basis for the verification study in **Appendix B)**. The gender distribution was 164 were male, 248 were female, and for two knees, no gender information was present. In addition, an equivalent dataset of 421 cadaver knees was used. Of those 146 were female, 273 were male and for two no gender information was available. The database was provided by Conformis (Conformis Inc., Billerica, MA, USA).

An existing framework for the evaluation of individual bone morphology of femur, tibia and patella was applied, which has been extended for the calculation of interbone parameters as described in **Appendix B)**. As subchondral bone degeneration is expected to be related to the degree of varus or valgus mal-alignment, the database analyzed is differentiated based on the hip-knee-ankle-angle (HKA). The knees were classified as neutrally aligned with an HKA between 177°-183°, varus aligned with an HKA below 174°, or valgus aligned with an HKA above 186°. The ranges in between were excluded to achieve a clear differentiation between varus, valgus, and physiological knee morphology.

To overcome the impact of height and gender on the morphological parameters, respective values were normalized depending on their direction of measurement. The normalized morphological parameter values of the varus and valgus groups were then compared against those of the neutral group. Statistical significance of the deviations in means was assessed using t-tests at a significance level of 5%. In addition, effect sizes were determined.

Results

The morphological analysis was successful for all femur and interbone parameters, and for over 99% of the tibiae and patellae. Of all cases, 26.0% were classified as neutral, 9.4% as valgus, and 64.6% as varus.

In the database analysis, statistically significant differences in mean were found for 10 morphological or alignment parameter of the distal femur, for one parameter of the proximal tibia, and for four interbone parameters. Several effects were present both for the valgus/ neutral and varus/ neutral comparison, suggesting a relationship of the HKA with the respective morphological parameter. Respective quantitative results of the analysis can be found in **Table 6-2**.

Table 6-2: Results of the statistical analysis of morphological parameters, comparing varus, valgus and neutral patient groups. The sub-populations were differentiated by their hip knee angle. Medium and large effect sizes according to Cohen et al. (Cohen 1988) are highlighted (color code below). Parameters were considered as deformity parameters, when there was a medium or large effect size for both the varus/neutral or valgus/neutral comparison.

Bone	Aspect	Parameter	Varus compared to neutral			Valgus compared to neural		
			Levene test	T test/ Welch	Effect size	Levene test	T test/ Welch	Effect size
Femur	Sizing	Condylar ML Width	0	1	0.27	1	0	0.88
		Overall AP Length	0	0	0.16	0	0	0.15
		Lateral Condylar Depth	**1**	**1**	**0.47**	**0**	**1**	**0.79**
		Medial Condylar Depth	1	0	0.12	0	0	0.04
	Trochlea	Anterior ML Width	0	0	0.17	**1**	**1**	**1.00**
		Lateral Elevation	**0**	**1**	**0.25**	**1**	**1**	**0.94**
		Medial Elevation	0	0	0.05	**0**	**1**	**1.04**
		Central Elevation	0	0	0.03	**0**	**1**	**0.57**
		Trochlear depth	**0**	**1**	**0.29**	**0**	**1**	**0.69**
		ML Sulcus Displacement	**0**	**1**	**0.20**	0	0	0.35
	J-Curve	Mediolateral Spacing	0	0	0.18	0	0	0.37
		Posterior Mediolateral Width	1	0	0.03	0	0	0.09
		Distal Condylar Offset	**0**	**1**	**0.57**	**0**	**1**	**0.83**
		PCO Lateral	1	0	0.14	**0**	**1**	**0.91**
		PCO Medial	1	0	0.19	0	0	0.34
		Lateral Distal Sagittal Radius	0	0	0.18	1	0	0.64
		Medial Distal Sagittal Radius	**1**	**1**	**0.96**	0	0	0.11
		Lateral Posterior Sagittal Radius	0	0	0.06	0	0	0.33
		Medial Posterior Sagittal Radius	**1**	**1**	**0.26**	0	0	0.20
		PCO Ratio Lateral	**1**	**0**	**0.03**	**0**	**1**	**0.88**
		PCO Ratio Medial	1	0	0.18	0	0	0.46
		Condyle Ratio	0	0	0.18	0	0	0.47
	Alignment	Mechanical LDFA	0	0	0.07	0	0	0.05
		Posterior Condylar Angle	**1**	**1**	**1.52**	**0**	**1**	**2.05**
Tibia	Sizing	ML Width	0	0	0.11	0	0	0.29
		AP Height	0	0	0.10	0	0	0.10
	Alignment	Medial Sagittal Tibial Slope	1	0	0.09	0	0	0.13
		Lateral Sagittal Tibial Slope	0	0	0.15	0	0	0.15
		Coronal Tibial Slope	0	**1**	**1.41**	**0**	**1**	**1.34**
Inter-bone	Alignment	Patella Tilt	**0**	**1**	**0.23**	0	0	0.15
		Patella Shift	**0**	**1**	**0.25**	**0**	**1**	**0.90**
		Congruence Angle	1	0	0.15	**0**	**1**	**0.75**
		TTTG	**0**	**1**	**0.91**	**0**	**1**	**0.61**
		Joint Rotation	0	0	0.01	0	0	0.14
		Insall Salvati 3D	**1**	**1**	**0.46**	**0**	**1**	**0.86**

Color code: Parameters with at least one medium (large) effect size are highlighted as followed: medium effect sizes= 0.5-0.8: □ | Large effect sizes > 0.8: ■

Discussion

Several studies investigated changes in knee shape with varus and valgus mal-alignment, by comparing varus and valgus knees (Cohen et al. 2019; Choi et al. 2022) or by comparison of varus and/or valgus knees against control knees (Chang et al. 2018; Lee et al. 2021; Matsuda et al. 2004). A relevant limitation of respective studies are the small sample sizes, which has been addressed by the presented analysis of 835 knees.

Femur shape changes with OA

The most frequently mentioned femoral morphological parameter, with statistically significant differences in mean between varus, valgus, and control knees, is the posterior condylar angle (Cohen et al. 2019; Chang et al. 2018; Matsuda et al. 2004). In addition, the lateral condylar depth (Matsuda et al. 2004) and the lateral distal femoral angle were listed as influenced by varus and/or valgus malalignment (Lee et al. 2021). These results are in agreement with the results of the present study, with statistically significant relationships identified for the normalized lateral condylar depth and the posterior condylar angle, both in the varus/neutral and valgus/neutral comparison. Also, the same direction of the relationship as reported in literature was found in the present study, with a decrease in the normalized lateral condylar depth with HKA and an increase of the posterior condylar angle with HKA.

Further statistically significant differences, consistent both in the varus/neutral and valgus/neutral comparison, were found for the lateral trochlear elevation, trochlear depth, and distal condylar offset in the present study. Additional mal-alignment specific, statistically significant parameter differences were found. For varus knees, those included changes in the condylar ML width, ML sulcus displacement, and medial sagittal radii. The impact on the medial sagittal radii is highly plausible, as OA in general is associated with a flattening of the femoral condyles, especially in the distal area (Neogi et al. 2013). An increase in ML width and in the dimensions of the posterior condylar region in the OA incidence group compared to the control group were also reported by Bedbrenner et al. (Bredbenner et al. 2010). Similarly, Neogi et al. (Neogi et al. 2013) reported wider femoral condyles in the OA incidence group of the OA initiative. While there was no information about the leg alignment in the incidence group, due to the generally higher prevalence of varus OA in the patient population, the agreement of the results with those of the varus/neutral comparison can be considered plausible. For

valgus knees, additional mal-alignment specific deviations included the anterior ML width, medial and central trochlear elevation, as well as the lateral PCO and lateral PCO ratio.

Tibia shape changes with OA

In the present study, there was a statically significant change in the coronal tibial slope, with a high effect size both for the varus/neutral and valgus/neutral comparison. A decrease in coronal tibial slope with the HKA was seen, with highest values in the varus group. This effect is plausible, as a degeneration of the medial (lateral) compartment is expected with severe cases of varus (valgus) OA (Kellgren-Lawrence grade 3-4 (Kellgren and Lawrence 1957)), resulting in an increase (decrease) of the coronal slope. Neogi et al. (Neogi et al. 2013), found a widening and flattening of the tibial compartments with OA. Similarly in the present database analysis, an increase in the ML width of the varus and compared to the control group was found. However, the difference was not statistically significant and the effect sizes was low.

Interbone parameter changes with OA

In the present study, an increase in TT-TG distance was seen with increasing HKA, both absolute and relative. This observations suggests valgus aligned knees to be of higher risk for a pathological TT-TG distance of over 20 mm (Dejour et al. 1994) or a pathological TT-TG Index of over 0.23 (Hingelbaum et al. 2014). These results are in agreement with the literature, reporting statistically significant positive correlations of the HKA with the TT-TG distance (Hochreiter et al. 2019; Chen et al. 2022). Further, in the present study an increase in Insall-Salvati Index (3D) was found in the varus and valgus compared to the control group. To the best of the author's knowledge, there are no studies reporting on both this relationship.

Conclusion

In conclusion, the results of the present study are in agreement with the available literature on effects of leg mal-alignment on knee morphological parameters. With a much more extensive data basis and comprehensive parameter list, the results represent a valuable basis for identifying cut-off values in the context of automated deformity correction as well as for other orthopedic applications.

D) Exemplary documentation of the virtual TKA implantation

Introduction

In this thesis, an automated virtual TKA implantation was implemented and applied to a representative database. The respective workflow and process is described in detail in **Chapter 5.3.1**. This chapter documents the virtual TKA for an exemplary case, which was selected from the database analyzed in **Chapter 5.4**. For each step of the process, visualizations are provided below.

Femur Workflow

1) Defining a bone-specific coordinate system

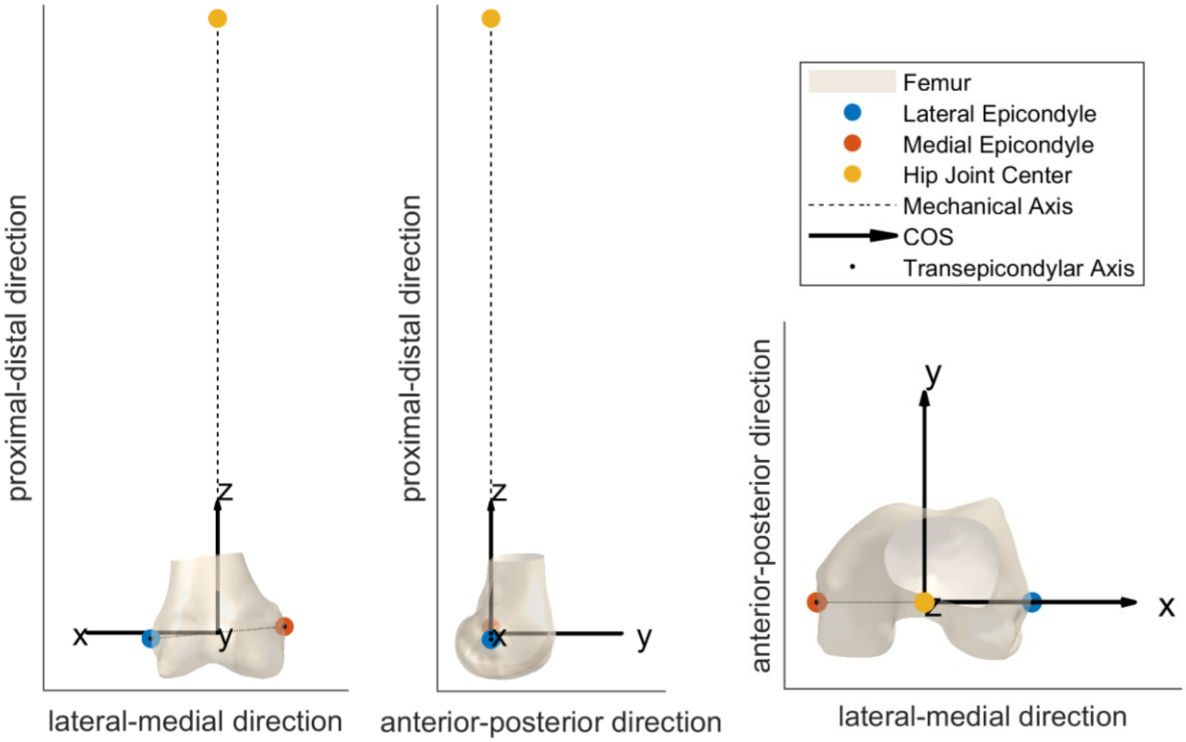

2) Identifying relevant bony reference points for implant positioning

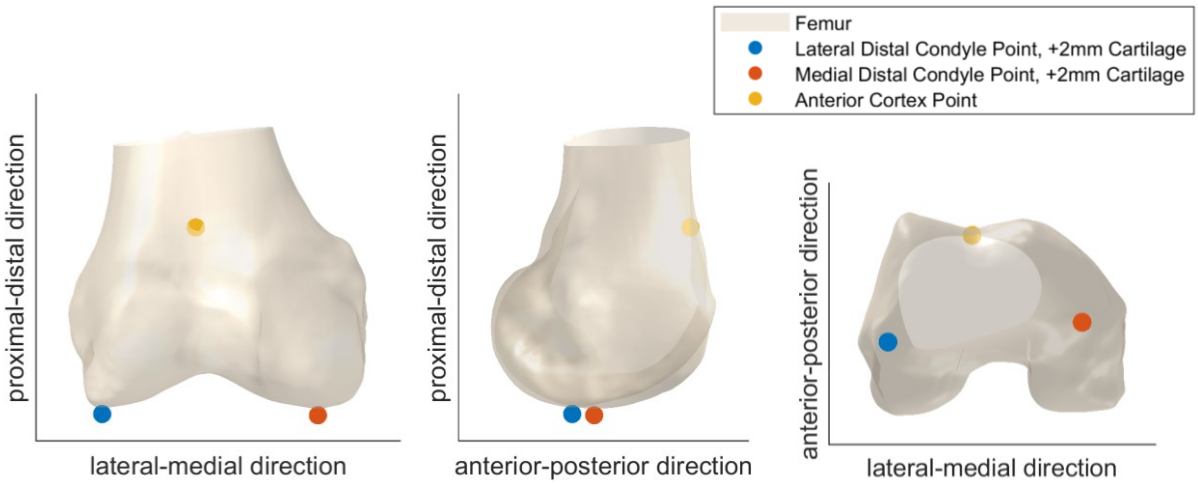

3) Positioning of the implant relative to the point based on reference points

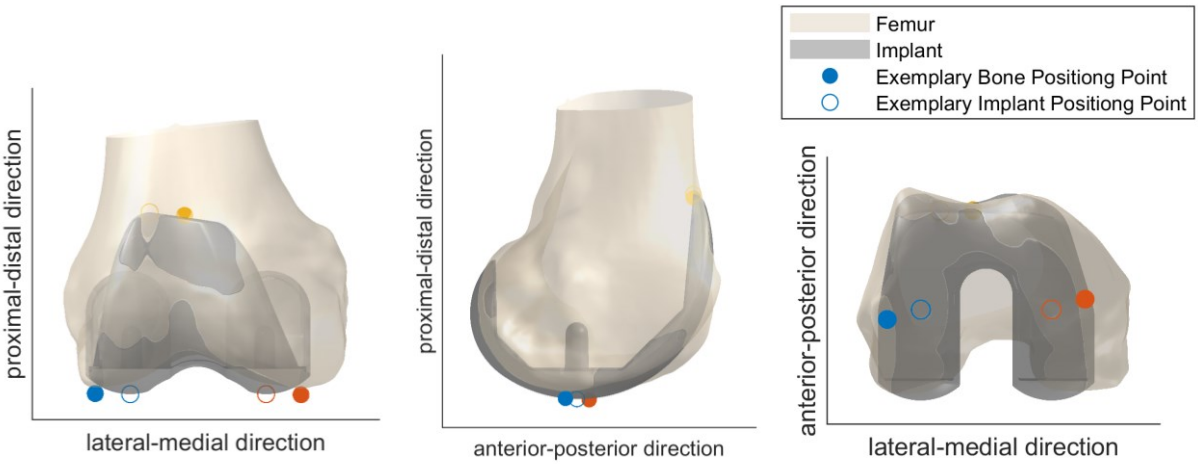

4) Performing the resection cuts defined by the implant backside information

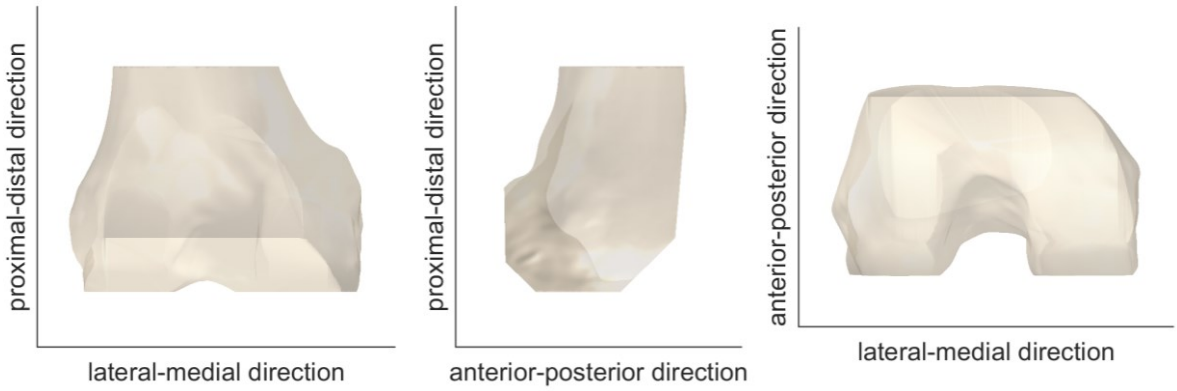

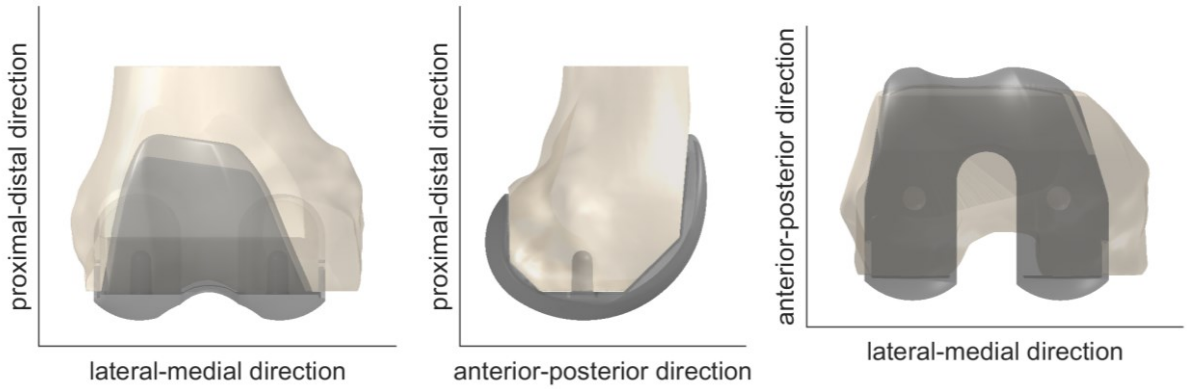

Tibia Workflow

1) Defining a bone-specific coordinate system

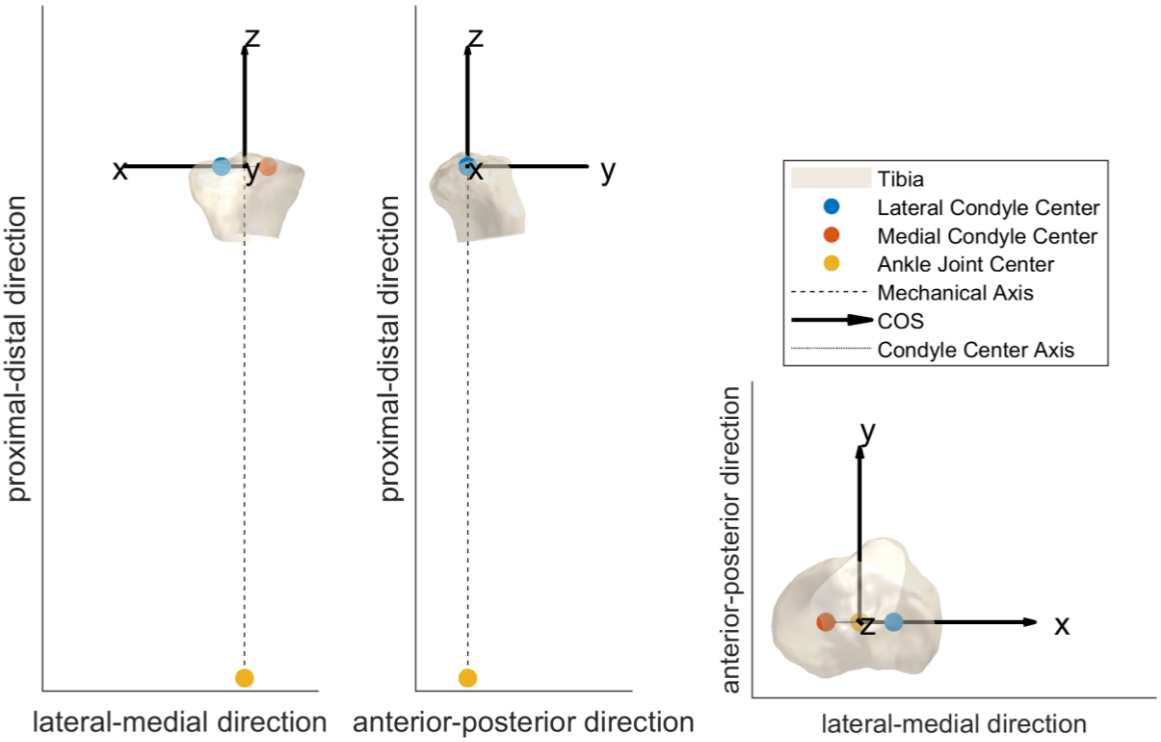

2) Identifying relevant bony reference points for implant positioning

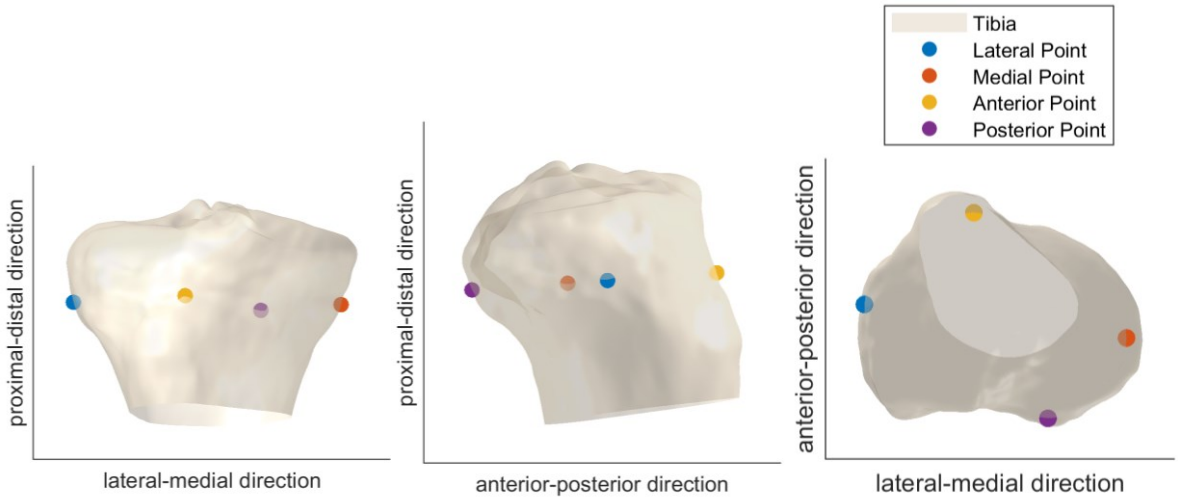

3) Positioning of the implant relative to the point based on reference points

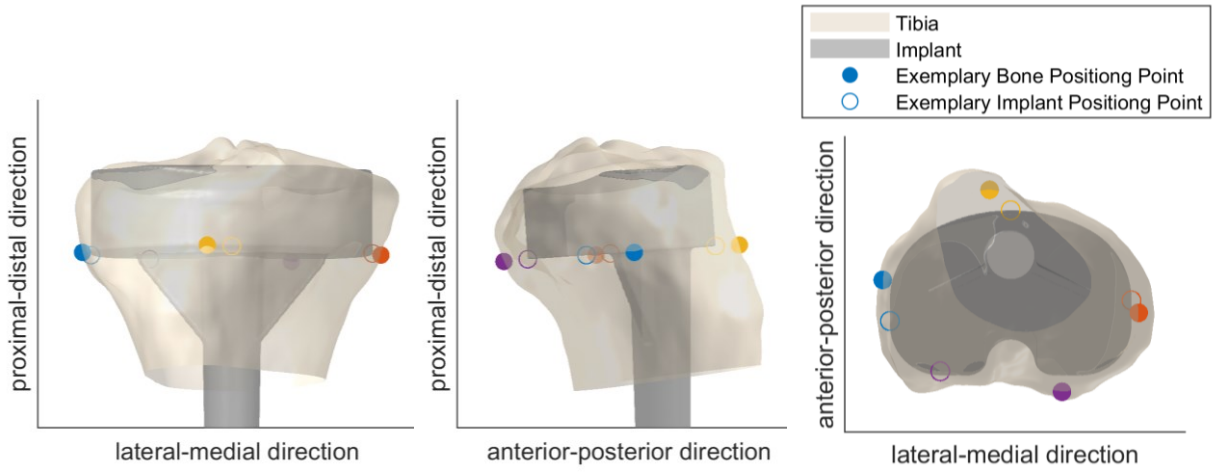

4) Performing the resection cuts defined by the implant backside information

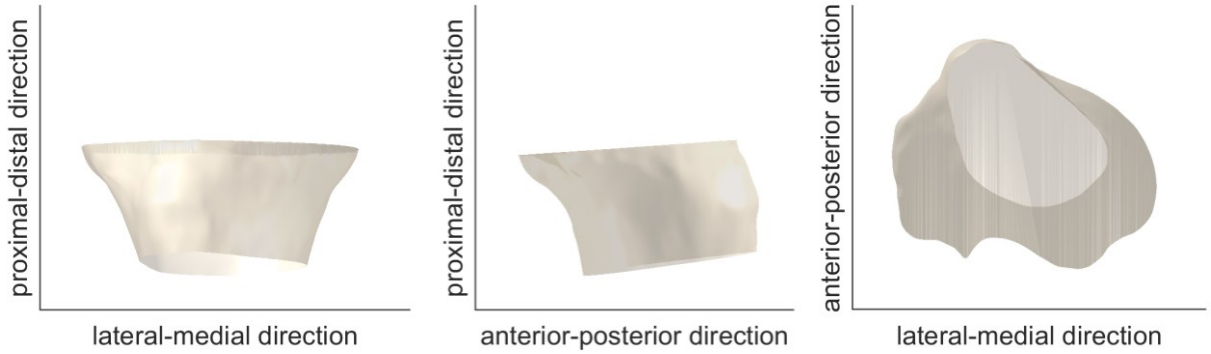

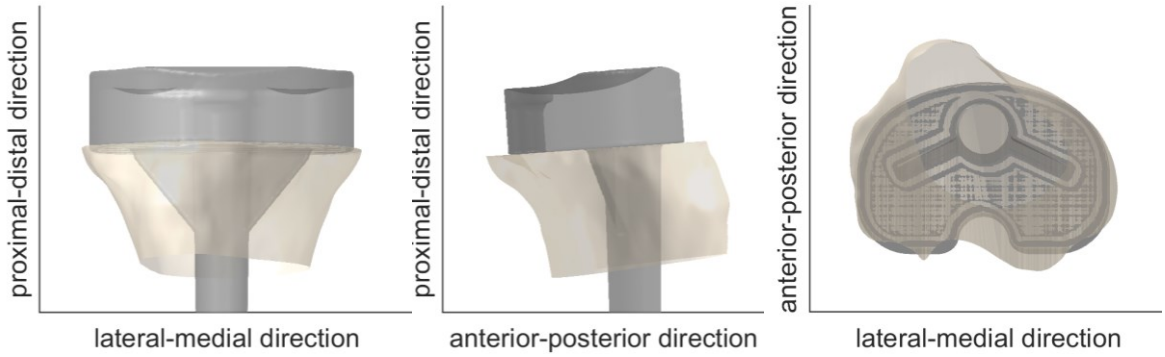
proximal-distal direction
lateral-medial direction
proximal-distal direction
anterior-posterior direction
anterior-posterior direction
lateral-medial direction